THE UNIVERSITY *of* EDINBURGH

Investigating Potential New Mechanisms of Regulating Autophagy

Agata Natalia Makar

THE UNIVERSITY *of* EDINBURGH

Thesis submitted for the degree of Doctor of Philosophy
The University of Edinburgh
April 2023

Abstract

Autophagy is a cellular recycling mechanism that can be upregulated in cancer cells to provide energy and nutrient supply and promote cell survival. It has previously been reported that autophagy deficiency can result in tumour growth inhibition and enhanced sensitivity to chemotherapy suggesting that targeting autophagy is an attractive treatment option for cancer patients. To efficiently target autophagy as a treatment strategy, it is necessary to investigate the molecular autophagy pathway and develop novel potent inhibitors. Previous work in the lab, utilising proximity labelling assays and a genome-wide CRISPR-Cas9 screen have identified potential novel mechanisms by which autophagy can be regulated. The goals of my PhD project are to develop the necessary tools and characterise these new modulators in order to further our understanding of the regulation of autophagy in cells.

Lay summary

Our cells are exposed to stress on regular basis, therefore multiple mechanisms tackling cellular stress have been developed. One of them is a pathway coined as autophagy, which involves degradation of material from within the cells by degradative organelles of a cell called lysosomes. The importance of autophagy is highlighted in neurodegenerative disorders when often autophagic activity is diminished, resulting in accumulation of unwanted materials in cells, toxicity and subsequent tissue degeneration. However, this highly conserved process is not always beneficial, cancer cells use autophagy to promote growth and to resist therapy. Therefore, targeting autophagy is an attractive treatment prospect for cancer therapy. Nevertheless currently used autophagy inhibitors are non-specific and toxic which raises a need for search of new autophagy regulators which could potentially be targeted in therapy. This thesis focuses on characterising a potential new autophagy regulator identified in a gene deletion screen. Moreover, a novel interaction of already established autophagy regulators will be studied. Both aspects of my thesis aim to contribute to the scientific research focused on understanding the molecular bases of autophagy regulation and multifaced roles of autophagy proteins.

Declaration

I confirm that the work presented in this thesis is my own, unless specified otherwise in the text. This work has not been submitted for any other degree or qualification.

Signed……. Date…….

Agata Natalia Makar

Acknowledgements

I would like to thank my PhD supervisor Dr Noor Gammoh for the support and encouragement I have received throughout the past 5 years. Noor has helped build my confidence and become a better scientist. On a more personal note, when I was facing a hard time and was ready to give up on myself, Noor did not let me do that. She was kind and compassionate and believed in me when I stopped believing in myself, I will be forever grateful for that. Once again, thank you so much Noor.

To my wonderful lab members, Joanne: for all our silly dances, venting sessions and finding humour in the most difficult situations; Najib: for the mental health coffee breaks and glow-up work you have done on me; Alina for encouraging me every step of the way and making me laugh on daily basis; the biggest thank you, I love you all so much!

To my best friend Asia, without a doubt I would not be able to do this without you. I could always count on you, whether it was a serious conversation or laughing so much we cannot breathe anymore, both did wonders to my mental state and helped me immensely when things got tough. You are the most wonderful person and you helped me get through countless weekends in the lab and believed in my strength when I couldn’t.

To my wonderful parents, your patience and encouragement meant so much to me. Thank you for supporting all my silly decisions and always being in my corner. Your love and kindness were a driving force for me, I really hope I made you proud.

Table of contents

Abstract 2
Lay summary 3
Declaration 4
Acknowledgements 5
Table of contents 6
List of figures 10
List of tables 12
List of abbreviations 13
Chapter 1. Introduction 16
1.1 Autophagy – an overview 16
1.1.1 Autophagosome biogenesis 17
1.1.2 Autophagosome-lysosome fusion 24
1.1.3 IAM degradation 26
1.1.4 Autophagy in development 27
1.1.5 Autophagy in aging and Alzheimer's disease 28
1.1.6 Autophagy in cancer 30
1.2 Lysosomes – an overview 31
1.2.1 V-ATPase proton pump 32
1.2.2 Lysosomal membrane proteins 33
1.2.3 Cathepsin proteases 36
1.2.4 Lysosomal lipases 37
1.2.5 Lysosomal enzymes trafficking 39
1.2.6 Lysosomal storage disorders 42
1.2.7 Lysosomal dysfunction and neurodegeneration 43
1.3 RNAseK – an overview 45
1.4 Conjugation of ATG8s to Single Membranes 46

1.5 Investigating mechanisms of autophagy regulation 48
1.5.1 Genome-wide CRISPR-Cas9 screen 50
1.5.2 TurboID-based proximity labelling 51
1.6 Aims of the thesis 54
Chapter 2. Materials and methods 55
2.1 Cell culture 55
2.2 SDS-PAGE and western blotting 55
2.3 Microscopy 56
2.4 Antibodies 57
2.5 Cloning 59
2.6 Plasmids and oligonucleotides 62
2.7 Transfections 67
2.8 Quantitative reverse transcription (qRT)-PCR 68
2.9 Binding assays 69
2.10 Autophagy loss of function screen 71
2.11 TurboID 71
2.12 Transmission Electron Microscopy 72
2.13 Proteinase K protection assay 72
2.14 EGFR degradation assay 73
2.15 Fluorescence-activated cell scanning (FACS) assays 73
2.16 Bodipy staining 74
2.17 Lipidomics 75
2.18 Secretome analysis 75
2.19 DexoMAG lysosomal enrichment 76
2.20 Peptide array 77
2.21 Statistical analysis 77
Chapter 3. Characterisation of autophagy function and cell localisation of RNAseK 78

3.1 Introduction 78
3.2 Aims and objectives 79
3.3 Results 80
3.3.1 Analysis of the autophagy pathway in the absence of RNAseK 80
3.3.2 Investigating the role of RNAseK in IAM degradation 87
3.3.3 Dissecting the cellular localisation of RNAseK 89
3.3.4 Identifying RNAseK interaction network 93
3.4 Discussion 96
Chapter 4. Role of RNAseK in lysosomal homeostasis 101
4.1 Introduction 101
4.2 Aims and objectives 102
4.3 Results 103
4.3.1 Analysis of lysosomal function in the absence of RNAseK 103
4.3.2 Investigating the role of RNAseK in lysosomal lipases delivery and maturation 107
4.3.3 Investigating lysosomal proteome and cellular secretome in the absence of RNAseK 115
4.4 Discussion 118
Chapter 5. Role of PLD3 and VPS4a in autophagy 122
5.1 Introduction 122
5.2 Aims and objectives 123
5.3 Results 125
5.3.1 Analysis of autophagy pathway in absence of PLD3 125
5.3.2 Role of RNAseK in VPS4a regulation 128
5.4 Discussion 133
Chapter 6. Summary and discussion 137
Chapter 7. Validation of ATG2 as a novel binding partner of ATG16L1 142
7.1 Introduction 142

7.2 Aims and objectives 143
7.3 Results 144
7.3.2 Validation of the ATG2-ATG16L1 interaction 144
7.3.3 Mapping the ATG2-ATG16L1 interaction sites 147
7.3 Discussion 152
Appendix 1 155
Appendix 2 157
List of references 159

List of figures

Figure 1.1 Schematic diagram of autophagy including autophagic flux markers. 18
Figure 1.2 Diagram of ATG8 conjugation machinery. 22
Figure 1.3 Effects of autophagy dysregulation on organismal health. 31
Figure 1.4 Proteins regulating lysosomal homeostasis. 39
Figure 1.5 Schematic diagram of canonical trafficking of lysosomal hydrolases. 41
Figure 1.6 Schematic diagram of PLD3 trafficking to lysosomes. 42
Figure 1.7 A diagram depicting APP processing pathway 44
Figure 1.8 Schematic diagram of RNAseK. 46
Figure 1.9 Schematic diagram of TurboID proximity labelling mechanism of action. 53
Figure 3.1 RNAseK knockout results in accumulation of autophagic markers and cargo. 83
Figure 3.2 RNAseK knockout does not inhibit autophagosome closure. 84
Figure 3.3 RNAseK knockout does not inhibit autophagosome-lysosome fusion..... 87
Figure 3.4 RNAseK knockout inhibit IAM degradation. 89
Figure 3.5 Validation of RNAseK-myc cell line. 90
Figure 3.6 RNAseK localises to multiple cell compartments. 93
Figure 3.7 RNAseK is in proximity of proteins on multiple membranous compartments. 96
Figure 3.8 Comparison of top hits identified in pulldown and proximity labelling of RNAseK……..96
Figure 4.1 RNAseK knockout does not disrupt lysosomal pH and proteases function. 107
Figure 4.2 RNAseK knockout disrupts lipid homeostasis. 108
Figure 4.3 RNAseK knockout causes an lysosomal accumulation of ATG9a. 109
Figure 4.4 RNAseK knockout disrupts cellular localisation of MPRs. 112
Figure 4.5 RNAseK knockout alerts maturation and activity of PLA2G15 and LIPA. 114
Figure 4.6 RNAseK knockout alters the lysosomal localisation of multiple proteins. 118

Figure 5.1 PLD3 is required for autophagy. 127
Figure 5.2 VPS4a accumulates on lysosomes in absence of RNAseK. 130
Figure 5.3 Dominant negative mutant of VPS4a inhibits autophagy. 131
Figure 5.4 RNAseK regulates VPS4a dynamics. 133
Figure 6 Graphical abstract. 137
Figure 7.1 ATG16L1 interacts with ATG2. 146
Figure 7.2 ATG16L1 interact with ATG2 via C-terminus. 148
Figure 7.3 ATG2a YFS mutant shows reduced interaction with ATG16L1. 149
Figure 7.4 Identification of residues on ATG2a essential for ATG16L1 binding. 152

List of tables

Table 1.1 A list of selected Lysosomal storage disorders (LSDs). 34
Table 1.2 Comparison of autophagy proteins needed for autophagy and CASM..... 48
Table 2.1 List of antibodies used in this thesis. 59
Table 2.2 Details of reagents used for PCR. 61
Table 2.3 Cycles and temperature steps used for PCR. 61
Table 2.4 Conditions used for mutagenesis of ATG2 construct. 61
Table 2.5 Details of plasmids used for gene knockout or protein expression. 63
Table 2.6 Details of oligonucleotides used for gene knockout or protein expression. 66
Table 2.7 Details of siRNA used for knockdown experiments. 68
Table 2.8 Cycles and temperature steps used for qRT-PCR. 69

List of abbreviations

4-MUP	4-Methylumbelliferyl Palmitate
AA	Amino acid
AD	Alzheimer’s disease
ALR	Autophagosome-lysosome reformation
AMPK	AMP-activated protein kinase
AP	Adaptor protein complex
APP	Amyloid precursor protein
Atg/ATG	Autophagy-related
Aβ	β-amyloid
Baf A1	Bafilomycin A1
CASM	Conjugation of ATG8s to Single Membranes
CCV	Clathrin-coated vesicles
CD-MPR	Cation-dependent Man-6-P receptor
CHMP	Charged multivesicular body protein
CI-MPR	Cation-independent Man-6-P receptor
CLEM	Correlative light and electron *microscopy*
CMA	Chaperone-mediated autophagy
CME	Clathrin-mediated endocytosis
CO2	Carbon dioxide
CQ	Chloroquine
CRISPR	Clustered regularly interspaced short palindromic repeats
DFCP1	Double FYVE-domain containing protein
DMEM	Dulbecco's Modified Eagle's Medium
DS	Down Syndrome
EDTA	Ethylenediaminetetraacetic acid
EGFR	Epithelial growth factor receptor
EGTA	Ethyleneglycoltetraacetic acid
ESCRT	Endosomal sorting complex required for transport
EV	Extracellular vesicle
FACS	Fluorescence-activated cell sorting
FBS	Foetal bovine serum
GBM	Glioblastoma multiforme

GFP	Green fluorescent protein
HCQ	Hydroxychloroquine
HEK	Human embryonic kidney cell
HOPS	Homotypic fusion and protein sorting
HRP	Horseradish peroxidase
IAM	Inner autophagosomal membrane
ILV	Intraluminal vesicles
LAMP	Lysosomal membrane protein
LAP	LC3-associated phagocytosis
LC3	Microtubule associated protein 1 light chain 3
LD	Lipid droplet
LIPA	Lysosomal acid lipase
LIR	LC3-interacting region
LMP	Lysosomal membrane protein
LSD	Lysosomal storage disease
LysoPC	Lysophosphatidylcholine
LysoPE	Lysophosphatidylethanolamine
Man-6-P	Mannose 6-phosphate
MEF	Mouse embryonic fibroblast
MS	Mass spectrometry
mTORC1	Mammalian target of rapamycin complex 1
MVB	Multivesicular body
OAM	Outer autophagosomal membrane
OGT	O-linked β-N-acetylglucosamine transferase
PAS	Phagophore assembly site
PBS	Phosphate-buffered saline
PCR	Polymerase chain reaction
PE	Phosphatidylethanolamine
PEI	Polyethylenimine
PFA	Paraformaldehyde
PI3KC3	Phosphatidylinositol 3-kinase catalytic subunit type 3
PI3P	Phosphatidylinositol 3-phosphate
PLA2	Phospholipase A2

PLD3	Phospholipase D3
PPI	Protein-protein interaction
PS	Phosphatidylserine
RFP	Red fluorescent protein
sgRNA	Single guide RNA
SH-SY5Y	Human neuroblastoma cell
SIM	Super resolution microscopy
siRNA	Small interfering RNA
SMAD4	Mothers against decapentaplegic homolog 4
SNARE	Soluble N-ethylmaleimide-sensitive factor attachment protein receptor
SNX	sorting nexins
SPIONs	Superparamagnetic Iron Oxide Nanoparticles
STX17	Syntaxin-17
TEM	Transmission electron microscopy
TFA	Trifluoroacetic acid
TFEB	Transcription factor EB
TGN	Trans-Golgi network
TiD	TurboID
U2OS	Human bone osteosarcoma epithelial cells
UBD	Ubiquitin binding domain
ULK	Unc-51-like kinase
UPS	Ubiquitin-proteasome system
UVRAG	UV radiation resistance-associated gene protein
VAMP	Vesicle-associated membrane protein
V-ATPase	Multi-subunit vacuolar-type ATPase
VPS	Vacuolar protein-sorting
VSVG	Vesicular stomatitis virus G protein
WIPI	WD40 repeat domain phosphoinositide-interacting family of proteins
β-ME	β-mercaptoethanol

Chapter 1. Introduction

1.1 Autophagy – an overview

Cells employ multiple pathways to ensure optimal intracellular environment for maintaining cell health and function. There are two main ways cells remove unwanted intracellular components: the ubiquitin-proteasome system (UPS) and autophagy. UPS is utilised for degradation of short-lived and misfolded proteins and involves multiple ubiquitination steps before the cargo is proteolytically degraded in the proteasome (Dikic, 2017). The term autophagy was initially coined by Christian de Duve and it originates from Greek words auto – “self” and phagein – “to eat” and it refers to delivery of intracellular substrates to lysosomes for degradation (Wesselborg and Stork, 2015). Autophagy complements UPS’s function by degrading long-lived proteins, but as opposed to UPS, in autophagy the cargo is not limited to proteins and includes more heterogenous substrates such as lipids, nucleic acids and carbohydrates (Glick et al., 2010).

There are three main types of autophagy: microautophagy, chaperone-mediated autophagy (CMA) and macroautophagy. The common denominator between those processes is the delivery of the cargo from within the cell to the lysosomes for degradation. Microautophagy is an invagination of lysosomes and direct engulfment of the cytosol (Li et al., 2012) and CMA is a direct targeting of proteins to lysosomes by chaperones (Cuervo and Wong, 2014). Macroautophagy describes a process of a *de novo* formed, morphologically distinct, double membrane autophagosomes, which enclose the cytoplasmic material. Closed autophagosomes then fuse with the lysosome which results in degradation of the autophagosomal inner membrane (IAM) together with its content by lysosomal hydrolases (Yim and Mizushima, 2020a). Macroautophagy is the most studied type of autophagy and the main focus of this thesis, therefore from now on will be referred to as autophagy.

Due to the large size of autophagic vehicles (approximately 1 μm in diameter), in addition to degradation of the forementioned substrates, autophagy is also the main mechanism by which cells remove whole organelles or their fragments, as well as the membrane-less organelles formed by liquid-liquid phase separation (Glick et al., 2010; Wilfling et al., 2020). This specific degradation of substrates occurring in a selective manner is broadly called selective autophagy and the precise name is based on the

cargo which is being degraded, for example, the degradation of mitochondria during mitophagy, peroxisome during pexophagy, glycogen during glycophagy and lipids during lipophagy (Gubas and Dikic, 2022). Selective autophagy relies on a multitude of specific receptors, which tether the cargo to the autophagic machinery. Over 30 autophagy receptors have been identified in mammalian cells thus far (Gubas and Dikic, 2022). Of these, p62 (also known as SQSTM1) is the first identified selective autophagy receptor and can recognise cellular cargo through its ubiquitin binding domain (UBD) and LC3-interacting region (LIR, discussed below) (Bjørkøy et al., 2005; Lin et al., 2013). P62 degradation is also widely used to monitor autophagic degradation (Yoshii and Mizushima, 2017).

In addition to quality control function within the cell, autophagy is also used as a survival mechanism and it has been shown to be upregulated during periods of stress (Kroemer et al., 2010). During nutrient starvation cells utilise a non-selective (bulk) autophagy and degrade unessential cytosolic material to provide nutrients in order to sustain core metabolism and therefore promote cell survival and avoid cell death (Kaur and Debnath, 2015). Initially, it was believed that bulk autophagy is exclusively activated in response to starvation (Mortimore and Schworer, 1977). However, throughout the years researchers have discovered that autophagy is also activated in response to the whole array of stimuli including hypoxia, reduced growth factor signaling or increased calcium levels in the cytosol, to name a few (Jung et al., 2010).

1.1.1 Autophagosome biogenesis

Due to autophagy being a highly conserved process, the yeast strain *Saccharomyces cerevisiae* was initially used to identify key autophagy related (ATG) genes. After the discovery of autophagosomes in yeast cells under nutrient deprivation (Takeshige et al., 1992), the research group of Yoshinori Ohsumi performed a genetic screen in which they have identified autophagy-deficient mutants unable to survive nitrogen starvation (Tsukada and Ohsumi, 1993). The screen provided a great insight into autophagy process and Ohsumi was awarded the Nobel prize in Physiology and Medicine in 2016 (Levine and Klionsky, 2017). Today we have a better understanding of autophagy which can be broadly separated to three main stages: autophagosome biogenesis, autophagosome-lysosome fusion and autolysosome degradation.

Autophagosome biogenesis begins with the formation of a double membrane phagophore, which elongates to engulf autophagic cargo. Expansion of the phagophore is followed by its closure and formation of autophagosome (Glick et al., 2010). In the following section, I will discuss molecular mechanisms governing those processes.

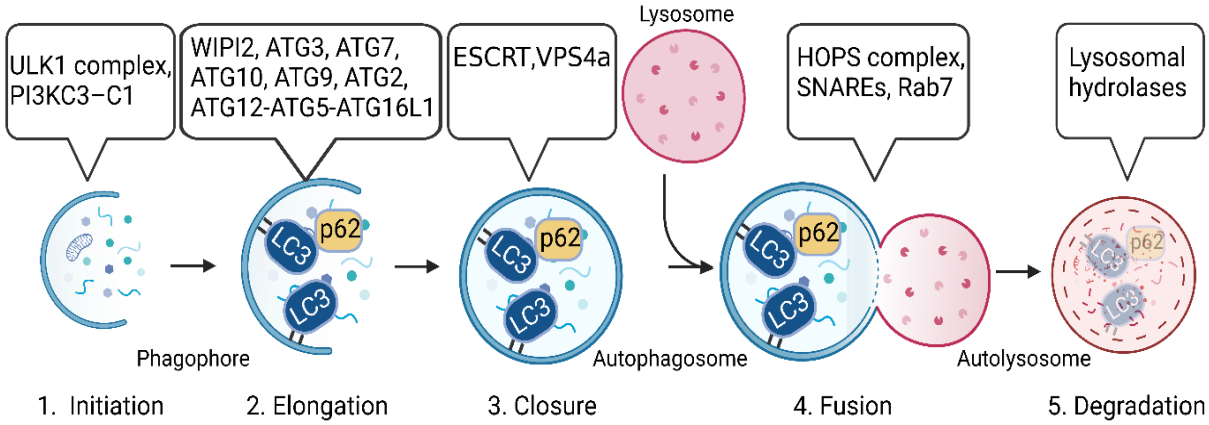

Figure 1.1 Schematic diagram of autophagy including autophagic flux markers.
The pathway starts with the assembly of a double membrane phagophore (1. Initiation), which then expands (2. Elongation) and closes to form the autophagosome encapsulating the cargo (3. Closure). The autophagosome fuses with lysosome to form autolysosome (4. Fusion). Autolysosomal cargo is degraded by lysosomal enzymes (5. Degradation). The core proteins regulating each stage of autophagy are listed above the diagram.

Upstream regulators of autophagy induction

Initiation of autophagosome biogenesis occurs due to variety of signals transmitted via different signalling pathways. Amongst them, mammalian target of rapamycin complex 1 (mTORC1) and (AMP- activated protein kinase) AMPK are the two key players which regulate autophagy in response to changes in the nutrient status of the cell (Kim et al., 2011).

mTORC1 consist of catalytic kinase subunit mTOR, regulatory associated protein of mTOR (Raptor), DEP domain containing mTOR-interacting protein (DEPTOR), mammalian lethal with Sec13 protein 8 (mLST8) and proline rich AKT substrate 40 kDa (PRAS40) (Takahara et al., 2020). mTORC1 is a negative regulator of autophagy and in nutrient rich conditions localises to the lysosome and phosphorylates multiple autophagy proteins, including Unc-51-like kinase 1 (ULK1), ATG13, ATG14 and WIPI2 (Dossou and Basu, 2019), thereby suppressing their

activities. Moreover, mTORC1 transcriptionally supresses autophagy by phosphorylating transcription factor EB (TFEB) (Puertollano et al., 2018). Upon nutrient starvation mTORC1 dissociate from lysosomes and becomes inactivated, these events leads to the initiation of autophagosome biogenesis (Yim and Mizushima, 2020b).

AMPK is a serine/threonine kinase which positively regulates autophagy. Upon glucose depletion AMPK senses the decrease in adenosine triphosphate (ATP) to adenosine diphosphate (ADP)/ adenosine monophosphate (AMP) ratio in cells (Hardie et al., 2012) and induces autophagy. AMPK inhibits mTORC1 indirectly by Tuberous Sclerosis Complex 2 (TSC2) phosphorylation and directly via Raptor phosphorylation (Gwinn et al., 2008; Inoki et al., 2003). Furthermore, AMPK promotes autophagosome biogenesis by activating ULK1 complex (Kim et al., 2011).

Autophagy initiation

The activity of upstream autophagy regulators results in ULK1 complex activation and recruitment to phagophore assembly site (PAS) which forms predominantly on ER (Yang et al., 2021). The ULK1 complex consists of ULK1/ULK2, ATG13, ATG101 and FAK Family interacting Protein of 200 kDa (FIP200) (Chan et al., 2007a; Ganley et al., 2009; Hara et al., 2008; Hosokawa et al., 2009; Yan et al., 1998). ULK1 is activated by autophosphorylation and in turn phosphorylates ATG13, FIP200 and ATG101 (Bach et al., 2011; Egan et al., 2015). Although ULK1 and ULK2 seem to be redundant during autophagy (Cheong et al., 2014), computational studies suggest distinct autophagic roles of ULK1 and ULK2 (Demeter et al., 2020). Deletion of the other complex components destabilise the ULK1 complex and results in a significant defect in autophagy initiation (Hara et al., 2008; Hosokawa et al., 2009; Mercer et al., 2009).

ULK1 activity is also crucial for activation of another autophagy complex, the class III lipid kinase complex I (PI3KC3–C1). PI3KC3–C1 is composed of vacuolar protein sorting 15 and 34 (VPS15 and VPS34, respectively), Beclin1 and ATG14 (Furuya et al., 2005; Itakura et al., 2008; Yan et al., 2009). The presence of ATG14 distinguishes between PI3KC3 complex I and complex II, where it is substituted with UV radiation resistance associated gene protein (UVRAG) in complex II (Itakura et al.,

2008). It is believed that ATG14 is responsible for targeting of PI3KC3–C1 to the PAS (Fan et al., 2011).

ULK1 phosphorylates Beclin1 and ATG14 which results in increased VPS34 enzymatic activity and phosphorylation of phosphatidylinositol (PI) to phosphatidylinositol 3-phosphate (PI3P) at the PAS (Egan et al., 2015; Russell et al., 2013; Wold et al., 2016). This activity is crucial for the formation of ER subdomains known as omegasomes, due to their Ω-like shapes. The omegasome provides a platform for phagophore formation and growth and is characterised by PI3P enrichment and the presence of Zink Finger FYVE domain-containing protein 1 (DFCP1) (Axe et al., 2008). Local accumulation of PI3P also results in the recruitment of the WD40 repeat domain phosphoinositide-interacting family of proteins (WIPIs). In mammalian cells four members of WIPI family have been identified; WIPI1, WIPI2, WIPI3/WDR45B and WIPI4/WDR45 (Proikas-Cezanne et al., 2015).

Phagophore elongation

WIPI2 plays a role in recruitment of the downstream ATG12-ATG5-ATG16L1 complex to the PAS via direct interaction with ATG16L1, and specifies the localisation and subsequent lipidation of the ubiquitin-like family of proteins (ATG8 proteins) (Dooley et al., 2014; Polson et al., 2010). Interestingly, in the absence of WIPI2-ATG16L1 binding, autophagy is diminished but not completely abolished, suggesting alternative ways of the complex recruitment to the phagophore (Lystad et al., 2019). Indeed, it has been reported that the interaction of ATG16L1 with FIP200 regulates the complex recruitment to the phagophore (Gammoh et al., 2013; Nishimura et al., 2013). Moreover, ATG16L1 contains multiple lipid binding residues crucial for its recruitment to the PAS and subsequent ATG8 lipidation (Dudley et al., 2019; Lystad et al., 2019).

ATG8 lipidation refers to the conjugation of cytosolic ATG8 to phosphatidylethanolamine (PE), which results in formation of membrane-bound ATG8 (also referred to as ATG8-II or ATG8-PE) (figure 1.2) (Kabeya et al., 2004). This process is crucial for phagophore elongation and includes multiple steps regulated by ATG proteins. Firstly, the cysteine protease ATG4 cleaves ATG8 and exposes a C-terminal glycine residue generating ATG8-I (Kabeya et al., 2000). ATG8-I is then activated by the E1-like enzyme ATG7. ATG7, together with ATG10 also play a role in

conjugation of ATG12 to ATG5 (to form ATG12-ATG5 conjugate), essential for the formation of ATG12-ATG5-ATG16L1 complex (Tanida et al., 2004). Conjugation of ATG8-I to membrane-associated PE and formation of ATG8-II requires the enzymatic activity of the E2-like ligase, ATG3. ATG3 recruitment to the lipidation site is regulated by the activity of the ATG12-ATG5-ATG16L1 complex known to harbour an E3-like ligase activity (Lystad et al., 2019; Sakoh-Nakatogawa et al., 2013; Tanida et al., 2004). Once lipidated, ATG8-II can stably associate with the phagophore membranes where it can also recruit cargo adaptor proteins. The ATG8s in mammalian cells consist of two families: LC3 (LC3A, LC3B and LC3C) and GABARAP (GABARAP, GABARAPL1 and GABARAPL2), and LC3B is the most commonly used to monitor autophagic activity (Mizushima et al., 2010). Cargo receptor proteins as well as other autophagy regulators bind to ATG8 proteins via conserved short peptide motifs called LC3-interaction region (LIRs) (Wirth et al., 2019). ATG8 proteins can associate with both inner and outer- autophagosomal membrane (IAM and OAM, respectively), and during autophagosome maturation the OAM-bound ATG8s are deconjugated by ATG4 (Maruyama and Noda, 2018).

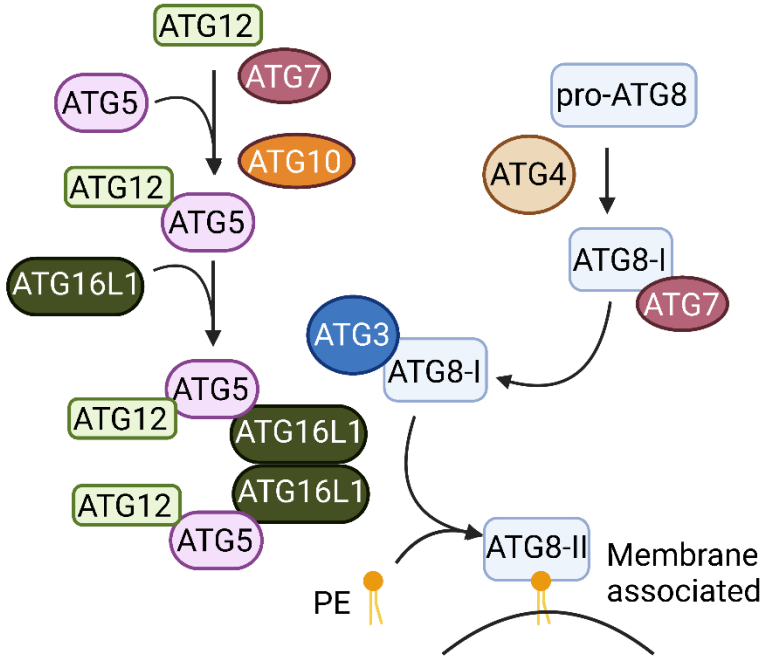

Figure 1.2 Diagram of ATG8 conjugation machinery.

Left: *assembly of ATG12-ATG5-ATG16L1 complex. ATG12 is activated by ATG7 (E1-like) and then together with ATG10 (E2-like) conjugate ATG12 to ATG5. ATG12-ATG5 is then associated with ATG16L1 to form E3-like enzyme complex.* ***Right:*** *pro-ATG8 protein is cleaved by ATG4 to form ATG8. ATG8 is activated by ATG7 (E1-like) to form ATG8-I and transferred to ATG3 (E2-like). ATG3 together with the ATG12-ATG5-ATG16L1 complex promote lipidation of ATG8 to PE which produces, membrane-bound ATG8-II.*

Elongation of the phagophore requires supply of lipids. ATG2 and ATG9 are the two ATG proteins that help supply lipids and membranes to the growing phagophore. The recruitment of ATG2 to PAS is crucial for phagophore elongation. In yeast, the interaction of Atg2 with Atg18 (a WIPI4 homologue) is essential for its recruitment to the phagophore (Suzuki et al., 2007). However, in mammalian cells the interaction of ATG2 with WIPI4 is dispensable for the recruitment of ATG2 to the phagophore (Rieter et al., 2013; Tang et al., 2019). This discrepancy between yeast and mammalian cells can be explained by a low homology between their respective Atg2 and ATG2 proteins. Indeed, the expression of human ATG2 in *Atg2*-deficient yeast strain does not rescue the autophagy knockout phenotype (Romanyuk et al., 2011). Mammalian ATG2 can localise to lipid droplets and autophagic membranes and was reported to possess membrane tethering and lipid transfer abilities (Maeda et al.,

2019; Valverde et al., 2019; Zheng et al., 2017). Deletion of the N-terminus region of ATG2 results in autophagy inhibition (Tamura et al., 2017). This observation further confirms the role of ATG2 in supplying lipids to the phagophore, as this N-terminal region exhibits high homology with VPS13, which is a lipid transporter protein (Osawa and Noda, 2019; Valverde et al., 2019). Moreover, studies showed ATG2 regulates retrograde transport of ATG9a protein from the phagophore (Tang et al., 2019) and that the two proteins form a heteromeric complex essential for autophagosome formation (van Vliet et al., 2022). Upon autophagy induction, ATG9a shuttles between multiple cell compartments and the phagophore (Orsi et al., 2012). ATG9a is the only transmembrane ATG protein identified thus far and it has been reported to promote phagophore elongation by transiently interacting with the phagophore membrane (Orsi et al., 2012). It was initially believed that ATG9a contributes to the elongation of the phagophore by supplying the donor membrane fragments (Orsi et al., 2012). However, recent studies suggest that ATG9a could also play a role in the equilibration of lipids on the phagophore due to its lipid scramblase activity (Maeda et al., 2020). A model of ATG9a assisting in equilibration of lipids delivered by ATG2 to the phagophore membrane has been proposed (van Vliet et al., 2022) further highlighting the role of the two proteins in phagophore elongation.

Phagophore closure

To completely encapsulate the cytosolic cargo and form an autophagosome, phagophore closure must occur. This process is regulated by multiple proteins including endosomal sorting complex required for transport (ESCRT) complexes and ATG proteins (Jiang et al., 2021).

The ESCRT machinery is required for multiple membrane remodeling events in cells, including phagophore closure. ESCRT proteins can be classified into ESCRT-I, ESCRT-II and ESCRT-III complexes and are recruited to the closure site in a successive manner (Jiang et al., 2021). ESCRT-III polymerises to form membrane-binding spirals and together with the AAA-ATPase VPS4a drive membrane remodeling (Adell et al., 2014; Chiaruttini et al., 2015). VPS4a also facilitates the disassembly and recycling of ESCRT-III. (Diaz et al., 2015). Of note, both ESCRT-III and VPS4a localise to the nascent autophagosome transiently and detach within 1-2 minutes (Zhen et al., 2020). Depletion of the ESCRT-I component VPS37A leads to accumulation of

unclosed autophagosomes (Takahashi et al., 2019). Similar phenotypes are observed in cells deficient of ESCRT-III subunits CHMP2A or CHMP4B (Takahashi et al., 2018a; Zhen et al., 2020). Further confirming the role of ESCRT proteins in the closure events, studies using dominant negative mutant of VPS4a (VPS4a^{E228Q}) demonstrated impairment of phagophore closure and subsequent autophagy inhibition (Takahashi et al., 2018a).

The involvement of ATG proteins in phagophore closure is represented by numerous studies. Depletion of either ATG3 or ATG5 results in the accumulation of unclosed autophagosomes (Kishi-Itakura et al., 2014; Tsuboyama et al., 2016). Simultaneous knockdown of both ATG2a and ATG2b (the two redundant homologues of Atg2 in mammalian cells) leads to autophagy block and the accumulation of phagophores (Velikkakath et al., 2012). The interaction of ATG2a with ATG8 has been shown to be essential for autophagosome closure and expression of a LIR mutant of ATG2a resulted in the accumulation of open autophagosomes (Bozic et al., 2020). Moreover, inhibition of GABARAP activity by the expression of dominant negative mutant of ATG4a (ATG4a^{C77A}) increased the number of open autophagic membranes (Weidberg et al., 2010). As ATG2 is also involved in phagophore elongation, it remains unclear whether the closure defects seen in ATG2 depleted cells are due to the expansion defects or due to an independent role of ATG2 in closure events.

1.1.2 Autophagosome-lysosome fusion

Following the sealing of phagophore and autophagosome formation, autophagosomes fuse with either endosomes to form transient amphisomes, and then lysosomes, or directly fuse with lysosomes (Parzych and Klionsky, 2014). Here, I will discuss molecular mechanisms governing autophagosome-lysosome fusion resulting in autolysosome formation.

Autophagosome-lysosome fusion is regulated by a series of factors. In brief, the small GTPase Ras-related protein (RAB7) controls autophagosome-lysosome membrane tethering. RAB7 recruits the homotypic fusion and protein sorting (HOPS) complex, which mediates membrane tethering and assembly of soluble NSF attachment protein receptors (SNARE) complexes that drive the fusion event (Itakura et al., 2012). Additional factors have also been associated with fusion and include

lipids, ATG8 proteins and other tethers and adaptors, such as EPG-5, ATG14L1, TECPR1 and PLEKHM1 (Lőrincz and Juhász, 2020).

RAB7 localises to late endosomes, lysosomes and late autophagic structures (Guerra and Bucci, 2016; Gutierrez et al., 2004; Jäger et al., 2004), and is required for the fusion between autophagosomes and lysosomes. RAB7 binds two subunits of the HOPS complex, VPS39, and VPS41 and this RAB7-HOPS interaction is key for membrane tethering (Lürick et al., 2017). Moreover, RAB7 effector protein Ectopic P-granules 5 autophagy tethering factor (EPG5) determines fusion specificity of autophagosomes with lysosomes (Wang et al., 2016). Inhibition of RAB7 recruitment to autophagosomes results in autophagy inhibition (Ganley et al., 2011). Conversely, expression of RAB7 restores cadmium-induced block of autophagosome-lysosome fusion (Wang et al., 2021b). Interestingly, RAB7 seems to be dispensable for autolysosome formation in nutrient rich conditions (Kuchitsu et al., 2018) suggesting additional factors regulating this process.

The main function of the HOPS complex is to facilitate the fusion of vesicles by membrane tethering (Spang, 2016). The molecular mechanisms governing HOPS complex recruitment to the fusion site remain largely unknown. The HOPS complex consist of 6 subunits: VPS11, VPS16, VPS18, VPS33A, VPS39 and VPS41. Multiple interactions between the complex subunits and other fusion regulators have been identified. In addition to VPS39/VPS41-RAB7 binding, VPS16 interaction with the PI3KC3-C2 component UVRAG stimulates autophagosome-lysosome fusion (Liang et al., 2008). Moreover, RAB7 effector protein Pleckstrin homology domain containing protein family member 1 (PLEKHM1) was identified as a regulator of HOPS complex recruitment and binds both HOPS complex and OAM-bound LC3 through an LIR motif (McEwan et al., 2015). All of the HOPS complex subunits can bind Syntaxin17 (STX17), a key SNARE protein present on autophagosomes (Jiang et al., 2014).

Structurally, SNARE proteins can be separated into two main groups depending on whether glutamine (Q-SNAREs) or arginine (R-SNAREs) are present in the central hydrophilic layer. The Q-SNAREs can be furthered classified into Q-a, Q-b, and Q-c SNAREs (Han et al., 2017). During autophagosome-lysosome fusion, the presence Q-SNAREs and R-SNAREs in the contact sites between the two vesicles results in the formation a trans-SNARE complex (Yoon and Munson, 2018). This complex is able to fuse the two membranes, ergo two vesicles, which results in the transient localisation

of all of the SNARE components on one, now fused membrane. (Han et al., 2017). In mammalian cells, two SNARE complexes responsible for autophagosome-lysosome fusion have been identified: STX17-SNAP29-VAMP8/VAMP7 and YKT6-SNAP29-VAMP7 (Itakura et al., 2012; Matsui et al., 2018).

To facilitate autophagosome-lysosome fusion, STX17 (Qa-SNARE) associates with the OAM via its transmembrane glycine-zipper motif (Itakura et al., 2012). The vesicle-associated membrane protein 7 or 8 (VAMP7 and VAMP8, respectively) are R-SNAREs located on the lysosomal membrane. STX17-VAMP7/8 together with Qbc-SNARE synaptosome associated protein 29 (SNAP29) form the trans-SNARE and mediate fusion between the two OAM and the lysosomal membrane. SNAP29 activity is regulated in a nutrient-dependent manner by O-linked β-N-acetylglucosamine (O-GlcNAc) transferase (OGT), which prevents spontaneous or ectopic formation of the SNARE complex (Guo et al., 2014).

It was initially believed that STX17 is recruited exclusively to closed autophagosomes, however multiple studies demonstrated that unclosed autophagic structures can also recruit STX17 and fuse with lysosome, however the fusion rate and autolysosome degradation are heavily impaired the absence of STX17 (Takahashi et al., 2018b; Tsuboyama et al., 2016). Interestingly, autophagosome-lysosome fusion is only completely blocked upon STX17 and Synaptobrevin homologue YKT6 precursor (YKT6) co-inhibition in cells and these proteins facilitate fusion via alternative complexes (Matsui et al., 2018).

1.1.3 IAM degradation

Following autophagosome-lysosome fusion and autolysosome formation, autolysosomal content is digested by lysosomal hydrolases, including proteases and lipases, discussed in chapter 1.2 (Trivedi et al., 2020). This final degradation step is essential for the completion of autophagy and is referred to as autophagic flux (Ueno and Komatsu, 2020). Autolysosomal content degradation results in the release of catabolites to be reused by cells. Lysosomal enzymes selectively degrade the IAM without disrupting the OAM (Yim and Mizushima, 2020b). IAM disintegration is crucial to expose the autophagosomal lumen and subsequent digestion of the autophagosomal cargo, whereas OAM protection results in the containment of

hydrolases within autolysosomal structures. Immunofluorescence analyses of autolysosomes revealed a formation of a transient acidified ring between the IAM and OAM, suggesting the separation of the two membranes (Tsuboyama et al., 2016). The initial ability of the inner membrane to resist degradation, delays IAM collapse and influx of lysosomal enzymes into the autophagosomal lumen, however, the comprehensive mechanisms of this transient resistance and subsequent collapse of IAM are yet to be determined. IAM degradation triggers STX17 release from autolysosomes and monitoring STX17 dissociation with autolysosomes provides a useful tool to study IAM degradation (Tsuboyama et al., 2016).

Mechanisms and regulatory network of IAM dynamics and autolysosomal degradation are poorly understood. The specific enzymes responsible for IAM degradation in mammalian cells have not been discovered. In yeast, integral vacuolar membrane protein Atg15/Cvt17 has been identified as an essential phospholipase required for the degradation of lipid vesicles (Maeda et al., 2015; Teter et al., 2001) and the disintegration of autophagic bodies within the yeast vacuole (Epple et al., 2001). This suggests that an enzymatic phospholipase activity could play a part in IAM degradation in mammalian cells.

Inhibition of autophagosome closure in cells depleted of ESCRT-III component CHMP2A results in the fusion of open autophagosomes with lysosomes and misdistribution of the glycosylated lysosomal membrane protein (LAMP1) on the IAM (Takahashi et al., 2018a). This atypical LAMP1 localisation disrupts IAM disintegration and delays the degradation of autophagosomal cargo, potentially due to LAMP1 protecting IAM from lysosomal hydrolases (Takahashi et al., 2018a). Once the content of autolysosome is degraded, autolysosome undergo autophagic lysosome reformation (ALR) and replenish the lysosome pool within the cell (Yim and Mizushima, 2020a).

1.1.4 Autophagy in development

Several studies have shown the importance of autophagy from embryo development to healthy aging and autophagy dysregulation has been connected to a number of diseases (Shintani and Klionsky, 2004). The significance of autophagy in development is represented by studies investigating the effects of autophagy inhibition

in animal models (Mizushima and Levine, 2010). Whole body knockout of *Beclin1* in mice results in embryonic lethality (Yue et al., 2003), similar phenotype is also observed in homozygous, gene-trapped allele mutant of *Ambra1* (Maria Fimia et al., 2007) and *FIP200*-null mice (Gan et al., 2006). Neonatal lethality is observed in mice lacking other autophagy regulators such at *Atg5* (Kuma et al., 2004); *Atg7* (Komatsu et al., 2005); *Atg3* (Sou et al., 2008); *Atg9* (Saitoh et al., 2009); or *ULK1/2* (Cheong et al., 2014). Whereas *GABARAP* or *LC3B* knockout mice do not exhibit a lethal phenotype (Cann et al., 2008; O'Sullivan et al., 2005). Interestingly, targeted reconstitution of autophagy in neurons of *Atg5*-null mice evaded the neonatal lethality and allowed mice to survive beyond the weaning age (Yoshii et al., 2016). This study showed a crucial role of autophagy in the brain and suggested that the neonatal lethality in autophagy deficient mice does not occur only due to nutrient insufficiency and role of autophagy in the development is more complex.

The differences between the knockout phenotypes of different autophagy machinery components in the forementioned studies could be explained in two ways. Firstly, deletion of certain proteins does not completely abolish autophagy and the residual autophagic activity could be sufficient to evade the more severe phenotypes. Secondly, it is possible that the phenotypes seen in these studies are a combination of autophagy inhibition as well as disruption of other, autophagy-independent processes those proteins participate in, such as the role of ATG9a in innate immune responses (Saitoh et al., 2009), or the role of FIP200 in apoptosis (Chen et al., 2016).

1.1.5 Autophagy in aging and Alzheimer's disease

Gradual decline in cell function and increased vulnerability to death are characteristic of aging. Stress response pathways limit tissue damage and promote organismal longevity (López-Otín et al., 2013). One of the main stress response pathways involved in healthy aging is autophagy, due to its role in the removal of potentially cytotoxic material. The decline in autophagic activity is correlated with aging (Aman et al., 2021) and expression of core autophagy regulators *ATG5*, *ATG7* and *BECN1* in human brain decreases with age (Lipinski et al., 2010). It was also reported that the activity of the negative autophagy regulator mTOR is elevated in the brain tissue of aged mice (Ott et al., 2016) and muscle-tissue specific deletion of *Atg7* in

mice results in the decreased lifespan (Carnio et al., 2014). Conversely, upregulation of autophagy has been linked to extended lifespan and improved healthspan. Mice on calorie-restricted diet exhibit an increase in mean and maximum survival times when compared to the control group (Weindruch and Walford, 1982). Similarly, enhancing autophagy by overexpression of *Atg5* or by suppressing interaction between Beclin1 with its negative regulator Bcl-2, extend the lifespan in mice (Fernández et al., 2018; Pyo et al., 2013). Furthermore, similar phenotype has been observed in mice treated with the autophagy inducer and mTOR inhibitor, rapamycin (Harrison et al., 2009). Altogether, these observations suggest that autophagy is a key regulator of aging.

Defective autophagy results in cellular dysfunction and/or cell death, which contribute to pathological aging and neurodegenerative disorders. Most studied neurodegenerative diseases associated with impaired autophagy include Alzheimer's disease, Parkinson's disease, Huntington's disease and amyotrophic lateral sclerosis (ALS) (Aman et al., 2021).

Alzheimer's disease (AD) is the most common cause of dementia and is characterised by accumulation of intracellular neurofibrillary tangles containing hyperphosphorylated tau protein and the deposition of extracellular β-amyloid (Aβ) plaques, pathological features that result in neuronal cell death and cognitive decline (Knopman et al., 2021). Accumulation of autophagic structures within dystrophic axons and dendrites is one of the hallmarks of AD (Nixon and Yang, 2011) and levels of Beclin1 in brains of AD patients are decreased (Pickford et al., 2008). Hyperactivation of autophagy caused by expression of gain-of-function mutant of Beclin1 reduces Aβ accumulation and delays cognitive decline in mice models (Rocchi et al., 2017). Moreover, mitophagy is reduced in the hippocampus of AD patients by 30 to 50 percent compared to healthy individuals and mitophagy induction reverses cognitive deficits in *C. elegans* AD model (Fang et al., 2019). In addition to disrupted autophagy, lysosomal overburden and dysfunction are major contributors to the AD phenotype (Nixon and Yang, 2011). The role of lysosomes in AD is discussed in chapter 1.2.5.

1.1.6 Autophagy in cancer

A role of autophagy in cancer is undisputable, however, whether autophagy is beneficial or detrimental in context of cancer depends on multiple factors, the main being tumour stage. At the early initiation stage, autophagy protects cells from early stages of malignant transformation by preventing the accumulation of cytotoxic material and genetic defects (Galluzzi et al., 2015). In accordance with this, *Beclin1* heterozygote mutant mice exhibit a high incidence of spontaneous tumours (Yue et al., 2003) and monoallelic deficiency in Beclin1 occurs in 75% of ovarian, 50% of breast and 40% of prostate cancers (Cao and Klionsky, 2007). Conversely, one of the observations in the calorie-restricted diet studies in mice was an inhibition of spontaneous lymphoma occurrence (Weindruch and Walford, 1982) suggesting tumour suppressing qualities of autophagy in the initiation of malignancy. Interestingly, in developed tumours, autophagy supports cell growth. Cancer cells are exposed to an increased cellular stress due to high proliferation rates and metabolic demand, as well as a poor vascularisation and reduced oxygen supply (Degenhardt et al., 2006). Cancer cells can depend on autophagy to survive and enhance growth in hostile conditions (Galluzzi et al., 2015) . Additionally, autophagy plays a role in treatment resistance and autophagy inhibition sensitises cancer to therapeutic agents. This tumour promoting qualities of autophagy in cancer progression makes autophagy inhibition an attractive target for cancer therapy (Kondo et al., 2005).

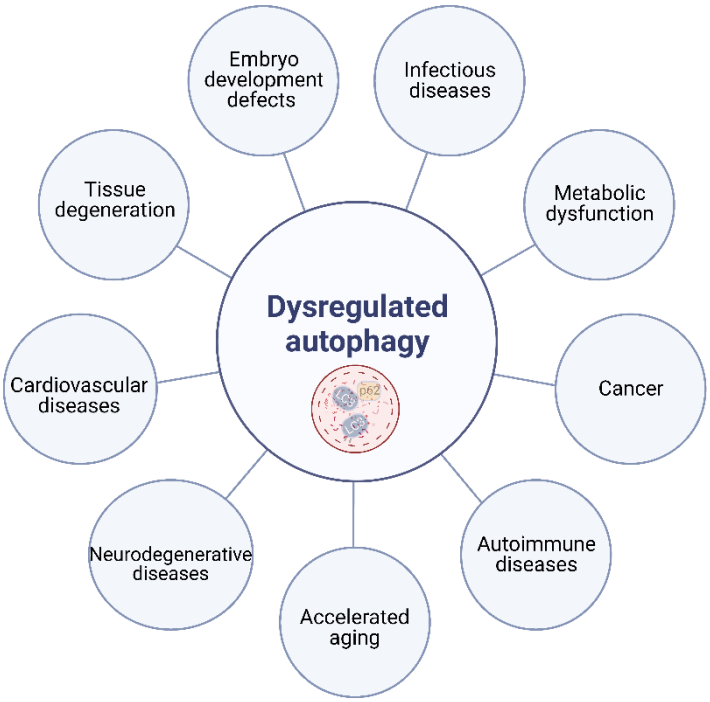

Figure 1.3 Effects of autophagy dysregulation on organismal health.

Consequences of dysregulated autophagy (middle circle) are shown in surrounding smaller circles.

1.2 Lysosomes – an overview

Lysosomes are a relatively small, membrane-limited organelles of approximately 0.3 μm in diameter (Bandyopadhyay et al., 2014). Although modest in size, their activity is crucial to ensure cell health and function. Lysosomes were discovered by Christian de Duve's research group in a series of biochemical experiments, where fractions of cells derived from liver rat tissue were shown to be enriched in hydrolytic enzymes. Enzymatic activity of these fractions was also increased upon treatments causing membrane disruption, which suggested the presence of a membrane-bound organelles containing the enzymes (de Duve et al., 1955). Dense, single-membrane organelles with enzymatic activity were subsequently shown by electron microscopy imaging (Novikoff et al., 1956; Sabatini and Adesnik, 2013). This discovery provided a tremendous insight into cell biology, and lysosome and peroxisome discovery by de Duve granted him a Nobel Prize in Physiology or Medicine in 1974 (Sabatini and Adesnik, 2013).

Although originally regarded solely as an endpoint of autophagy, multiple

studies demonstrated a role of lysosomes in different stages of autophagy. Nutrient sensing qualities of lysosomes regulate autophagy induction by releasing of mTORC1 from the lysosomal membrane (Sancak et al., 2010). Moreover, release of lysosomal calcium to the cytosol induce autophagy by stimulating the nuclear translocation of TFEB and recruiting of PI3P-binding proteins to PAS (Medina et al., 2015; Scotto Rosato et al., 2019). Fusion of autophagosomes with late endosomes or lysosomes is influenced by lysosomal membrane proteins (LMPs) (Huynh et al., 2007; Sarkar et al., 2013), further underscoring the importance of lysosomes in autophagy. In addition to autophagy regulation, lysosomes regulate multiple processes such as metabolic adaptation, cell signalling and secretion (Trivedi et al., 2020). Here, I will discuss lysosomal proteins and the mechanisms governing lysosomal enzymes delivery and function, as well as lysosome related diseases.

1.2.1 V-ATPase proton pump

Lysosomal lumen contains a multitude of degradative enzymes making lysosomes the main cellular compartment responsible for the digestion of extra- and intra-cellular material (figure 1.3) (Piao and Amaravadi, 2016). This activity of lysosomes explains their name which is a combination of the Greek words *Lysis* (meaning loosen/destroy/dissolve) and *Soma* (meaning body) and can be translated into lytic body (Piao and Amaravadi, 2016). The key characteristic of lysosomes is their low pH (between 4.5 and 5.0) which distinguishes lysosomes from other endocytic vesicles (Li et al., 2019). This acidic pH is crucial for the optimal activity of lysosomal enzymes. Lysosomes located at the cell periphery are relatively less acidic and the pH of the lysosomal lumen decreases when they migrate towards the perinuclear region, which could be one of the ways cells control lysosomal activity (Johnson et al., 2016). This retrograde movement of the lysosomes also facilitates efficient autophagic flux and was observed upon nutrient depletion (Korolchuk et al., 2011). The pH-dependent activity of lysosomal hydrolases could also be a protective mechanism against uncontrolled degradation of cellular content upon lysosomal damage and enzyme leakage to the cytosol (Wang et al., 2018).

Lysosomes maintain acidic pH by the activity of a multi-subunit vacuolar-type ATPase (V-ATPase) proton pump. V-ATPases are ATP-dependent proton pumps

operating by a rotary motion driven, unidirectional translocation of protons across membranes (Imamura et al., 2003; Ohkuma and Poole, 1978). In mammalian cells, V-ATPase complex subunits can be divided into two domains: V_0 comprised of eight subunits (a1, c, c″, d1, e1, f, ATP6AP1 and ATP6AP2) and V_1 comprised of eight subunits (A, B2, C1, D, E1, F, G1 and H) (Wang et al., 2020). The V_0 domain is responsible for the transport of protons from the cytosol into the lysosomal lumen, whereas V_1 domain hydrolyses ATP to provide energy required for the rotation of the complex. The proton pump activity of the complex is negatively regulated by the separation of the V_1 domain from the membrane-embedded V_0 domain (Oot et al., 2017). Interestingly, recent studies showed that mTOR regulates V-ATPase complex assembly and when active, blocks the recruitment of V_1 domain to the lysosomal membrane (Ratto et al., 2022).

During autophagy, lysosomal activity is crucial for IAM degradation and subsequent digestion of autophagosome cargo. The V-ATPase pump inhibitor Bafilomycin A1 (Baf A1) binds to the proteolipid ring of the V_0 domain of the complex inhibiting proton translocation (Bowman and Bowman, 2002). Baf A1 treatment leads to an increase in the lysosomal pH and disruption of lysosomal degradative activities, which was shown to cause the accumulation of lysosomal cargo (Yoshimori et al., 1991). In some cases, Baf A1 treatment can also lead to a disruption of autophagosome-lysosome fusion however, this phenotype is not a result of Baf A1-induced alkylation of lysosomes (Mauvezin et al., 2015). Due to the inhibition of autophagic cargo degradation and ATG8-II accumulation in Baf A1 treated cells, this inhibitor is widely used as a control to measure autophagic activity in cells (Yoshii and Mizushima, 2017).

1.2.2 Lysosomal membrane proteins

In addition to the V-ATPase complex, lysosomal membrane contains over 700 LMPs (figure 1.3) (Rudnik and Damme, 2021). Although the functions of many of these proteins are not clearly understood, multiple disorders are connected to LMP dysfunction (table 1.1), highlighting the role of lysosomal membrane integrity in cell homeostasis (Platt et al., 2018).

Disease name	Accumulated substrate	Affected lysosomal protein	Reference
Gaucher disease (types I, II, III)	Glucosylceramide	Glucosylceramidase	(Brady et al., 1965)
Fabry disease	Globotriasylceramide	α-Galactosidase	(Sweeey and Klionsky, 1963)
Pompe disease	Glycogen	Acid maltase	(Hers et al., 1963)
Niemann-Pick (type A, B)	Sphingomyelin	Acid sphingomyelinase	(Brady et al., 1966)
Niemann-Pick (type C)	Cholesterol, glycosphingolipids	NPC1, NPC2	(Crocker, 1961)
Farber disease	Ceramide	Acid ceramidase	(Ehlert et al., 2007)
Wolman disease	Cholesterol esters	Lysosomal acid lipase	(Maehira et al., 1984)
Danon disease	Glycogen	LAMP2	(Danon et al., 1981)
Tay-Sachs disease	GM2, ganglioside, glycolipids	β-Hexosaminidase A	(Mahuran, 1999)
Juvenile Batten disease	Ceroid lipofuscin	Cathepsin D, CLN3	(Koike et al., 2000)

Table 1.1 A list of selected Lysosomal storage disorders (LSDs).

Affected enzymes and substrates accumulating in the lysosomes are shown in the selected LDSs. The disease relevance of selected LDSs will be discusses in later chapters.

Lysosomes have a low pH and reducing conditions. They also contain a high concentration of degradative enzymes which could potentially digest the lysosomal membrane. To protect lysosomes, the luminal side of the lysosomal membrane contains many glycosylated proteins forming a ‘glycocalyx’-like surface coat (Rudnik and Damme, 2021). The most abundant and highly glycosylated LMPs are the lysosomal associated membrane proteins (LAMPs). LAMP1 and LAMP2 account for 50% of all LMPs and are widely used to identify lysosomes (Cook et al., 2004;

Eskelinen, 2006). These transmembrane proteins contain heavily N-glycosylated luminal part and short cytosolic C-terminal tail and display 37% sequence identity (Tanaka et al., 2000). Depletion of LAMP1 leads to increased expression of LAMP2 suggesting a potential overlap in protein function (Andrejewski et al., 1999). LAMP1 and LAMP2 double knockout mice are embryonically lethal (Eskelinen et al., 2004). However, it was reported that LAMP1 knockout mice exhibit milder phenotypes than LAMP2 deletion, which suggests that although some functions of LAMP1 and LAMP2 overlap, they also play independent roles in cells (Andrejewski et al., 1999). For an example, LAMP2a but not LAMP1, is required for CMA (Kaushik et al., 2006). Additionally loss-of-function mutations of LAMP2, but not LAMP1, are associated with the glycogen storage disorder, Danon disease (table 1.1) (Yang et al., 2010). LAMPs also have glycocalyx-independent functions such as lysosomal cholesterol export (Li and Pfeffer, 2016). They also control lysosomal movement from the cell periphery through dynein-mediated transport along microtubules (Huynh et al., 2007). Altogether, these published findings highlight the crucial roles of LAMPs in proper lysosomal function.

Ion channels regulate ionic gradient by transporting cations across the lysosomal membrane in a uni- or bi-directional manner. Ion channels can be grouped into chloride channels, potassium channels and non selective cation channels (Trivedi et al., 2020). Non-selective cation channels include Transient Receptor Potential Cation Channel 1 (TRPML1), two-pore channels (TPCs) and P2X4 channel, where TRMPL1 being the most studied lysosomal cation channel. TRMPL1 is permeable to Ca^{2+}, Na^{+}, K^{+}, Zn^{2+} and Fe^{2+} (Staudt et al., 2016) and has been shown to regulate lysosomal size and exocytosis by lysosomal Ca^{2+} release (Cao et al., 2017; Samie et al., 2013). TRMPL1 also regulates retrograde migration of lysosomes (Li et al., 2016). Moreover, TRMPL1-mediated Ca^{2+} release from the lysosomes activates calcinurin and inhibits autophagy (Medina et al., 2015). Loss-of-function mutations of TRPML1 cause type IV mucolipidosis (table 1.1) (Sun et al., 2000). Moreover, TRMPL1 depletion leads to the accumulation of Zn^{2+} and Fe^{2+}, confirming the role of TRMPL1 in release of heavy metals from lysosomes (Dong et al., 2008).

Although several lysosomal exporters have been identified, proteins governing efflux of lysosomal macromolecules to cytoplasm are poorly characterised. A small number of amino acid exporters have been identified thus far. These include,

Cystinosin for cysteine export, PQLC2 for arginine and lysine export, and SLC38A9 and SLC36A1 responsible for export of multiple amino acids, such as glutamine, arginine, histidine and lysine (Wang et al., 2021a; Xu and Ren, 2015). Amino acid release from the lysosome post autolysosome degradation is a crucial step for maintaining their intracellular levels and regulating autophagic activity (Dossou and Basu, 2019). Only two lipid exporters have been identified. Niemann-Pick disease, type C1 (NPC1), together with NPC2, release cholesterol from the lysosomes (Infante et al., 2008). Blocking NPC1-mediated cholesterol release was shown to inhibit amphisome formation (Sarkar et al., 2013). Moreover, NPC1 dysfunction leads to Niemann-Pick (type C) disorder (table 1.1).

1.2.3 Cathepsin proteases

Cathepsins are the most abundant proteases in the lysosomal lumen. According to their catalytic activity, cathepsins are classified into three groups: serine proteases (cathepsins A and G), aspartic acid proteases (cathepsin D and E) and cysteine proteases (cathepsins B, C, F, H, K, L, O, S, V, X, and W). The main role of cathepsins in lysosomes is the digestion of proteins delivered to the lysosomal lumen. Moreover, cathepsins activate multiple lysosomal proteins ensuring their optimal function. (Yadati et al., 2020). Although cathepsin activity is highest in acidic pH, several cathepsins are also active in alkaline conditions (Yadati et al., 2020). Cathepsins are synthesised as inactive pre-pro-enzymes, which limits uncontrolled protease activity within cells. Pre-pro-enzyme is cleaved to the pro-form in the ER lumen and once delivered to acidic environment, the pro-enzyme is cleaved again to become fully active (Turk et al., 2012). Some cathepsins can undergo auto-activation, where the same class of cathepsin cleaves the inactive pro-version of the enzyme, but this activation sometimes requires the activity of other cathepsin groups (Laurent-Matha et al., 2006; Pungercar et al., 2009). Some lysosomal hydrolases, such as lipases or nucleases do not harbour any proteolytic activity and rely on cathepsins for their cleavage and maturation (Gonzalez et al., 2018a). The wide range of proteolytic activity in a spectrum of pH highlights not only cathepsins versatility but also the importance lysosomal membrane integrity to contain the proteolytic activity. Indeed, leakage of Cathepsin D from lysosomes to the cytoplasm triggers cell death (Di et al., 2021). Moreover, cathepsin dysfunction has been associated with multiple disorders

(table 1.1).

1.2.4 Lysosomal lipases

Lipases are also found within lysosomes and are responsible for the digestion of a range of lipid substrates to maintain cell metabolism and signalling. Lysosomal/vacuolar lipase involved in autophagy has been characterised in yeast. Atg15/Cvt17 was shown to have a phospholipase activity crucial for the degradation of IAM within the vacuole (the yeast degradative compartment equivalent to mammalian lysosomes) (Teter et al., 2001). Moreover, Atg15 is required for the degradation of lipid droplets targeted to the vacuole via microautophagy (van Zutphen et al., 2014). Other vacuolar lipases are yet to be discovered in yeast. In mammalian cells, lysosomal acid lipase (LIPA) is the most studied lysosomal hydrolase due to its association with Wolman disease. In addition to LIPA, multiple phospholipases have been identified thus far, including phospholipase D3 (PLD3). In this section, I will focus on discussing LIPA and PLD3 because of their significance in disease and a potential role in autophagy. These two enzymes are also relevant to my PhD project.

LIPA is responsible for the digestion of cholesteryl esters and triglycerides to free cholesterol and fatty acids, respectively (Li and Zhang, 2019). To be activated, LIPA requires to undergo proteolytic processing. Purification of human LIPA showed two variants of the proteins of 56 kDa and 41 kDa corresponding to pro-enzyme and mature enzyme, respectively (Ameis et al., 1994). Although the enzymatic activity of LIPA has been reported, the catalytic site remains unknown. LIPA is the only identified lysosomal enzyme responsible for cholesteryl ester digestion and it plays a crucial role in lipid metabolism by removing excess of cholesterol from cells (Li and Zhang, 2019). LIPA activity indirectly regulates autophagy as abnormal accumulation of cholesterol in lysosomes leads to the inhibition of fusion events between autophagosomes and late endosomes (Sarkar et al., 2013). Moreover, expression of this enzyme is induced upon nutrient starvation, presumably to facilitate lipid droplet degradation via lipophagy (Lettieri Barbato et al., 2013). Additionally, LIPA is upregulated during macrophage differentiation in order to accommodate augmented lysosomal degradation activities within macrophages (Ries et al., 1998). Low activity of LIPA has been observed in non-alcoholic fatty liver disease (Gomaraschi et al., 2019) and complete loss of

function leads to Wolman disease, a lysosomal storage disorder which results in premature death due to malnutrition and liver failure (table 1.1) (Li and Zhang, 2019).

PLD3 is a member or phospholipase D (PLD) protein family (Selvy et al., 2011). PLD enzymes digest phosphatidylcholine to phosphatidic acid and choline and their activity is necessary for membrane dynamics (Brown et al., 2017). This subset of enzymes share a conserved HxKxxxxD (HKD) motif responsible for catalytic activity. PLD3 was identified as a member of the PLD family based on the presence of two HKD motifs located within the middle and the C-terminal end of the protein (Pedersen et al., 1998). The C-terminal HKD domain within PLD3 contains an glutamate residue instead of an aspartate, although the significant of this substitution is unclear (Pedersen et al., 1998). PLD3 has been also attributed an exonuclease activity, which was shown to regulate endosomal nucleic acid sensing (Gavin et al., 2018). Confirming the phospholipase activity of PLD3 has been challenging due to the lack of accurate tools to measure lysosomal phospholipase activity in cell culture and due to low expression levels of PLD3 in most cell types. Expression of PLD3 is however greater in neuronal cells (Pedersen et al., 1998). Although reports on the phospholipase activity of PLD3 had been conflicting, several recent studies confirmed this activity in neuroblastoma cell line (Gonzalez et al., 2018b; Nackenoff et al., 2021; Nibbeling et al., 2017). Initially, PLD3 was thought to be an ER protein and sorting defects in PLD3 mutants result in accumulation of the protein on the ER and inhibition of the nuclease function (Gonzalez et al., 2018b). However, endogenous PLD3 in human neurons was shown to colocalise with LAMP1 and cathepsins B and D (Nackenoff et al., 2021). Moreover, inhibition of PLD3 trafficking or processing leads to changes in lysosomal morphology (Gonzalez et al., 2018a).

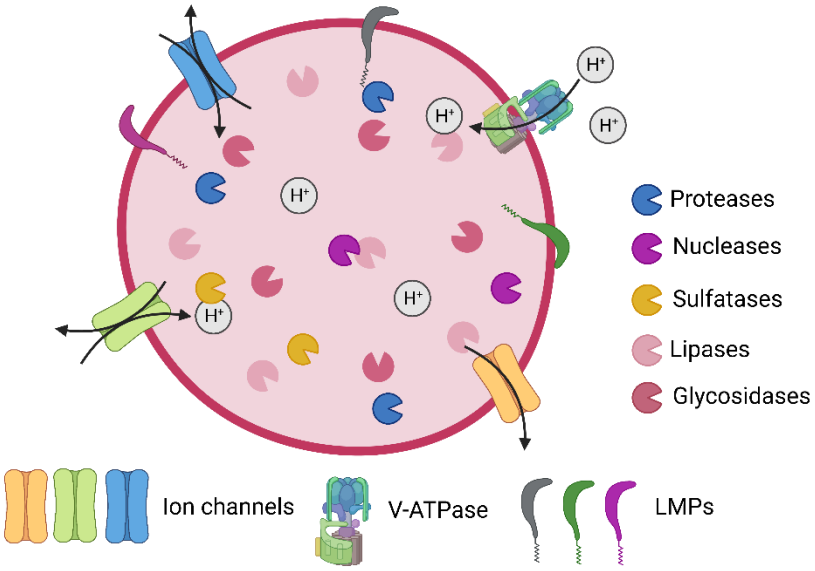

Figure 1.4 Proteins regulating lysosomal homeostasis.

The lysosomal lumen contains multiple groups of hydrolases including proteases, nucleases, sulfatases, lipases and glycosidases. Lysosomal membrane contains LMPs, V-ATPase proton pumps and selective and non-selective ion channels.

1.2.5 Lysosomal enzymes trafficking

The degradative function of lysosomes depends on efficient trafficking and activation of lysosomal enzymes (figure 1.4). Lysosomal hydrolase precursors are synthesised in the ER and targeted to the Golgi apparatus. While passing through the trans-Golgi network (TGN), the N-linked oligosaccharidic chains of the enzymes are tagged with a mannose 6-phosphate (Man-6-P) residues (Brown et al., 1986). This residue is then recognised by two type transmembrane receptors: the cation-dependent (CD) and the cation-independent (CI) Man-6-P receptors (MPRs) (Dahms et al., 1987; Hoflack and Kornfeld, 1985). Binding of the receptors to the tagged hydrolases is crucial for the export from TGN. MPRs contain cytosolic YXXF and [D/E]XXXL[L/I] signals recognised by adaptor protein complexes (APs) (Höning et al., 1997). This recognition of tyrosine- and dileucine-based motifs of MPR-bound enzymes by APs results in their packaging into clathrin-coated vesicles (CCVs) which are then transported from TGN. CCVs can be targeted into late endosomes directly or via early endosomes (Staudt et al., 2016). Moreover, CI-MPR can mediate transport

of hydrolases from the plasma membrane, which plays a role in lysosomal delivery of secreted hydrolases (Jadot et al., 1992). The acidic lumen of endocytic compartments facilitates the uncoupling of MPRs from their cargos, which allows enzyme migration towards lysosomes (Olson et al., 2008). Once uncoupled, the receptors are recycled back to TGN in a manner regulated by the retromer complex. The retromer complex consists of sorting nexins 1 and 2 (SNX1 and SNX2, respectively), VPS35, VPS29 and VPS26 (Haft et al., 1998, 2000) and is stabilised by RAB7 (Rojas et al., 2008). Disruptions in either retromer assembly or function lead to insufficient lysosomal enzyme delivery and accumulation of undigested cargo within the lysosomal lumen (Rojas et al., 2008). Interestingly, ATG9 also plays a role in MPRs trafficking and ATG9-depleted cells show disruption in the trafficking and maturation of several cathepsins (Jia et al., 2017). Mutations in enzymes involved in Man-6-P synthesis have been also associated with the missorting of lysosomal enzymes and mucolipidosis type II and III (table 1.1) (Tiede et al., 2005; Velho et al., 2019), In addition to the canonical MPR-dependent trafficking of lysosomal enzymes, alternative pathways also exist. This was initially observed when CI- and CD-knockout where mice exhibited cell-type specific, residual delivery of lysosomal enzymes (Qian et al., 2008). Since this discovery, multiple additional receptors and delivery pathways have been reported (Staudt et al., 2016).

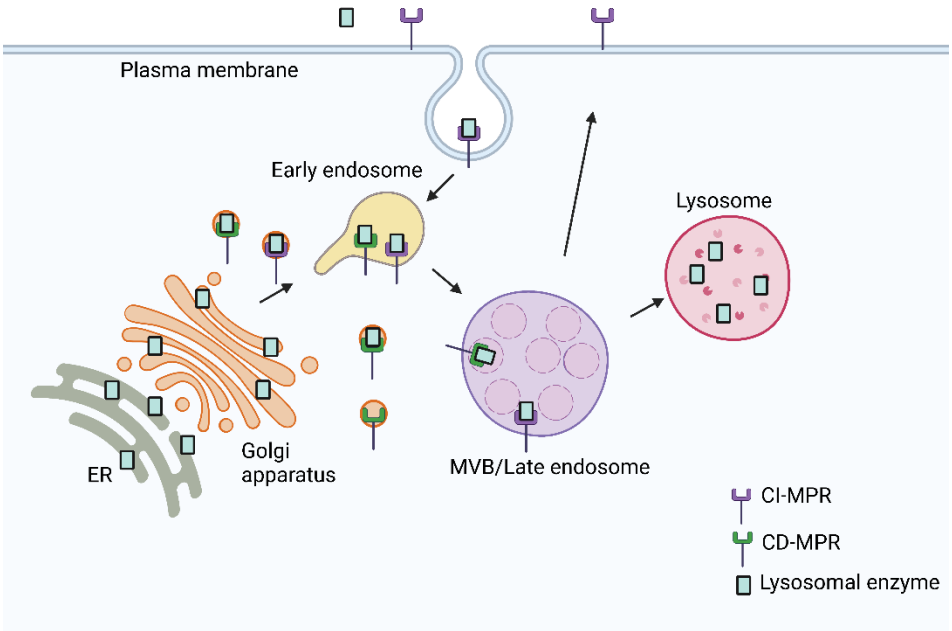

Figure 1.5 Schematic diagram of canonical trafficking of lysosomal hydrolases.
The pathway begins with delivery of enzymes from the ER to the Golgi apparatus. Enzymes are then tagged with Man-6-P, which is recognised by either CD-MPR and CI-MPR. MPR-bound hydrolases are delivered to late endosomes directly or via early endosomes and released from the receptors to allow their maturation. Receptors are then recycled and transported back to the Golgi apparatus or plasma membrane.

PLD3 lysosomal delivery

PLD3 is a transmembrane protein which potentially contributes to its MPR-independent lysosomal delivery pathway (figure 1.5) (Gonzalez et al., 2018a). PLD3 is glycosylated in the Golgi apparatus. Disruption of PLD3 glycosylation results in its abnormal cellular localisation and the accumulation of enlarged lysosomes (Demirev et al., 2019). Inactive full length PLD3 was detected in early endosomes suggesting its potential trafficking via early endosomes (Gonzalez et al., 2018a). Subsequently, PLD3 is delivered to multivesicular bodies (MVBs) and sorted into intraluminal vesicles (ILV) within MVBs. The delivery from early endosomes to MVBs is dependent on the presence of PI3P on endosomal membranes and is disrupted when the activity of PI3KC3 complex is inhibited (Gonzalez et al., 2018a). PLD3 was shown to be ubiquitinated at the N-terminus and is recognised by the ESCRT complex, which leads to sorting of the enzyme into ILVs. ESCRT complexes and VPS4a activity are crucial for proper packaging of PLD3 into ILVs and overexpression of a dominant negative

mutant of VPS4a disrupts proper processing of PLD3 (Gonzalez et al., 2018a). Once PLD3 is exposed to the acidic lumen in late endosomal compartments, it is then proteolytically cleaved by cysteine proteases resulting in the separation of the N-terminal transmembrane domain from the remainder of the proteins containing the HKD domains. The stable luminal enzyme is then delivered to the lysosomal lumen, whereas the N-terminal fragment is degraded by cathepsins B and L (Gonzalez et al., 2018a). Disruption is PLD3 processing is associated with AD (Demirev et al., 2019) and will be discussed in the chapter 1.2.5.

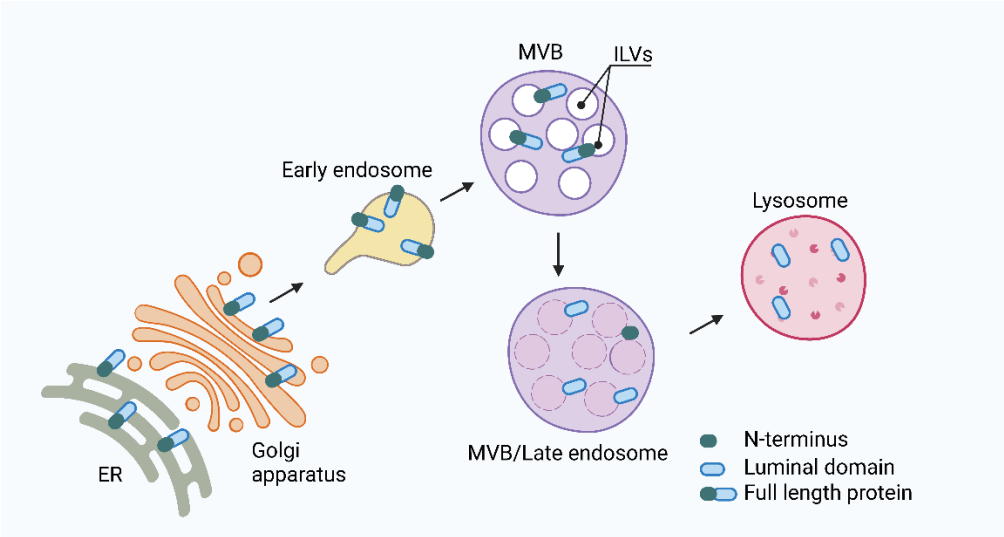

Figure 1.6 Schematic diagram of PLD3 trafficking to lysosomes.

The pathway begins with the delivery of enzymes from the ER to the Golgi apparatus where PLD3 is glycosylated. PLD3 is then delivered to MVBs via early endosomes and sorted into ILVs. Upon ILV degradation, the full length protein is cleaved and the N-terminal is degraded. The remaining luminal fragment (harbouring the catalytic HKD domains) is then delivered to lysosomes.

1.2.6 Lysosomal storage disorders

Mutations in proteins associated with lysosomes can lead to a gradual build-up of substrates within the lysosomal lumen (Platt et al., 2018). This abnormal substrate accumulation within lysosomes can cause cellular damage, which with time leads to cell death and subsequent tissue degeneration. A broad term for diseases caused by such lysosomal metabolism dysfunction is lysosomal storage disease (LSD) (Parenti et al., 2021). Liver is one organ that is susceptible to lysosomal dysfunction. For an

example, low levels of glucocerebrosidase enzyme is associated with Gaucher disease type I (table 1.1) (Platt et al., 2018). This tissue specific degeneration can affect organismal health and in many cases lead to premature death (Parenti et al., 2021). Although 70 LSDs have been reported thus far (Platt et al., 2018), most of them lack an effective treatment. In cases of diseases caused by defective lysosomal hydrolases, enzyme replacement therapy could potentially rescue the disease phenotype. However, enzyme replacement therapy has only been approved for a fraction of LSDs (Ohashi, 2012). LSDs are characterised by lysosomal proteins with reduced or completely abrogated function and the accumulated substrates. Selected LSDs are described in table 1.1.

1.2.7 Lysosomal dysfunction and neurodegeneration

In addition to a plethora of LSDs, dysfunctional lysosomes have been associated with multiple diseases such as cancer, autoimmune disorders and neurodegenerative diseases (Cao et al., 2021). Multiple studies have shown connections between impaired lysosomal function and AD. Loss of lysosomal acidity associated with aging is considered a catalyst of AD (Nixon, 2020). In patients with Down Syndrome (DS) who are prevalent to developing AD, oxidative damage of V_0 domain of lysosomal V-ATPase proton pump was observed prior to AD neuropathology development (Di Domenico et al., 2013). Moreover, pathogenic processing of amyloid precursor protein (APP) (figure 1.7) can disrupt lysosomal acidification by inhibition of V-ATPase proton pump assembly in DS patients (Im et al., 2022). Mouse models of AD confirm this phenotype and show decline in lysosome acidification of neurons prior Aβ plaques deposition (Lee et al., 2022). In addition to acidification defects, mutations in retromer complex also have been associated with AD. Hippocampal dysfunction and Aβ accumulation was observed in VPS26 knockout mice or VPS35 neuronal-selective knockout mice, recapitulating features of AD (Muhammad et al., 2008; Qureshi et al., 2022). AD has also been associated with defects of the lysosomal hydrolase PLD3. Patients bearing mutant of PLD3 ($PLD3^{VM}$) are more likely to suffer from late-onset AD (Cruchaga et al., 2014). Expression $PLD3^{VM}$ leads to enlarged lysosomes and Aβ accumulation in flies (Demirev et al., 2019). Interestingly, this mutation is located close to the HKD motif, suggesting that phospholipase activity of PLD3 might be disrupted. Alternatively, the phenotype seen

in PLD3^{VM} could also be a result of improper processing and trafficking of PLD3 (Cruchaga et al., 2014; Demirev et al., 2019). Depletion of PLD3 leads to increased amyloidogenic processing of APP and elevated extracellular Aβ levels (Cruchaga et al., 2014; Mukadam et al., 2018). Moreover, mRNA levels of *PLD3* are reduced in the brains of AD patients (Satoh et al., 2014). Interestingly, PLD3 can also accumulate on extracellular Aβ plaques in AD brains suggesting potential defects in its trafficking (Satoh et al., 2014). As opposed to neuroprotective role of PLD3 in brain, increased cathepsin D activity is correlated with AD (Schwagerl et al., 1995). Studies have shown that cathepsin D activity leads to the formation of hyperphosphorylated tau fragments observed in AD (Bi et al., 2000). However, this increased activity of cathepsin D in AD could also be a compensatory mechanism to degrade substrates accumulating in neurons (Perez et al., 2015) and therefore requires to be further investigated. Altogether, these studies show a crucial role of lysosomes in AD development and progression.

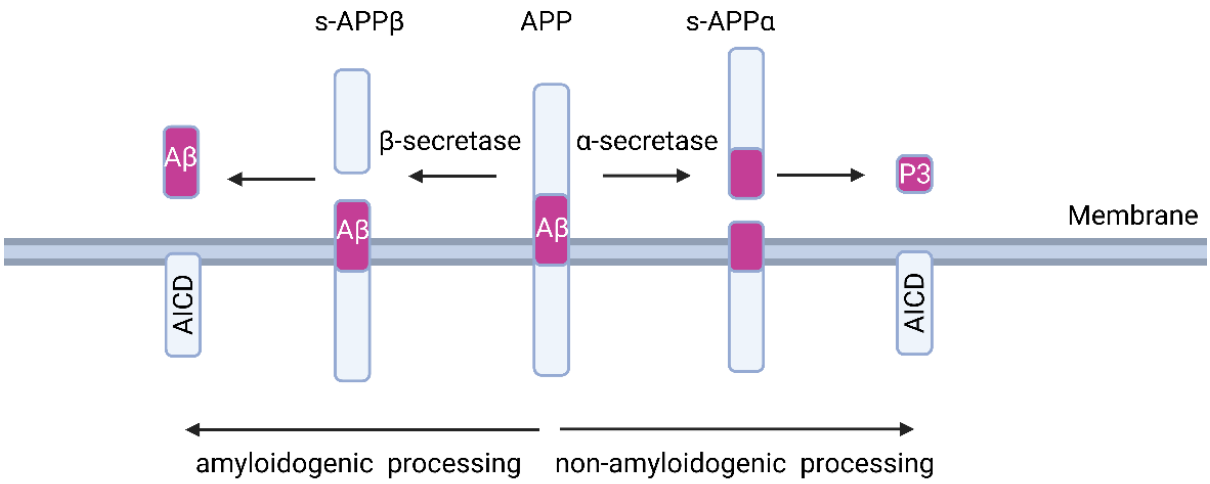

Figure 1.7 A diagram depicting APP processing pathway.

The transmembrane protein APP can be processed in nonamyloidogenic and amyloidogenic pathways. In the nonamyloidogenic pathway, APP is cleaved to form a soluble APP fragment α (sAPP-α). The APP C-terminal fragment is then cleaved to release the APP intracellular domain (AICD) and P3 fragment. In the amyloidogenic pathway, cleavage of APP to produce the soluble APP fragment β (sAPP-β) which is then produce pathogenic Aβ and AICD.

1.3 RNAseK – an overview

RNase kappa (RNAseK) is a small protein consisting of two transmembrane domains with the N- and C-termini of the protein predicted to face the cytoplasm (figure 1.8) (Perreira et al., 2015). The protein was in initially described as an endoribonuclease with an ability to hydrolyse ApU, ApG and UpU bonds *in vitro* (Economopoulou et al., 2007; Kiritsi et al., 2012). This enzymatic activity of RNAseK has not been further validated in cells as structural data suggest that it involves residues embedded within the transmembrane region (figure 1.8) (Kiritsi et al., 2012). Recent studies indicate that RNAseK is a mammalian homologue of the *S. cerevisiae* rotary subunit f in the V-ATPase proton pump (Vma7) (Abbas et al., 2020). RNAseK and Vma7 display 32% sequence identity and 52% sequence similarity. Structural analyses of mammalian brain V-ATPase revealed RNAseK positioning in the f subunit of the pump V_0 region (Abbas et al., 2020).

RNAseK has been identified as a crucial factor for viral entry via endocytosis (Carro and Cherry, 2020; Hackett et al., 2015; Perreira et al., 2015). Depletion of RNAseK does not disrupt binding of viruses to the cell surface receptors but abrogates their internalisation via clathrin-mediated endocytosis (CME) and non-CME (Perreira et al., 2015). Lymphocyte antigen 6 locus E (LY6E) mediates uptake of multiple flaviviruses via CME (Hackett and Cherry, 2018). Depletion of RNAseK abrogates LY6E tabularisation inhibiting the virus internalisation (Hackett and Cherry, 2018). Although initially reported as an essential factor for CME, subsequent analyses have shown that RNAseK is dispensable for the uptake of transferrin and dextran by CME and micropinocytosis, respectively (Hackett et al., 2015; Perreira et al., 2015). Interestingly, coupling of transferrin to beads 40 nm in diameter disrupted its uptake in RNAseK depleted cells (Hackett and Cherry, 2018). On the other hand, RNAseK was not required for the uptake of transferrin coupled to 20 nm beads suggesting that its role in the endocytic uptake depends on the size of the cargo (Hackett and Cherry, 2018). In addition to its role in virus uptake, RNAseK was shown to be a positive regulator of type I interferon secretion and apoptosis (Sun et al., 2021). Moreover, increased *RNAseK* expression has been observed in certain cancers. Upregulation of *RNAseK* positively correlated with the differentiation of osteoclast precursors and enhanced breast cancer to bone metastasis (Yue et al., 2022). Similarly, upregulation

of RNAseK was observed in glioblastoma multiforme (GBM) tumour tissues and correlated with resistance to temozolomide, the most commonly used chemotherapeutic drug in GBM treatment (Hsu et al., 2021). Although progress has been made in determining the function of RNAseK in cell homeostasis, its detailed role and regulatory network remain unclear. In addition, despite the involvement of RNAseK in endocytosis, its involvement in autophagy has not been previously studied.

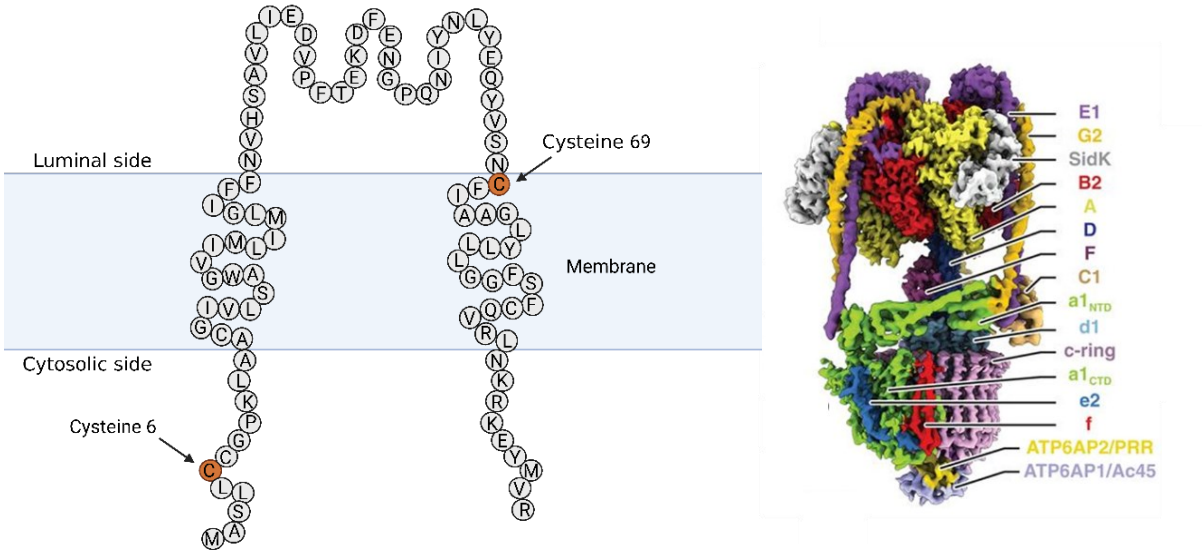

Figure 1.8 Schematic diagram of RNAseK.

Left: *transmembrane regions and membrane adjacent fragments of RNAseK protein. Cysteine 6 and cysteine 69 required for the putative RNAse activity in vitro are highlighted in orange.* ***Right:*** *Composite cryo-EM model (right) of brain V-ATPase in rotational state. RNAseK (subunit f) is represented in red in the lower part of the complex. Image taken from Abbas et al., 2020.*

1.4 Conjugation of ATG8s to Single Membranes

ATG8 lipidation was initially only associated with the biogenesis of a double-membraned autophagosomes (described in previous chapters). However, numerous studies have shown that ATG8 lipidation can also occur on single membranes. This non-canonical form of autophagy was recently coined as Conjugation of ATG8s to Single Membranes (CASM) (Durgan et al., 2021). CASM plays role in immunity, cancer and neurodegeneration (Durgan and Florey, 2023). CASM processes include: LC3-associated phagocytosis (LAP) (Sanjuan et al., 2007); LAP-like processes

(Florey et al., 2011a; Jacquin et al., 2017); LC3-associated endocytosis (LANDO) (Heckmann et al., 2019); and LC3-dependent extracellular vesicle loading and secretion (LDELS) (Leidal et al., 2020). Interestingly, ATG8 can be conjugated to both PE and phosphatidylserine (PS) during CASM, whereas in autophagy its conjugation is exclusively to PE (Durgan et al., 2021). Therefore, ATG8-PS conjugate is a potential "molecular signature" for CASM (Durgan and Florey, 2023).

Although autophagy and CASM share multiple regulators, the required molecular machinery varies (Table 1.2). This could be because autophagy requires the *de novo* formation of phagophores, whereas CASM relies on pre-formed membranes where for lipidation to take place. The difference in the molecular machinery required for CASM or autophagy can be utilised to distinguish the induction of either pathway during ATG8 lipidation. For instance, the ULK complex (including ULK1/2, ATG13, and FIP200) and ATG14L1 are dispensable for CASM (Florey et al., 2011b; Martinez et al., 2015). On the other hand, the lipidation machinery (including ATG3, ATG7, ATG5, ATG12 and ATG16L1) is crucial for both autophagy and CASM (Florey et al., 2011b; Martinez et al., 2015). Interestingly, despite the requirement of ATG16L1 for both CASM and autophagy, the C-terminal WD40 domains of ATG16L1 are essential for CASM but not autophagy (Fletcher et al., 2018). Mutating key residues within the WD40 domains or deleting the entire WD40 domains of ATG16L1 allow the study of CASM without disrupting autophagy (Fletcher et al., 2018; Rai et al., 2019).

Ionophores and lysosomotropic drugs such as monensin and chloroquine (CQ), respectively, can induce LAP-like CASM processes (Jacquin et al., 2017). These agents change the endosomal ion balance and raise the pH. On the contrary, Baf A1 treatment, which also raises endosomal pH, inhibits CASM (Florey et al., 2015; Jacquin et al., 2017). These observations suggested that CASM inhibition by Baf A1 is independent of the changes in pH and V-ATPase proton pumping function. Indeed, recent studies showed that the association between V_0 and V_1 domain of V-ATPase complex, rather than acidification status, is required for CASM activation (Hooper et al., 2022). The assembled V-ATPase complex binds to WD40 domain of ATG16L1 which specifies the lipidation site on the single membrane compartments (Hooper et al., 2022). Although multiple factors regulating CASM have been discovered, the full regulatory network is yet to be characterised.

Protein/complex	Autophagy	CASM	Reference
ULK1 complex	✓	X	(Florey et al., 2011a)
Rubicon	X	✓	(Martinez et al., 2015)
WIPI2	✓	X	(Martinez et al., 2015)
ATG7, ATG3, ATG5-ATG12	✓	✓	(Martinez et al., 2015)
ATG9	✓	X	(Kageyama et al., 2011)
ATG16L1 WD40 domain	X	✓	(Fletcher et al., 2018)

Table 1.2 Comparison of autophagy proteins needed for autophagy and CASM.

The ✓ symbol means that the complex/protein/protein fragment is needed for the process, whereas X indicate dispensable factors.

1.5 Investigating mechanisms of autophagy regulation

Since the initial discovery of the core ATG proteins, a plethora of regulators has been identified (Glick et al., 2010). Nevertheless, not all mechanisms governing efficient autophagic flux are known. This includes recruitment and release of ATG proteins to and from autophagic membranes or proteins involved in different stages of autophagy such IAM degradation. Due to autophagy being a complex and dynamic process comprising of multiple finely orchestrated steps, it is challenging to define all of the proteins directly or indirectly involved in the pathway. The role of autophagy in maintaining cell health and its dysregulation in disease underscores the importance of understanding its regulatory network in order to identify ways to therapeutically modulate it (Shintani and Klionsky, 2004). Furthermore, FDA approved drugs used to regulate autophagy (for an example those used in cancer treatment) are unspecific and toxic (Mohsen et al., 2022). This suggests the need to identify new autophagy regulators in order to find more specific targets to modulate autophagy during therapy. In the next chapters, I will discuss two screens I have performed prior to the start of my PhD that were used as bases of my PhD thesis. These screens, genome-wide knockout screen and proximity labelling approach, were aimed to give an insight into the autophagy regulatory network.

Assays to monitor autophagy

A number of methods have been developed to monitor autophagic flux in a cell population that can be used to test the modulation of autophagy by genetic or pharmacological approaches (Yoshii and Mizushima, 2017). Here, I will discuss selected assays based on the dynamics of the ATG8 protein, LC3B, during autophagy. As previously mentioned LC3-I is conjugated to PE during autophagy to form LC3-II (Kabeya, 2000). This conjugation results in a faster migration of LC3-II, compared to unconjugated LC3-I, on a SDS-PAGE gel (Yoshii and Mizushima, 2017). The induction of an autophagic flux results in LC3 lipidation and degradation by lysosomal hydrolases (Runwal et al., 2019). Accumulation of LC3-I or LC3-II under conditions that stimulate autophagy (e.g. amino acid starvation) would suggest a block in autophagy either prior to or post LC3 lipidation, respectively. For instance, the build-up of LC3-I is observed in cells treated with VPS34 inhibitors and LC3-II accumulation is observed during Baf A1 treatment (Fedele and Proud, 2020; Ronan et al., 2014). These phenotypes can also be replicated upon genetic depletion of essential autophagy proteins (such as ATG7 and ATG2). Degradation of autophagy cargo receptors (such as p62) can also be used to monitor autophagy (Yoshii and Mizushima, 2017). Both LC3B and p62 are commonly used autophagy markers and can be investigated by western blotting (to assess levels and migration), fluorescent microscopy (to assess their subcellular localisation), and FACS analyses (to quantify their levels) (Ueno and Komatsu, 2020).

Targeting of fluorescent reporters to the lysosome for degradation is useful to measure autophagy in cells. LC3 N-terminally tagged with Green Fluorescent Protein (GFP) only, or together with Red Fluorescent Protein (RFP), is targeted to lysosomes for degradation when autophagy is induced. Upon delivery to lysosomes and IAM degradation, exposure to the acidic environment of lysosomes leads to quenching of the GFP signal, whereas RFP signal remains intact (Liang and Corn, 2022). These qualities of fluorescent reporters allow to monitor autophagic flux by measuring the intensity of green and red fluorescence whereby if autophagy is inhibited cells retain the GFP and RFP signals and if autophagy is induced then only the GFP signal is lost (Liang and Corn, 2022). Similarly, using autophagic cargo receptors tagged with fluorescent proteins led to the identification of multiple regulators of selective autophagy (Kanfer et al., 2021; Liang et al., 2020; Ohnstad et al., 2020).

Multiple additional assays to investigate different stages of autophagy exist, such as phosphorylation events of known regulators or autophagic cargo degradation to test selective autophagy (Alsaadi et al., 2019). Methods used in this thesis will be described in later chapters.

1.5.1 Genome-wide CRISPR-Cas9 screen

Fluorescently tagged autophagy reporters are commonly used to identify new regulators of autophagy in high-throughput genome-wide screens, including RNA interference (RNAi)-mediated gene silencing- and gene editing-based assays (Chan et al., 2007b; Hale et al., 2016; Orvedahl et al., 2011). However, the major disadvantage of RNAi-based screens is the incomplete knockdown of protein expression, rather than a complete abolishment, which could result in residual activity of the targeted proteins and lack of apparent effects on autophagy (Bethani et al., 2009). This impediment can be overcome by using a Clustered regularly interspaced short palindromic repeats-Cas9 (CRISPR-Cas9) tools. CRISPR-Cas9 was originally discovered in bacteria, where it is an immune response mechanism against viral infection (Deltcheva et al., 2011). This system is based on Cas9 endonuclease which can cleave target DNA at a specific site (Deltcheva et al., 2011; Jinek et al., 2012) although additional Cas9-related endonucleases have also been discovered. Cas9 can be targeted to genomic sequences by binding a complementary sequence of a short guide RNA (sgRNA) leading to double-strand break (Jinek et al., 2012). Double-strand break triggers DNA repair mechanisms through non-homologous end-joining and homologous recombination (Shrivastav et al., 2008). Non-homologous end-joining can result in indel mutations and therefore gene knockout. On the other hand, homologous recombination can restore wild type sequence of a gene and is used to incorporate specific mutations and tags (Shrivastav et al., 2008).

In screens utilising CRISPR/Cas9-mediated gene editing aimed at identifying autophagy regulators, a fluorescently tagged reporter protein, such as GFP-LC3, can be used as an autophagy readout. If a certain gene is essential for autophagy, knocking it out would lead to autophagy inhibition and an accumulation of the fluorescence signal. Fluorescent cells can be distinguished in a mixed cell population by fluorescence-activated cell sorting (FACS). Genome-wide or selected gRNA

sequences (Shalem et al., 2014) can be introduced to cells as a pool aiming to introduce one gRNA sequence per cell. After separating cells depending on the fluorescent signal by FACS, the individual gRNA can be identified by genomic sequences. Genome-wide CRISPR-Cas9 screens have been used to identify multiple autophagy regulators (Dejesus et al., 2016; Liang et al., 2020; Mimura et al., 2021; Morita et al., 2018). It was also used to identify RNAseK as a potential autophagy regulator in the screen I have performed prior to the start of my PhD. Discovery of CRISPR-Cas9 in bacteria and subsequent development of tools for using CRISPR-Cas9 for targeted gene knockouts revolutionised the scientific field. Many scientific advances were made using these tools and Jennifer Doudna and Emmanuelle Charpentier won Nobel Prize in Chemistry in 2020 for their seminal work on CRISPR/Cas9 (Westermann et al., 2021).

1.5.2 TurboID-based proximity labelling

Identification of protein-protein interactions (PPIs) required for autophagy is important to understand the regulatory network governing different stages of the pathway. It is also another approach which could lead to discovery of novel autophagy regulators. Multiple tools have been developed to facilitate the detection of PPIs especially those that are more challenging to uncover due to their transient nature. One of the best tools utilised to identify transient or weak interactions is biotin ligase-based proximity labelling assays (Qin et al., 2021). This proximity labelling technique is based on the ability of a promiscuous biotin ligase to label proximal proteins with biotin (figure 1.9). This labelling involves an ATP-dependent, covalent attachment of biotin to nucleophilic residues such as lysine (Choi-Rhee et al., 2004). One of the advantages of biotin ligase-based assays is low toxicity, which means it can be used in live cell culture or a live organism for prolonged periods of time (Qin et al., 2021). Biotin labelled proteins can are enriched by streptavidin pulldown and analysed by mass spectrometry (MS). Moreover, due to the covalent binding between biotin and labelled proteins, stringent conditions can be used for the pulldown which reduces unspecific binding and the pulldown background signal. However, labelling that occurs in the biotinylation radius of the enzyme results in labelling of true PPIs, but also of proteins in proximity of the bait protein rather than interacting with it. Therefore, the data from proximity labelling assays need to be analysed carefully and confirmed by

additional methods. The labelling time, biotin concentration and labelling radius depends on the enzyme used.

The original enzyme used for proximity-based labelling was developed by mutating *Escherichia coli* biotin ligase at residue 118, to enable promiscuous biotinylation (Choi-Rhee et al., 2004). This promiscuous biotin ligase was named BirA*/BioID and has been widely used to study PPIs (Roux et al., 2012). Subsequently, improved BioID variants have been engineered, such us BioID2 or BASU (Kim et al., 2016; Ramanathan et al., 2018). More recently, a new BioID variant was developed called TurboID (Branon et al., 2018). TurboID is a promiscuous biotin ligase developed by expressing a recombinant ligase on yeast surface (Cherf and Cochran, 2015) followed by multiple rounds of mutagenesis to direct the evolution of the protein in order to obtain a more efficient enzyme (Packer and Liu, 2015). This newly generated BioID variant was shown to exhibit more efficient catalytic activity compared to other promiscuous biotin ligases (Branon et al., 2018). For an example, TurboID can catalyse the biotinylation of protein targets within 10 min of incubation with biotin, whereas other biotin ligases, such as BioID, BioID2 or BASU, require up to 18 hr to catalyse the biotinylation of a similar amount of protein targets (Branon et al., 2018). Moreover, TurboID is functional under wider temperature spectrum when compared to BioID thus making it a more versatile tool (Branon et al., 2018). However, biotinylation radius of TurboID is increased to 35 nm, compared to 10 nm BioID radius, which increases unspecific labelling. Moreover, if TurboID is expressed ubiquitously, it can utilise endogenous biotin and promote chronic biotinylation, increasing toxicity. Chronic biotinylation can also saturate proximal labelling sites which leads to reduction in the labelling specificity. These drawbacks of TurboID need to be taken under consideration when designing experiments using this enzyme. Altogether, when used carefully, TurboID is an attractive tool to use for proximity labelling and identification of proximal proteins and potential interactors.

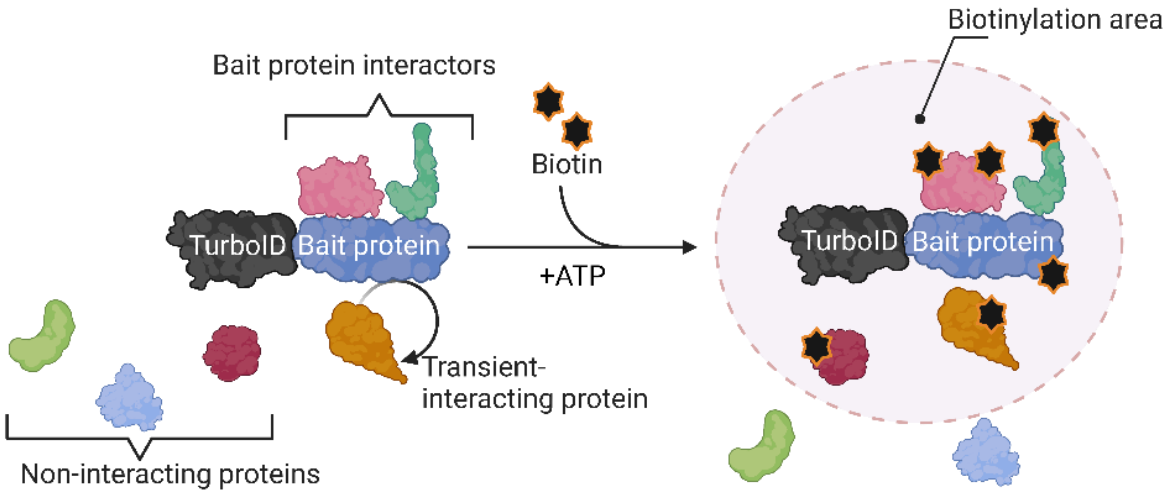

Figure 1.9 Schematic diagram of TurboID proximity labelling mechanism of action.

Bait protein fused to TurboID construct is expressed in cells. Incubation with exogenous biotin results in biotinylation of proteins in proximity of the bait. This includes direct and indirect binding partners, transient interactors and non-interactors.

1.6 Aims of the thesis

The main goal of this thesis is to understand the role of RNAseK in autophagy and lysosomal function. RNAseK was identified as a potential autophagy regulator in a Genome-Wide CRISPR-Cas9 knockout screen. RNAseK is a poorly characterised protein and the role of RNAseK in autophagy has not been studied before. Chapter 3 will focus on identifying the stage of autophagy affected in absence of RNAseK. Moreover, the interacting network and cellular localisation of RNAseK will be analysed. In chapter 4, the role of RNAseK in lysosomal function will be investigated. Finally, chapter 5 will focus on characterising the role in autophagy of selected proteins disrupted in the absence of RNAseK.

Moreover, the aim of this thesis is to validate the interaction between two autophagy proteins ATG2 and ATG16L1. These two proteins were shown in close proximity in a TurboID proximity assay. Although, both proteins are established autophagy regulators, an interaction between ATG2 and ATG16L1 has not been described thus far.

Chapter 2. Materials and methods

2.1 Cell culture

Mouse embryonic fibroblasts (MEFs), U2OS, human neuroblastoma cells (SH-SY5Y) and HEK293T were cultured in Dulbecco's Modified Eagle's Medium (DMEM) containing 4.5 g/L glucose (Gibco, 21969035) and supplemented with 10% FBS (Gibco, 10473-028), 2 mM L-glutamine (Gibco, 25030-081), 10 U/mL penicillin and 100 µg/mL streptomycin (Gibco, 15140-122) in a humidified chamber maintained at 37°C and 5% carbon dioxide (CO_2). For passaging, cells were washed with phosphate-buffered saline (PBS) followed by a dissociation with 0.05% trypsin (Gibco, 25300054) and neutralisation with DMEM. A fraction of the cell suspension was then transferred to a new cell culture dish and topped up with cell media.

To induce autophagy, cells were washed twice with PBS and incubated for the indicated amount of time in amino acid-free or serum-free DMEM. To disrupt lysosomal degradative function, Baf A1 was used at 20 nM final concentration (Sigma, B1793), unless indicated otherwise. To inhibit early stages of autophagy, VPS34-IN1 was used at 2 µM final concentration (Cayman Chemical, 17392).

2.2 SDS-PAGE and western blotting

Cells were washed twice with ice-cold PBS and lysed in RIPA buffer (10 mM Tris, 100 mM NaCl, 1 mM ethylenediaminetetraacetic acid (EDTA), 1 mM ethyleneglycoltetraacetic acid (EGTA), 0.1% SDS, 1% Triton X-100 (Sigma, T9284), 1 mM β-mercaptoethanol (β-ME) (Sigma, 444203), 0.5% sodium deoxycholate, 10% glycerol (Fisher Scientific UK, 10675872), supplemented with protease inhibitors cocktail V (Millipore, 539137-10VL). Samples were transferred to 1.5 mL Eppendorf tubes and vortexed, if p62 was analysed, samples were also sonicated. This was followed by centrifugation at 20,000 g for 10 min at 4°C. The supernatants were collected and mixed with SDS sample loading buffer dye (200 mM Tris-HCl pH 6.8, 2 g/mL SDS, 10% glycerol (v/v), 143 mM β-ME, bromophenol blue) and further denatured by heating at 95°C for 5 min.

Protein lysates were loaded on gels and separated at 120 V in for ~1.5 h on either 10% or 15% SDS-polyacrylamide gels. PageRuler (Thermo Scientific, 26619)

was used as a protein standard. Separated proteins were subsequently transferred onto nitrocellulose membranes (Bio-Rad, 1620115) for 10% gels, or PVDF membranes (Bio-Rad, 1620177) for 15% gels. Proteins were transferred by wet transfer by applying constant 385 milliamps for 70 min for 10% gels, or constant 100 V for 100 min to the blotting chamber containing transfer buffer (15% methanol, 96 mM Tris, 78 mM glycine). Membranes were blocked with 5% non-fat milk in TBST buffer [TBS, 0.05% Tween 20 (Sigma, P9416)] for 30 min. Subsequently membranes were incubated with primary antibodies (table 2.1) diluted in TBST and 5% non-fat milk for 2 h at room temperature or overnight at 4°C. Membranes were then washed with TBST and incubated with horseradish peroxidase-linked (HRP) secondary antibodies (table 2.1) at room temperature for 1-2 h. Membranes were washed with TBST and developed using Clarity Western ECL substrate (Bio-Rad, 1705061) or SuperSignal West Femto (Thermo Scientific, 34094). To visualise protein bands, Bio-Rad ChemiDoc XRS+ Imaging System was used.

2.3 Microscopy

For immunofluorescence staining, cells were plated on glass coverslips in 6-well plates for 24-48 h prior indicated treatment. Following the treatment cells were washed twice with PBS and fixed with 3.7% paraformaldehyde (PFA) (Sigma, P6148) in 20 mM HEPES pH 7.5 for 15 min at room temperature in the dark. Fixation buffer was then washed off with PBS and cells were permeabilised using in 0.1% Triton X-100 (Sigma, T9284) in PBS for 5 min at room temperature or ice-cold MeOH for 2 min on ice. Cells were washed twice with PBS and blocking was then performed using 1% bovine serum albumin (BSA) in PBS for 30 min at room temperature. Coverslips were then incubated with primary antibodies (table 2.1) for 3 hrs at 37ºC, followed by washes in PBS and incubation with the indicated secondary Alexa Fluor secondary antibodies (table 2.1) for 30 min at room temperature in the dark. After washing the coverslips twice with PBS, nuclei were stained with 4’,6-diamidino-2-phenylindole (DAPI; Sigma, D9542) prior to mounting on microscope slides with Prolong Diamond Antifade mountant (Invitrogen, P3696). Microscope slides were left at room temperature for 24 h before acquiring images. Images were acquired on a Nikon A1R point scanning confocal microscope with a 60X objective. Analyses were performed using ImageJ software. EzColocalization plugin was used to quantify Pearson’s

correlation coefficient between the indicated proteins. VPS4a puncta per cell was assessed manually using a multi-point feature in ImageJ software.

For imaging of live cells, GFP-STX17 expressing cells were plated on glass-bottom plates (World Precision Instruments, FD35-100) for 24 h. Cells were then washed twice with PBS and incubated in Hank's balanced salt solution (HBSS) (Gibco, 14025092) for 2 h. To visualise acidic lysosomal compartments LysoTracker Deep Red (Invitrogen, L12492) was added. Live cell imaging was performed using a Nikon A1R point scanning confocal microscope with a 100X objective. LysoTracker ring and dot structures per cell were assessed manually using multi-point feature in ImageJ software.

2.4 Antibodies

Antibodies used in this thesis were diluted in 5% (w/v) non-fat milk in TBST (15 mM NaCl, 10 mM Tris-HCl pH 7.5, and 0.05% Tween 20 (Sigma, P9416) when used for immunoblotting. For immunofluorescence analyses antibodies were diluted in 1% (w/v) BSA, 0.02% (v/v) sodium azide in PBS. Details of the antibodies used in this thesis are listed in the table below.

Antibodies						
Target	**Species**	**Clone**	**Supplier**	**Cat. number**	**Dilution WB**	**Dilution IF**
β-Actin	Mouse	AC-74	Sigma Aldrich	A5316	1:3000	---
ATG16L1	Rabbit	---	MBL	PM040	1:200	1:300
ATG3	Mouse	3E8	MBL	M133-3	1:3000	---
ATG5	Rabbit	---	Sigma Aldrich	A0731	1:3000	---
ATG7	Rabbit	---	Sigma Aldrich	A2856	1:2000	---
ATG9A	Rabbit	D4O9D	CST	13509	---	1:200
Cathepsin B	Goat	---	R&D systems	AF965	1:3000	---

CD63	Mouse	sc-5275	Santa Cruz	MX-49.129.5	---	1:300
CD-MPR	Rabbit	EPR7691	Abcam	ab134153	---	1:300
CI-MPR	Rabbit	EPR6599	Abcam	ab124767	1:3000	1:300
EGFR	Rabbit	sc-5275	Santa Cruz	1005	1:2000	---
FIP200	Rabbit	---	Abcam	176816	1:1000	---
GFP	Mouse	7.1 and 13.1	Roche	11814460001	---	1:300
GFP	Rabbit	---	Chromotek	PABG1-100	1:3000	1:300
GM130	Mouse	---	BD biosciences	610822	---	1:300
HA-tag	Rat	3F10	Roche	11867423001	1:1000	---
LAMP1	Rat	1D4B	Abcam	ab25245	---	1:1000
LC3B	Rabbit	---	Sigma Aldrich	L7543	1:3000	---
MYC-tag	Mouse	9B11	CST	2276	1:1000	1:300
MYC-tag	Rabbit	71D10	CST	2278s	---	1:300
p62	Rabbit	---	Enzo Life Sciences	BML-PW9860-0100	---	1:300
p62	Rabbit	---	CST	5114	1:2000	---
PLA2G15	Rabbit	---	Atlas Antibodies	HPA041702	1:500	---
PLD3	Rabbit	---	Atlas Antibodies	HPA012800	1:1000	1:200
RAB7	Rabbit	D95F2	CST	9367S	---	1:300
RFP	Rabbit	---	Rockland	600-401-379	1:2000	---

RNAseK	Rabbit	S4806-1	Proteintech	Custom production	1:2000	1:600
Mouse IgG-HRP	Goat	---	CST	7076	1:3000	---
Rabbit IgG-HRP	Goat	---	CST	7074	1:3000	---
Goat IgG-HRP	Rabbit	---	Invitrogen	61-1620	1:5000	---
AlexaFluor488 anti-mouse	Goat	---	Invitrogen	A1101	---	1:500
AlexaFluor488 anti-rabbit	Goat	---	Invitrogen	A11008	---	1:500
AlexaFluor594 anti-mouse	Goat	---	Invitrogen	A11032	---	1:500
AlexaFluor594 anti-rabbit	Goat	---	Invitrogen	A11012	---	1:500
AlexaFluor594 anti-rat	Goat	---	Invitrogen	A11007	---	1:500
AlexaFluor647 anti-mouse	Goat	---	Invitrogen	A32728	---	1:500
AlexaFluor647 anti-rat	Goat	---	Invitrogen	A21247	---	1:500

Table 2.1 List of antibodies used in this thesis.

2.5 Cloning

For cloning of guide RNAs (gRNAs) into lentiviral vectors, 1 µg of sgRNA vector (table 2.5) was digested with 2 µL of BsmBI enzyme (NEB, R0739S) in the presence of digestion buffer 3.1 (NEB, B7203). A total reaction volume of 50 µL was incubated for 2 h at 55ºC. Subsequently, the digestion temperature was lowered to 37ºC and 1 µL of calf intestinal alkaline phosphatase (CIP) (NEB, M0525S) was added for 5 min. The digested plasmid was run on 1% agarose gel and purified using QIAGEN gel extraction kit (Qiagen, 28115) according to manufacturer's instructions. Each pair (forward and reverse) of the gRNA oligonucleotides (table 2.6) were phosphorylated using T4 Polynucleotide kinase (NEB, M0201S) in T4 ligation buffer (NEB, B0202S) for 30 min at 37ºC. Annealing was then performed by heating sample up to 95ºC for 5

min and ramping down temperature to 25ºC at 5 ºC/min. The digested plasmid together with annealed oligonucleotides were ligated using T4 DNA ligase (NEB, M0202) in T4 ligation buffer for 1 h at room temperature. The ligation product was transformed into or Stbl3 competent cells (Invitrogen, C737303) and plated on lysogeny broth (LBroth) agar plates containing ampicillin. After overnight incubation at 37ºC, single colonies were selected and grown in LBroth containing ampicillin. Positive clones were confirmed by Sanger sequencing and subsequently amplified using QIAGEN plasmid midi kit (Qiagen, 12145).

For cloning of RNAseK into TurboID vector (table 2.5), 2 µg of pQCXIN-TurboID vector was digested with 1 µL of NotI enzyme (NEB, R0189S) and 1 µL of BamHI (NEB, R0136S) in presence of 3.1 digestion buffer (total reaction volume 50 µL) for 4 h at 37ºC.

For cloning of ATG16L1 into the TurboID vector, 2 µg of pQCXIN-TurboID vector was digested with 1 µL of BsiWI enzyme (NEB, R0553S) in 3.1 digestion buffer for 2 h at 55ºC, followed by purification using QIAquick PCR purification kit (Qiagen, 28104). The purified vector was subsequently digested with 1 µL of PacI enzyme (NEB, R0547S) in CutSmart digestion buffer (NEB, B7204) (total reaction volume 50 µL) for 2 h at 37ºC.

The digested vectors were run on 1% agarose gel and purified using QIAGEN gel extraction kit according to manufacturer's instructions. The insert constructs were amplified by polymerase chain reaction (PCR) according to tables 2.2 and 2.3, gel purified, and subsequently digested with the indicated enzymes in the presence of the suitable digestion buffer for 1 h. Digested insert was purified using QIAquick PCR purification kit according to manufacturer’s instruction. Digested vectors together with amplified insert fragment were ligated using 0.5 µL of T4 DNA ligase (400,000 units/mL stock concentration) in presence of T4 ligation buffer (total reaction volume 10 µL) for 1 h at room temperature. The ligation product was transformed into or DH5α competent cells (Invitrogen, 18265017) and plated on LBroth agar plates containing ampicillin. After overnight incubation at 37ºC single colonies were selected and grown in LBroth containing ampicillin. Positive clones were confirmed by Sanger sequencing and subsequently amplified using QIAGEN plasmid midi kit.

Reagent	Volume (µL)
5x HF Phusion reaction buffer (NEB, B0518S)	10
2.5 mM dNTP	3
10 µM forward primer	2.5
10 µM reverse primer	2.5
Phusion polymerase (NEB, M0530S)	1
DMSO	1
100 ng/µL DNA template	1
Nuclease-free ddH_2O	Up to 50

Table 2.2 Details of reagents used for PCR.

Number of cycles	Step	Temperature (°C)	Time (min)
1	Initial denaturation	98	2
25-30	Denaturation	98	0.5
	Annealing	53-68	0.5
	Elongation	72	1 per kb
1	Final extension	72	10
1	Hold	10	---

Table 2.3 Cycles and temperature steps used for PCR.

For cloning of ATG2 plasmid HA-ATG2 plasmid (table 2.5) was used as a template for site directed mutagenesis. Using the indicated primers (table 2.6), plasmids were amplified using Q5 Site-directed mutagenesis kit (NEB, E0552S) according to the manufacturer's instructions. The PCR reaction was set up according table 2.4.

Step	Temperature (ºC)	Time (sec)
Initial denaturation	98	30
25-35 cycles	98	10
	68	30
	72	600
Final extension	72	120
Hold	10	---

Table 2.4 Conditions used for mutagenesis of ATG2 construct.

The amplification product was then digested using KLD enzyme mix (NEB, M0554) and digestion product were then transformed into DH5α competent cells (Invitrogen, 18265017) and plated on LBroth agar plates containing ampicillin. After

overnight incubation at 37ºC single colonies were selected and grown in LBroth containing ampicillin. Successful cloning was confirmed by Sanger sequencing and positive clones were amplified using QIAGEN plasmid midi kit.

2.6 Plasmids and oligonucleotides

The plasmids and oligonucleotides used for gene knockout or protein expression in this thesis are detailed in tables 2.6 and 2.7, respectively. Flag-S-ATG16L1 constructs have been described previously (Gammoh et al., 2013).

Insert	Vector	Other details
GFP-LC3	pBabe	---
Cas9 sgRNA	lentiCRISPR v2	Addgene #52961
Cas9	pFUGW	Addgene #52962
sgRNA	lentiCRISPR v1	Addgene #70662
TiD-myc-ATG16L1	pBabe	---
Flag-S-ATG16L1	pBabe	(Gammoh et al., 2013)
Flag-S-ATG16L1 (AA 1–335	pBabe	(Gammoh et al., 2013)
Flag-S-ATG16L1 (AA 336–623)	pBabe	(Gammoh et al., 2013)
sgRNAseK#1	lentiCRISPR v2	---
sgRNAseK#2	lentiCRISPR v2	---
RNAseK-myc	pQCXIN	---
GFP-RNAseK	pBabe	---
RNAseK-myc-TiD	pQCXIN	---
Myc-TurboID	pQCXIN	---
GFP-STX17	pMRXIP	Addgene #45909
GFP	pBabe	---
PLA2G15-HA	pCMV6-Entry	Sinobiological #MG52099-CY
GFP-VPS4a	pLNCX2	Addgene #116924
GFP-VPS4a E228Q	pEGFP	Addgene #80351
mCheery-VPS4a	pLNCX2	Addgene #115334
ATG2a-GFP	pMRXIP	---

Flag-HA-ATG2a	pMSCV	Gift from Dr David McEwan
Flag-HA-ATG2a YFS	pMSCV	Gift from Dr David McEwan
Flag-HA-ATG2a 221-227	pMSCV	---
GFP-ATG2b	pEGFP	Gift from Dr Li Yu
Flag-HA-ATG2b	pMSCV	Gift from Dr David McEwan
GAG-POL	---	---
PAX2	---	---
VSVG	---	---

Table 2.5 Details of plasmids used for gene knockout or protein expression.

Oligonucleotide	SEQUENCE (5' TO 3')	Application
Illumina Forward Set 1	AATGATACGGCGACCACCGAGATCTACACTCTTTCCCTACACGACGCTCTTCC GATCTTAAGTAGAGTCTTGTGGAAAGGACGAAACACCG	Appendix 1
Illumina Forward Set 2	AATGATACGGCGACCACCGAGATCTACACTCTTTCCCTACACGACGCTCTTCC GATCTATACACGATCTCTTGTGGAAAGGACGAAACACCG	Appendix 1
Illumina Forward Set 3	AATGATACGGCGACCACCGAGATCTACACTCTTTCCCTACACGACGCTCTTCC GATCTGATCGCGCGGTTCTTGTGGAAAGGACGAAACACCG	Appendix 1
Illumina Forward Set 4	AATGATACGGCGACCACCGAGATCTACACTCTTTCCCTACACGACGCTCTTCC GATCTCGATCATGATCGTCTTGTGGAAAGGACGAAACACCG	Appendix 1
Illumina Forward Set 5	AATGATACGGCGACCACCGAGATCTACACTCTTTCCCTACACGACGCTCTTCC GATCTTCGATCGTTACCATCTTGTGGAAAGGACGAAACACCG	Appendix 1
Illumina Forward Set 6	AATGATACGGCGACCACCGAGATCTACACTCTTTCCCTACACGACGCTCTTCC GATCTATCGATTCCTTGGTTCTTGTGGAAAGGACGAAACACCG	Appendix 1
Illumina Forward Set 7	AATGATACGGCGACCACCGAGATCTACACTCTTTCCCTACACGACGCTCTTCC GATCTGATCGATAACGCATTTCTTGTGGAAAGGACGAAACACCG	Appendix 1
Illumina Forward Set 8	AATGATACGGCGACCACCGAGATCTACACTCTTTCCCTACACGACGCTCTTCC GATCTCGATCGATACAGGTATTCTTGTGGAAAGGACGAAACACCG	Appendix 1
Illumina Forward Set 9	AATGATACGGCGACCACCGAGATCTACACTCTTTCCCTACACGACGCTCTTCC GATCTACGATCGATAGGTAAGGTCTTGTGGAAAGGACGAAACACCG	Appendix 1
Illumina Forward Set 10	AATGATACGGCGACCACCGAGATCTACACTCTTTCCCTACACGACGCTCTTCC GATCTTAACAATGGTCTTGTGGAAAGGACGAAACACCG	Appendix 1
Illumina Forward Set 11	AATGATACGGCGACCACCGAGATCTACACTCTTTCCCTACACGACGCTCTTCC GATCTATACTGTATCTCTTGTGGAAAGGACGAAACACCG	Appendix 1
Illumina Forward Set 12	AATGATACGGCGACCACCGAGATCTACACTCTTTCCCTACACGACGCTCTTCC GATCTGATAGGTCGCATCTTGTGGAAAGGACGAAACACCG	Appendix 1
Illumina Reverse Set 1	CAAGCAGAAGACGGCATACGAGATAAGTAGAGGTGACTGGAGTTCAGACGTG TGCTCTTCCGATCTTTCTACTATTCTTTCCCCTGCACTGT	Appendix 1
Illumina Reverse Set 2	CAAGCAGAAGACGGCATACGAGATACACGATCGTGACTGGAGTTCAGACGTG TGCTCTTCCGATCTATTCTACTATTCTTTCCCCTGCACTGT	Appendix 1

Illumina Reverse Set 3	CAAGCAGAAGACGGCATACGAGATCGCGCGGTGTGACTGGAGTTCAGACGTG TGCTCTTCCGATCTGATTCTACTATTCTTTCCCCTGCACTGT	Appendix 1
Illumina Reverse Set 4	CAAGCAGAAGACGGCATACGAGATCATGATCGGTGACTGGAGTTCAGACGTG TGCTCTTCCGATCTCGATTCTACTATTCTTTCCCCTGCACTGT	Appendix 1
Illumina Reverse Set 5	CAAGCAGAAGACGGCATACGAGATCGTTACCAGTGACTGGAGTTCAGACGTG TGCTCTTCCGATCTTCGATTCTACTATTCTTTCCCCTGCACTGT	Appendix 1
Illumina Reverse Set 6	CAAGCAGAAGACGGCATACGAGATTCCTTGGTGTGACTGGAGTTCAGACGTG TGCTCTTCCGATCTATCGATTCTACTATTCTTTCCCCTGCACTGT	Appendix 1
Illumina Reverse Set 7	CAAGCAGAAGACGGCATACGAGATAACGCATTGTGACTGGAGTTCAGACGTG TGCTCTTCCGATCTGATCGATTCTACTATTCTTTCCCCTGCACTGT	Appendix 1
Illumina Reverse Set 8	CAAGCAGAAGACGGCATACGAGATACAGGTATGTGACTGGAGTTCAGACGTG TGCTCTTCCGATCTCGATCGATTCTACTATTCTTTCCCCTGCACTGT	Appendix 1
Illumina Reverse Set 9	CAAGCAGAAGACGGCATACGAGATAGGTAAGGGTGACTGGAGTTCAGACGTG TGCTCTTCCGATCTACGATCGATTCTACTATTCTTTCCCCTGCACTGT	Appendix 1
Illumina Reverse Set 10	CAAGCAGAAGACGGCATACGAGATAACAATGGGTGACTGGAGTTCAGACGTG TGCTCTTCCGATCTTTCTACTATTCTTTCCCCTGCACTGT	Appendix 1
Illumina Reverse Set 11	CAAGCAGAAGACGGCATACGAGATACTGTATCGTGACTGGAGTTCAGACGTG TGCTCTTCCGATCTATTCTACTATTCTTTCCCCTGCACTGT	Appendix 1
Illumina Reverse Set 12	CAAGCAGAAGACGGCATACGAGATAGGTCGCAGTGACTGGAGTTCAGACGTG TGCTCTTCCGATCTGATTCTACTATTCTTTCCCCTGCACTGT	Appendix 1
myc-TiD-ATG16L1 Forward	GCAGCACGTACGATGTCGTCGGGCCTGCGCGC	Appendix 2
myc-TiD-ATG16L1 Reverse	GCAGCATTAATTAATCAAGGCTGTGCCCACAGCACAG	Appendix 2
sgRNAseK#1 Forward	CACCGCCATTCTGCTGTGTTAATTG	Chapter 3
sgRNAseK#1 Reverse	AAACCAATTAACACAGCAGAATGG	Chapter 3
sgRNAseK#2 Forward	CACCGGTGGCATCGTCCTCAGCGCC	Chapter 3
sgRNAseK#2 Reverse	AAACGGCGCTGAGGACGATGCCACC	Chapter 3
sgRNAseK endogenous tagging Forward	CACCGATACATGGTGCGCTAGAGCG	Chapter 3

sgRNAseK endogenous tagging Reverse	AAACCGCTCTAGCGCACCATGTATC	Chapter 3
RNAseK-myc donor DNA	GCTACAACTGTTTCATCGCCGCGGGCCTCTACCTCCTCCTCGGAGGCTTCTCCTTCTGCCAAGTTCGTCTCAACAAGCGCAAGGAATACATGGTGCGCGAACAAAAACTTATTTCTGAAGAAGATCTGTAGAGCGCGCTCCGCCTCTCCCTCCCCAGCCCCCTTCTCTATTTAAAGACTCCGCAGACTCCGTCCCACTCATCTGGCGTCCTTTGGGACTT	Chapter 3
RNAseK-myc-TiD NotI Forward	GCAGCAGCGGCCGCATGGCGTCGCTCCTGTGCTG	Chapter 3
RNAseK-myc-TiD BamHI Reverse	GCAGCAGGATCCGCGCACCATGTATTCCTTGC	Chapter 3
GFP-RNAseK XhoI Forward	GCAGCACTCGAGATGGCGTCGCTCCTGTGCTGT	Chapter 5
GFP-RNAseK EcoRI Reverse	GCAGCAGAATTCCTAGCGCACCATGTATTCCTT	Chapter 5
qRT-PCR-PLD3 Forward	ATCCATCGATGCGGTCCTTC	Chapter 5
qRT-PCR-PLD3 Reverse	CCAGACCAGTTGGAGGTTCC	Chapter 5
qRT-PCR-Actin Forward	GATGAGGCTCAGAGCAAGAGAG	Chapter 5
qRT-PCR-Actin Reverse	GTCCCGGCCAGCCAGGTCCAG	Chapter 5
ATG2a AA 221-227 Forward	GGCGGCGGCGCAGCTGGCAGGGGTCCGC	Chapter 7
ATG2a AA 221-227 Reverse	GCCGCCGCCGCAGGCGGCTGATGCACGTC	Chapter 7

Table 2.6 Details of oligonucleotides used for gene knockout or protein expression.

2.7 Transfections

For retroviral particles production, HEK293Ts were seeded in 10 cm dishes for 24 h. Next day 6 µg of construct, 3 µg of vesicular stomatitis virus G protein (VSVG), 3 µg of GAGPOL with 50 µL of polyethylenimine (PEI) in 500 µL of Opti-MEM (Gibco, 31985062) were incubated for 10 min at RT and then added to cells.

For lentiviral particles production, HEK293Ts were seeded in 10 cm dishes for 24 h. Next day 5 µg of construct 1.25 µg of VSVG, 3.75 µg of PAX2 with 50 µL of PEI in 500 µL of Opti-MEM were incubated for 10 min at RT and then added to cells.

72 h post-transfection, the viral media was passed through a 0.45 µm syringe filter (Fisher Scientific UK, 15216869) and used for cells transduction. For transduction of MEF or U2OS, cells were seeded in 6-well plate for 24 h. Next day, viral media was added to the cells with 1 µg/mL polybrene (Sigma Aldrich, TR-1003-G) and centrifuged at 210 g for 10 min, After 24 h, viral media was replaced with complete media and selection marker was added 48 h post-transduction.

For transient transfections, HEK293Ts were seeded in 10 cm dishes for 24 h. Next day, 1-3 µg of the construct and 50 µL of PEI in 500 µL of Opti-MEM were incubated for 10 min and then added to the cells. After 48-72 h, cells were used for the specified experiments.

For endogenous tagging of *Rnasek* at the C-terminal end with a MYC tag (RNAseK-MYC), MEF cells were seeded 24 h prior to transient transfection with Cas9, pBabe-GFP, sgRNA-RNAseK constructs, and a donor synthesised DNA (tables 2.5 and 2.6). Transient transfection was performed by mixing of the forementioned constructs with 5 µL of Lipofectamine 2000 transfection reagent (Invitrogen, 11668019) in 400 µL Opti-MEM. Transfection mix was incubated for 20 min and added to the cells. After 5 h incubation at 37ºC, transfection mix was replaced by complete media. 24 h post transfection, cells were selected with puromycin (2 µg/mL) for 72 hr followed by single cell sorting based on GFP fluorescence. Successful tagging in cells was confirmed by sequencing and immunofluorescence staining for MYC tag.

For siRNA transfections, MEF or SH-SY5Y cells were seeded onto 6 well plate. Next day, the indicated siRNA duplexes (table 2.7) were incubated with 5 µL of Dharmafect 1 transfection reagent (Dharmacon, Horizon Discovery Biosciences Ltd, T-2001-03) in 400 µL of Opti-MEM for 20 min at room temperature. Transfection mix

was added to cells and incubated for 24 h. The final concentration of siRNA was 25 nM. 24 h later, the transfection media was changed to complete media. Cells were analysed 72 h post transfection and knockdown efficiency was confirmed by qRT-PCR.

Target	Gene ID	Dharmacon product code
Mouse *Rnasek*	52898	L-054958-01-0005
Human *RNASEK*	440400	L-032392-02-0005
Mouse *Pld3#1*	18807	J-049108-09-0002
Mouse *Pld3#2*	18807	J-049108-10-0002
Mouse *Pld3#3*	18807	J-049108-11-0002
Human *PLD3*	23646	L-009659-01-0005
Non-targeting control	---	D-001810-10-05

Table 2.7 Details of siRNA used for knockdown experiments.

2.8 Quantitative reverse transcription (qRT)-PCR

To measure the efficiency of RNA interference-mediated gene knockdown, RNA was isolated from cells using RNeasy Mini Kit (Qiagen, 74104) according to the manufacturer's instructions. RNA was measured using Nanodrop (Thermo Scientific) at 285 nm wavelength. 400 ng of RNA was used for cDNA synthesis SuperScript double stranded cDNA synthesis kit (Invitrogen, 11917010). Quantitative PCR was performed using Brilliant II SYBR (Agilent Technologies, 600828) on a StepOne Plus Real-Time PCR System (Applied Biosystems, 4376600) (table 2.8). Gene expression was calculated by deltadelta Ct method and Pld3 transcript levels were normalised to Actin, by PCR amplification using primer sequences listed in table 2.6.

Number of cycles	Step	Temperature (°C)	Time (s)
1	Denaturation	95	600
40	Denaturation	95	30
	Annealing	60	30
	Elongation	72	60
1	Denaturation	95	15
	Annealing	60	60
	Melt curve	+0.3 (up to 95)	15

Table 2.1 Cycles and temperature steps used for qRT-PCR.

2.9 Binding assays

For protein-protein interactions, HEK293T cells were seeded in 100 mm plates for 24 h. Next day, cells were transfected with the indicated individual constructs using PEI transfection reagent as described above. 72 h post transfection, cells were washed twice with PBS and harvested by direct lysing in pulldown (PD) buffer [150 mM NaCl, 20 mM Tris-HCl pH 7.5, 5 mM EDTA, 1% Triton-X or 10 mM Tris/Cl pH 7.5, 150 mM NaCl, 0.5 mM EDTA, 0.5 % NP40 (Abcam, ab142227)] supplemented with protease inhibitors cocktail V (Millipore, 539137-10VL) and lysates were cleared by spinning at 20,000 g for 10 min at 4°C. Cleared lysates expressing the individual transgenes were then mixed, incubated with GFP-Trap agarose beads (Chromotek, gta-20) or anti-HA agarose (Roche, 60789700) and rotated at 4ºC overnight. Beads were then washed 3 times in PD buffer and proteins were eluted by boiling for 5 min in SDS sample buffer diluted in PD buffer (final concentrations: 50 mM Tris pH 6.8; 2% SDS; 10% glycerol; 1 mM β-ME). Eluted proteins were analysed by SDS-PAGE and western blot.

For unbiased analyses of protein-protein interactions in U2OS, sgControl or sgRNAseK#2 cells stably expressing GFP-VPS4a^{WT} were seeded in 100 mm dishes for 24 h. Cells were then treated with amino acid-free DMEM for 3 h. Cells were subsequently harvested by direct lysing in PD buffer supplemented with protease inhibitors as above. Cell lysates were cleared by centrifiguation at 20,000 g for 10 min at 4°C and incubated with GFP-Trap agarose beads (Chromotek, gta-20) while rotating overnight at 4ºC. Beads were then washed 3 times in PD buffer followed by 3

washes in TBS buffer (15 mM NaCl, 10 mM Tris-HCl pH 7.5). Supernatant was removed and beads were stored at -80ºC for mass spectrometry (MS) processing.

For unbiased analyses of protein-protein interactions in RNAseK-myc cell line, RNAseK-myc MEF or wild type MEF cells were seeded in 100 mm dishes for 24 h. Cells were then treated with amino acid-free DMEM for 2 h and harvested by direct lysing in PD buffer supplemented with protease inhibitors as above. Cell lysates were cleared by centrifugation at 20,000 g for 10 min at 4°C and incubated with anti-myc antibody (table 2.1) while rotating overnight at 4ºC. Recombinant Protein G agarose beads were then added to the cell lysates for 10 min. Beads were then washed 3 times in PD buffer followed by 3 washes in TBS buffer (15 mM NaCl, 10 mM Tris-HCl pH 7.5). Supernatant was removed and beads were stored at -80ºC for MS processing.

For MS analyses, 5 µg/mL trypsin (Thermo Scientific, 90058) in proteolysis buffer (2 M urea, 50 mM Tris-HCl pH 7.5, 1 mM DTT) was added to the PD beads and incubated at 27°C for 30 min. Supernatants were then transferred into fresh 1.5 mL Eppendorf tubes. Beads were additionally washed with proteolysis buffer and supernatants were pooled together and digested overnight. The next day, samples were alkylated by incubation with iodoacetamide (Sigma, I6125-25G) in the dark for 30 min, and the reaction was stopped by the addition of TFA (Thermo Scientific, 28901) followed by vortexing. For desalting of the samples, C18 columns were activated with MeOH followed by 0.1% TFA wash. Sample were added to the C18 columns and spun at 500 g for 5 min. The C18 columns were washed twice with 50 µL of 0.1% TFA. Samples were eluted from C18 columns with 20 µL of elution buffer (50% acetonitrile, 0.05% TFA). The eluted samples were evaporated in a vacuum concentrator for 20 min and resuspended in 12 µL of 0.1% TFA. The samples were analysed by the core mass spectrometry facility using an Orbitrap Fusion Lumos Tribrid Mass Spectrometer (Thermo Scientific). Data obtained from the MS was analysed using Perseus software.

For binding experiments between recombinant ATG16L1 and ATG2 pulled down from cells, HEK293T cells were seeded in 100 mm dishes for 24 h followed by transfection with GFP-ATG2 constructs or GFP empty control using PEI. Cell lysates were obtained 72 h post transfection by direct lysing in RIPA buffer. Cell lysates were cleared by spinning at 20,000 g for 10 min at 4°C, and incubated with GFP-Trap agarose beads for 2 hours. Beads were then washed 3 times in PD buffer

supplemented with 300 mM NaCl and re-suspended in PD buffer. Re-suspended beads were incubated with 10 ng of recombinant wild-type ATG16L1 purified from insect cells (Dudley et al., 2019b) and 0.1 mg/mL BSA. After 1 h incubation at 4°C, beads were then washed 3 times with PD buffer and bound proteins were eluted by boiling for 5 min in SDS sample buffer diluted in PD buffer. Eluted proteins were analysed by SDS-PAGE and western blot.

2.10 Autophagy loss of function screen

MEF cells stably expressing pBabe-GFP-LC3 and SpCas9 were transduced with the mouse GeCKOv2 CRISPR knockout pooled library B (Addgene #1000000053) followed by 8 days of cell expansion and selection with puromycin (2 µg/mL, Millipore, 540411). Cells were then washed twice with PBS and starved for 16 h in amino acid-free DMEM supplemented with 10% dialysed FBS to induce autophagy. Cells were disassociated with 0.05% trypsin and trypsin was neutralised by adding DMEM. This was followed by centrifugation at 200 g for 3 min, cell pellet was resuspended in PBS. After washing cells twice with PBS, cell pellet was resuspended in PBS containing 1% dialysed FBS. Cells were then FACS sorted to separate GFP positive and negative cells using BD Aria II flow cytometer. Genomic DNA of GFP positive cells was extracted using DNeasy Blood & Tissue Kit (Qiagen, 69504). Integrated sgRNA cassettes were amplified with PCR using Illumina primers (table 2.6) followed by next-generation sequencing. Illumina library preparation, and sequencing (MiSeq v2 100PE to yield at least 11M + 11M reads) and bioinformatics analyses were performed by Edinburgh Genomics Facility.

2.11 TurboID

For proximity labelling experiments, MEF cells stably expressing TurboID constructs were seeded in 100 mm dishes for 24 h. Cells were then washed twice with PBS and treated with amino acid-free DMEM supplemented with 500 µM biotin (Sigma, B4639) for 2 h. Cells were then lysed in RIPA buffer supplemented with protease inhibitor cocktail V. Samples were centrifuged at 20,000 g for 10 min at 4°C and the supernatant collected and incubated with Streptavidin Sepharose High

Performance beads (GE Healthcare, 17511301) while rotating overnight at 4°C. Beads were then washed twice in RIPA buffer, once in RIPA buffer containing 1 M NaCl, twice in 2 M urea in Tris-HCl (pH 8.0), and finally 3 washes in TBS. Samples were then processed for MS analyses, as outlined above.

2.12 Transmission Electron Microscopy

For ultrastructural visualisation, MEF or U2OS cells were seeded in 100 mm dishes for 24 h. Cells were then washed twice with PBS and treated with amino acid-free DMEM and Baf A1 as indicated for 3 hr followed by cell disassociation with 0.05% trypsin which was neutralised by adding DMEM. Cells were pelleted by centrifugation at 200 g for 3 min. Cell pellets were then washed twice with PBS and fixed for 3 h and 15 min in fixation buffer. The fixation buffer consisted of 2.5% Glutaraldehyde (Sigma, G5882-10ML), 2% Paraformaldehyde (Thermo Scientific, 28908), 120 mM PIPES (Sigma, P6757), 50 mM HEPES (Fisher Scientific, 10081113), 4 mM MgCl2.6H2O (Sigma, 442611), 20 mM EGTA (Sigma, 324626). Sections were prepared for imaging by the University of Edinburgh electron microscopy facility and visualised using Philips/FEI BioTwin CM120 Transmission Electron Microscope.

2.13 Proteinase K protection assay

Cells were seeded in 100 mm dishes. The next day, cells were washed twice with PBS and treated with amino acid-free DMEM and 100 nM Baf A1 for 3 h. Following the treatment, cell were washed twice with PBS and homogenisation buffer (20 mM HEPES pH 7.6, 220 mM mannitol, 70 mM sucrose, 1 mM EDTA) was added to the cells. Cells were scraped off the dishes, transferred to 1.5 mL Eppendorf tubes and passed 10 times through a 27G needle followed by centrifugation at 500 g for 5 min at 4°C. Collected supernatants were aliquoted into three new tubes. In each tube, either homogenisation buffer, Proteinase K (New England Biolabs, P8107S) (25 µg/mL final concentration) or Proteinase K with Triton X-100 (1% final concertation) were added. The samples were incubated for 10 min at 30°C and reactions were stopped by adding protease inhibitors cocktail V (Millipore, 539137-10VL) on ice. Samples were then precipitated with 10% Trichloroacetic acid (TCA) (Sigma, T4885) for 30 min at 4°C and

centrifuged at 4°C at 20,000 g for 15 min. Pellets were washed ice-cold acetone and sonicated, which was followed by a 5 min centrifugation at 20,000 g at 4°C. Protein pellets were re-suspended in loading buffer and heated at 95°C for 10 min. Samples were analysed by SDS-PAGE and western blotting with the indicated antibodies.

2.14 EGFR degradation assay

For analyses of EGFR degradation rates, cells were seeded in 6-well dishes for 24 h. Subsequently, cells were washed twice with PBS and treated with serum-free DMEM supplemented with 2 mM L-glutamine for 4 hr. EGFR internalisation and degradation was induced by adding 20 ng/mL EGF (PreproTech, AF-100-15) for the indicated times. Cells were then washed twice with PBS and lysed in RIPA buffer supplemented with protease inhibitors (Millipore, 539137-10VL), followed by analysis using SDS-PAGE and western blotting with indicated antibodies.

2.15 Fluorescence-activated cell scanning (FACS) assays

For lysosomal acidity analysis, sgControl or sgRNAseK were seeded in 60 mm dishes. The next day, cells were washed twice with PBS and treated with amino acid-free DMEM for 2 h. LysoSensor Green (Invitrogen, L7535) at 1 μM final concentration was added to cells for 30 min. Following the treatment, cell were washed twice with PBS and disassociated with 0.05% trypsin which was neutralised by adding 10% FBS diluted in DMEM. This was followed by centrifugation at 200g for 3 min, cell pellet was resuspended in PBS. After washing cells twice with PBS, cell pellet was resuspended in PBS containing 1% dialysed FBS. LysoSensor Green signal intensity was then analysed using BD Fortessa flow cytometer.

For lysosomal Cathepsin B activity analysis, sgControl or sgRNAseK were seeded in 60 mm dishes. The next day, cells were washed twice with PBS and treated with amino acid-free DMEM for 2 h. Cathepsin B fluorogenic substrate III (Calbiochem, 219392), final concentration of 10 μM, was added for 30 min. Following the treatment, cells were washed twice with PBS and disassociated with 0.05% trypsin which was neutralised by adding DMEM. This was followed by centrifugation at 200 g for 3 min. Cell pellets were resuspended in PBS. After washing twice with PBS, cell pellets were

resuspended in PBS containing 1% dialysed FBS. Cathepsin B fluorescent product signal intensity was then analysed using BD Fortessa flow cytometer.

For analysis of LIPA activity, sgControl or sgRNAseK cells were seeded in 60 mm dishes. The next day cells were washed twice with PBS and treated with serum free DMEM for 24 h in the presence of 4-Methylumbelliferyl Palmitate (4-MUP) (Cayman Chemical, 16089) at final concentration of 30 μM Following the treatment, cell were washed twice with PBS and disassociated with 0.05% trypsin which was neutralised by adding DMEM. This was followed by centrifugation at 200 g for 3 min. Cell pellets were washed twice with PBS and resuspended in PBS containing 1% dialysed FBS. 4-MUP fluorescent product signal intensity was then analysed using BD Fortessa flow cytometer.

2.16 Bodipy staining

For analyses of lipid droplets, cells were plated on glass coverslips in 6-well plates for 24 h prior treatment with amino acid-free DMEM for 2 h. Following the treatment, cells were washed twice with PBS and fixed with 3.7% paraformaldehyde (PFA) (Sigma, P6148) in 20 mM HEPES pH 7.5 for 15 min at room temperature in the dark. Fixative was then washed off with PBS and cells were permeabilised using in 0.1% Triton X-100 (Thermo Scientific, 13454259) in PBS for 5 min at room temperature. Cell were washed twice with PBS and incubated with BODIPY™ 558/568 (Invitrogen, D3835) at 0.5 μM final concentration for 10 min in the dark. After washing the coverslips twice with PBS, nuclei were subsequently stained with 4’,6-diamidino-2-phenylindole (DAPI; Sigma, D9542) prior to mounting on microscope slides Prolong Diamond Antifade mountant (Invitrogen, P3696). Microscope slides were left at room temperature for 24 h before acquiring images. Images were acquired on a Nikon A1R point scanning confocal microscope with a 60X objective.

For FACS analyses, cells were seeded in 100 mm dishes. The next day, cells were washed twice with PBS and treated with amino acid-free DMEM for 2 h and BODIPY™ 558/568 at 0.5 μM final concentration was added to cells for 30 min. Following the treatment, cell were washed twice with PBS and disassociated with 0.05% trypsin which was neutralised by adding DMEM. This was followed by centrifugation at 200 g for 3 min. Cell pellets were washed twice with PBS and

resuspended in PBS containing 1% dialysed FBS. BODIPY signal intensity was then analysed using BD Fortessa flow cytometer.

2.17 Lipidomics

For lipidomics analyses, cells were plated in triplicates in 6-well plates for 24 h. Cells were then washed twice with cold PBS and polar solvent [50% methanol (Thermo Scientific, 10767665), 30% acetonitrile (VWR, 83640.290), MS 20% water (Supelco, 1153332500)] was added. To extract lipids, cells were incubated with the solvent on dry ice for 15 min. The extraction solution from each well was then transferred into a 1.5 mL Eppendorf tube and centrifuged at 16 000 g for 10 min at 4°C. The supernatants were transferred to fresh Eppendorf tube and stored at -75°C prior to MS analyses. MS sample preparation and data analyses were performed by Gio Rodriguez Blanco, IGC MS facility.

2.18 Secretome analysis

For analyses of proteins secreted to the media, cells were seeded in 100 mm dishes. The next day, cells were washed twice with PBS and treated with serum-free DMEM supplemented with 2 mM L-glutamine for 24 h. Cell media was collected and cleared by centrifugation at 2000 g for 20 min. Supernatants were then precipitated by the addition of 10% TCA (Sigma, T4885) and incubation for 30 min at 4°C followed by centrifugation at 20,000 g for 15 min at 4°C. Pellets were washed in ice-cold acetone followed by sonication and centrifugation at 20,000 g for 5 min at 4°C. Pellets were resuspended in 6 M guanidine hydrochloride containing 1.5 mg/mL Tris(2-carboxyethyl)phosphine hydrochloride (TCEP) (Sigma, C4706) and 1 mg/mL chloroacetamide (Sigma, C0267) and digested with Lysyl (FUJIFILM Wako Pure Chemicals U.S.A. Corporation, 121-05063) for 4 h at 37°C. Subsequently, samples were digested overnight using Trypsin (Thermo Scientific, 90058). To stop the digestion reaction, Trifluoroacetic acid (TFA) (Thermo Scientific, 28901) was added to the sample followed by vortexing. For desalting of the samples, C18 columns were activated with MeOH, followed by 0.1% TFA wash. Sample were added to the C18 columns and spun at 500 g for 5 min. The C18 columns were washed twice with 50

µL of 0.1% TFA. Samples were eluted from C18 columns with 20 µL of elution buffer (50% acetonitrile, 0.05% TFA). The eluted samples were evaporated in a vacuum concentrator for 20 min and resuspended in 12 µL of 0.1% TFA. The samples were analysed by the core mass spectrometry facility using an Orbitrap Fusion Lumos Tribrid Mass Spectrometer (Thermo Scientific). Data obtained from the MS was analysed using Perseus software.

2.19 DexoMAG lysosomal enrichment

For isolation of lysosome preparations, MEF cells were seeded into 100 mm dishes for 24 h. Next day cells were treated with 10% Dextran coated magnetite (DexoMAG, 40 kDa, Liquids Research Ltd) in complete media. 24 h later, media was replace with fresh complete media and cells cultured for another 24 h. Cells were then pelleted and resuspended in isolation buffer (250 mM sucrose, 10 mM HEPES pH 7.4, 1 mM CaCl2, 15 mM KCl, 1 mM MgCl2, 1.5 mM MgAc, 1 mM DTT) followed by mechanical lysing using a 23G needle and centrifugation at 600 g for 10 min. Supernatants were loaded on a LS magnetic separation column (Miltenyi Biotec, 130-042-401), washed three times in isolation buffer. Magnet was then removed and bound lysosomal fractions eluted using isolation buffer. Lysosomal integrity was confirmed by β-Hexosaminidase enzyme assay (Thelen et al., 2017). β-Hexosaminidase enzyme chromogenic substrate solution (10 mM 4-Nitrophenyl N-acetyl-β-D-glucosaminide (Sigma, N9376) in 0.1 M sodium citrate containing 0.2% (w/v) BSA) was incubated with lysosomal fractions. The enzyme product intensity was measured using microplate reader (Tecan Spark 20) at 405 nm absorbance. Lysosomal fractions containing 1% Triton X-100 were used as a negative control. Once lysosomal integrity was confirmed, proteins were precipitated with 10% TCA (Sigma, T4885) for 30 min at 4°C and centrifuged at 4°C at 20,000 g for 15 min. Pellets were washed in ice-cold acetone and sonicated, which was followed by a 5 min centrifugation at 20,000 g at 4°C. Proteins pellets were frozen on dry ice and sent to Dominic Winter (University of Bonn, Germany) for MS sample preparation and analyses.

2.20 Peptide array

For the ATG2a peptide array, peptide fragments consisting of 15 amino acids (with the overlap length between fragments of 7 amino acids) of mouse ATG2a were bound to cellulose membrane (JPT Peptide Technologies). The membrane with peptide fragments was hydrated in MeOH for 5 min followed by 3 washed with TBST. The membrane was blocked overnight in Superblock T20 (Thermo Scientific, 37536) at 4°C. To asses background binding, the membrane was first incubated with Rabbit IgG-HRP (1:2000 dilution in Superblock T20) for 1 h at room temperature. The membrane was then washed three times for 5 min with TBST and developed using Clarity Western ECL substrate.

For regeneration, the membrane was washed three times, 10 min each, with water. This was followed by incubation with the regeneration buffer (62.5 mM TRIS; 2% SDS; pH adjusted to 6.7 with HCl) at 50°C for 30 min. This process was repeated four times. The membrane was then washed three times with PBS for 20 min, followed by three washes with TBST for 20 min and subsequently three washes with TBS for 10 min, all done at room temperature. The membrane was then blocked overnight in Superblock T20. Subsequently, the membrane was incubated with 0.1 µg/mL Flag-His-ATG16L1 diluted in 3 mL blocking buffer for 3 h at room temperature. The membrane was washed three times for 5 min with TBST and incubated for 3 h in rabbit anti-ATG16L1 antibody solution (1:1000 in Superblock T20). Following primary antibody incubation, the membrane was washed three times for 5 min with TBST and incubated with secondary antibody as described above. The membrane was then washed three times for 5 min with TBST and developed using Clarity Western ECL substrate.

2.21 Statistical analysis

All experiments in this thesis were performed at least three times, unless indicated otherwise. Statistical analyses were performed on Prism 8 (GraphPad) except for MS data statistical analyses which were performed on Perseus software. Microscopy images analyses were performed using ImageJ software.

Chapter 3. Characterisation of autophagy function and cell localisation of RNAseK

3.1 Introduction

As discussed in chapter one, autophagy is a highly complex pathway governed by multiple proteins and protein complexes (Glick et al., 2010). Although significant progress has been made to identify factors crucial for autophagy, it is highly likely that not all regulators are known. Moreover, we do not know the functions of all of the established autophagy players. For example, what is the function of DFCP1 or what are the factors regulating the recruitment and release of already known autophagy regulators to and from autophagic membranes?

Identifying novel proteins regulating autophagy is an exciting area of scientific research. A better understanding of the molecular mechanisms governing autophagy could potentially provide more specific targets for the treatment of various disease, including cancer (Degenhardt et al., 2006). N-terminal tagging of LC3 with GFP has been widely used to monitor autophagic activity in a cell population (Mizushima et al., 2010). Autophagy induction leads to targeting of GFP-LC3 to lysosomes for degradation. This process can be halted by chemical inhibitors of autophagy or by knockout of core autophagy machinery (appendix 1a). Prior to the start of my PhD, I utilised GFP-LC3 reporter to perform a Genome-wide CRISPR-Cas9 screen using a GeCKO library of sgRNAs (Sanjana et al., 2014). MEF cell line stably expressing GFP-LC3 and Cas9 was infected with a library of sgRNAs targeting the whole genome and packaged into lentiviruses. After expansion and selection of cells successfully transduced with sgRNAs, autophagy was induced by amino acid (AA) starvation. A small population of cells retained GFP signal during AA starvation, which indicated autophagy inhibition (appendix 1c). DNA was extracted from GFP-positive cells followed by amplification of sgRNA cassettes and Illumina sequencing (appendix 1b). Amongst a multitude of *Atg* genes, one of the top hits obtained from this screen was *RNAseK*. RNAseK is a poorly characterised transmembrane protein recently reported to be subunit f of the V-ATPase proton pump (Abbas et al. 2020; Perreira et al., 2015). The proton pumping activity of the V-ATPase complex is crucial for autophagic flux, as it ensures acidic milieu of autolysosomes and efficient degradation of IAM and

autophagic cargo by lysosomal hydrolases (Bowman and Bowman, 2002). Genetic, or chemical inhibition of pump complex, results in accumulation of LC3-II within autolysosomal structures (Yim and Mizushima, 2020b; Yoshimori et al., 1991). Interestingly, subunit f of the pump was shown to be dispensable for the assembly and proton pumping of the complex (Mazhab-Jafari et al., 2016). Moreover, depletion of RNAseK does not lead to increased alkylation of lysosomes (Perreira et al., 2015). This suggests that the GFP-LC3 retention in RNAseK knockout cells, as seen in the forementioned screen, is unrelated to a defect in lysosomal acidification. The localisation of RNAseK in cells appears to vary between species. In human cells, RNAseK was localised to plasma membrane and endosomal pathway, including lysosomes (Abbas et al. 2020; Perreira et al., 2015). However, in grass carp RNAseK was shown to localise to endosome and the ER, but not lysosomes (Sun et al., 2021). The cellular localisation and regulatory network of RNAseK in mouse cells remain to be elucidated.

3.2 Aims and objectives

To better understand the role of RNAseK during autophagy, it is important to characterise the step in autophagy blocked in its absence. Moreover, studies of cell localisation and proteins in proximity of RNAseK would allow to gain an insight into RNAseK dynamics and help define its role in cell homeostasis. Objectives to achieve the aims of this chapter are listed as follows:

1. Characterisation of the autophagy pathway in RNAseK depleted cell. Firstly, the degradation of autophagy markers and autophagic cargo will be monitored in the absence of RNAseK. Moreover, distinct stages of autophagy pathway will be analysed in control and RNAseK knockout cells.
2. The cellular localisation of RNAseK varies between different species, and it is not clear where this protein would localise in a mouse cell line. Moreover, the molecular interactors of RNAseK are poorly characterised. Cellular localisation of RNAseK in MEF cells and the regulatory network of RNAseK will be analysed using endogenously tagged RNAseK-myc MEF cell line and PPIs assays. Understanding the localisation and interactors of RNAseK will help aid identifying its role in autophagy.

3.3 Results

3.3.1 Analysis of the autophagy pathway in the absence of RNAseK

To confirm the results from the genome-wide knockout screen, I aimed to test whether RNAseK is required for autophagy. MEF cells were infected with two different sgRNA constructs targeting RNAseK. To exclude off-target effects of the sgRNAs used in the initial screen, these sgRNA sequences targeted different regions of the *Rnasek* gene. Due to a low quality of commercially available antibodies, the efficiency of the knockout was confirmed by genomic PCR (performed by a former MSc student in Dr Gammoh's group, Tim Michelberger) (data not shown). Since these results were obtained, we have acquired a custom antibody against RNAseK. This antibody was used to check RNAseK knockout efficiency and showed that using either of the two sgRNA against RNAseK results in the protein knockout (figure 3.1a). Western blot analyses of autophagic markers LC3 and p62 showed accumulation of p62 and lipidated form of LC3 (LC3-II) under basal and AA starvation conditions in RNAseK knockout cells compared to control cells (figure 3.1b). In control cells treated with AA starvation together with the lysosomal inhibitor Baf A1, we observed an increased accumulation of LC3-II and p62 in comparison to AA starvation treatment alone. Baf A1 is used as a control of autophagic flux as it disrupts lysosomal acidity and prevents the degradation of autophagy cargo. This allows the measurement of autophagic activity within cells. In cells depleted of RNAseK and treated with AA starvation and Baf A1, LC3-II and p62 levels remained unchanged compared to AA starvation alone, suggesting that autophagic degradation is inhibited in the absence of RNAseK (figure 3.1b). Densitometric analyses of LC3-II and p62 levels in the two RNAseK knockout cells confirmed the significant accumulation of both markers compared to control cells (figure 3.1c,d). Inhibition of autophagic flux in RNAseK knockout cells was also confirmed by BODIPY staining. BODIPY is a fluorescent dye, which has an ability to stain neutral lipids. This characteristic of BODIPY can be used to label lipid droplets (LD) in cells (Rumin et al., 2015). LDs are cellular organelles made of a phospholipid monolayer that surrounds the hydrophobic core of neutral lipids. They serve as lipid storage units and regulate lipid homeostasis. In addition to lipolysis, selective

degradation of LDs by lipophagy regulates lipid homeostasis and LD levels in cells (Schott et al., 2019). Fluorescent imaging of BODIPY in control and RNAseK knockout cells showed an increase in LDs in the absence of RNAseK (figure 3.1e). Subsequently, FACS was used to measure the intensity of BODIPY signal and showed a significant increase in LDs in the absence of RNAseK (figure 3.1f). Altogether, these findings confirm the results of the initial knockout screen and show that RNAseK is an essential factor for autophagic flux. Accumulation of lipidated form of LC3 in absence of RNAseK indicates autophagy is blocked at later stages of the pathway, such as autophagosome closure, fusion with lysosomes or autolysosomal degradation. These stages of the pathway were analysed in cells lacking RNAseK and will be described below.

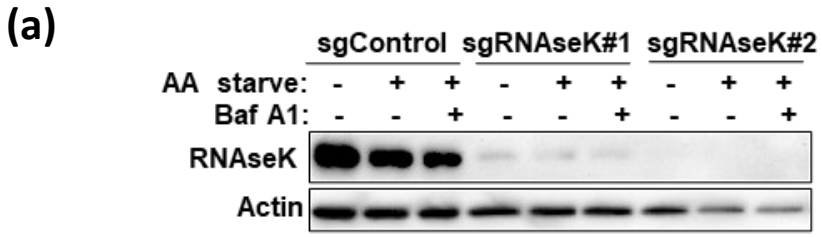
(a)
sgControl
sgRNAseK#1
sgRNAseK#2
AA starve:
Baf A1:
RNAseK
Actin

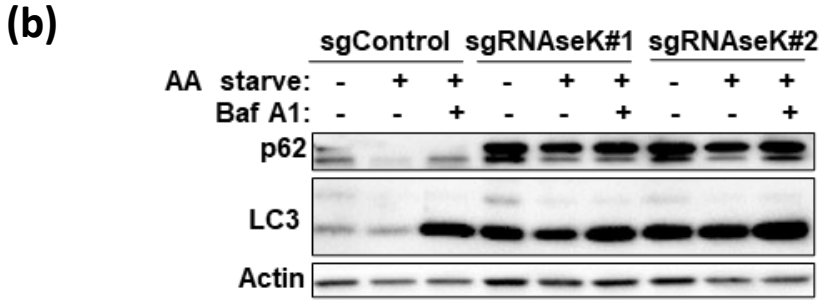
(b)
sgControl
sgRNAseK#1
sgRNAseK#2
AA starve:
Baf A1:
p62
LC3
Actin

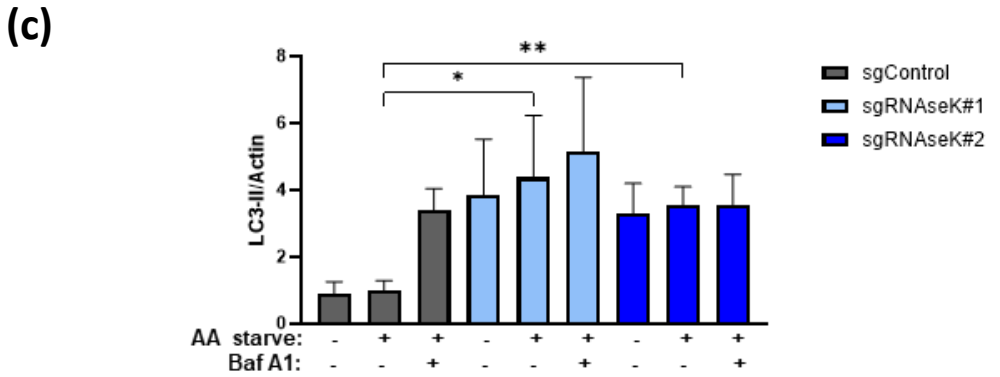
(c)
LC3-II/Actin
AA starve:
Baf A1:
sgControl
sgRNAseK#1
sgRNAseK#2

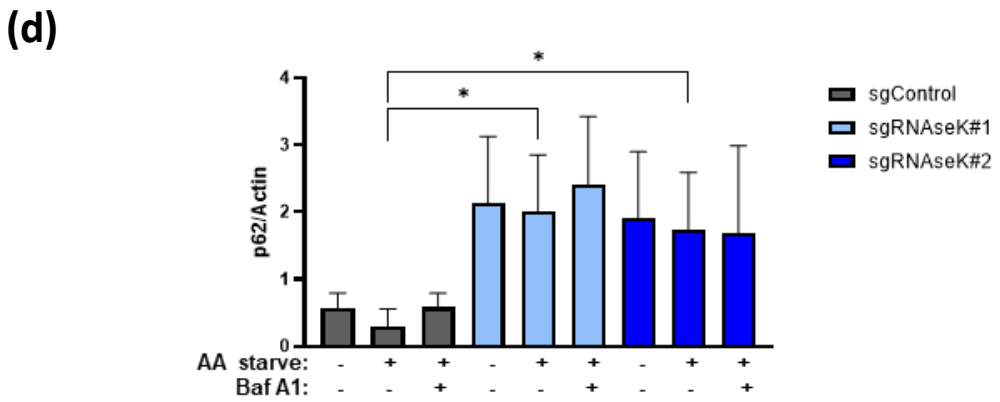
(d)
p62/Actin
AA starve:
Baf A1:
sgControl
sgRNAseK#1
sgRNAseK#2

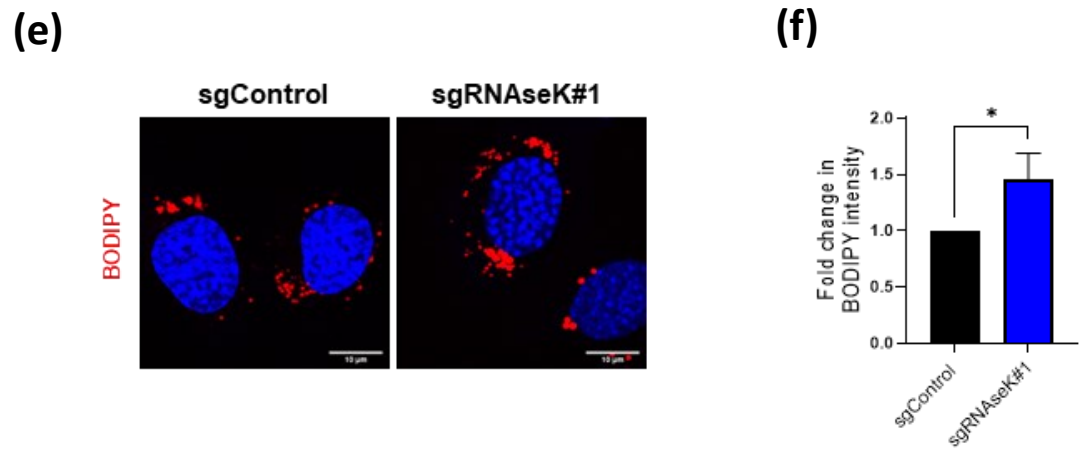
(e)
sgControl
sgRNAseK#1
BODIPY
(f)
Fold change in BODIPY intensity
sgControl
sgRNAseK#1

Figure 3.1 RNAseK knockout results in the accumulation of autophagic cargo.
(a) *Western blot analyses of endogenous RNAseK in sgControl MEF cells and two RNAseK knockout cell lines. Cells were either untreated or AA starved in the presence or absence of Baf A1.* ***(b)*** *Western blot analyses of sgControl and RNAseK knockout cells using the indicated antibodies. Cells were left treated as in (a).* ***(c)*** *Quantification of LC3-II levels normalised to actin in (b).* ***(d)*** *Quantification of p62 levels normalised to actin in (b).* ***(e)*** *Representative images of sgControl and sgRNAseK cells stained with BODIPY.* ***(f)*** *Quantification of BODIPY signal fold change in control and RNAseK knockout cells relative to signal in sgControl cells. In all panels mean + SD is shown from at least three independent experiments. *p<0.05, **p<0.01, assessed by unpaired Student's t-test.*

Defects in autophagosome closure lead to the accumulation of phagophores, drastically reduce fusion rates of the autophagic structures with lysosomes, and block autophagic flux (Takahashi et al., 2018a; Tsuboyama et al., 2016; Velikkakath et al., 2012). As the closure events take place post LC3 lipidation, increased levels of lipidated form of LC3 are observed in cells with autophagosome closure defects (Velikkakath et al., 2012). This accumulation of LC3-II and p62 resembles the phenotype seen in RNAseK knockout (figure 3.1b). To test whether autophagosome closure is disrupted in RNAseK knockout cells, we utilised a proteinase K (PK) protection assay (figure 3.2a). In this assay, cells are treated with AA starvation and Baf A1 to induce autophagic activity without cargo degradation by lysosomal hydrolases. Cells were lysed and incubated with or without PK. Treatment of cell lysates without PK serves as a control of the starting material. Treatment with PK results in degradation of available proteins, including p62 on the growing phagophore, unclosed autophagosome, or cytosol. Once the autophagosome is sealed, the autophagic membrane protects the cargo within from degradation by PK enzyme (Velikkakath et al., 2012). Treatment with PK and Triton X-100 (TX) is used as a positive control for the enzyme activity as TX is a detergent which is able to disturb autophagic membranes. Therefore, treatment with TX exposes p62 from autophagosomes and autolysosomes to the degradative activity of PK. The levels of p62 degradation in the PK assay did not show significant differences between control and RNAseK knockout cells (figure 3.2b,c) suggesting that in cells lacking RNAseK autophagosome closure is intact and that autophagy inhibition happens post closure events.

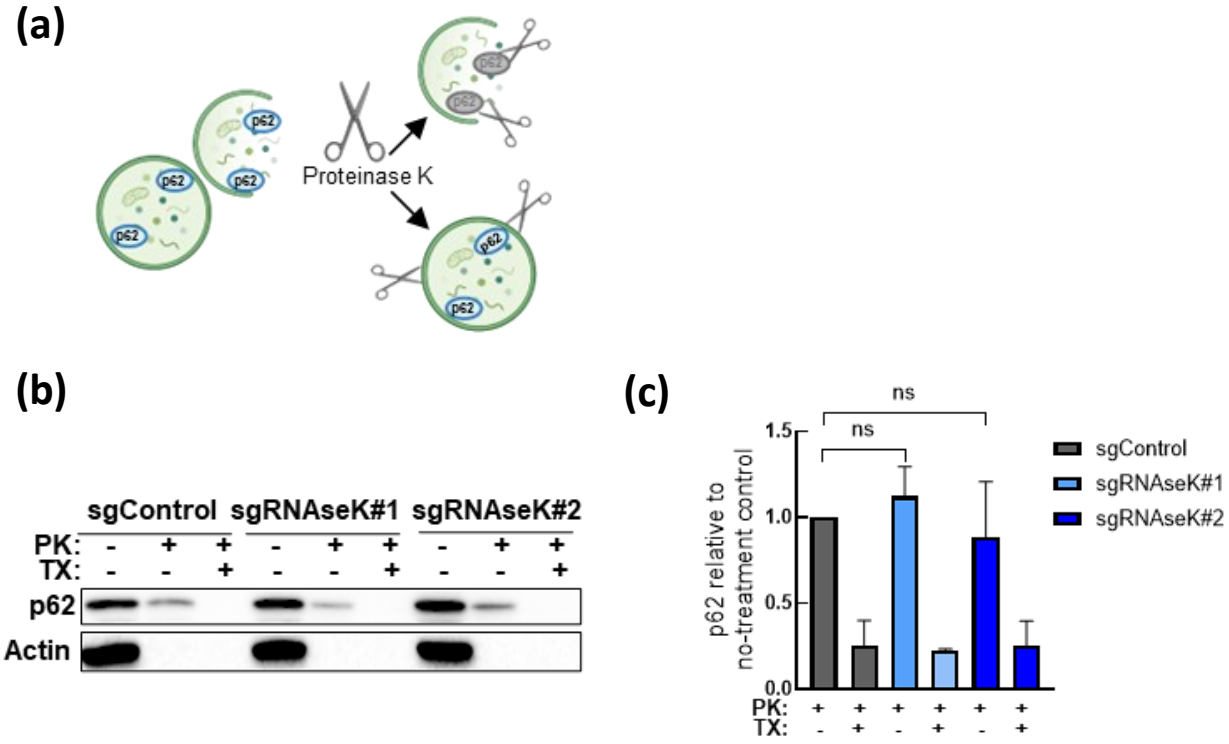

Figure 3.2 RNAseK knockout does not inhibit autophagosome closure.

Schematic diagram of proteinase K (PK) protection assay. Unclosed autophagosome contents are susceptible to PK degradation while closed autophagosomes protect their content from degradation. ***(b)*** *Western blot analyses of sgControl and sgRNAseK MEF cells cultured in AA starvation media and Baf A1 for 3 h. Cell lysates were incubated with buffer only or with PK in the presence or absence of 0.1% Triton (TX).* ***(c)*** *Quantification of (b) with values normalised to buffer only controls. Mean + SD is shown from at three independent experiments. (ns) non-significant, assessed by unpaired Student's t-test.*

To address whether the fusion of autophagosomes with lysosomes is abrogated in the absence of RNAseK, we visualised GFP-LC3 or p62 together with the lysosomal membrane protein LAMP1, a widely used lysosomal membrane marker (Eskelinen, 2006). Fusion defects result in increased levels of autophagic markers and LC3 puncta accumulation adjacent to LAMP1-marked lysosomes (Ebner et al., 2018). Immunofluorescence analyses showed a dramatic accumulation of LAMP1 structures in the absence of RNAseK (figure 3.3a,b). The size of lysosomes appeared to be larger in the RNAseK depleted cells. This lysosomal swelling, resembles the phenotype observed upon treatment with known autophagy inhibitor, Chloroquine (CQ). CQ accumulates in lysosomes which leads to lysosomal alkylation and swelling (Poole

and Ohkuma, 1981). Moreover, fusion between autophagosomes and lysosomes is inhibited in certain cell lines treated with CQ (Mauthe et al., 2018). However, as opposed to cells treated with CQ, in RNAseK knockout GFP-LC3 accumulated within the lysosomal lumen (figure 3.3a). Similar phenotype was observed during siRNA-mediated knockdown of RNAseK knockdown cells and subsequent staining for endogenous p62 and LAMP1 (figure 3.3b). This suggests that although lysosomal morphology appears to be changed in the absence of RNAseK, the fusion events remain intact. Accumulation of autolysosomal structures was confirmed by transmission electron microscopy (TEM). In TEM, high energy beam of electrons is directed at a thin section of the cell (approximately 50-80 nm thickness). Images obtained by TEM have higher magnification and resolution than the images obtained by a confocal microscope (Franken et al., 2017). Whereas in control cells we observed mostly autophagosome structures, in cells depleted of RNAseK, autolysosomal structures accumulated (figure 3.3c). RNAseK knockout phenotype mimics the phenotype seen in control cells treated with Baf A1 (figure 3.3c). This suggests that the absence of RNAseK inhibited autophagy post fusion of autophagosomes with lysosomes and is most likely related to lysosomal function.

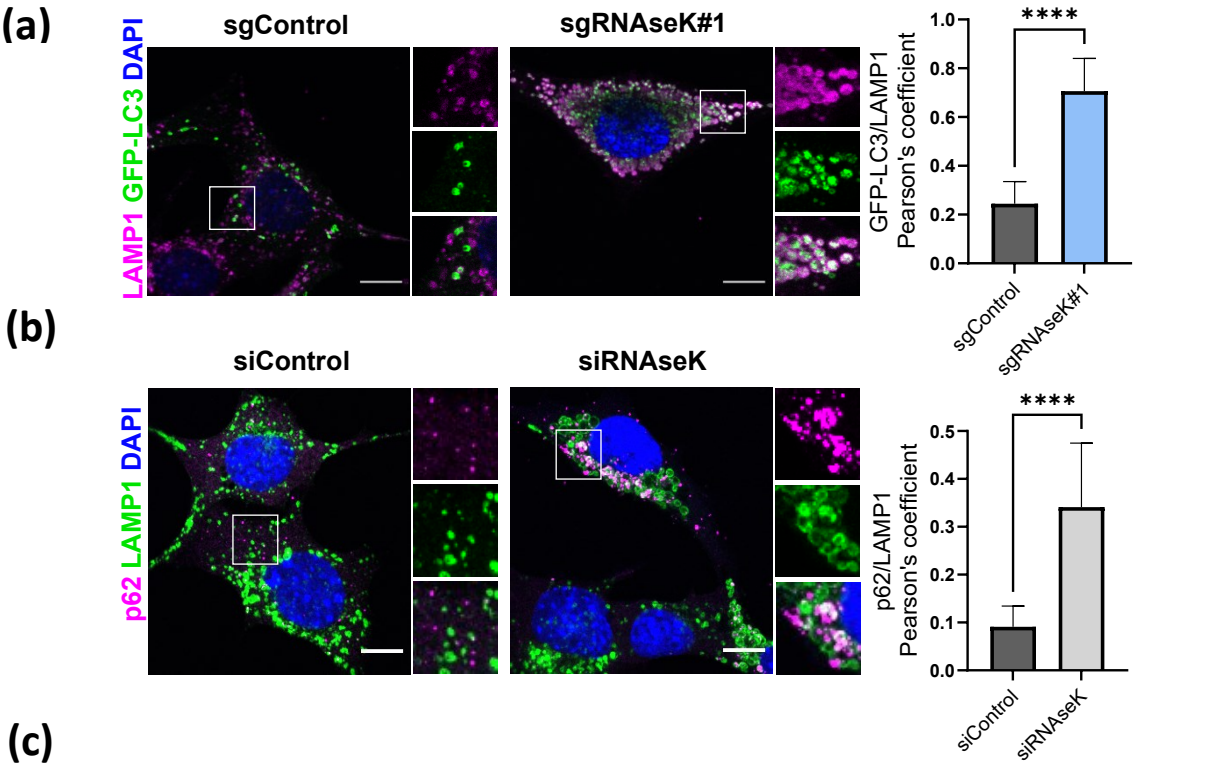
(a)
sgControl
sgRNAseK#1
LAMP1 GFP-LC3 DAPI
GFP-LC3/LAMP1
Pearson's coefficient
****
1.0
0.8
0.6
0.4
0.2
0.0
sgControl
sgRNAseK#1
(b)
siControl
siRNAseK
p62 LAMP1 DAPI
p62/LAMP1
Pearson's coefficient
****
0.5
0.4
0.3
0.2
0.1
0.0
siControl
siRNAseK

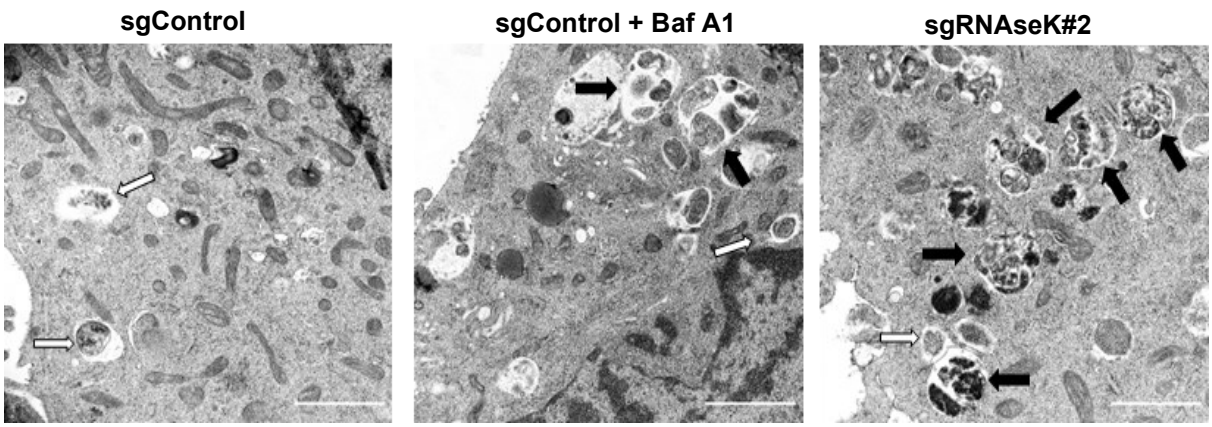
(c)
sgControl
sgControl + Baf A1
sgRNAseK#2

Figure 3.3 RNAseK knockout does not inhibit autophagosome-lysosome fusion.
(a) *Representative immunofluorescence images of GFP-LC3 and endogenous LAMP1 in sgControl or sgRNAseK MEFs cultured in the absence of AAs for 2 h. Scale bar: 10 μm. Quantification of Pearson's colocalization coefficient between GFP-LC3 and LAMP1 is shown on the right.* ***(b)*** *Representative immunofluorescence images of endogenous p62 and LAMP1 in siControl or siRNAseK MEFs treated as in (a). Scale bar: 10 μm. Quantification of Pearson's colocalization coefficient between p62 and LAMP1 is shown on the right. In (a) and (b), mean + SD is shown from at least three independent experiments. **** p<0.0001, assessed by unpaired Student's t-test.* ***(c)*** *Representative electron microscopy images of sgControl and sgRNAseK U2OS cells treated in the absence of AA for 3 h. Baf A1 is added as indicated. Arrows indicate autophagosomes (white arrows) and autolysosomes (black arrows). Scale bar: 1 μm.*

3.3.2 Investigating the role of RNAseK in IAM degradation

Autophagosome-lysosome fusion is facilitated by the SNARE protein STX17. STX17 localises to several cellular compartments, such as mitochondria, ER and cytosol (Koyama-Honda and Mizushima, 2022). During autophagy, autophagosome closure results in the translocation of STX17 to the closed autophagosome, to promote fusion with lysosomes (Itakura et al., 2012). Once the fusion is complete, the subsequent stage of autophagy is the degradation of IAM. STX17 was shown to associate with autolysosomes post fusion and the disassociation of STX17 from the autolysosomes is triggered by IAM degradation (Tsuboyama et al., 2016). These characteristics of STX17 can be used to study IAM degradation. To check whether this stage of autophagy is blocked in the absence of RNAseK, we used a previously described technique whereby STX17 is co-localised with LysoTracker (figure 3.4a) (Tsuboyama et al., 2016). LysoTracker stains acidic compartments in cells such as lysosomes. Based on the staining pattern of LysoTracker, autolysosomes containing intact IAM can be visualised as ring structures during LysoTracker staining. Once IAM is degraded and the acidic mileu of lysosomes enters the autophagic lumen, LysoTracker localisation will change to dot-like structures (figure 3.4a) (Tsuboyama et al., 2016). LysoTracker signal was detected in RNAseK knockout cells, indicating that the acidity of lysosomes is not abrogated in these cells (figure 3.4b). When compared

to control cells, RNAseK knockout cells exhibited a significant increase of STX17 positive LysoTracker rings and a decrease in LysoTracker dots (figure 3.4b). These data indicate that IAM degradation is blocked in the absence of RNAseK.

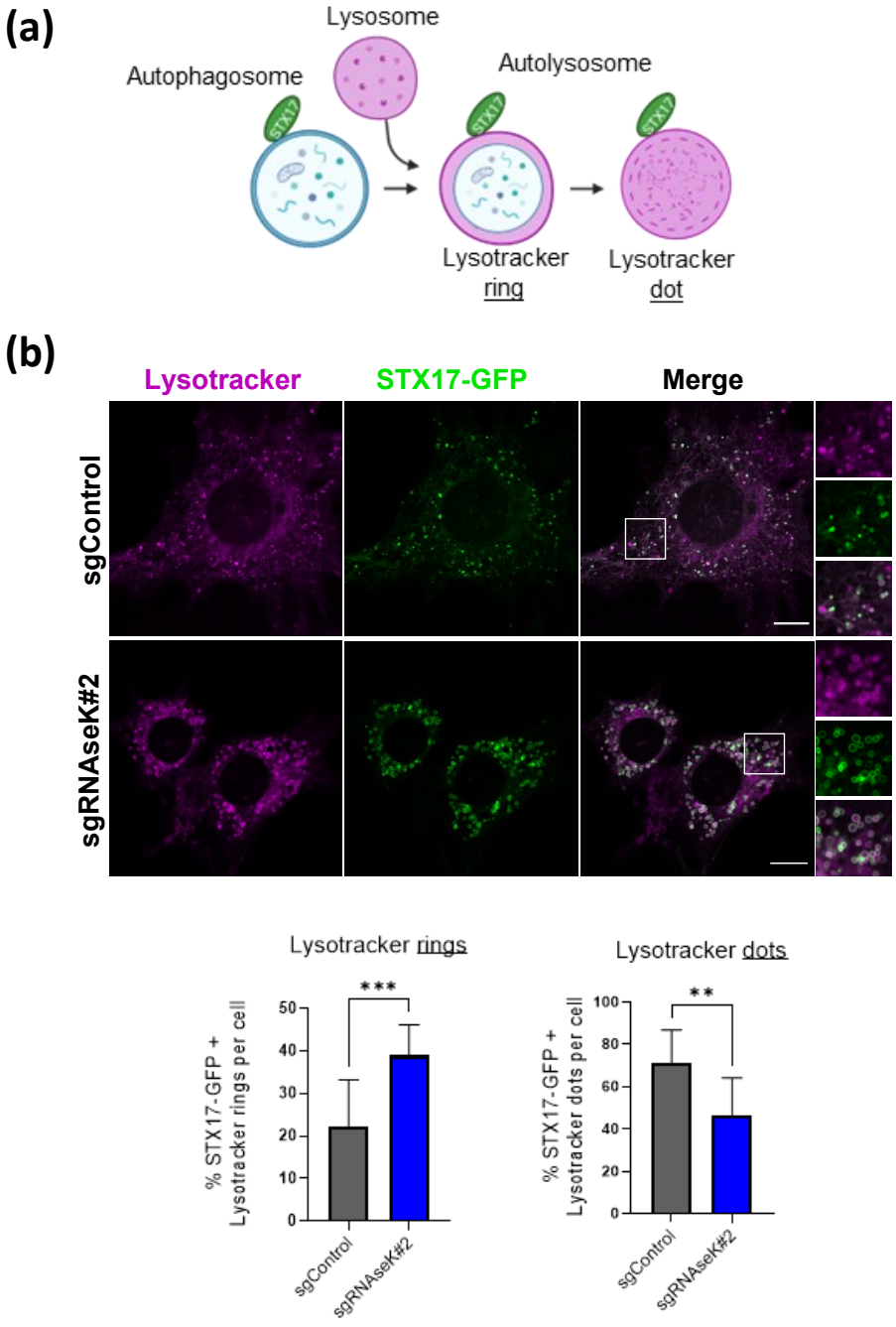

Figure 3.4 RNAseK knockout inhibit IAM degradation.

(a) *Model for studying IAM degradation whereby STX17 association with undegraded or degraded autolysosomes are observed as a lysotracker ring or dots, respectively.* ***(b)*** *Representative images of sgControl and sgRNAseK MEFs stably expressing STX17-GFP and stained with Lysotracker red. Quantifications of the percentage of STX17 with Lysotracker rings or dots are shown below, mean + SD is shown from at least three independent experiments. **p<0.01, ***p<0.001, assessed by unpaired Student's t-test. Scale bar: 10 μm.*

3.3.3 Dissecting the cellular localisation of RNAseK

The cellular localisation of RNAseK varies between species (Perreira et al., 2015; Sun et al., 2021). Therefore, it was crucial to gain a better understanding of the cellular localisation of RNAseK in mouse cells used in my experiments. As overexpression of proteins may not be representative of endogenous protein activities (Moriya, 2015), I generated an endogenously tagged RNAseK-myc cell line. Endogenous tagging minimises genomic disruption and can be achieved by CRISPR-Cas9 mediated knock-in of a DNA fragment into the genome (Koch et al., 2018). To edit endogenous sequence of *Rnasek* we used an sgRNA targeting the C-terminus of *Rnasek* gene to direct the Cas9 nuclease and a single stranded synthetic DNA containing myc tag sequence followed by a stop codon and flanked by homology arms based on the 3'end of *Rnasek*. MEF cells were transfected with these constructs and single clones were amplified. The efficiency of the knock-in in the single clones was checked by sequencing of the amplified DNA fragments (figure 3.5a). Expression of RNAseK-myc was confirmed by western blot analyses, whereby RNAseK was detected at a correct molecular weight using an antibody against myc tag (figure 3.5b). Endogenous tagging of RNAseK was shown not disrupt its function in autophagy, as demonstrated by LC3 turnover (figure 3.5b). Expression of RNAseK-myc was also confirmed by immunofluorescence using an antibody against myc and showed a punctate cytosolic localisation (figure 3.5c).

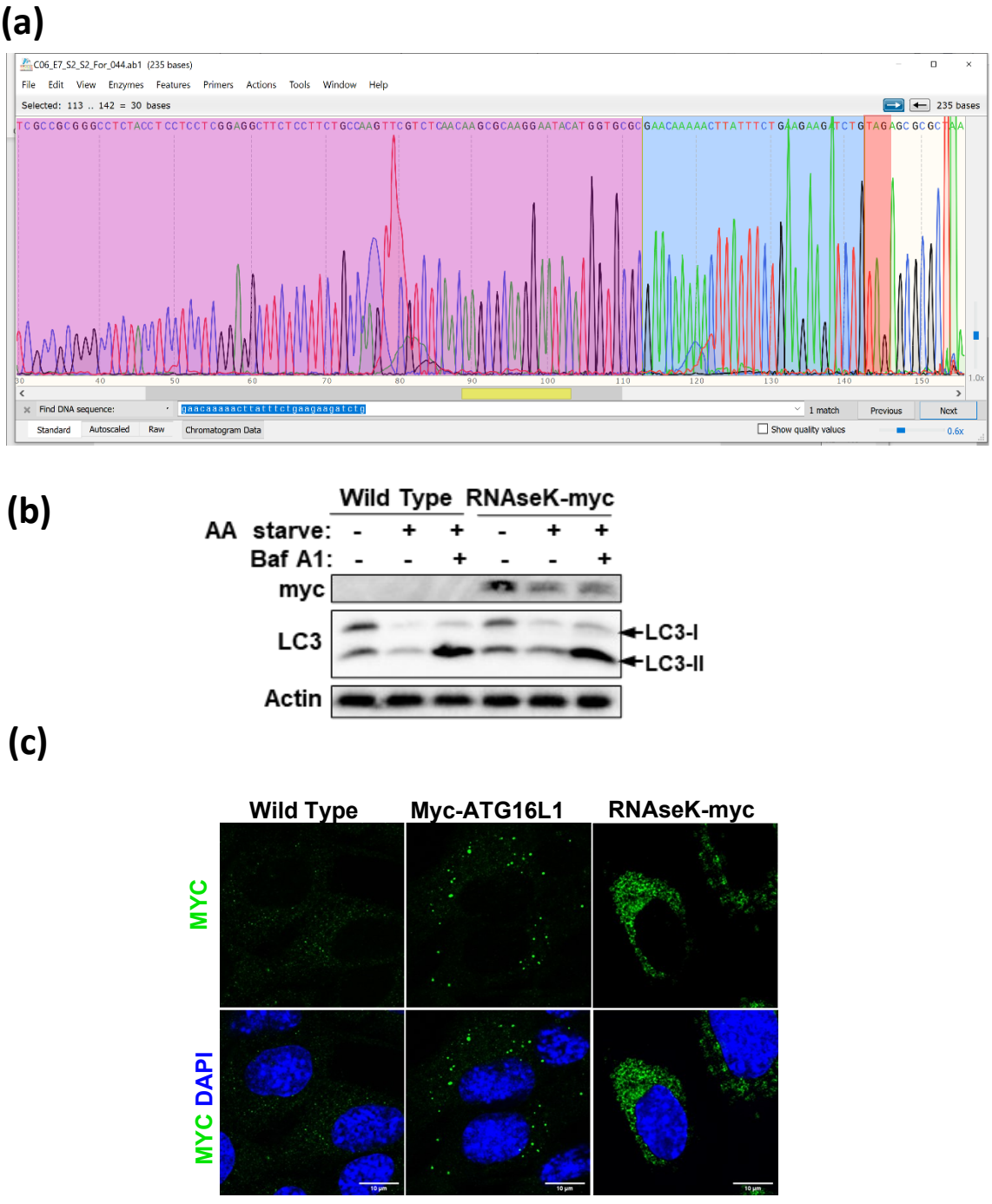

Figure 3.5 Validation of RNAseK-myc cell line.

(a) Sequencing histogram of C-terminus of endogenous RNAseK. Genomic RNAseK sequence is represented in purple, myc tag is highlighted in blue, followed by STOP codon in orange. (b) Western blot analyses of wild type and RNAseK-myc tagged MEF cells using the indicated antibodies. Cells were untreated or AA starved for 2 h in the presence or absence of Baf A1. (c) Representative immunofluorescence images of wild type cells or cells expressing ATG16L1-myc (positive control for myc staining) or RNAseK-myc stained using the indicated antibodies. Cells were cultured in the absence of AAs for 2 h. Scale bar: 10 μm.

Following their validation, RNAseK-myc cells were used for immunofluorescence analyses to determine the subcellular localisation of RNAseK (figure 3.6a-e). In agreement with previous reports in human cells, RNAseK-myc showed a high degree of co-localisation with late endosome and lysosome markers, RAB7 and LAMP1, respectively (figure 3.6a,b). In addition to these cellular compartments, RNAseK showed a significant co-localisation with the Golgi apparatus marker GM130 and also a partial co-localisation with the autophagy markers, ATG9 and ATG16L1 (figure 3.6c-e). These results suggest that RNAseK could shuttle within the cell and interact with proteins at multiple organelles. RNAseK-myc cell line was also subjected to a pulldown experiment using anti-myc antibodies. Proteins that co-precipitated with the bait were analysed using MS. The results obtained from the MS analyses were plotted according to their fold change and statistical significance relative to the wild type MEFs used as negative control (figure 3.6f). RNAseK showed association with multiple subunits of the V-ATPase complex and late endosomal/lysosomal proteins, such as LAMTOR proteins, which supports the subcellular localisation of RNAseK analysed in this thesis and in published reports (Abbas et al.; Hackett and Cherry, 2018; Perreira et al., 2015).

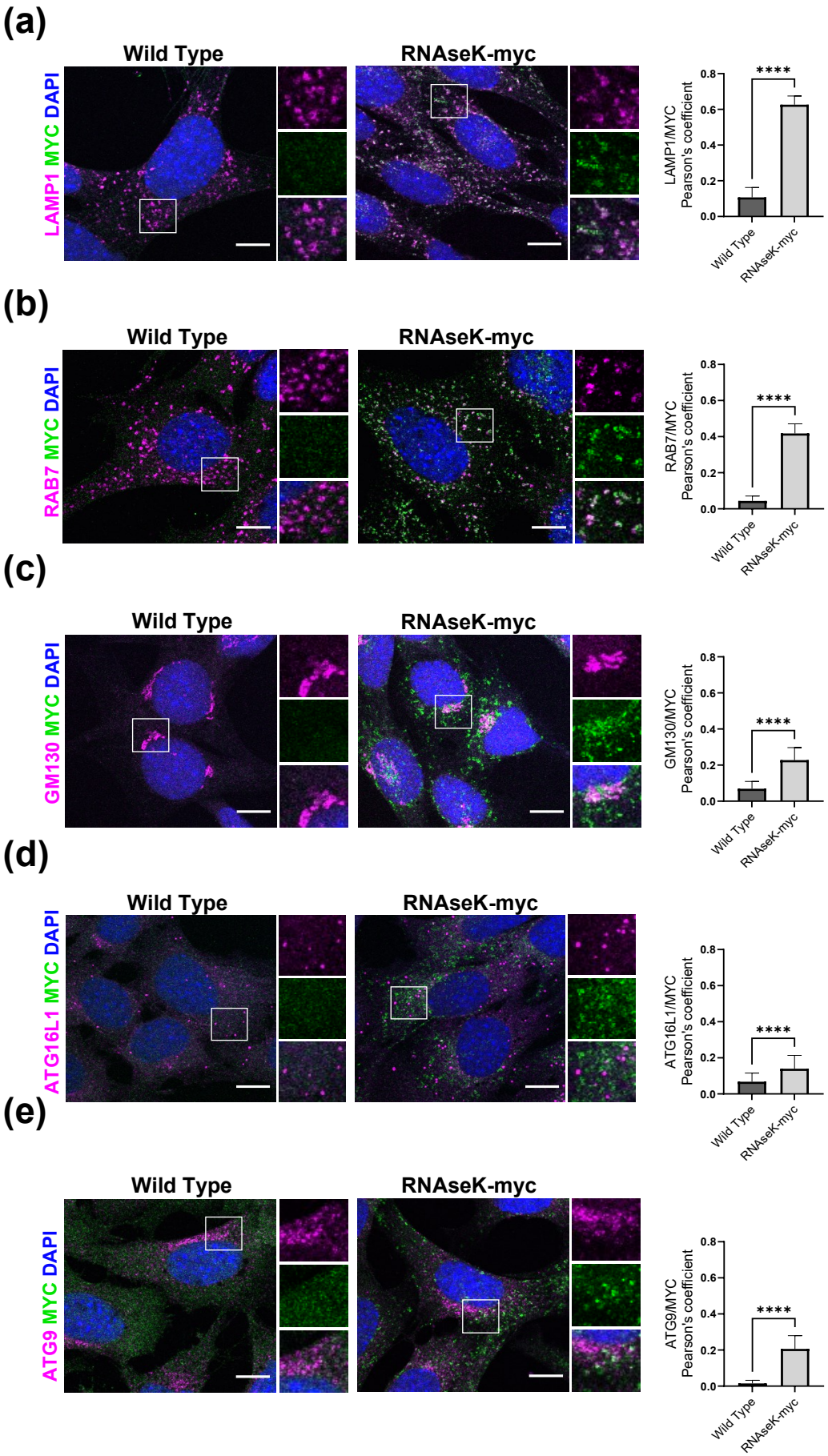
(a)
Wild Type
RNAseK-myc
LAMP1 MYC DAPI
LAMP1/MYC Pearson's coefficient
****
Wild Type
RNAseK-myc
(b)
Wild Type
RNAseK-myc
RAB7 MYC DAPI
RAB7/MYC Pearson's coefficient
****
Wild Type
RNAseK-myc
(c)
Wild Type
RNAseK-myc
GM130 MYC DAPI
GM130/MYC Pearson's coefficient
****
Wild Type
RNAseK-myc
(d)
Wild Type
RNAseK-myc
ATG16L1 MYC DAPI
ATG16L1/MYC Pearson's coefficient
****
Wild Type
RNAseK-myc
(e)
Wild Type
RNAseK-myc
ATG9 MYC DAPI
ATG9/MYC Pearson's coefficient
****
Wild Type
RNAseK-myc

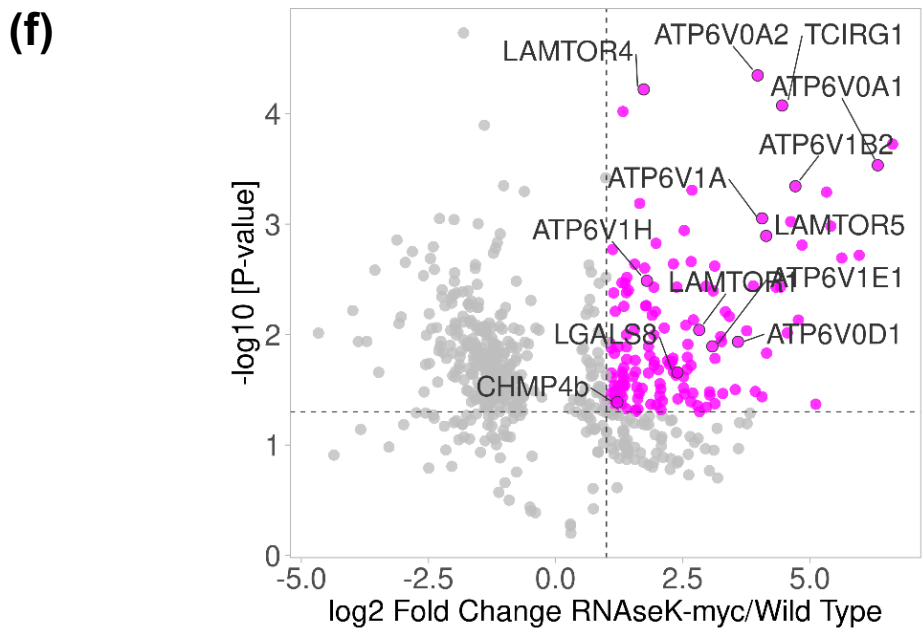

Figure 3.6 RNAseK localises to multiple cell compartments.

(a-e) *Representative immunofluorescence images of wild type or RNAseK-myc MEFs cultured in AA free media for 2 h. Cells were fixed and stained against myc and the indicated endogenous protein. Scale bar: 10 µm. Quantifications of Pearson's colocalization coefficient between RNAseK-myc and the indicated markers are shown on the right. In all panels, mean + SD is shown from at least three independent experiments. ****p<0.0001, assessed by unpaired Student's t-test.* ***(f)*** *Volcano plot analyses of RNAseK-myc pulldown hits identified by MS presented as relative values to hits obtained from wild type cells. Significant hits (P > 0.05; Fold Change > 2) are represented in magenta.*

3.3.4 Identifying RNAseK interaction network

The above results suggest that RNAseK does not reside in a single cellular compartment but co-localises with different cellular markers including autophagy players. To confirm the results from the IP MS and to investigate any transient interactions of RNAseK, I generated an RNAseK constructs with a C-terminal TurboID-myc tag. Overexpression of RNAseK-myc-TurboID or empty-myc-TurboID constructs in MEF cells was confirmed by western blot analyses. Both of the constructs were detected at the correct molecular size using anti-myc antibody (figure 3.7a). Correct cellular localisation of RNAseK-myc-TurboID protein was confirmed by immunofluorescence analyses, where it co-localised with the late endosomal marker

RAB7, whereas cells expressing empty-myc-TurboID showed a diffused localisation (figure 3.7b).

The validated cell lines were treated with AA free media and exogenous biotin, followed by pulldown using streptavidin-coupled beads. The biotinylated proteins were analysed by MS. Similar to RNAseK-myc IP MS analyses, hits from TurboID MS were plotted according to fold change and statistical significance (figure 3.7c). Multiple positive controls were highly biotinylated in RNAseK-myc-TurboID cells, including V-ATPase proton pump subunits and lysosomal membrane proteins (figure 3.7c). Amongst the significantly biotinylated proteins were also the Golgi apparatus protein (GPR89) and endosomal trafficking pathway protein (SNX11) (figure 3.7c). Gene ontology analyses of biological processes of proteins enriched in RNAseK-myc-TurboID cell line showed vesicle mediated transport as one of the most common process associated with proteins in proximity to RNAseK (figure 3.7d).

Comparison of top hits identified by MS in the forementioned pulldown and proximity labelling experiments of RNAseK showed enrichment of multiple proteins in both experimental settings. Majority of overlapping hits were lysosomal proteins such as LAMTOR and subunits of V-ATPase proton pump (figure 3.8). Interestingly, multiple LEM-domain proteins were also identified including EMD, LEMD3 and TMPO (figure 3.8). These proteins reside on the inner nuclear membrane which furthers confirm that RNAseK is not confined to the lysosomes and associates with proteins residing on various membranous compartments in cells.

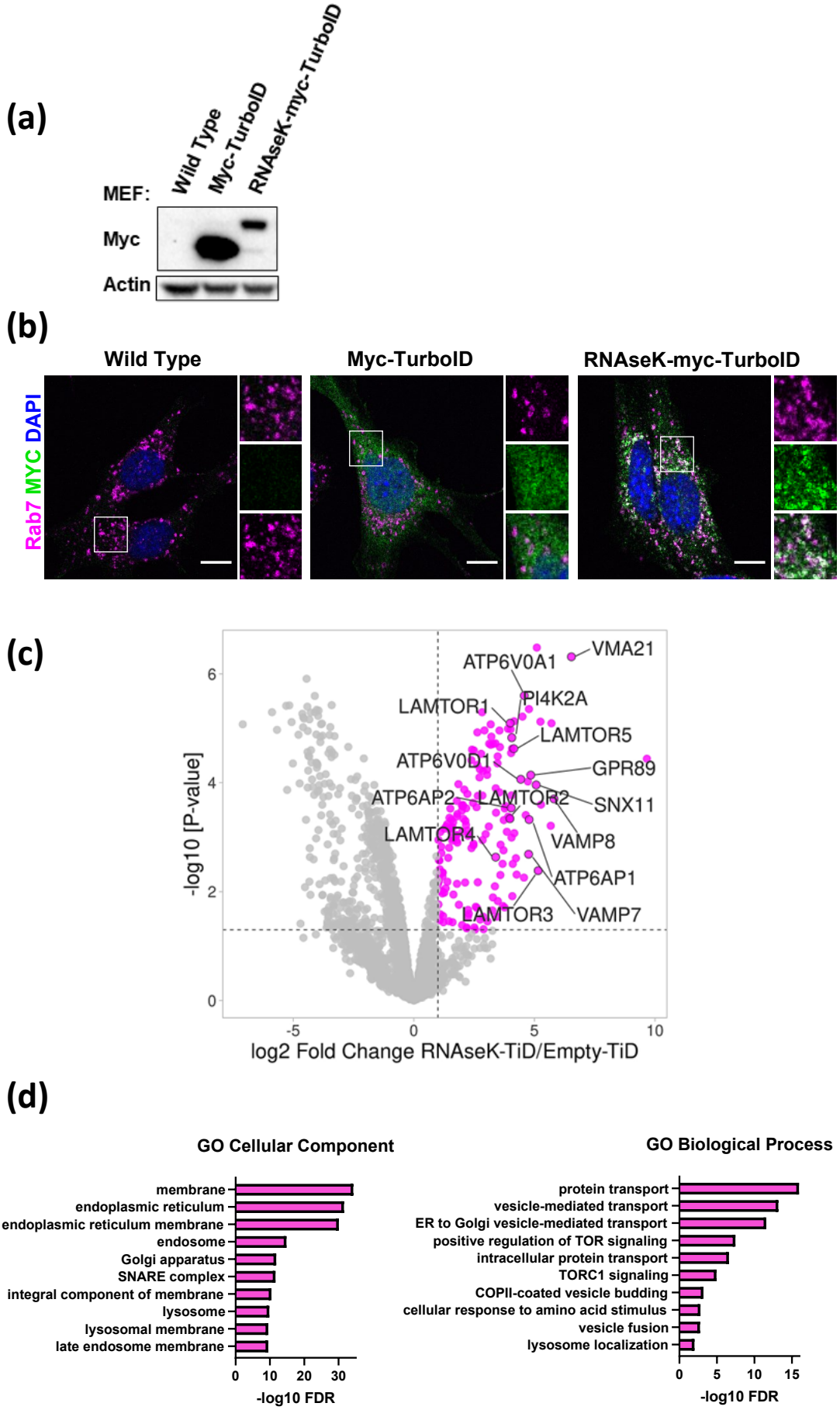
(a)
Wild Type
Myc-TurboID
RNAseK-myc-TurboID
MEF:
Myc
Actin
(b)
Wild Type
Myc-TurboID
RNAseK-myc-TurboID
Rab7 MYC DAPI
(c)
VMA21
ATP6V0A1
PI4K2A
LAMTOR1
LAMTOR5
ATP6V0D1
GPR89
ATP6AP2
LAMTOR2
SNX11
LAMTOR4
VAMP8
ATP6AP1
LAMTOR3
VAMP7
-log10 [P-value]
log2 Fold Change RNAseK-TiD/Empty-TiD
(d)
GO Cellular Component
membrane
endoplasmic reticulum
endoplasmic reticulum membrane
endosome
Golgi apparatus
SNARE complex
integral component of membrane
lysosome
lysosomal membrane
late endosome membrane
-log10 FDR
GO Biological Process
protein transport
vesicle-mediated transport
ER to Golgi vesicle-mediated transport
positive regulation of TOR signaling
intracellular protein transport
TORC1 signaling
COPII-coated vesicle budding
cellular response to amino acid stimulus
vesicle fusion
lysosome localization
-log10 FDR

Figure 3.7 RNAseK is in proximity of proteins on multiple membranous compartments.
(a) *Western blot analyses of wild type, myc-TurboID and RNAseK-myc-TurboID expressing cells using the indicated antibodies.* ***(b)*** *Representative immunofluorescence images of wild type cells or cells expressing myc-TurboID or RNAseK-myc-TurboID stained using the indicated antibodies. Cells were cultured in the absence of amino acids for 2 h. Scale bar: 10 µm.* ***(c)*** *Volcano plot analyses of RNAseK-TurboID (TiD) proximity labelling hits identified by MS presented as relative values to hits obtained from TurboID empty cells. Significant hits (P > 0.05; Fold Change > 2) are represented in magenta.* ***(d)*** *Top 10 cellular components (left) and biological processes (right) of top hits obtained in (F). GO enrichment analysis plotted according to −log10 False Discovery Rate (FDR). The statistical significance was calculated by a one-way Fisher's exact test.*

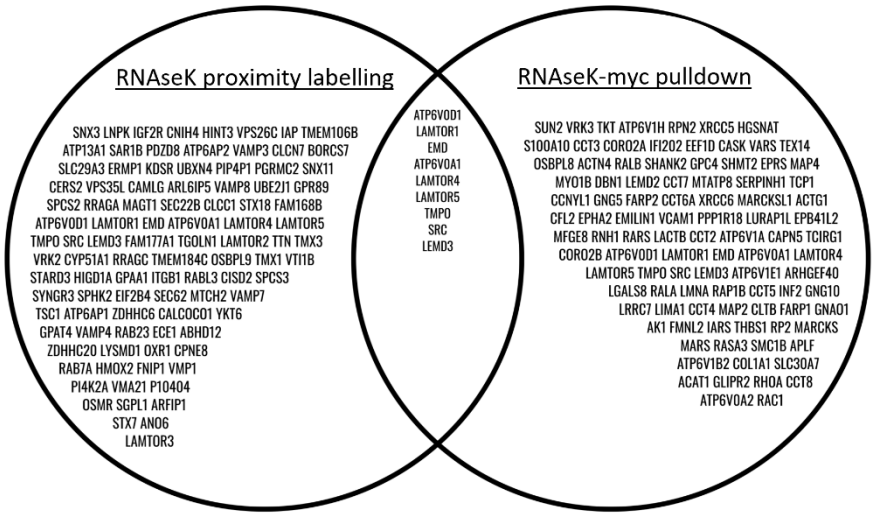

Figure 3.8 Comparison of top hits identified in pulldown and proximity labelling of RNAseK.
Venn diagram of top hits identified by MS from RNAseK proximity labelling (left) and RNAseK-myc pulldown (right). Overlapping hits are shown in the middle.

3.4 Discussion

This chapter has highlighted a role of RNAseK in autophagy and gave an insight into the cellular localisation of RNAseK. RNAseK knockout leads to the accumulation of autophagic markers LC3 and p62 and was shown to be crucial for an efficient autophagic flux. This result potentially contradicts a study on Vma7, the yeast homologue of RNAseK, where it was shown to be dispensable for mitophagy (Mijaljica et al., 2011). The difference in the observed phenotypes, could explained by relatively low homology between the two proteins. Moreover, functions of autophagy proteins

can vary between yeast and mammals, for example Atg18 protein in yeast is crucial for autophagy, whereas the mammalian homologue of Atg18, WIPI4 is dispensable for an efficient autophagic flux (Suzuki et al., 2007; Tang et al., 2019). Immunofluorescence analyses of endogenously tagged RNAseK showed a partial co-localisation with ATG16L1. However, the build-up of LC3-II and no accumulation of LC3-I in RNAseK knockout cells indicate that RNAseK does not regulate the function of the conjugation machinery and the autophagy block takes place post the lipidation events. Although RNAseK co-localises with ATG9, which is involved in phagophore elongation, this process is also intact in cells depleted of RNAseK. EM images of autophagic structures accumulating in RNAseK knockout cells do not resemble phagophore elongation defects (Tamura et al., 2017). Autophagosome closure was tested by measuring levels of p62 protected from digestion by proteinase K. P62 was partially protected from digestion by this enzyme, in both control and RNAseK knockout cells. P62 is involved in other cellular functions, such as the delivery of ubiquitylated proteins to the proteasome for degradation, which explains only partial protection by autophagic membranes (Liu et al., 2016). It is possible for unclosed autophagosome to still fuse with the lysosome, which would protect p62 from the degradation by proteinase K (Tsuboyama et al., 2016). However, fusion rate of on open autophagic structures with lysosomes in significantly lower than closed autophagosome and it would lead to increased levels of p62. Altogether, these observations indicate, that the elongation and closure of autophagosomes are intact in cells lacking RNAseK.

Immunofluorescence analyses of autophagic players with LAMP1 were used to study the fusion between autophagosomes and lysosomes in control and RNAseK knockout cells. Disruption in fusion events leads to accumulation of cargo receptor proteins adjacent to lysosomes (Ebner et al., 2018). In RNAseK knockout, both LC3 and p62 accumulated within LAMP1 structures. This suggests that autophagosomes undergo fusion with lysosomes regardless of RNAseK status. Moreover, the accumulation of LC3 in autolysosomal lumen confirms a block in autophagy rather than CASM, where LC3 is found on the lysosomal membrane, instead of the lysosomal lumen (Hooper et al., 2022). To exclude CASM, further studies are required such as analyses of LC3 lipidation and degradation upon RNAseK depletion in autophagy deficient cells such as ATG13 knockout cells.

Autophagosome-lysosome fusion is facilitated by STX17 localised to the autophagosomal membrane. Once fused with the lysosomes, IAM is degraded by the lysosomal hydrolases, which triggers STX17 release from autolysosomes (Tsuboyama et al., 2016). In cells lacking RNAseK, we observed accumulation of STX17 on autolysosomes denoted with LysoTracker signal. Although RNAseK associates with multiple fusion machinery and could potentially regulate STX17 detachment from autolysosomes, I concluded that STX17 phenotype seen in RNAseK knockout is due to impairment of IAM degradation. This is due to the accumulation of LysoTracker rings with STX17 and decrease of LysoTracker dot structures, which indicate the presence of IAM and reduced influx of lysosomal hydrolases to autophagosomal lumen. Molecular machinery governing IAM degradation is poorly characterised and tools to study IAM are limited, therefore it is difficult to confirm this hypothesis using alternative methods. EM images show the accumulation of autolysosomes, similar to Baf A1 treated cells, but whether these structures contain IAM is open to interpretation. Lysosomes of RNAseK knockout cells, stained positive for LysoTracker, in agreement with previous reports (Perreira et al., 2015). This characteristic could be used to confirm the presence of lysosomal lumen ring in autolysosomes of RNAseK knockout cells, by visualising LysoTracker using correlative light and electron microscopy (CLEM). However, this method is technically challenging and is not easily accessible. It would be interesting to test, whether this membrane degradation defect in lysosomes is specific to autophagic membranes. Is the degradation of ILVs, delivered to lysosomes via MVBs, disrupted in cells lacking RNAseK? Could these two processes be regulated by RNAseK activity or is RNAseK exclusively involved in IAM degradation? Investigation of membrane composition differences between the two compartments would help to access specificity of RNAseK in membrane degradation processes.

Autolysosomes appear to increase in size in RNAseK knockout cell line. Lysosomal swelling can lead to lysosomal membrane permeabilization and reduction in degradative function of the lysosome (Wang et al., 2018). It remains to be elucidated whether lysosomal swelling occurs due to autophagic cargo accumulation within the autolysosomes or this change of lysosomal morphology is autophagy-independent. This could be clarified by imaging of LAMP1 upon RNAseK depletion in autophagy

deficient cells such as ATG13 knockout cells or cells treated with autophagy inhibitors (e.g. VPS34 inhibitor).

Recent structural analyses identified RNAseK as a subunit f of lysosomal V-ATPase proton pump (Abbas et al. 2020). RNAseK was shown to localise to lysosomes and plasma membrane (Abbas et al. 2020; Perreira et al., 2015). Immunofluorescence and proteomics analyses of tagged RNAseK, confirmed its localisation to the lysosomes and late endosomes. However, RNAseK is not confined to those organelles and showed association with proteins on Golgi apparatus, ER, nuclear membrane and endocytic vesicles. Interestingly, plasma membrane proteins were not amongst top hits in our RNAseK analyses. Could RNAseK be translocated to the plasma membrane upon viral infection but on most occasions shuttle between the intracellular organelles? It would be interesting to investigate the significance of RNAseK co-localisation with ATG9. ATG9 was shown to be involved in trafficking of lysosomal proteins (Jia et al., 2017). Perhaps the potential interaction of ATG9 and RNAseK regulates the localisation of RNAseK. RNAseK exhibited partial co-localisation with organelles where V-ATPase proton pumps are present, such as lysosomes, late endosomes or Golgi apparatus (Toei et al., 2010). It remains to be determined whether RNAseK shuttles between different cell compartments exclusively as a part of the V-ATPase pump or it can disassociate from the complex. Moreover, it is unclear if the function of RNAseK during autophagy depends on its association with the V-ATPase complex.

In addition to lysosomal proteins, comparison of top hits identified in pulldown and proximity labelling of RNAseK revealed enrichment of multiple LEM-domain proteins. These proteins reside on inner nuclear membrane and share a conserved LEM motif (Cai et al., 2001). In-depth analyses of nuclear membrane proteins association with RNAseK could provide insight into regulatory network of RNAseK. For example, it would be interesting to determine whether RNAseK binds to the LEM motif and what would be the consequences of disrupting this binding. Although nuclear pore complexes have been shown to be degraded by selective autophagy (Capella et al., 2020; Lee et al., 2020), enrichment of nuclear membrane proteins seen in proximity labelling and pulldown analyses could also suggest autophagy-independent role of RNAseK in maintaining cellular homeostasis.

Due to the multi-organelle localisation of RNAseK which includes lysosomes, I next aimed to investigate whether the absence of RNAseK could impact lysosomal homeostasis and the ability of lysosomes to degrade autophagosomes. These aspects will be discussed in the next chapter.

Chapter 4. Role of RNAseK in lysosomal homeostasis

4.1 Introduction

As discussed in chapter 1.2, lysosomal homeostasis depends on multiple factors. Maintaining lysosomal acidity is crucial for proper maturation and activation of lysosomal hydrolases (Li et al., 2019). Lysosomal acidity is maintained by lysosomal V-ATPase complex, which pumps protons across the membrane, lowering the pH of the lysosomal lumen (Imamura et al., 2003; Ohkuma and Poole, 1978). Acidic lysosomes are essential for an efficient degradation of autolysosomal cargo (Li et al., 2019). This is represented by numerous studies showing that chemical or genetical modulation of lysosomal pH abrogates autophagic flux (Bagh et al., 2017; Yoshimori et al., 1991). Indeed, Baf A1, which inhibits the assembly of lysosomal V-ATPase proton pump, is commonly used as an autophagy inhibitor (Mizushima et al., 2010)

Degradation of cargo within lysosomes can be an end point to pathways other than autophagy, such as endocytosis (Sigismund et al., 2008). Therefore, disrupting lysosomal acidity inhibits multiple processes and has a more global effect on a cell function. From a therapeutic perspective, specifically inhibiting autophagy without disrupting other processes within the lysosomes, would be beneficial.

Lysosomal homeostasis is also ensured by an efficient delivery of hydrolases to the lysosome (Staudt et al., 2016). Canonical pathway of lysosomal enzyme delivery is based on receptor proteins CD-MPR and CI-MPR, which recognise and bind the enzymes within the TGN and facilitate their delivery to the lysosomes. Upon exposure to the acidic environment of late endosomal compartments, the receptors disassociate from enzymes and are recycled back to TGN or the plasma membrane (Haft et al., 1998, 2000; Olson et al., 2008). This uncoupling of enzymes from receptors is crucial for a proper maturation of the hydrolases. Maturation involves cleavage of a pro-enzyme, which results in the formation of a mature and active hydrolase (Laurent-Matha et al., 2006; Pungercar et al., 2009). Disruption of enzyme delivery and maturation can result in an impairment of the degradative function of lysosomes (Qian et al., 2008).

Lysosomal hydrolases can be categorised based on their substrates. Activity of a lysosomal family of proteases called cathepsins is crucial for maintaining lysosomal homeostasis. In addition to cargo degradation delivered to the lysosomal lumen, cathepsins are also involved in the maturation of hydrolases released from MPRs. Disruptions in cathepsin function has been associated with Juvenile Batten disease (table 1.1). Moreover, abrogated trafficking of Cathepsin D and Cathepsin L was shown to result in the accumulation of autophagy markers (Jia et al., 2017).

Although the role of lysosomal lipases in autophagy is not well characterised, there is a clear connection between lipases and autophagy. LIPA has been shown to facilitate degradation of LDs delivered to lysosomes via autophagy (Zhang et al., 2022). Moreover, lipid imbalances in lysosomes can inhibit autophagic flux (Maharjan et al., 2022; Sarkar et al., 2013). It is highly likely that IAM degradation, which proceeds the hydrolytic degradation of autophagic cargo, depends on lipases activity. However, mammalian lipases involved in this this process have not been identified thus far.

Numerous studies have shown that a disruption of lysosomal homeostasis, results in changes in protein secretion. Alkalisation of the lysosomal milieu by chemical modulators, such as Baf A1 or CQ, increases the secretion of extracellular vesicles (EVs) (Alvarez-Erviti et al., 2011). Moreover, abnormal cholesterol accumulation in the lysosomal lumen, as seen in Niemann Pick Type C disease, was shown to correlate with an increase in EV release (Strauss et al., 2010). Lysosomal accumulation of VPS4a, which ordinarily associates with lysosome in a transient manner, was also shown to cause hypersecretion of proteins (Hasegawa et al., 2011). Altogether, these published findings suggest that biochemical properties of lysosomes and lysosomal proteome play an important role in regulating cell secretome.

4.2 Aims and objectives

RNAseK is a subunit of V-ATPase proton pump and associates with multitude of lysosomal proteins (figure 3.7) (Abbas et al., 2020; Perreira et al., 2015). In the previous chapter, I have shown that the knockout of RNAseK results in the disruption of IAM degradation and the accumulation of autolysosomes, indicating alerted lysosomal function (figure 3.4). Therefore, the aim of this chapter is to define the role

of RNAseK in lysosomal biology. Objectives to achieve the aims of this chapter are as follows:

1. Firstly, I will test whether the absence of RNAseK can affect lysosomal acidity and proteases function. Lysosomal acidity will be tested using a pH-dependent, fluorescent dye. Maturation and activity of the lysosomal protease Cathepsin B will be assessed by western blot analyses and ability to cleave a fluorogenic substrate, respectively. A more general proteolytic activity of the lysosomes, will be assessed by monitoring the degradation rates of EGF receptor (EGFR) delivered to the lysosomes via endocytosis.
2. As IAM degradation requires the activity of lipases, I will test whether RNAseK knockout causes any lipid imbalances in cells. Lipidomics will be used for the analysis of lipid levels in RNAseK knockout cells and compared to control cells.
3. To test whether the absence of RNAseK causes disruption in the delivery and/or maturation of selected lysosomal hydrolases, immunofluorescence analyses of proteins involved in enzyme trafficking will be performed. Moreover, maturation and activity of lysosomal lipases will be tested by western blot analyses and fluorogenic substrate.
4. To gain an unbiased overview on the lysosomal content in the presence or absence of RNAseK, lysosomal enrichment followed by proteomics analyses will be performed. As altered proteome of lysosomes can cause changes in protein secretion, the secretome in control and RNAseK knockout will also be analysed.

4.3 Results

4.3.1 Analysis of lysosomal function in the absence of RNAseK

The autolysosome accumulation observed in RNAseK knockout cells prompted us to study lysosomal function in these cells. The main characteristic of lysosomes is their low pH (Li et al., 2019). RNAseK is a subunit of the V-ATPase proton pump, a complex which maintains the acidity of lysosomes and ensures proper maturation and

activation of enzymes within the lysosomal lumen (Futai et al., 2019). Although it has been reported that the depletion of RNAseK does not decrease lysosomal acidity (Perreira et al., 2015), I aimed to verify that the effects of RNAseK on autophagy are unrelated to disruption of lysosomal acidification in our cells. Lysosomal acidity was tested using a lysosomal fluorescent dye LysoSensor green. The intensity of fluorescent signal emitted by LysoSensor depends on the acidity of lysosomes and increases when lysosomes are more acidic (Zhou et al., 2013). LysoSensor signal was comparable between control and RNAseK knockout cells under basal conditions (figure 4.1a). Similarly, the increase in dye intensity induced by AA starvation did not vary significantly between control and RNAseK knockout cells (figure 4.1a). Lysosomal acidification was also detected in RNAseK knockout cells treated with LysoTracker red (figure 3.4), as discussed in chapter 3.3.1. In agreement with previous reports, these findings suggest that lysosomal acidity is not disrupted in the absence of RNAseK.

We next proceeded to test whether the function of lysosomal proteases could be halted in cells lacking RNAseK. As mentioned in chapter 1.2.3, cathepsins are trafficked to lysosomes in a form of pro-enzyme and undergo cleavage to mature and become active in the lysosomal lumen (Turk et al., 2012). This cleavage of cathepsins can be monitored by western blot analyses, whereby a higher molecular weight band represents a pro-enzyme and lower band represents a mature form of the enzyme (Pungercar et al., 2009). Western blot analyses of lysosomal Cathepsin B showed no differences in its proteolytic processing when compared between control and RNAseK knockout cells (figure 4.1b). In addition to Cathepsin B proteolytic processing, we also tested whether the mature form of the enzyme is functional in lysosomes in the absence of RNAseK. This was tested using a fluorogenic Cathepsin B substrate, which fluorescence is quenched because of a quencher attached to it (Poreba et al., 2019). When delivered to the lysosomes, the cleavage of the substrate by Cathepsin B in the lysosomal lumen results in the separation of the fluorescent dye from the quencher and the emission of a fluorescent signal. Therefore, the intensity of the fluorescence signal correlates to the enzymatic activity of Cathepsin B (figure 4.1c). Comparison of the fluorescence signal intensity between control and RNAseK knockout cells showed no significant differences in basal conditions or under AA starvation (figure 4.1d) confirming that Cathepsin B is functional in RNAseK knockout cells. The overall proteolytic activity of lysosomes was also confirmed by EGFR degradation assay in

which stimulation of cells with EGF results in the internalisation of its receptor (EGFR) and endocytic targeting to lysosomes for degradation (figure 4.1e) (Sigismund et al., 2008). Western blot analyses of EGFR levels showed comparable EGFR degradation rates between control and RNAseK knockout cells (figure 4.1f,g). Altogether, these results indicate that protein degradation within the lysosomal lumen is preserved in the absence of RNAseK.

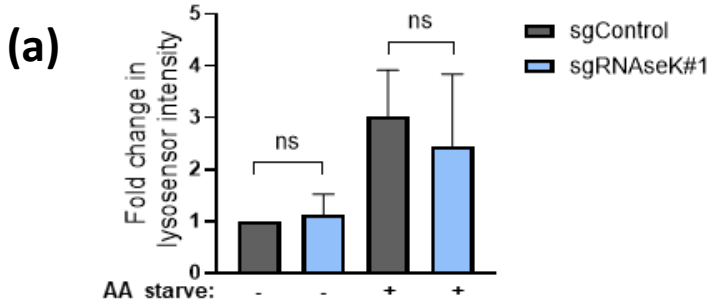
(a)
Fold change in lysosensor intensity
5
4
3
2
1
0
ns
ns
sgControl
sgRNAseK#1
AA starve: - - + +

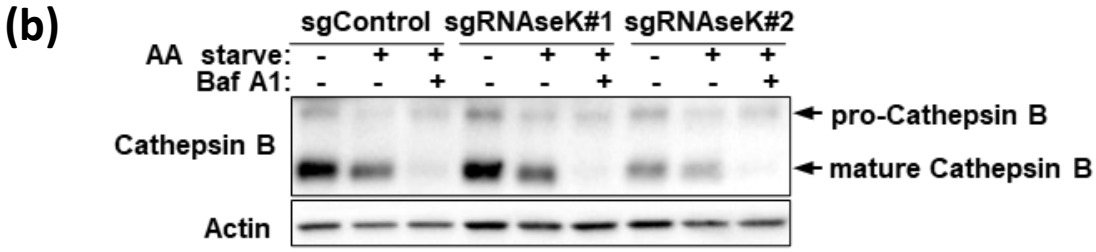
(b)
sgControl sgRNAseK#1 sgRNAseK#2
AA starve: - + + - + + - + +
Baf A1: - - + - - + - - +
Cathepsin B
pro-Cathepsin B
mature Cathepsin B
Actin

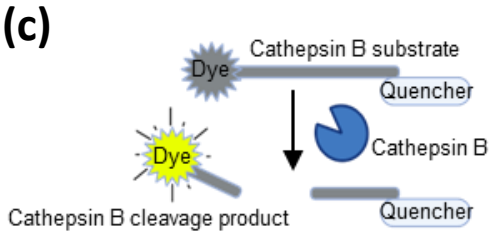
(c)
Cathepsin B substrate
Dye
Quencher
Cathepsin B
Dye
Cathepsin B cleavage product
Quencher

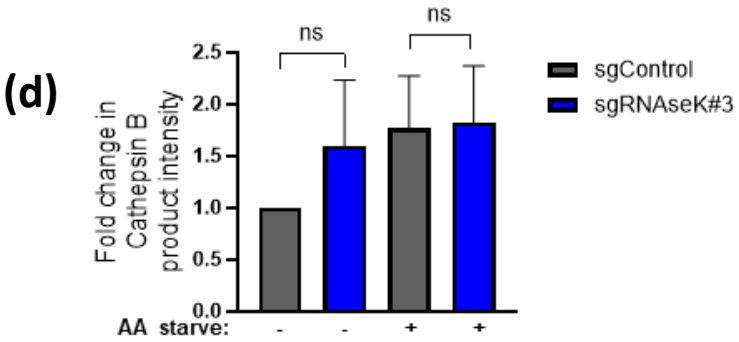
(d)
Fold change in Cathepsin B product intensity
2.5
2.0
1.5
1.0
0.5
0.0
ns
ns
AA starve: - - + +
sgControl
sgRNAseK#3

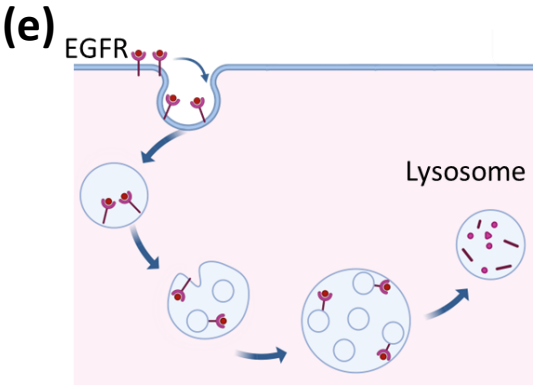
(e)
EGFR
Lysosome

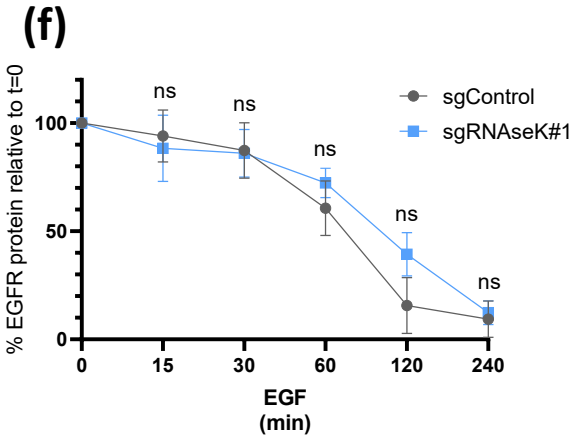
(f)
% EGFR protein relative to t=0
100
50
0
ns
ns
ns
ns
ns
sgControl
sgRNAseK#1
0 15 30 60 120 240
EGF (min)

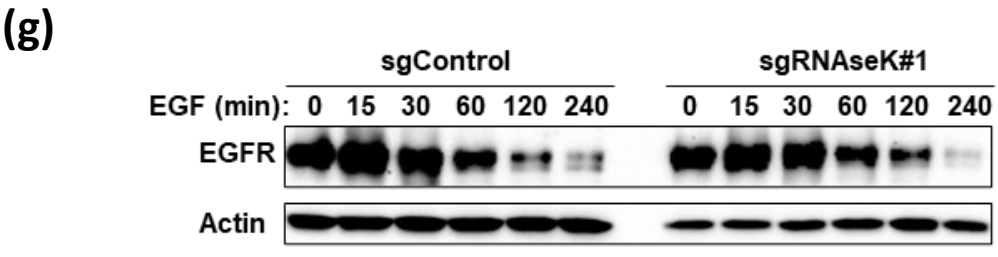
(g)
sgControl
sgRNAseK#1
EGF (min): 0 15 30 60 120 240 0 15 30 60 120 240
EGFR
Actin

Figure 4.1 RNAseK knockout does not disrupt lysosomal pH and protease function.
(a) *Quantification of LysoSensor Green signal fold change in control and RNAseK knockout cells relative to signal in sgControl cells. MEFs were left untreated or AA starved and incubated with LysoSensor Green followed by FACS analyses for fluorescence intensity.* ***(b)*** *Western blot analyses of Cathepsin B in sgControl and RNAseK knockout cells (sgRNAseK). Cells were untreated or AA starved in the presence or absence of Baf A1.* ***(c)*** *Schematic diagram of Cathepsin B activity assay where cleavage of Cathepsin B substrate results in the fluorescence of the cleavage product.* ***(d)*** *Quantification of Cathepsin B substrate fluorescence in sgControl and sgRNAseK cells. Signal was normalised relative to sgControl cells. MEFs were left untreated or AA starved and incubated with the Cathepsin B substrate followed by FACS analyses.* ***(e)*** *Schematic diagram of EGRR uptake and lysosomal targeting.* ***(f)*** *Quantification of EGFR levels following EGF stimulation in (H) expressed as a percentage of the EGFR levels at time 0 in the relative cell line.* ***(g)*** *Western blot analyses of EGFR levels in sgControl and sgRNAseK cells. Cells were cultured without serum for 4 h, followed by stimulation with EGF (20 ng/mL) for the indicated times. In all panels, mean + SD is shown from at least three independent experiments. (ns) non-significant, assessed by unpaired Student's t-test.*

4.3.2 Investigating the role of RNAseK in lysosomal lipases delivery and maturation

The intact activity of proteases in the absence of RNAseK led me to hypothesise that IAM degradation, potentially mediated by a lipase activity, could be defective in RNAseK knockout due to reduced lipase activity. To test whether depletion of RNAseK has any effect on lipid homeostasis, I performed lipidomics MS analyses of whole cell lysates (Wu et al., 2020). These analyses allow the detection of any imbalances in lipid metabolism, which would give us an insight into the enzymatic activity of lipases in the absence of RNAseK. Whole cell lipidomics (performed by Gio Rodriguez Blanco) of control and RNAseK knockout MEFs showed that the levels of most lipids were unaffected by the absence of RNAseK (data not shown). However, we noticed a decrease in levels of lysophosphatidylcholine (LysoPC) and lysophosphatidylethanolamine (LysoPE) in RNAseK knockout cells (figure 4.2). These two lipids are product of a phospholipase activity, mainly phospholipase A2 (PLA2) (Burke and Dennis, 2009). Although this class of phospholipase is not exclusively

lysosomal, Phospholipase A2 Group XV (PLA2G15) is a member of PLA2 family present within the lysosomal lumen (Shayman and Tesmer, 2019). Therefore, reduced levels of LysoPC and LysoPE may be caused by a defect in the activity of PLA2G15 or other lysosomal phospholipase in the absence of RNAseK, which could explain the inhibition of IAM degradation.

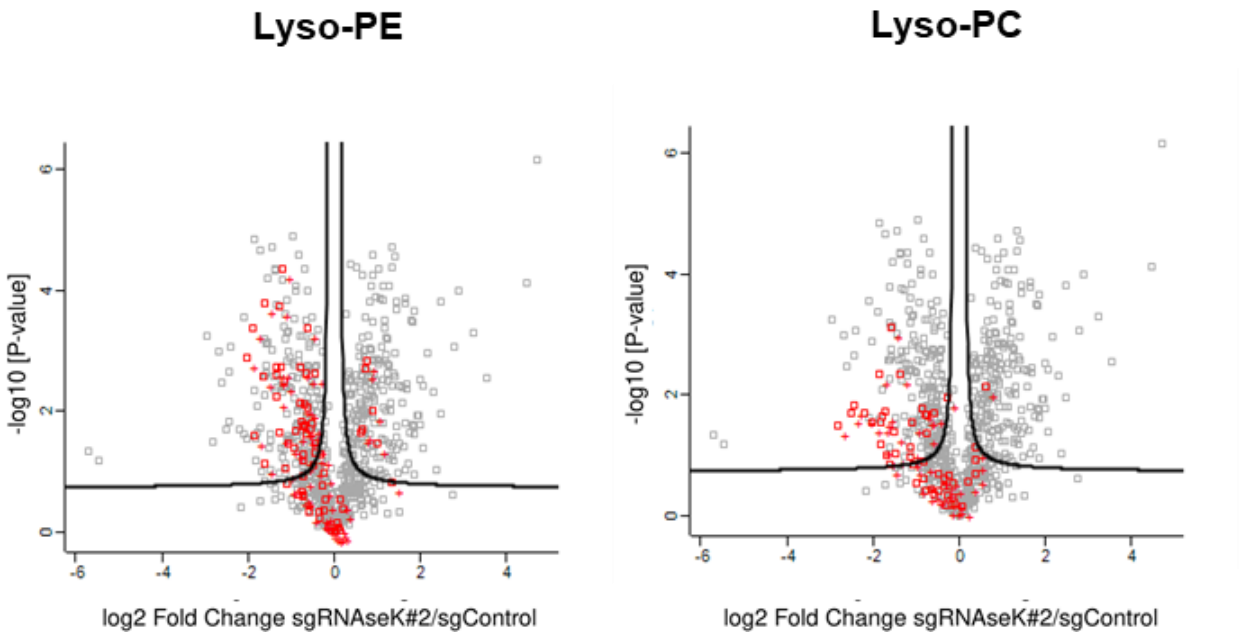

Figure 4.2 RNAseK knockout disrupts lipid homeostasis.
Volcano plot of lipids identified by MS analyses in sgRNAseK or sgControl MEF cells. Highlighted in red are LysoPE (left) and LysoPC (right) lipids. Data obtained by Gio Rodriguez Blanco.

Immunofluorescence and MS analyses described in chapter 3.3.3, highlighted the association of RNAseK with compartments involved in hydrolases trafficking to the lysosomes, such as endosomal compartments, Golgi apparatus and TGN (figure 3.7). Moreover, RNAseK exhibited a partial co-localisation with ATG9a, an autophagy protein which contributes to the delivery of certain hydrolases to the lysosome (Jia et al., 2017). To test whether ATG9a cell localisation is altered in the absence of RNAseK, we performed immunofluorescence analyses of endogenous ATG9a with GM130 and LAMP1. In control cells, ATG9a showed a perinuclear localisation and

highly co-localised with Golgi apparatus, in agreement with published findings (Orsi et al., 2012). The co-localisation of ATG9a with lysosomes, marked by LAMP1 staining, was marginal in control cells (figure 4.3). In RNAseK knockout cells, the co-localisation between ATG9a and GM130 was significantly diminished. Moreover, ATG9a accumulated on lysosomes, suggesting that the retrograde trafficking of ATG9a was disrupted (figure 4.3). As proteolytic activity of the lysosomes in cells depleted of RNAseK appears to be intact, I suspected that the phenotype seen in RNAseK knockout cells could be due to a disruption in lysosomal delivery of selected but not all hydrolases.

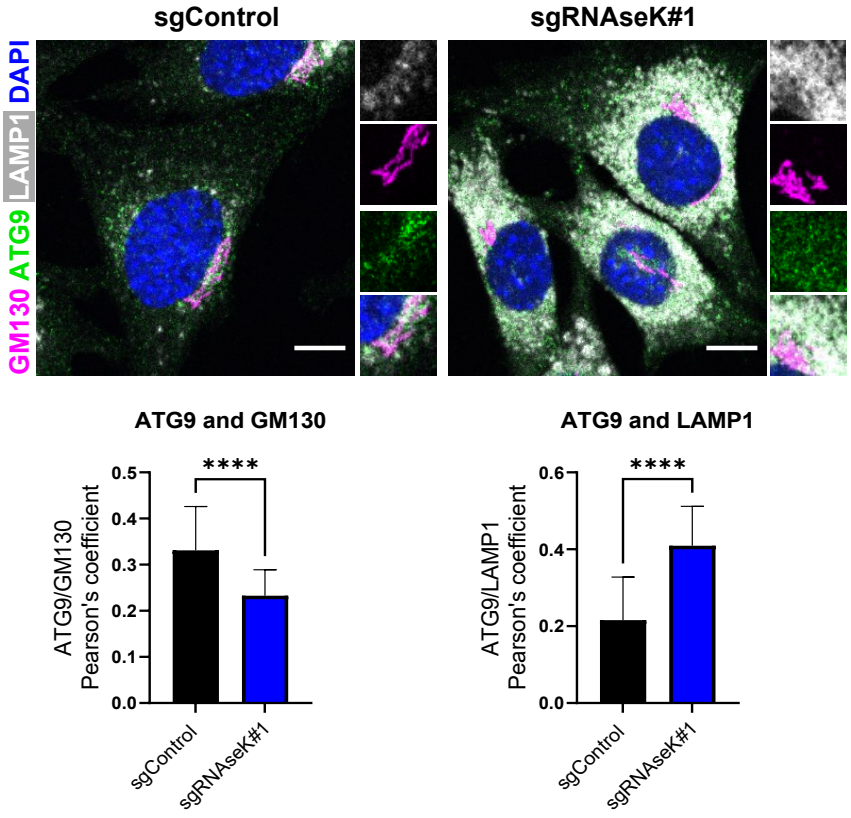

Figure 4.3 RNAseK knockout causes a lysosomal accumulation of ATG9a.
*Representative immunofluorescence image of ATG9a, GM130 and LAMP1 in sgControl or sgRNAseK MEFs cultured in the absence of AAs for 2 h. Scale bar: 10 μm. Quantification of Pearson's colocalization coefficient between ATG9a and LAMP1 or ATG9a and GM130 is shown below. Mean + SD is shown from at least three independent experiments. ****p<0.0001, assessed by unpaired Student's t-test.*

To test whether CD-MPR and CI-MPR, the two main receptors involved in canonical hydrolase trafficking to lysosomes, are affected by RNAseK knockout, I analysed their localisation by fluorescence microscopy. Both receptors shuttle between the Golgi apparatus and endosomal vesicles and transiently associate with late endosomes/lysosomes (Brown et al., 1986). Upon de-coupling of enzymes from MPRs in the acidic milieu of endosomes, MPRs are trafficked back to the Golgi apparatus. Therefore, MPRs predominantly localise to Golgi apparatus and TGN in cells (Brown et al., 1986). Immunofluorescence co-staining of the receptors with GM130 or LAMP1 showed significant differences in MPRs localisation in the absence of RNAseK. Co-localisation of both receptors with the Golgi apparatus was significantly diminished (figure 4.4a,b). Whereas CD-MPR did not exhibit increased co-localisation the lysosome marker LAMP1, CI-MPR seems to be accumulating on lysosomes (figure 4.4a,b). Interestingly, control cells treated with Baf A1 exhibited alerted localisation of CI-MPR but not CD-MPR (figure 4.4a,b). Super resolution microscopy (SIM) analyses of CI-MPR and LAMP1 in control cells treated with Baf A1 and RNAseK knockout cells was performed to further study CI-MPR association with lysosomes. Whereas in control cells most CI-MPR puncta seems to be adjacent to LAMP1 structures, in the absence of RNAseK a fraction of CI-MPR localised to the lysosomal lumen (figure 4.4c). This phenotype of CI-MPR in RNAseK knockout suggests that certain hydrolases could be misdelivered to lysosomes. Alternatively, the accumulation of CI-MPR on lysosomes could mean that enzymes are trafficked to the lysosome but do not disassociate from CI-MPR which abrogates their maturation and function.

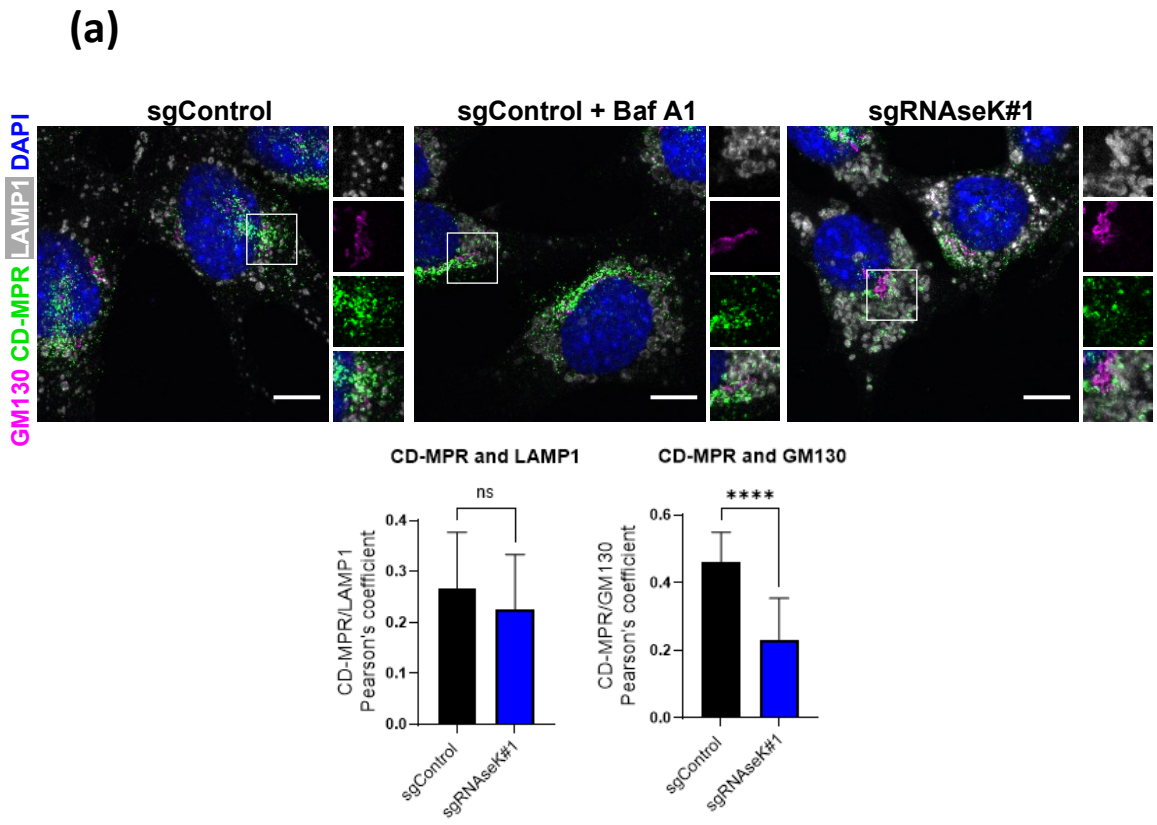
(a)
sgControl
sgControl + Baf A1
sgRNAseK#1
GM130 CD-MPR LAMP1 DAPI
CD-MPR and LAMP1
CD-MPR and GM130
ns
****
CD-MPR/LAMP1 Pearson's coefficient
CD-MPR/GM130 Pearson's coefficient
0.0
0.1
0.2
0.3
0.4
0.6
sgControl
sgRNAseK#1

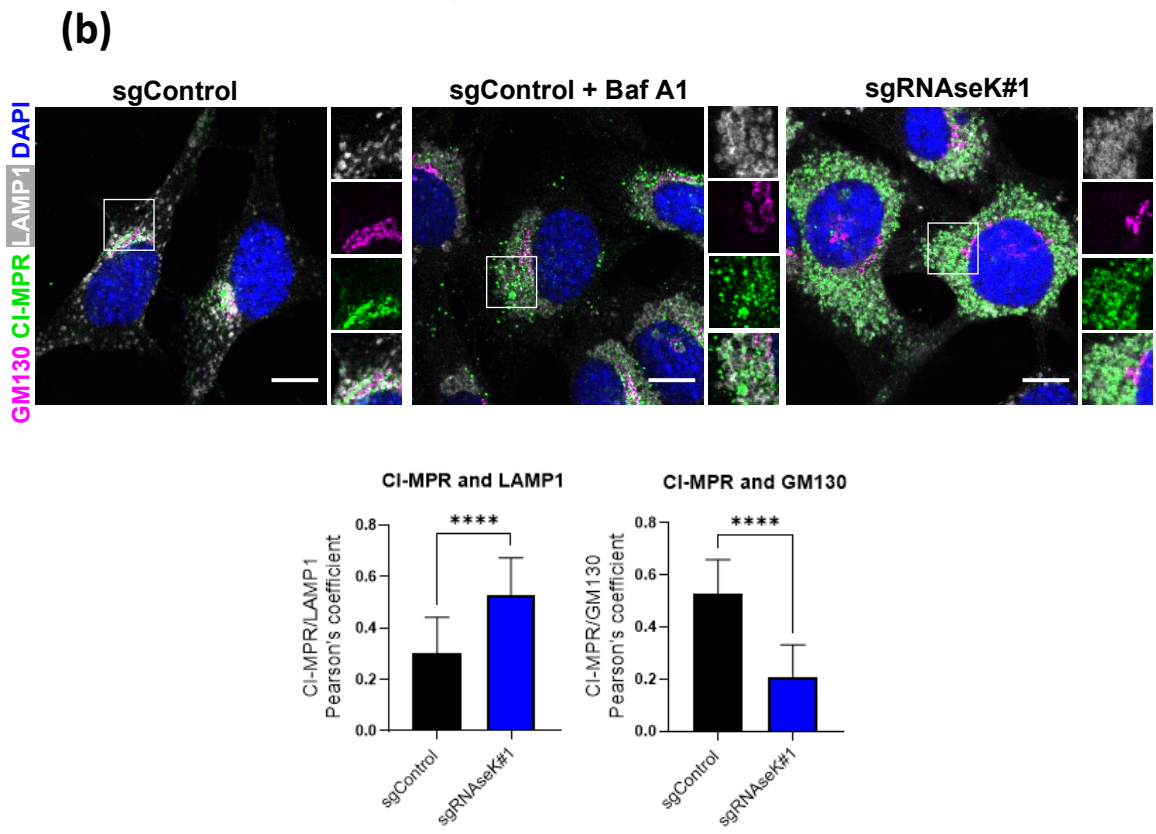
(b)
sgControl
sgControl + Baf A1
sgRNAseK#1
GM130 CI-MPR LAMP1 DAPI
CI-MPR and LAMP1
CI-MPR and GM130
****
CI-MPR/LAMP1 Pearson's coefficient
CI-MPR/GM130 Pearson's coefficient
0.0
0.2
0.4
0.6
0.8
sgControl
sgRNAseK#1

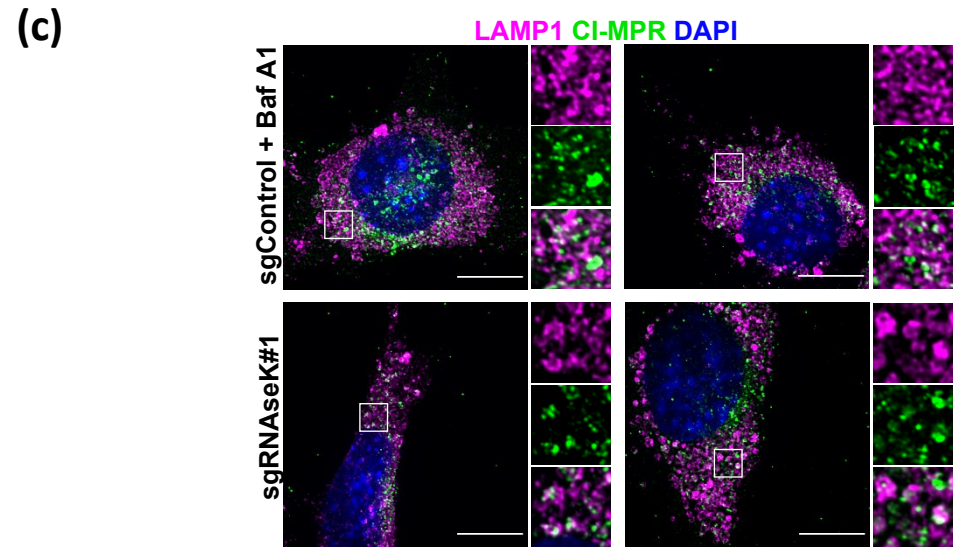

Figure 4.4 RNAseK knockout disrupts cellular localisation of MPRs.

(a) *Representative immunofluorescence images of CD-MPR, GM130 and LAMP1 in sgControl or sgRNAseK MEFs cultured in the absence of AAs for 2 h. Baf A1 was added for 2 h as indicated. Scale bar: 10 μm. Quantification of Pearson's colocalization coefficient between CD-MPR and LAMP1 or CD-MPR and GM130 is shown below, sgControl + Baf A1 n=2* ***(b)*** *Representative immunofluorescence images of CI-MPR, GM130 and LAMP1 in sgControl or sgRNAseK MEFs cultured in the absence of AAs for 2 h. Baf A1 was added for 2 h as indicated. Scale bar: 10 μm. Quantification of Pearson's colocalization coefficient between CI-MPR and LAMP1 or CI-MPR and GM130 is shown below, sgControl + Baf A1 n=2 . Mean + SD is shown from at least three independent experiments. ****p<0.0001, (ns) non-significant, assessed by unpaired Student's t-test.* ***(c)*** *Representative SIM image of CI-MPR and LAMP1 in sgControl or sgRNAseK MEFs cultured in the absence of AAs for 2 h. Baf A1 was added for 2 h as indicated, n=1. Scale bar: 10 μm.*

To test whether the disassociation of CI-MPR from hydrolases is disrupted in the absence of RNAseK , we assessed the levels of PLA2G15 co-immunoprecipitation (co-IP) with CI-MPR, in control and RNAseK knockout cells. PLA2G15 is phospholipase present in lysosomes, which was recently associated with IAM degradation in *C. elegans* (Li et al., 2022). Overexpression and pulldown of tagged PLA2G15 in control and RNAseK knockout cells showed an increased co-IP of CI-MPR in RNAseK knockout cells (figure 4.5a). This indicates an increased association of CI-MPR with PLA2G15 upon RNAseK depletion. Similarly to Cathepsin B, PLA2G15 is cleaved in the acidic milieu of the lysosomes (Hiraoka et al., 2005). To test whether

depletion of RNAseK disrupts the proteolytic processing of PLA2G15, we examined the levels of PLA2G15 by western blot (figure 4.5b). The processing from pro- to mature PLA2G15, induced by AA starvation, seems to be attenuated in the absence of RNAseK (figure 4.5b). Altogether, these studies suggest that certain hydrolases could be misdelivered, or delivered to the lysosome but are dysfunctional, potentially due to impaired disassociation from CI-MPR.

LIPA is another lysosomal lipase delivered to the lysosomes via MPR-mediated pathway (Qian et al., 2008). Due to the poor quality of commercially available antibodies and low levels of this protein in MEFs, I was unable to test LIPA proteolytic processing by western blot analyses. However, I was able to test the activity of LIPA by introducing a specific fluorogenic substrate (4-MUP) to cells. Cleavage of 4-MUP by LIPA results in the release of 4-MU fluorescent product (Dairaku et al., 2014) (figure 4.5c). Measurement of 4-MU intensity in control and RNAseK knockout cells showed reduced activity of LIPA in the absence of RNAseK (figure 4.5d). The levels of fluorescent product detected in RNAseK knockout cells were comparable to control cells treated with Baf A1, suggesting a complete inhibition of enzyme function. However, it is unclear whether this phenotype is observed due to defect in maturation or lysosomal delivery of LIPA.

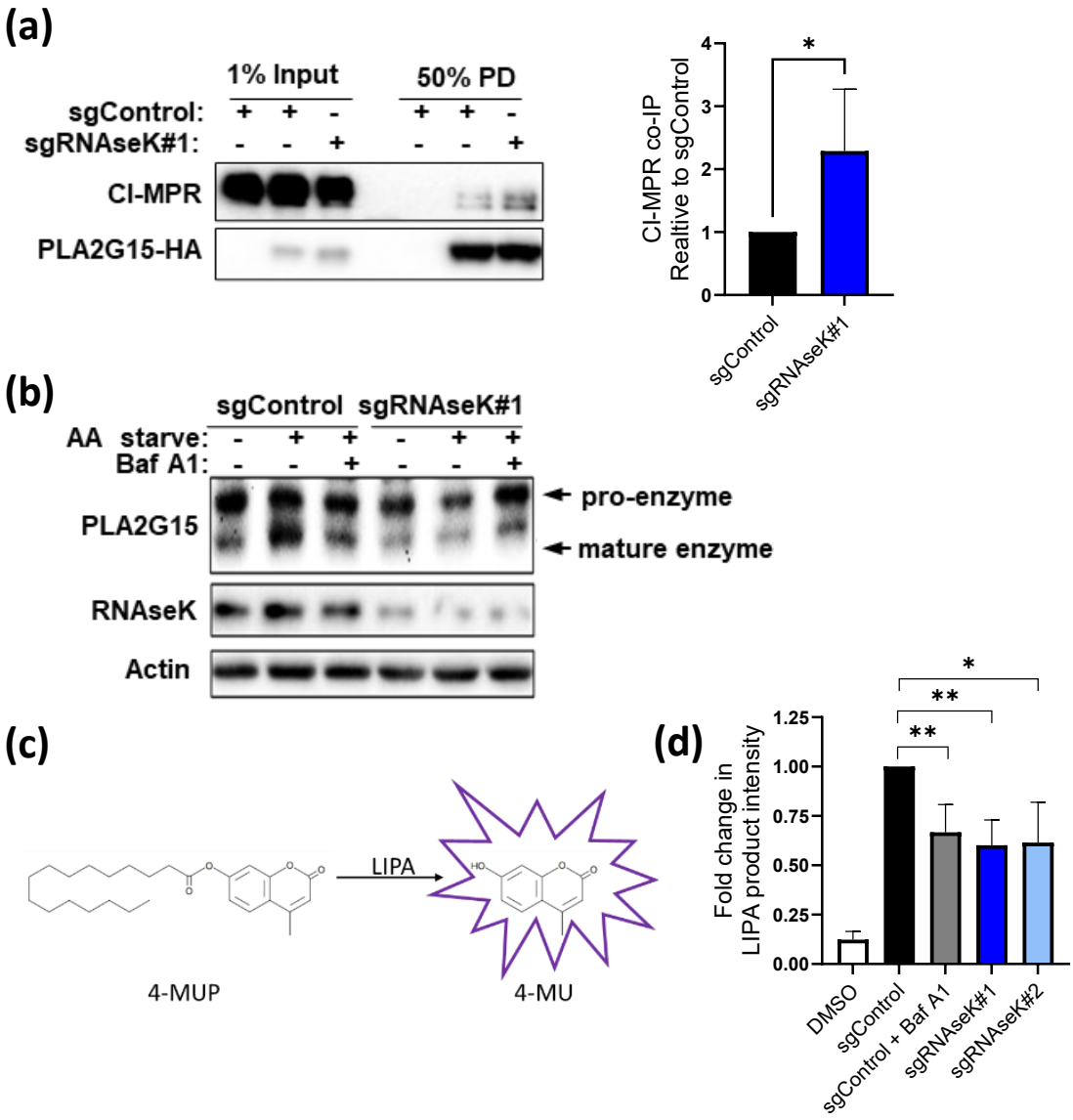

Figure 4.5 RNAseK knockout alters maturation and activity of PLA2G15 and LIPA.

(a) *sgControl or sgRNAseK MEFs were transfected with PLA2G15-HA plasmid. Cell lysates were then mixed and subjected to anti-HA pulldown, followed by western blotting using the indicated antibodies. Quantification of CI-MPR pulldown levels normalised to sgControl.* ***(b)*** *Western blot analyses of PLA2G15 in sgControl and sgRNAseK MEFs. Cells were untreated or AA starved in the presence or absence of Baf A1.* ***(c)*** *Schematic diagram of LIPA activity assay where cleavage of LIPA substrate results in the fluorescence of the cleaved product.* ***(d)*** *Quantification of LIPA substrate fluorescence in control and RNAseK knockout cells. Signal was normalised relative to sgControl cells. MEFs were left untreated or AA starved for 2 h and incubated with the LIPA substrate followed by FACS analyses. In all panels mean + SD is shown from at least three independent experiments. ****p<0.0001, assessed by unpaired Student's t-test.*

4.3.3 Investigating lysosomal proteome and cellular secretome in the absence of RNAseK

To determine whether certain hydrolases are misdelivered or dysfunctional in RNAseK knockout cells and to obtain an unbiased an overview of lysosomal content, I examined the proteome of enriched lysosomal fractions. To obtain lysosomal fractions, cells were treated with Superparamagnetic Iron Oxide Nanoparticles (SPIONs), which upon prolonged incubation in cells result in their accumulation in lysosomes (figure 4.6a) (Singh et al., 2020). Lysosomal fractions were then enriched using magnetic columns and analysed by MS. As expected, the levels of ATG8 proteins and selective autophagy receptors were significantly increased in the lysosomes of RNAseK knockout cells (figure 4.6b). Of note, although this technique allows for enrichment of lysosomal proteins, the obtained fractions could contain proteins from other cell compartments. This is represented by ATG9a and CI-MPR levels which did not significantly vary between control and RNAseK knockout cells (data not shown), despite an increased association with RNAseK in immunofluorescence analyses. Two lysosomal lipases, LIPA and PLD3, were significantly decreased in the lysosome fractions of sgRNAseK cells, whereas PLA2G15 levels remained unchanged (figure 4.6b). Most cathepsins remained unchanged in the absence of RNAseK, with a few exceptions of decreased levels of Cathepsin O and Cathepsin F in RNAseK knockout cells. Altogether, these results indicate a role of RNAseK in the selective delivery of specific lysosomal hydrolases.

One of the proteins significantly increased in the lysosomal fractions in RNAseK knockout cells was VPS4a (figure 4.6b). As discussed in chapter 1.2.5, VPS4a is involved in the trafficking of PLD3 to the lysosomes (Gonzalez et al., 2018a). Moreover, alerted cell localisation of VPS4a and accumulation on the lysosomes results in hypersecretion of selected proteins (Hasegawa et al., 2011). To test whether selected lipases are increasingly secreted in the absence of RNAseK, MS analyses of the secretome was performed. Proteomics analyses of cell media in control and RNAseK knockout cells showed significantly increased levels of secreted PLD3 in the absence of RNAseK (figure 4.6c). LIPA and PLA2G15 were not detected in the secretome in either of cell lines. Because lysosomal alkylation causes increased secretion of certain proteins (Leidal et al., 2020), secretome of control cells treated

with Baf A1 was also analysed. Consistent with previous reports, secretome of cells treated with Baf A1 contained increased levels of LC3B, when compared to control (Leidal et al., 2020) (figure 4.6d). However, PLD3 was not detected in the secretome of cells treated Baf A1, suggesting that the phenotype seen in the secretome of RNAseK knockout cannot be replicated by inhibiting the V-ATPase proton pump assembly.

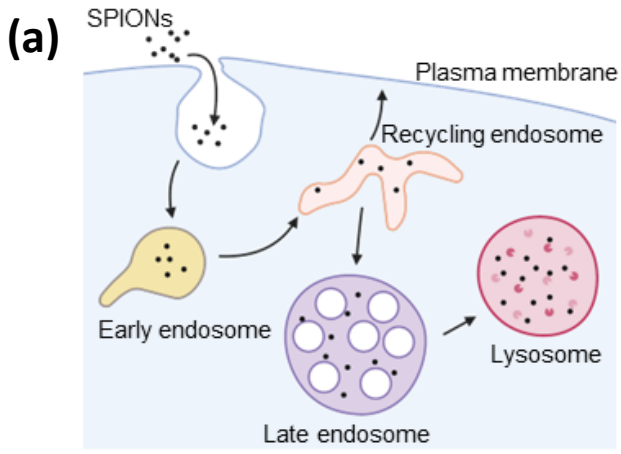
(a)
SPIONs
Plasma membrane
Recycling endosome
Early endosome
Late endosome
Lysosome

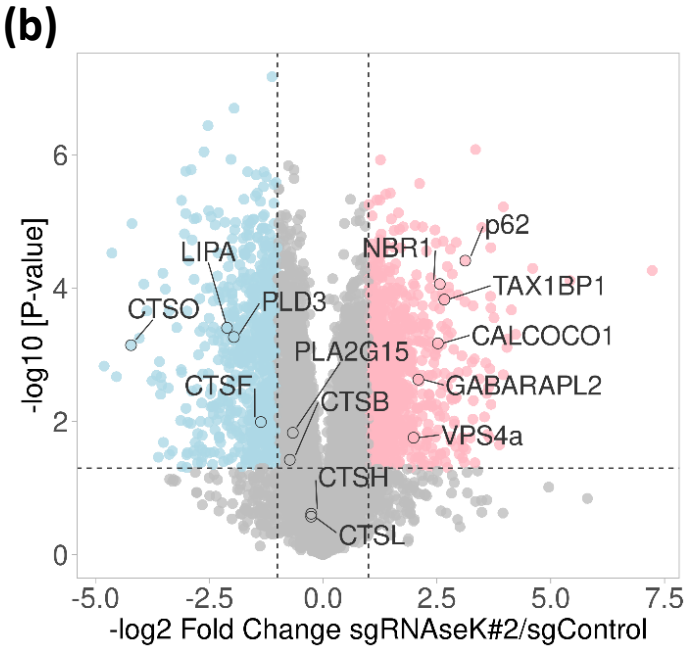
(b)
-log10 [P-value]
-log2 Fold Change sgRNAseK#2/sgControl
LIPA
CTSO
PLD3
CTSF
PLA2G15
CTSB
CTSH
CTSL
NBR1
p62
TAX1BP1
CALCOCO1
GABARAPL2
VPS4a

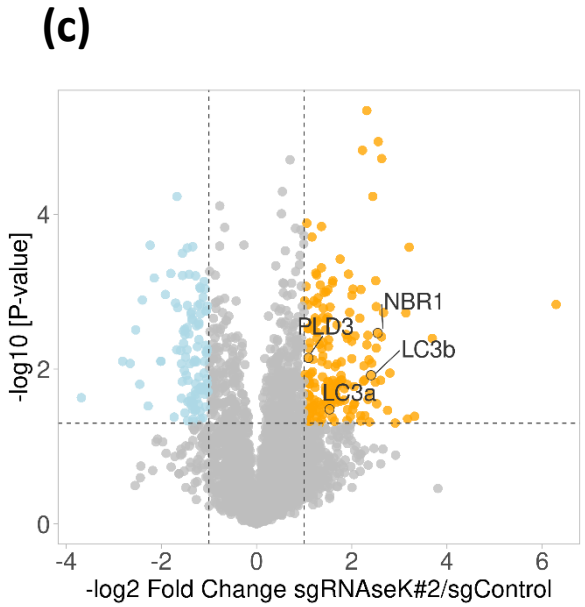
(c)
-log10 [P-value]
-log2 Fold Change sgRNAseK#2/sgControl
NBR1
PLD3
LC3b
LC3a

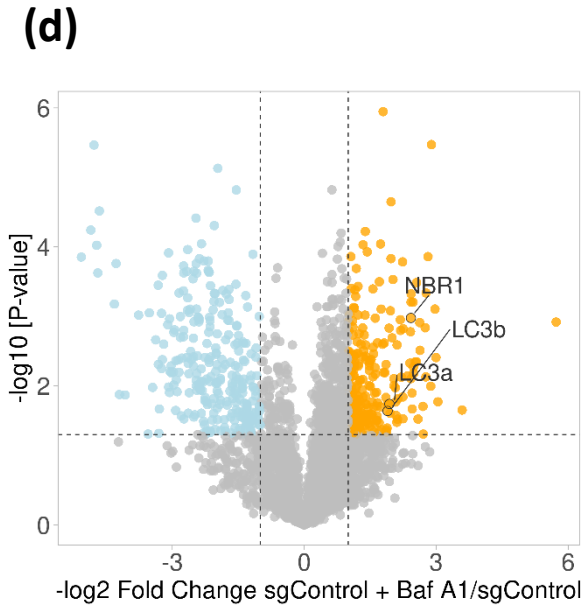
(d)
-log10 [P-value]
-log2 Fold Change sgControl + Baf A1/sgControl
NBR1
LC3b
LC3a

Figure 4.6 RNAseK knockout alters the lysosomal localisation of multiple proteins.
(a) *Schematic diagram depicting the method used to label cells with SPIONs.* ***(b)*** *Volcano plot of proteins identified by MS analyses of lysosomal preparations derived from sgControl or sgRNAseK MEFs. Highlighted in pink are proteins showing significant enrichment in the lysosomal fraction of sgRNAseK cells (P > 0.05; FC > 2) and in blue are those that are significantly decreased (P > 0.05; FC < -2).* ***(c)*** *Volcano plot of proteins identified by MS analyses of cell media derived from sgRNAseK or sgControl MEF cultures. Highlighted in orange are significantly enriched proteins in sgRNAseK cells (P > 0.05; FC > 2) and in blue are those that are significantly decreased (P > 0.05; FC < -2).* ***(d)*** *Volcano plot of proteins identified by MS analyses of the cell media derived from sgControl cells in the presence or absence of Baf A1. Highlighted in orange are significantly enriched proteins in sgRNAseK cells (P > 0.05; FC > 2) and in blue are those that are significantly decreased (P > 0.05; FC < -2).*

4.4 Discussion

Chapter 3 highlighted that the role of RNAseK in autophagy is related to its specific function in lysosomes. In this chapter, biochemical properties and proteomics of lysosomes were analysed. RNAseK is a subunit of V-ATPase proton pump, a complex which ensures lysosomal acidification (Perreira et al., 2015). Similar to the phenotype observed in the absence of RNAseK, inhibition of V-ATPase-mediated acidification of lysosomes results in the accumulation of undigested autophagic cargo within the lysosomal lumen (Bagh et al., 2017; Fedele and Proud, 2020). Moreover, Baf A1 treatment, which inhibits V-ATPase complex assembly, was shown to inhibit CME due to abrogated recycling of cholesterol to the plasma membrane (Kozik et al., 2013). As mentioned in chapter 1.3, depletion of RNAseK also causes size-dependent inhibition of CME, somewhat resembling Baf A1 treatment phenotype. Efficient acidification of cellular compartments by the V-ATPase complex is crucial for cell survival and prolonged inhibition of the complex activity is lethal to cells (Pamarthy et al., 2018). Therefore, the role of RNAseK in maintaining lysosomal acidity was the first aspect tested in this chapter.

The V-ATPase complex consists of multiple subunits and several of them were shown to be dispensable for complex assembly and proton pumping (Mo et al., 2020; Xia et al., 2019). Analyses of LysoSensor signal showed no significant differences in lysosomal acidification between control and RNAseK knockout cells indicating that the

proton pumping activity of V-ATPase complex remains intact in absence of RNAseK. These results confirmed already published data and suggested that the role of RNAseK is not related to the regulation of lysosomal pH (Abbas et al. 2020; Perreira et al., 2015). Indeed, the V-ATPase pump activity is not restricted to maintaining lysosomal acidification was shown to have additional roles in cells, such as mTORC1 activation, CASM induction, and autophagosome-lysosome fusion (Hooper et al., 2022; Xia et al., 2019; Zoncu et al., 2011). Analyses of Cathepsin B maturation and activity showed that RNAseK is not essential for its activity. Interestingly, although the lysosomal levels of most cathepsins remained unchanged in the absence of RNAseK, Cathepsin O and Cathepsin F were significantly reduced. The roles of both cathepsins are poorly characterised, however depletion of Cathepsin F was shown to result in lysosomal accumulation of fluorescent proteins and lipids (lipofuscin) *in vivo* (Tang et al., 2006). Comparison of proteolytic degradation of EGFR between control and RNAseK knockout cells suggests that these cathepsins are dispensable for the proteolytic degradation of this endocytic cargo.

ATG9a levels in proteomics analyses of lysosomal fractions did not show significant differences between control and RNAseK knockout cells, perhaps due to impurities of lysosomal fractions. However, immunofluorescence analyses of ATG9a showed its increased co-localisation with LAMP1 in the absence of RNAseK. ATG9a was previously reported to transiently interact with late endosomal compartments and is required for the maturation of Cathepsin D and Cathepsin L (Jia et al., 2017). Trafficking of ATG9a is regulated by TBC1 domain family member 5 (TBC1D5). In the absence of TBC1D5, ATG9a accumulates in lysosomes (Popovic and Dikic, 2014) as seen in RNAseK knockout cells. However, ATG9a depletion was shown to result in the inhibition of the proteolytic degradation of EGFR (Jia et al., 2017), which was not the case in RNAseK knockout cells. Moreover, depletion of ATG9a inhibits LC3 lipidation and phagophore elongation unlike RNAseK depletion (Young et al., 2006). Therefore, although the cellular localisation of ATG9a seems to be affected by the absence of RNAseK, it is unlikely to contribute to the defect in autolysosome degradation seen in these cells.

Immunofluorescence analyses of CI-MPR and CD-MPR, the two receptors involved in the canonical delivery of hydrolases to lysosomes, also showed altered cellular localisation in the absence of RNAseK. The Golgi localisation of both receptors

is diminished in RNAseK knockout cells. Moreover, CI-MPR, but not CD-MPR, co-localised with LAMP1 in sgRNAseK cells. The discrepancy in the lysosomal accumulation of the two receptors, observed in RNAseK knockout cells, could occur due to a difference in size of these two MPRs. The molecular weight of CI-MPR is ~300 kDa whereas CD-MPR is ~45 kDa (Ghosh et al., 2003). It is possible that, similar to its role during CME at the plasma membrane, RNAseK could be selectively involved in trafficking of the larger receptor (Hackett and Cherry, 2018). However, the details of the altered cellular localisation of CI-MPR need to be further investigated. SIM analyses showed that CI-MPR localised within the lysosomal lumen, on the lysosomal membrane and adjacent to lysosomes in sgRNAseK cells. Proteomics analyses of lysosomal fractions did not show increased CI-MPR levels in RNAseK knockout cells. However, the association of CI-MPR with PLA2G15 was increased upon RNAseK depletion, which correlates with an impaired maturation of the enzyme, suggesting that the release of PLA2G15 from CI-MPR is disrupted. The differences observed in CI-MPR localisation investigated by fluorescence microscopy or lysosomal proteomics could be explained by the differences in sample preparation. It is possible that the enhanced association of CI-MPR and PLA2G15 with lysosomal membrane in sgRNAseK cells was disturbed by mechanical cell lysing and the proteins were lost during enrichment of lysosomal fractions. Moreover, as previously mentioned, the enriched lysosomal fractions could contain other cell compartments such as the Golgi apparatus. However, it is unlikely that the defect in autophagy detected in RNAseK-depleted cells is a result of in the redistribution of CI-MPR as previous studies have shown that the defective trafficking of the receptor results in enlarged lysosomes but does not impede autophagic flux (Cui et al., 2019; Rawat et al., 2022).

Accumulation of PLA2 substrates and disrupted maturation of PLA2G15 in the absence of RNAseK suggest that lipase activity is regulated by RNAseK. Recently, PLA2G15 was shown to promote IAM degradation in *C.elegans* (Li et al., 2022). However, the survival of mice with a systemic deletion of *Pla2g15* was comparable to the wild type and mice did not exhibit a phenotype comparable to the deletion of any of the essential autophagy genes (Hiraoka et al., 2006). This suggests that if PLA2G15 is indeed involved in IAM degradation in mammalian cells, it is not the sole phospholipase involved in this process. Analyses of another lysosomal lipase, LIPA, showed reduced activity of this enzyme in RNAseK knockout cells. Previous reports

showed that *Lipa* expression is upregulated upon nutrient starvation and that LIPA activity is crucial for LD degradation via lipophagy (Lettieri Barbato et al., 2013). IAM degradation in LIPA deficient cells has not been tested before. However, silencing of LIPA disrupts the acidification of lysosomes and reduces the lipidation of LC3 in liver cells, whereas in preadipocyte cell line, LIPA knockdown does not affect autophagic flux (Gamblin et al., 2021; Li et al., 2021).

Another lysosomal lipase analysed in this chapter is PLD3, a putative phospholipase associated with AD. mRNA levels of *PLD3* are reduced in the brains of AD patients and PLD3 was shown to be enriched in Aβ plaques (Nackenoff et al., 2021; Satoh et al., 2014). Although improper lysosomal trafficking of PLD3 leads to changes in lysosomal morphology, the role of PLD3 in the degradation of autophagic cargo has not been studied before (Gonzalez et al., 2018a). Proteomics analyses of enriched lysosomal fractions showed a significant decrease in PLD3 levels in the absence of RNAseK. PLD3 is delivered to the lysosomes via non-canonical pathway, which involves the ESCRT complex and VPS4a-depedent packaging of PLD3 into ILVs (Gonzalez et al., 2018a). Proteomics analyses of lysosomal fraction showed an accumulation of VPS4a in the absence of RNAseK. This suggests that abrogated activity of VPS4a might be the reason for the disrupted trafficking of PLD3 to lysosomes as observed in RNAseK knockout cells. Accumulation of VPS4a on late endosomal compartments was shown to increase protein secretion (Hasegawa et al., 2011). Indeed, secretome analyses of cell media from control and RNAseK knockout cells showed increased secretion of PLD3 in the absence of RNAseK, confirming disrupted targeting of PLD3 to lysosomes. Interestingly, PLD3 secretion was not observed in cell treated with Baf A1, highlighting that the role of RNAseK in the proper trafficking of PLD3 is independent of V-ATPase complex assembly.

Altogether these data show that although RNAseK is not essential for lysosomal acidification or proteolytic activities of tested proteases, it has a function in maintaining lysosomal homeostasis. RNAseK depletion causes altered localisation of certain lysosomal hydrolases and proteins that normally only transiently associate with lysosomes. The crosstalk between PLD3 and VPS4a phenotypes in the absence of RNAseK prompted me to investigate the two proteins more closely, which will be the focus of the next chapter.

Chapter 5. Role of PLD3 and VPS4a in autophagy

5.1 Introduction

The autophagic cargo includes lipids, membranous cell compartments and fragments thereof (Gubas and Dikic, 2022). Moreover, IAM degradation must occur prior to the degradation of autolysosomal cargo by hydrolases (Tsuboyama et al., 2016; Yim and Mizushima, 2020). Therefore, it is highly likely that lipases play a role in an efficient autophagic flux. Nevertheless, the specific lipases contributing to autophagic flux in mammalian cells have not been well studied. PLD3 is one of the hydrolases identified in lysosomes containing a putative phospholipase activity and depletion of PLD3 results in changes in lysosomal morphology and increase in cellular levels of LAMP1 (Gonzalez et al., 2018a; Mukadam et al., 2018; Nackenoff et al., 2021).

Although the specific role of PLD3 in autophagy has not been described, previous studies showed that expression of PLD3 mutants with reduced enzymatic activity results in diminished autophagy (Tan et al., 2019). Moreover, reduced PLD3 activity is associated with AD, the neurodegenerative disorder characterised by, amongst other features, a decline in autophagic activity (Cruchaga et al., 2014; Satoh et al., 2014; Tan et al., 2019). PLD3 depletion was shown to cause increase in CI-MPR levels and affect the cellular localisation of CI-MPR (Mukadam et al., 2018). Unlike the phenotype seen upon RNAseK depletion, CI-MPR does not seem to accumulate within lysosomes in siPLD3 cells (Mukadam et al., 2018). PLD3 is delivered to lysosomes via non-canonical pathway, which requires sorting of the enzyme to ILVs. This packaging of PLD3 into ILV is mediated by ESCRT-III and VPS4 and abrogating VPS4 activity results in disrupted processing and activity of PLD3 (Gonzalez et al., 2018a).

In addition to a role in ILV formation and trafficking of PLD3 to lysosomes, VPS4 has been associated with multiple processes within cells, including autophagy. Previous reports showed that the AAA-ATPase activity of VPS4 is crucial for efficient autophagosome closure in human cells (Takahashi et al., 2018a, 2019). Moreover, expression of a dominant negative mutant of VPS4a with abrogated enzymatic activity

resulted in the accumulation of autophagic markers (Takahashi et al., 2018; Wang et al., 2019), impaired cholesterol trafficking from lysosomes (Bishop and Woodman, 2000) and changes in the morphology of late endosomal vesicles (Bishop and Woodman, 2000; Gonzalez et al., 2018a). VPS4 also plays an important role in lysosomal damage repair and transiently associates with lysosomes to mediate the disassociation of ESCRT-III components from the lysosomal membrane (Radulovic et al., 2018; Skowyra et al., 2018). However, while VPS4 associates with lysosomes during lysosomal damage, the detection of VPS4 on lysosomes can also be indicative of a disruption in other cellular pathways related to protein trafficking and vesicular budding (Scheuring et al., 2001). Moreover, VPS4 regulates disassembly of ESCRT-III machinery during multitude of processes in the cell including plasma membrane repair, cell cycle progression and maintaining nuclear membrane morphology (Vietri et al., 2020). Depletion of both mammalian paralogs of VPS4 (VPS4a and VPS4b) is lethal to cells, further underscoring the crucial role of these proteins in cell homeostasis (Szymańska et al., 2020). VPS4 interacts with multiple cellular compartments in a transient manner making studies of this protein technically challenging and its regulatory network poorly characterised.

5.2 Aims and objectives

Because we observed an altered localisation of PLD3 and VPS4a in the absence of RNAseK, in this chapter I aim to investigate whether the improper localisation of these proteins has an effect on autophagic flux in cells. Moreover, I hypothesised that the increased association of VPS4a with lysosomes, as seen by MS analyses, happens upstream of PLD3 secretion. Therefore, I aim to test whether RNAseK knockout phenotype can be recapitulated by inhibiting VPS4 activity. The VPS4a phenotype seen upon RNAseK depletion indicated that RNAseK could be involved in controlling the dynamics of VPS4a and its release from lysosome. This could be potentially regulated by an interaction of the two proteins, making RNAseK a novel regulator of VPS4a. Objectives to achieve the aims of this chapter are as follows:

1. The first part of the chapter will be focused on characterising the knockdown phenotype of PLD3. LC3 lipidation and degradation, together with p62 levels, will assessed in MEFs and neuronal cells. Moreover, co-localisation

of endogenous LAMP1 and p62 will be analysed by immunofluorescence in the presence or absence of PLD3. To test whether autophagic structures accumulate upon the knockdown of PLD3, TEM analyses will be performed and compared to the phenotype seen in control and RNAseK knockdown cells. A more general endo-lysosomal activity in cells depleted of PLD3 will be assessed by monitoring the degradation rates of EGFR delivered to the lysosomes via the endocytic pathway.

2. The second part of this chapter will be focused on assessing the relationship between RNAseK and VPS4a. Firstly, the increased association of VPS4a with lysosomal fractions in RNAseK knockout, as seen in proteomics analyses of lysosomal fractions, will be assessed by colocalising VPS4a with late endosomal and autophagy markers. To further analyse the altered localisation of VPS4a, MS analyses of VPS4a pulldown in the presence or absence of RNAseK will be performed.
3. To test whether forced accumulation on lysosomes of VPS4a can mimic RNAseK knockout phenotype, CI-MPR association with GM130 and LAMP1 will be tested by immunofluorescence analyses and compared between wild type cells and cells expressing dominant negative mutant of VPS4a ($VPS4a^{E228Q}$). Moreover autophagic flux efficiency will also be analysed by western blotting in these cells.
4. To test whether RNAseK can regulate VPS4a directly, the potential interaction between the two proteins will be tested. Moreover, common cellular localisation of VPS4a and RNAseK will be assessed by immunofluorescence analyses of endogenously tagged RNAseK with overexpressed VPS4a.

5.3 Results

5.3.1 Analysis of autophagy pathway in absence of PLD3

In the absence of RNAseK, we observed significantly decreased levels of PLD3 in the lysosomal fractions and its increased secretion (figure 4.6b,c). To test whether this mislocalisation of PLD3 contributes to the deficiency in autophagy seen in RNAseK knockout cells, I tested LC3 and p62 degradation in cells depleted of PLD3. Individual small interfering RNAs (siRNAs) were used to knockdown PLD3 in MEFs. Due to poor quality of commercially available antibodies and low protein level of endogenous PLD3, knockdown of PLD3 in MEF cells was confirmed by qRT-PCR. Transfection of MEF cells with three different siRNAs against PLD3 resulted in an efficient knockdown of the protein (figure 5.1a). Western blot analyses of autophagic markers in basal conditions showed an accumulation of lipidated form of LC3 and p62 in siPLD3 cells in a manner comparable to control cells treated with Baf A1 (figure 5.1b). These findings suggest that siPLD3 leads to a block in autophagic flux as seen in RNAseK knockout cells (figure 3.1b). The effect of PLD3 knockdown on autophagy was also confirmed in human neuroblastoma cells (SH-SY5Y), which express higher levels of endogenous PLD3 (figure 5.1c). Similarly to MEF cells, LC3-II accumulated upon PLD3 depletion. The levels of LC3-II accumulation were comparable to control cells treated with Baf A1 and siRNAseK (figure 5.1c). Block in autophagic flux upon PLD3 depletion was also observed by immunofluorescence analyses of endogenous p62 and LAMP1 were their increased co-localisation were detected in siPLD3 in MEF cells under AA starvation (figure 5.1d,e), mimicking the phenotype seen in siRNAseK MEF cells (figure 3.3b). TEM was used to asses autophagic structures in RNAseK and PLD3 depleted cells where comparable accumulation of autolysosomal structures was detected when compared to control cells (figure 5.1f). Altogether, these observation confirmed a disruption in LC3 and p62 degradation and an accumulation of autolysosomal structures in the absence of PLD3. Next we tested EGFR degradation rates, which upon EGF stimulation is delivered to lysosomes for degradation via endocytosis. Similar to RNAseK knockout cells, the degradation of EGFR remains intact in siPLD3 MEFs (figure 5.1g). This indicates that the block in proteolytic degradation in the absence of PLD3 is specific to autophagy and does not occur due

to a general defect in lysosomes. Altogether, these data suggest that the disrupted lysosomal delivery of PLD3 in the absence of RNAseK may contribute to the block in autophagy seen upon RNAseK depletion.

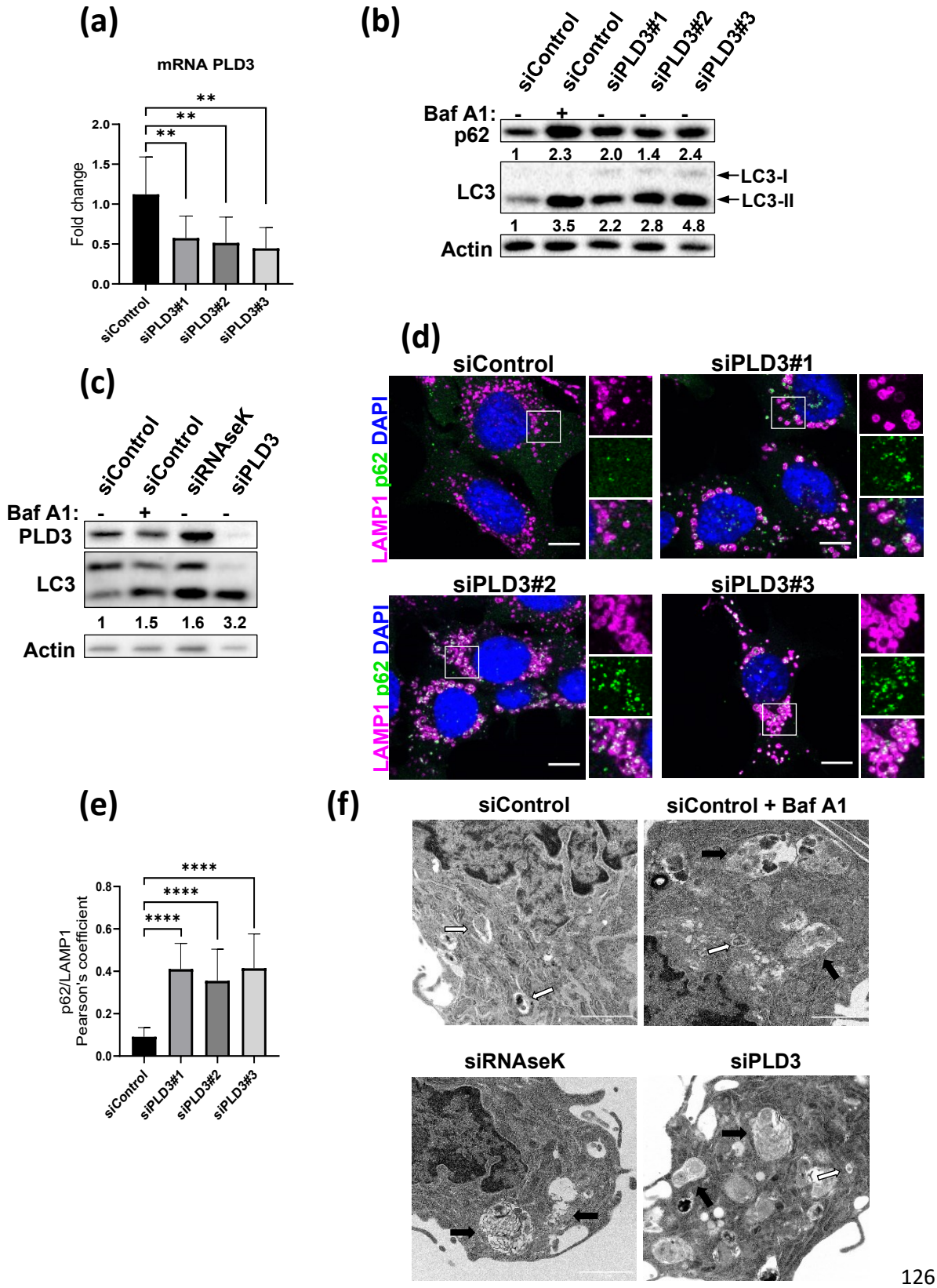

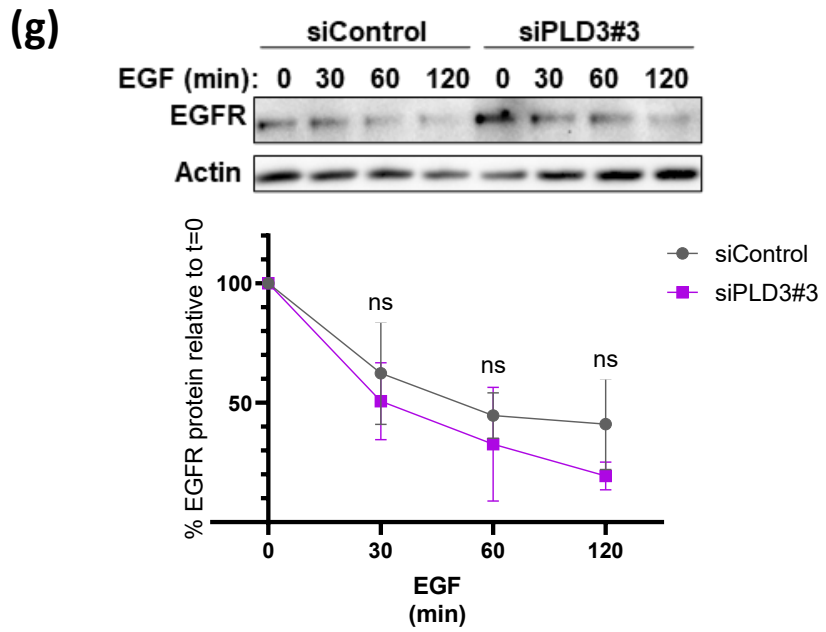

Figure 5.1 PLD3 is required for autophagy.

(a) *qRT-PCR analyses of mRNA extracted from MEFs transfected with non-targeting siRNA siControl or siPLD3. Pld3 mRNA levels were normalised to Actin. Fold change in expression was compared to siControl cells.* ***(b)*** *Western blot analyses of lysates derived from MEF cells transfected with siControl or three different siRNA sequences targeting PLD3 using the indicated antibodies. Baf A1 treatment for 2 h was included in siControl cells. Quantification of p62 and LC3-II band intensity normalised relative to siControl (lane 1) is shown below the relevant blot lanes.* ***(c)*** *Western blot analyses of lysates derived from SH-SY5Y cells transfected with siControl or pool siRNAs targeting RNAseK or PLD3 using the indicated antibodies. Baf A1 treatment for 3 h was included in siControl cells. Quantification of LC3-II band intensity normalised relative to siControl (lane 1) is shown below the relevant blot lanes.* ***(d)*** *Representative immunofluorescence images of MEF cells (as in a) using the indicated antibodies. Cells were cultured in absence of amino acids for 2 h. Scale bar: 10 μm.* ***(e)*** *Quantification of Pearson's colocalization coefficient between p62 and LAMP1 in siControl and siPLD3 in (d).* ***(f)*** *Representative transmission electron microscope (TEM) images of siControl, siPLD3 and siRNAseK MEF cells treated in the absence of amino acids for 2 h. Baf A1 is added as indicated. Arrows indicate autophagosomes (white arrows) and autolysosomes (black arrows). Scale bar: 1 μm.* ***(g)*** *Western blot analyses of EGFR levels in siControl and siPLD3 MEF cells. Cells were cultured without serum for 4 h, followed by stimulation with EGF (20 ng/mL) for the indicated times. Quantification of EGFR levels expressed as a percentage of time 0 is shown below. In all panels mean + SD is shown from at least three independent experiments.* $^{**}p<0.01$, $^{****}p<0.0001$, *(ns) non-significant, assessed by unpaired Student's t-test.*

5.3.2 Role of RNAseK in VPS4a regulation

Previous reports have shown that trafficking of PLD3 to lysosomes requires activity of VPS4a (Gonzalez et al., 2018a). Therefore, I hypothesised that the accumulation of VPS4a on lysosomes may potentially partially inhibit its activity and cause the mislocalisation of PLD3 in RNAseK knockout cells. To address whether VPS4a is indeed accumulating on lysosomes, I used a U2OS cell line stably expressing GFP-tagged VPS4a (GFP-VPS4a). In control cells, GFP-VPS4a showed mostly a diffused localisation, in agreement with previous reports (Nickerson et al., 2010). However, upon RNAseK depletion, GFP-VPS4a accumulated in punctate structures (figure 5.2a). Interestingly, in cells treated with Baf A1 I observed a diffused localisation of VPS4a suggesting that inhibiting V-ATPase proton pump assembly does not cause changes in VPS4a localisation (figure 5.2a). To further investigate on which structures VPS4a is accumulating in the absence of RNAseK, immunofluorescence analyses of VPS4a with different organelle markers was performed. Upon RNAseK depletion, VPS4a showed a significantly increased co-localisation with the late endosomal markers RAB7 and CD63 and the autophagy receptor p62 (figure 5.2b-d). This aberrant localisation of VPS4a was then confirmed by MS analyses of GFP-VPS4a pulldown in control and RNAseK knockout cells, which showed increased association of VPS4a with RAB7, STX17 and p62 in the absence of RNAseK (figure 5.2e). As previously mentioned, cells depleted of RNAseK harbour an accumulation of p62 and STX17 on the lysosomes. Altogether, these data confirm alerted localisation of VPS4a in RNAseK knockout and its increased association with lysosomal compartments, suggesting that RNAseK has a role in regulating VPS4a.

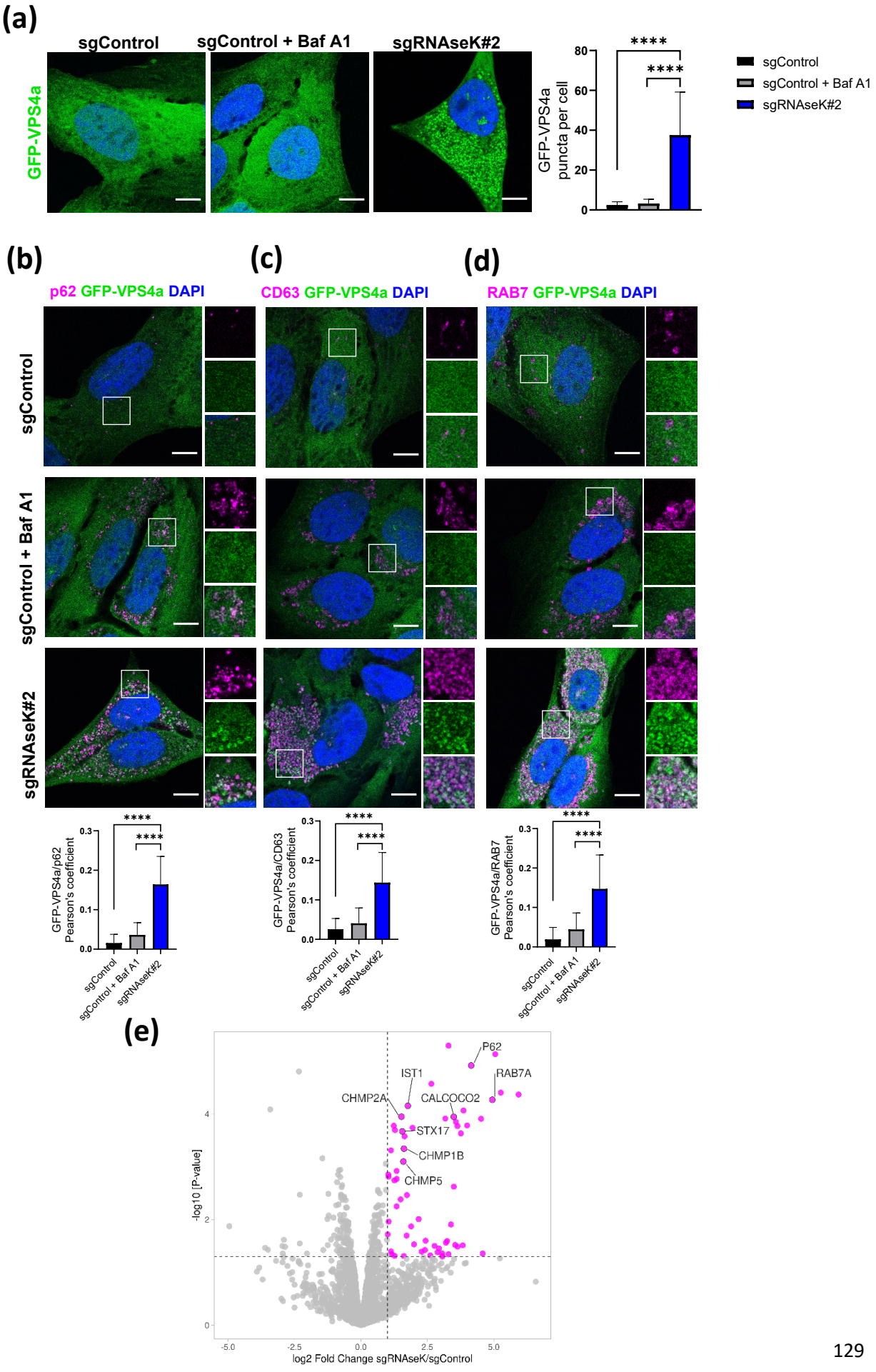
(a)
sgControl
sgControl + Baf A1
sgRNAseK#2
GFP-VPS4a
GFP-VPS4a puncta per cell
****
****
sgControl
sgControl + Baf A1
sgRNAseK#2
(b)
p62 GFP-VPS4a DAPI
(c)
CD63 GFP-VPS4a DAPI
(d)
RAB7 GFP-VPS4a DAPI
sgControl
sgControl + Baf A1
sgRNAseK#2
GFP-VPS4a/p62 Pearson's coefficient
GFP-VPS4a/CD63 Pearson's coefficient
GFP-VPS4a/RAB7 Pearson's coefficient
(e)
P62
IST1
RAB7A
CHMP2A
CALCOCO2
STX17
CHMP1B
CHMP5
-log10 [P-value]
log2 Fold Change sgRNAseK/sgControl

Figure 5.2 VPS4a accumulates on lysosomes in the absence of RNAseK.

(a) *Representative confocal microscopy images of GFP-VPS4a transduced into sgControl or sgRNAseK U2OS cells and cultured in AA starvation media. Baf A1 was added 3 h as indicated. Scale bar: 10 μm. Quantification of VPS4a puncta is shown on the right.* ***(b-d)*** *Representative immunofluorescence image of GFP-VPS4a stably expressed in U2OS cells as in (a) and stained using antibodies against the indicated endogenous proteins. Scale bar: 10 μm. Quantifications of Pearson's colocalization coefficient between GFP-VPS4a and indicated markers are shown below.* ***(e)*** *Volcano plot of interacting proteins identified by MS following GFP-TRAP pulldown of GFP-VPS4a transfected into sgControl or sgRNAseK cells. Hits showing significantly association with GFP-VPS4a in sgRNAseK cell line (P > 0.05; FC > 2) are highlighted in magenta.*

Since VPS4a accumulation presumably happens upstream of PLD3 mislocalisation and subsequent autophagy inhibition, we wanted to test whether it is possible to mimic autophagy phenotype seen in RNAseK depleted cells by modifying VPS4a activity. Dominant negative mutant of VPS4a (VPS4a^{E228Q}) is a point mutant of VPS4a lacking its AAA-ATPase activity (Vajjhala et al., 2008) and previous reports have shown that this mutant accumulates on late endosomal compartments (Nickerson et al., 2010). To test the consequences of enforcing lysosomal localisation of VPS4a on autophagic flux, we analysed the levels of LC3 and p62 in cells expressing either wild type or dominant negative mutant of VPS4a. Cells expressing GFP empty vector or wild type VPS4a were able to induce efficient LC3 and p62 degradation during AA starvation (figure 5.3). However, expression of VPS4a^{E228Q} resulted in an accumulation of LC3-II and p62 under basal condition and AA starvation (figure 5.3). These findings indicate that proper cellular localisation and activity of VPS4a is required for efficient autophagic flux.

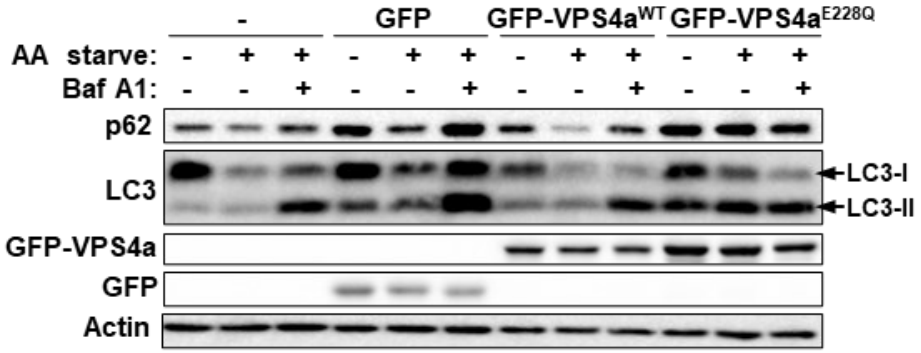

Figure 5.3 Dominant negative mutant of VPS4a inhibits autophagy.

Western blot analyses of U2OS cells transiently expressing the indicated constructs using the indicated antibodies. Cells were AA starved in the presence or absence of Baf A1 for 3 h.

To further underscore the similarities in the phenotype seen in RNAseK depleted cells and cells expressing VPS4a^{E228Q} mutant, I assessed by immunofluorescence analyses the co-localisation of CI-MPR with GM130 and LAMP1. Expression of VPS4a^{E228Q} resulted in an altered cellular localisation of CI-MPR, when compared to cells expressing wild type VPS4a. Dominant negative mutant showed a decreased co-localisation of CI-MPR with GM130 (figure 5.4a). Moreover, CI-MPR co-localisation with LAMP1 was significantly increased upon VPS4 inhibition (figure 5.4b), similar to the phenotype observed in RNAseK knockout cells (figure 4.4b). We speculated that RNAseK could interact with VPS4a in order to regulate its release from lysosomes. To test this, pulldown experiments were performed by mixing cell lysates expressing either GFP-VPS4a or RNAseK-myc followed by GFP-TRAP pulldown, which showed an interaction of the two proteins (figure 5.4c). Similar results were observed in a reciprocal pulldown where GFP-RNAseK could co-precipitate with mCherry-VPS4a (figure 5.4d). This association between RNAseK and VPS4a was further analysed by immunofluorescence imaging. Considering the diffused phenotype of VPS4a in cells and its transient interaction with lysosomes, I used cells expressing VPS4a^{E228Q} mutant and show its co-localisation with endogenously tagged RNAseK-myc (figure 5.4e). Altogether these data indicate that RNAseK could potentially have a role in regulating VPS4a localisation and activity and subsequently PLD3 trafficking.

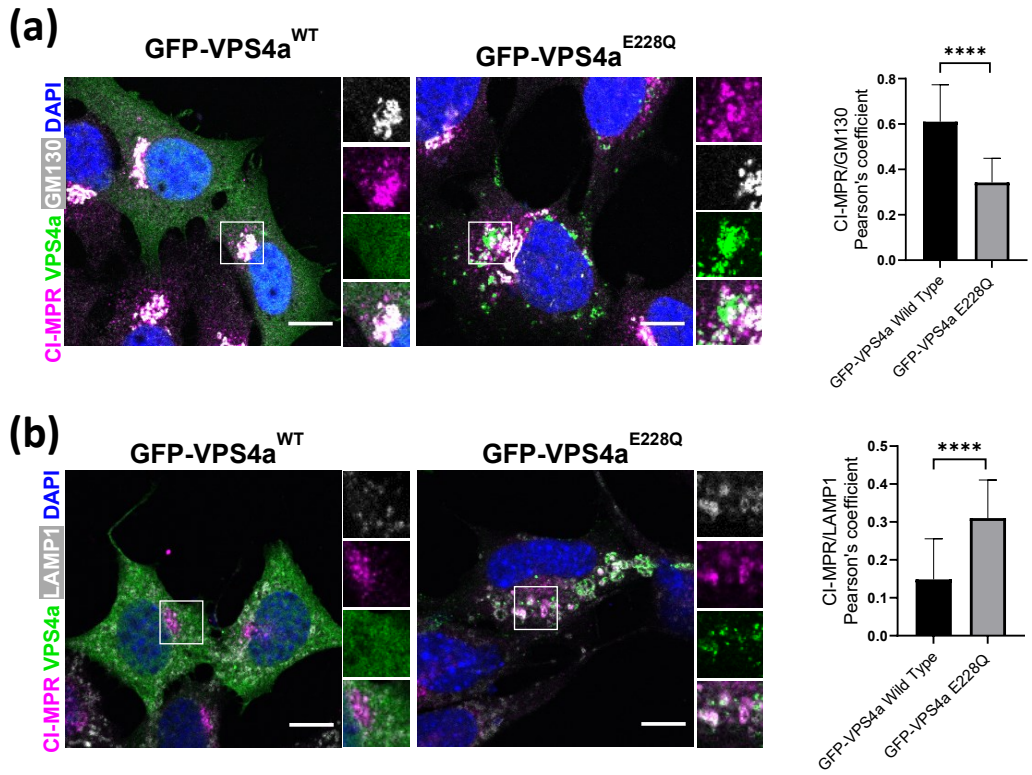
(a)
GFP-VPS4a WT
GFP-VPS4a E228Q
CI-MPR VPS4a GM130 DAPI
CI-MPR/GM130 Pearson's coefficient
****
GFP-VPS4a Wild Type
GFP-VPS4a E228Q
(b)
GFP-VPS4a WT
GFP-VPS4a E228Q
CI-MPR VPS4a LAMP1 DAPI
CI-MPR/LAMP1 Pearson's coefficient
****
GFP-VPS4a Wild Type
GFP-VPS4a E228Q

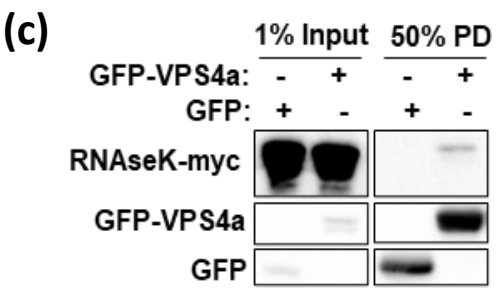
(c)
1% Input
50% PD
GFP-VPS4a: - + - +
GFP: + - + -
RNAseK-myc
GFP-VPS4a
GFP

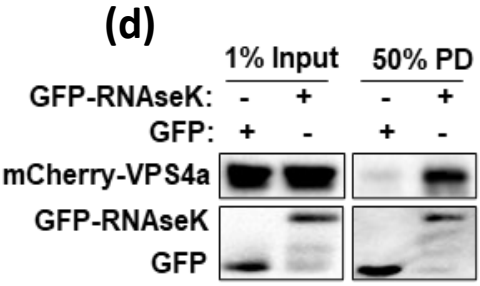
(d)
1% Input
50% PD
GFP-RNAseK: - + - +
GFP: + - + -
mCherry-VPS4a
GFP-RNAseK
GFP

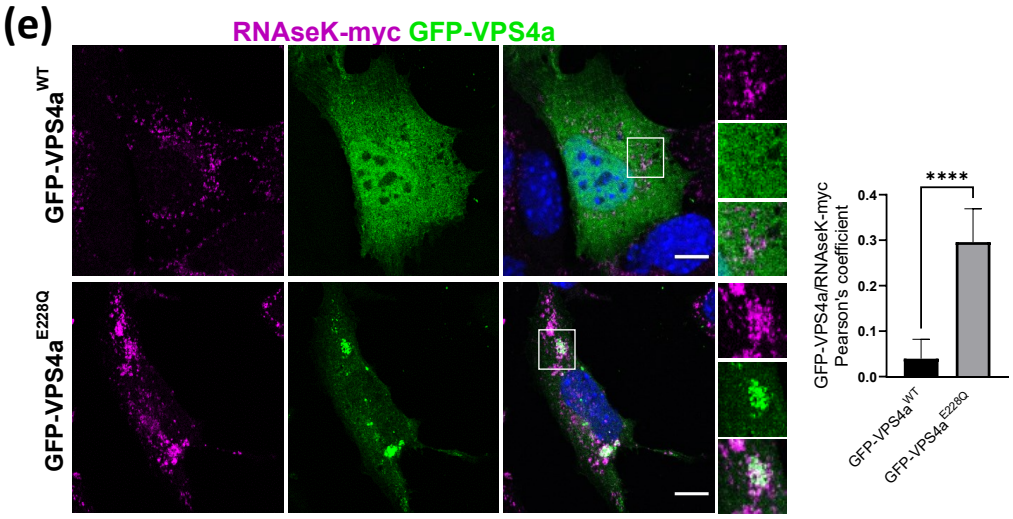
(e)
RNAseK-myc GFP-VPS4a
GFP-VPS4a WT
GFP-VPS4a E228Q
GFP-VPS4a/RNAseK-myc Pearson's coefficient
****
GFP-VPS4a WT
GFP-VPS4a E228Q

Figure 5.4 RNAseK regulates VPS4a dynamics.
(a) *Representative immunofluorescence images of MEF cells transfected with GFP-VPS4a^{WT} or GFP-VPS4a^{E228Q} and cultured in the absence of amino acids for 2 h. Cells were fixed and stained using the indicated antibodies. Scale bar: 10 µm. Quantification of Pearson's colocalization coefficient between CI-MPR and GM130 is shown on the right.* ***(b)*** *Representative immunofluorescence images of MEF cells transfected with GFP-VPS4a^{WT} or GFP-VPS4a^{E228Q} and cultured in the absence of amino acids for 2 h. Cells were fixed and stained using the indicated antibodies. Scale bar: 10 µm. Quantification of Pearson's colocalization coefficient between CI-MPR and GM130 is shown on the right.* ***(c)*** *HEK293T cells were transfected with GFP or GFP-VPS4a plasmids along with RNAseK-myc expressing plasmid. Cell lysates were then mixed and subjected to GFP-TRAP pulldown (PD) followed by western blotting analyses using the indicated antibodies.* ***(d)*** *HEK293T cells were transfected with GFP or RNAseK-GFP plasmids along with mCherry-VPS4a expressing plasmid. Cell lysates were treated as in (c).* **(e)** *Representative immunofluorescence images of RNAseK-myc MEF cells transfected with GFP-VPS4a^{WT} (top panel) or GFP-VPS4a^{E228Q} (bottom panel) and cultured in the absence of amino acids for 2 h. Cells were fixed and stained using antibodies against myc. Scale bar: 10 µm. Quantification of Pearson's colocalization coefficient between RNAseK-myc and GFP-VPS4a is shown on the right. In all experiments, ****p<0.0001, assessed by unpaired Student's t-test from three independent experiments.*

5.4 Discussion

This chapter has highlighted a role for PLD3 and VPS4a in efficient autophagic flux. Details of the regulatory network and an exact functions of PLD3 are yet to be fully characterised. However, my data show that PLD3 is essential for autophagy in mouse and human cells. Previous studies reported a reduced autophagic activity in cells co-expressing mutants of PLD3 with diminished phospholipase activity together with mutant of APP protein (Tan et al., 2019). Expression of these mutants resulted in increased mTORC1 activity, decreased LC3-II and increased p62 levels (Tan et al., 2019). These results differ from the phenotype I observed upon the depletion of PLD3 in mouse fibroblasts and human neuronal cells with regards to LC3 status. The discrepancies between the two observation might be due to a difference between PLD3 knockdown and expression of PLD3 mutants. Moreover, these PLD3 constructs were expressed in cell lines stably expressing the Swedish mutant of APP protein

APP(695), which causes an increased amyloidogenic processing of APP and possibly could change the dynamics of PLD3 (Belyaev et al., 2010; Tan et al., 2019). Reduction in PLD3 activity has been connected to a disruption in the endolysosomal network and enlarged LAMP1 structures (Fazzari et al., 2017; Yuan et al., 2022). On the other hand, overexpression of PLD3 was also shown to result in enlargement and accumulation of endolysosomal vesicles in neurons suggesting that the levels of PLD3 need to be carefully regulated in cells (Yuan et al., 2022). Similar to previous reports, lysosomal morphology appears to be enlarged in MEFs upon PLD3 knockdown in this study. Interestingly, because PLD3 is trafficked to lysosomes via MVBs and is sorted into ILVs, it has been proposed that the aberrant endolysosomal structures appearing in cells with reduced PLD3 activity are a consequence of improper ILV formation (Yuan et al., 2022). However, my data show that EGFR degradation in cells depleted of PLD3 remains intact. This indicates that ILV formation in the absence of PLD3 is not disrupted as EGFR is trafficked to the lysosomes via ILVs (Futter et al., 1996).

PLD3 is targeted to lysosomes in a VPS4a-depedent manner (Gonzalez et al., 2018a). In agreement with these reports, VPS4a mislocalisation seen in RNAseK knockout cells could disrupt the trafficking of PLD3 to lysosomes. As previously mentioned, depletion of PLD3 increases the extracellular Aβ levels and phospholipase deficient mutant of PLD3 ($PLD3^{VM}$) has been associated with late-onset of AD (Cruchaga et al., 2014). Moreover, in brains of AD patients, extracellular levels of PLD3 are increased (Satoh et al., 2014). However, in early stages of AD, before extracellular deposits of Aβ plaques build-up, Aβ accumulates intracellularly in enlarged late endosomal compartments (Willén et al., 2017). This phenotype can be recapitulated by the expression of a dominant negative mutant of VPS4a ($VPS4a^{E228Q}$) and could be used to model early pathological features reported in AD (Willén et al., 2017). Indeed, $VPS4a^{E228Q}$ accumulates on late endosomal compartments causing their enlargement and subsequent accumulation of Aβ and tau phosphorylation, thereby mimicking the changes seen on a cellular level in early AD models (Willén et al., 2017). Thus, it would be interesting to test whether the phenotype seen in early AD model is a consequence of improper trafficking of PLD3 caused by VPS4a arrest on late endosomal compartments. Comparison of PLD3 levels in the secretome of cells expressing wild type VPS4a or $VPS4a^{E228Q}$ could help address this question.

Disrupted localisation of VPS4a in the absence of RNAseK was confirmed by proteomics and immunofluorescence analyses (figure 5.2a-e). My study shows that VPS4a accumulates on lysosomes in RNAseK knockout cells, similarly to the phenotype seen by overexpression of dominant negative mutant of VPS4a (VPS4a^{E228Q}). Expression of VPS4a^{E228Q} results in inhibited autophagic flux and accumulation of lipidated LC3, similarly to what is seen upon RNAseK depletion. Moreover, I observed increased lysosomal localisation of CI-MPR when VPS4a^{E228Q} was overexpressed in the cells. The alerted CI-MPR localisation upon the expression of VPS4a^{E228Q} and RNAseK depletion suggest that ESCRT-III complex components may be involved in the canonical delivery of hydrolases to the lysosomes via CI-MPR and arrested VPS4a localisation disrupt these processes. Further investigation of the cellular localisation and activity of lysosomal proteins and receptors involved in trafficking of hydrolases in cells expressing VPS4a^{E228Q} is required to address this hypothesis.

Although similarities between RNAseK knockout and VPS4 inhibition are apparent, VPS4a^{E228Q} does not fully recapitulate the phenotype seen in RNAseK depleted cells. Expression of the dominant negative mutant of VPS4a was shown to disrupt autophagosome closure (Takahashi et al., 2018a). However, these processes remain intact in RNAseK knockout cells. This suggests that although VPS4a appears to be arrested on lysosomes in the absence of RNAseK, its activity may not be fully abrogated. The differences in the phenotypes observed when VPS4a is arrested on lysosomes due to the absence of RNAseK and when VPS4a^{E228Q} is overexpressed require more investigation. For example, it would be interesting to test whether the functions of VPS4a in other cell processes are disrupted upon RNAseK depletion.

Pulldown experiments and immunofluorescence analyses suggest common subcellular localisation of RNAseK and VPS4a and suggest that RNAseK could potentially play a role in releasing of VPS4a from lysosomes. Although I did not observe an accumulation of VPS4a on lysosomes in cells treated with Baf A1, other subunits of V_0 domain of V-ATPase proton pump could be involved in efficient release of VPS4a from lysosomes. It would be interesting to test whether a similar arrest of VPS4a on lysosomes can be detected upon the depletion of other subunits of the V-ATPase proton pump. Pulldown experiments in whole cell lysates do not distinguish whether the interaction between RNAseK and VPS4a is direct. Because RNAseK is a

dual transmembrane protein, it is technically challenging to test its interaction with VPS4a using purified proteins. Pulldown assays using VPS4a truncations would allow to specify the binding region required to interact with RNAseK. Moreover, multiple point mutants of VPS4a leading to its reduced activity were identified in mammalian cells. Overexpression of these mutants results in enlarged lysosomes as seen upon VPS4a^{E228Q} overexpression (Rodger et al., 2020). Testing the ability of these point mutants to bind RNAseK would allow me to determine whether the binding site is located within the ATP catalytic site of VPS4a and whether the expression of these inactive mutants of VPS4a could be used to recapitulate the effects of RNAseK knockout in cells.

Altogether, these data show that PLD3 is a lysosomal lipase essential for autophagic flux in mammalian cells. Lysosomal localisation of PLD3 is required for efficient cargo degradation by autophagy and PLD3 activity depends on proper VPS4a cellular localisation. VPS4a accumulation on lysosomes upon RNAseK depletion results in aberrant localisation of certain lysosomal hydrolases and proteins involved in enzyme trafficking.

Chapter 6. Summary and discussion

The main aim of my thesis was to characterise the function of a novel autophagy regulator RNAseK identified in genome-wide CRISPR-Cas9 screen conducted prior to the start of my PhD. My findings show that RNAseK mainly localises to lysosomes and depletion of RNAseK from the cells dysregulates the localisation of multiple hydrolases and proteins which associate with lysosomes. I hypothesise that RNAseK can regulate the dynamics of VPS4a on lysosomes, which in turn ensures efficient lysosomal trafficking of PLD3. Therefore, in the absence of RNAseK, the arrest of VPS4a on lysosomes may be the cause for the misdelivery of PLD3 to lysosomes and its increased secretion. I showed that PLD3 is essential for autophagic flux and I predict that the IAM accumulation upon RNAseK depletion could be a result of diminished activity of PLD3 in these cells. The graphical abstract of my working model is depicted below (figure 6.1).

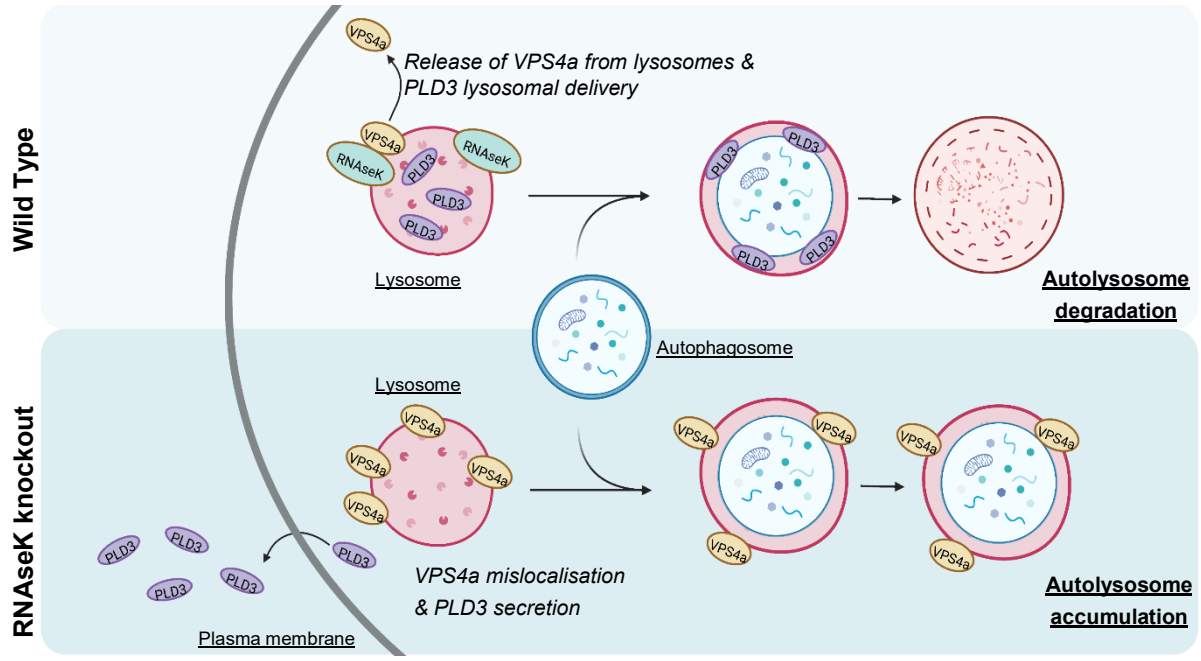

Figure 6.1 Graphical abstract.

Summary depicting a role of RNAseK in releasing VPS4a from lysosomes to allow efficient lysosomal localisation of PLD3 required for autophagosome degradation. In the absence of RNAseK, VPS4a accumulates on lysosomes and leads to enhanced secretion of PLD3 thereby disrupting autophagosome degradation.

RNAseK is a poorly characterised protein. Therefore, my study includes multiple novel findings for the role on RNAseK in autophagy and overall lysosomal homeostasis. Depletion of RNAseK disrupts IAM degradation and the balance of certain lipids in cells. Interestingly, all three tested lysosomal lipases, LIPA, PLA2G15, and PLD3, were affected by RNAseK depletion albeit in a different manner. LIPA and PLD3 levels in the lysosomal fractions are reduced and LIPA's activity is abrogated upon depletion of RNAseK. Although PLA2G15 levels in the lysosomal proteomics did not show significant differences between control and RNAseK knockout cells, maturation of this enzyme seems to be disrupted in the absence of RNAseK, potentially due to its increased association with CI-MPR. It would be interesting to see whether the depletion of all three lipases results in more dramatic autophagy phenotype when compared to PLD3 knockdown alone. LIPA and PLA2G15 have been previously connected to autophagy in *C.elegans* through to their potential roles in lipophagy and IAM degradation, respectively (Li et al., 2022; Zhang et al., 2022). Detailed analyses of each the three lysosomal lipases in RNAseK knockout cells would be interesting although challenging due to lack of information about these proteins, such as cleavage sites, and precise tools to study the activity of each lipase. Whilst robust antibodies to detect these lipases are not available, their overexpression in cells might not recapitulate the dynamics of the endogenous protein. This could be overcome by endogenous tagging. However, due to the proteolytic cleavage of the lipases upon their maturation, an endogenous tag would have to be inserted at the N- and C-termini of the protein, which makes this process labour intensive and technically challenging.

I focused on studying the lysosomal lipase PLD3, which levels are reduced in lysosomes of RNAseK knockout cells and is preferentially secreted. PLD3 exhibits similarities to Atg15, a yeast lipase crucial for IAM degradation (Epple et al., 2001; Teter et al., 2001). Both of these proteins contain transmembrane domains and are delivered to the lysosome via MVB, which is unusual for lysosomal hydrolases (Gonzalez et al., 2018a; Hirata et al., 2021). PLD3 depletion resulted in autophagy block and the accumulation of LC3 and p62. These findings make PLD3 the first mammalian lipase identified to be essential for autophagy, possibly due to its role in IAM degradation. It would be interesting to confirm whether IAM degradation is disrupted upon PLD3 depletion, as seen in cells lacking RNAseK. PLD3 activity in IAM

degradation could potentially be tested in *in vitro* settings of isolated autophagic membranes. However, such experiments would be and technically challenging due to the resistance of the OAM resistant to hydrolysis. Moreover, the exact sequence of mature PLD3 remains unknown, therefore it cannot be expressed in an active form further underscoring the technical difficulties I have been experiencing throughout my PhD studies.

In the absence of RNAseK, EGFR delivery to the lysosomes via ILVs and lysosomal degradation remains intact. This was an interesting observation because VPS4a was shown to be involved in ILV formation (Adell et al., 2014). Therefore, the accumulation of VPS4a on lysosomes observed in RNAseK knockout cells in theory should disrupt this process. However, previous studies have shown that co-depletion of VPS4a and VPS4b, but not VPS4a alone, inhibits EGFR degradation (Fraile-Ramos et al., 2007). Therefore, it is possible that VPS4b takes over that some functions of VPS4a in RNAseK knockout cells. The differences in membrane composition between IAM and ILV are unclear, therefore it is challenging to determine why ILVs presumably remain to be degraded in the absence of RNAseK, whereas IAM accumulates in the lysosomal lumen. This could be due to different factors required for efficient membrane degradation of ILVs, which remain unaffected upon RNAseK depletion. Moreover, EGFR is also incorporated into the membrane of ILV rather than fully encapsulated by it, therefore part of the protein is exposed to the lysosomal lumen (Raiborg and Stenmark, 2009). This partial exposure could suffice for EGFR and ILV to be degraded.

The effects of RNAseK depletion on VPS4a prompted me to look more closely into VPS4a function in autophagy and lysosomal enzyme delivery. In addition to the already established role of VPS4a in autophagosome closure (Takahashi et al., 2018a), I have discovered a novel role for VPS4a in IAM degradation during autophagy. Although VPS4a was previously implicated in an efficient trafficking of PLD3 to the lysosomes (Gonzalez et al., 2018a), it seem that the role of VPS4a in the trafficking of hydrolases is not confined to PLD3. This is represented by increased lysosomal localisation of CI-MPR in cells expressing inactive form of VPS4a. This accumulation of CI-MPR on lysosomes could cause an imbalance in lysosomal content, therefore the use of a dominant negative mutant of VPS4a to model early AD events, as proposed in a published studies (Willén et al., 2017), should be analysed

with caution as it could result in generation of misleading data due to the potential role of VPS4a in regulation of CI-MPR. It would be interesting to test whether the early AD events, such as accumulation of Aβ and tau phosphorylation, could be seen upon RNAseK depletion in early AD cell models.

Another aspects of the project that remain to be elucidated are the upstream events that lead to the recruitment of VPS4a to the lysosomes in the absence of RNAseK. Upon lysosomal damage, Galectin-3 recruits the ESCRT machinery to the damage site to promote repair, which results in transient association of VPS4a with lysosomes (Jia et al., 2020). Could lysosomal damage be prevalent in the absence of RNAseK? Immunofluorescence imaging of Galectin-3 in RNAseK knockout lines could help address this. However, prolonged lysosomal damage leads to a disruption in lysosomal acidity and function (Eriksson et al., 2020), which was not observed in RNAseK knockout cells.

The activity of the V-ATPase complex is not restricted to proton pumping and the complex is involved in multiple other cellular processes. For an example, studies in yeast have shown that the V_0 domain promotes membrane fusion invents (Peters et al., 2001). V-ATPase complex assembly is also crucial for CASM (Hooper et al., 2022). Moreover, the V-ATPase was shown to be involved in insulin secretion from pancreatic β-cells (Sun-Wada et al., 2006) and exocytosis of synaptic vesicles (Hiesinger et al., 2005). My PhD studies have shown a novel function of RNAseK, a subunit of the V-ATPase proton pump, that is independent of lysosomal acidification. However, whether the activity of RNAseK requires its interaction with the V-ATPase complex remains to be addressed. This could be investigated by testing if the phenotype seen upon RNAseK knockout can be recapitulated by the depletion of other subunits of the V-ATPase complex. Interestingly, Baf A1 treatment, which inhibits V-ATPase pump assembly, did not mimic the phenotype seen upon RNAseK depletion. Therefore, I predict that the phenotype seen upon RNAseK depletion would not be observed upon the knockout of proteins within the V_1 domain of the complex.

The phenotype seen in cells upon the depletion of RNAseK suggests that this protein might be a novel candidate for a less toxic and more efficient cancer treatment. RNAseK depletion inhibits autophagy pathway but does not seem to disrupt general proteolytic activity of lysosomes. This differs from other approaches to inhibit autophagy in cancer, like HCQ or CQ treatment, where degradative qualities of the

lysosomes are abrogated (Verbaanderd et al., 2017). Moreover, it is possible that the upregulation of *RNASEK* seen in a percentage of glioblastoma patients could play a role in increasing autophagic activity in tumour cells. Upregulation of *RNASEK* expression was shown to corelate with resistance to chemotherapy, in agreement with reports related to the cytoprotective role of autophagy during anticancer treatment (Filippi-Chiela et al., 2015; Hsu et al., 2021; Yan et al., 2016). Therefore, targeting RNAseK and inhibiting its expression or function in cells could result in more effective treatment and prevent therapy resistance.

Targeting of RNAseK could also play vital a role in therapy specific subset of cancers. Mothers against decapentaplegic homolog 4 (*SMAD4*) is a tumour suppressor gene deleted or mutated in almost 30% of all cancers and (Neggers et al., 2020). Loss of *SMAD4* is associated with 60%–90% of pancreatic adenocarcinomas and corelates with poor prognosis (Fei et al., 2021). Studies evaluating cancer dependencies have shown that tumours depleted of SMAD4 often lack VPS4b as the two genes reside next to one another on chromosome 18 (McDonald et al., 2017; Neggers et al., 2020). The absence of VPS4b in these tumours makes them vulnerable to the loss of VPS4a, whereas depletion of VPS4a in a healthy cell is not lethal. Therefore, drugs designed to inhibit the function of VPS4a could potentially result in the death of SMAD-depleted cancer cells (McDonald et al., 2017; Neggers et al., 2020). As discussed in previous chapters, loss of RNAseK results in abnormal localization of VPS4a and potentially reduced activity of VPS4a. Therefore, it is possible to target VPS4a indirectly by inhibiting RNAseK. SMAD4-deficient pancreatic tumours often exhibit resistance to therapy by upregulating autophagy (Fei et al., 2021). Studies have shown that the inhibition of autophagy by HCQ significantly improved response to therapy in patients with SMAD4 depletion (Fei et al., 2021). These data suggest that targeting RNAseK in SMAD4-deficient tumours could be an attractive therapy target due to its dual role in VPS4a regulation and autophagic flux. Using just one target, as opposed to combination therapy, would provide less toxic alternative to anticancer treatment and possibly fewer off-target effects.

Chapter 7. Validation of ATG2 as a novel binding partner of ATG16L1

7.1 Introduction

Autophagy is a highly complex pathway governed by multitude of factors. In recent years, research provided a great insight into the regulation of autophagy, however many questions remain unanswered. In addition to search for novel regulators of the pathway, it is important to further characterise already known autophagy players, as the dynamics of these proteins are poorly characterised. Understanding the regulation of recruitment and release of autophagy proteins to the autophagosomal membrane could provide insights to the modulation of autophagy in disease. To gain an insight into the regulation of autophagy proteins in an unbiased way, I utilised proximity labelling tools. Prior to the start of my PhD, I performed a screen in search for new regulators of multiple autophagy proteins, including ATG16L1. ATG16L1 was tagged to the promiscuous biotin ligase, TurboID (TiD) (Branon et al., 2018) and expressed in ATG16L1 knockout cells (appendix 2a). Tagging the N-terminus of ATG16L1 with TiD (TiD-ATG16L1) did not the disrupt its function in autophagy and the construct was able to biotinylate known interacting partners of ATG16L1 upon treatment with exogenous biotin (appendix 2a,b). Therefore, I used cells expressing TiD-ATG16L1 and induced autophagy by AA starvation in the presence of biotin and biotinylated proteins were precipitated using streptavidin coated beads followed by MS analyses. In addition to already known interactors of ATG16L1 (such as FIP200 and WIPI2), MS analyses of biotinylated proteins showed ATG2b as one of the top hits in the screen (appendix 2c). This result indicated that ATG2b is in close proximity of ATG16L1, which suggested that the two proteins could potentially be interacting partners. This drew our attention because although both proteins are known autophagy regulators, the interaction between them has not been identified before. Both ATG16L1 and ATG2 proteins are crucial for autophagy and their depletion results in the inhibition of autophagic flux (Fujita et al., 2008; Velikkakath et al., 2012). Although the biotinylation was performed under nutrient stress, which is an autophagy inducer, it is possible that the functional relevance of this potential interaction between ATG16L1 and ATG2 is unrelated to canonical autophagy. Both proteins have additional roles in processes other than

autophagy. Indeed, ATG2 was shown to have a role in the regulation of lipid droplets size and distribution, whereby the C-terminal end of the protein is crucial for these processes but dispensable for the role of ATG2 in autophagy (Tamura et al., 2017; Velikkakath et al., 2012). ATG16L1 also plays a role during immune response upon bacterial infection (Sorbara et al., 2018), exosome production (Guo et al., 2017), hormone secretion (Ishibashi et al., 2012) and CASM (Fletcher et al., 2018). To determine whether the binding between ATG16L1 and ATG2 is required for autophagy, I aimed to assess the domain required for this interaction. N-terminal and middle regions of ATG16L1 are crucial for lipidation processes during autophagy, whereas the WD40 region at the C-terminus of the protein is dispensable for canonical autophagy (Fletcher et al., 2018; Gammoh et al., 2013; Lystad et al., 2019; Matsushita et al., 2007). On the other hand, ATG16L1 function during CASM relies on the C-terminus of ATG16L1 and deletion or mutation of this fragment results in the inhibition of LC3 lipidation on single membranes (Fletcher et al., 2018). These reports show that a complete protein depletion or deletion of large fragments of the proteins can disrupt multiple processes in cells. Therefore, when studying the functional relevance of an interaction between two proteins, it is important to find a specific binding site in order to distinguish the contribution of the studied protein-protein interaction in any biological pathway tested instead of relying on the deletion of the whole proteins or large fragments.

7.2 Aims and objectives

TurboID-based screen allows the identification of proteins in proximity of the bait protein fused to the promiscuous biotin ligase, however, it does not necessarily mean that highly biotinylated proteins are directly interacting with the bait protein (Branon et al., 2018; May et al., 2020). Therefore it is crucial to confirm whether ATG2 interacts with ATG16L1. Moreover, ATG2b was one of the top hits in MS analyses obtained from cells overexpressing TiD-ATG5, similarly to the results seen with TiD-ATG16L1 (data not shown). These observations suggest that the interaction of ATG2 with ATG16L1 could be ATG5-dependent. ATG2a and ATG2b are the two homologues of yest Atg2 (Velikkakath et al., 2012). Thus it is possible that both

proteins are able to bind ATG16L1 due to sequence similarity. Base on these observations, the objectives of this chapter are listed below.

1. To investigate the interaction between the two ATG2 proteins with ATG16L1 by co-immunoprecipitation experiments in the presence or absence of ATG5.
2. To test whether the interaction between ATG2 and ATG16L1 could be direct using in vitro binding experiment.
3. To specify the region mediating ATG2-ATG16L1 interaction using co-immunoprecipitation experiments and mutagenesis.

7.3 Results

7.3.2 Validation of the ATG2-ATG16L1 interaction

Although biotin ligase-based proximity assays are a great tool to investigate proteins surrounding the bait of interest, data obtained from these approaches need to be further validated. Firstly, I aimed to test whether ATG16L1 is able to interact with ATG2b, as suggested by the TiD-ATG16L1 proximity screen MS analyses. Because the two ATG2 proteins exhibit sequence similarity and have been shown to be functionally redundant (Velikkakath et al., 2012), binding of ATG2a to ATG16L1 was also tested. When tested in HEK293T cells, Co-expression of ATG16L1 and ATG2 constructs in the same dish led to high variability in protein expression levels (data not shown). For this reason, lysate mixing approach was used whereby each constructs was overexpressed in a separate dish and cell lysates were mixed before incubation with the indicated affinity beads. Pulldown of GFP-tagged ATG2 constructs resulted in the co-precipitation of overexpressed ATG16L1 protein indicating that both ATG2a and ATG2b are interacting partners with ATG16L1 (figure 7.1a). To check whether ATG5 is required for ATG2-ATG16L1 binding, pulldown experiments were also performed in HEK293T cells lacking ATG5. ATG16L1 was still able to bind to ATG2 in the absence of ATG5 indicating that ATG5 is dispensable for this interaction (figure 7.1a).

Pulldown assays in whole cell lysates do not provide the information whether the interaction between ATG2 and ATG16L1 is direct. Binding assays of purified

recombinant proteins would help us answer this question. As purified recombinant ATG2 proteins were not available in our lab, we overexpressed GFP-tagged ATG2 or empty GFP in cells and used GFP-Trap pulldown followed by stringent detergent washes to purify GFP-tagged proteins and reduce contamination. Purity of the ATG2 proteins was assessed by Ponceau staining (data not shown). These GFP beads-bound proteins were then incubated with ATG16L1 recombinant protein (Dudley et al., 2019a). Pulldown assays showed significant interaction of ATG2a and ATG2b with ATG16L1, when compared to empty GFP control (figure 7.1b), which suggests a potential direct binding between these proteins. As ATG2a showed a higher association with recombinant ATG16L1 (figure 7.1b) and ATG2b antibodies exhibited non-specific bands (figure 7.1a), we used ATG2a constructs in our experimental settings henceforth.

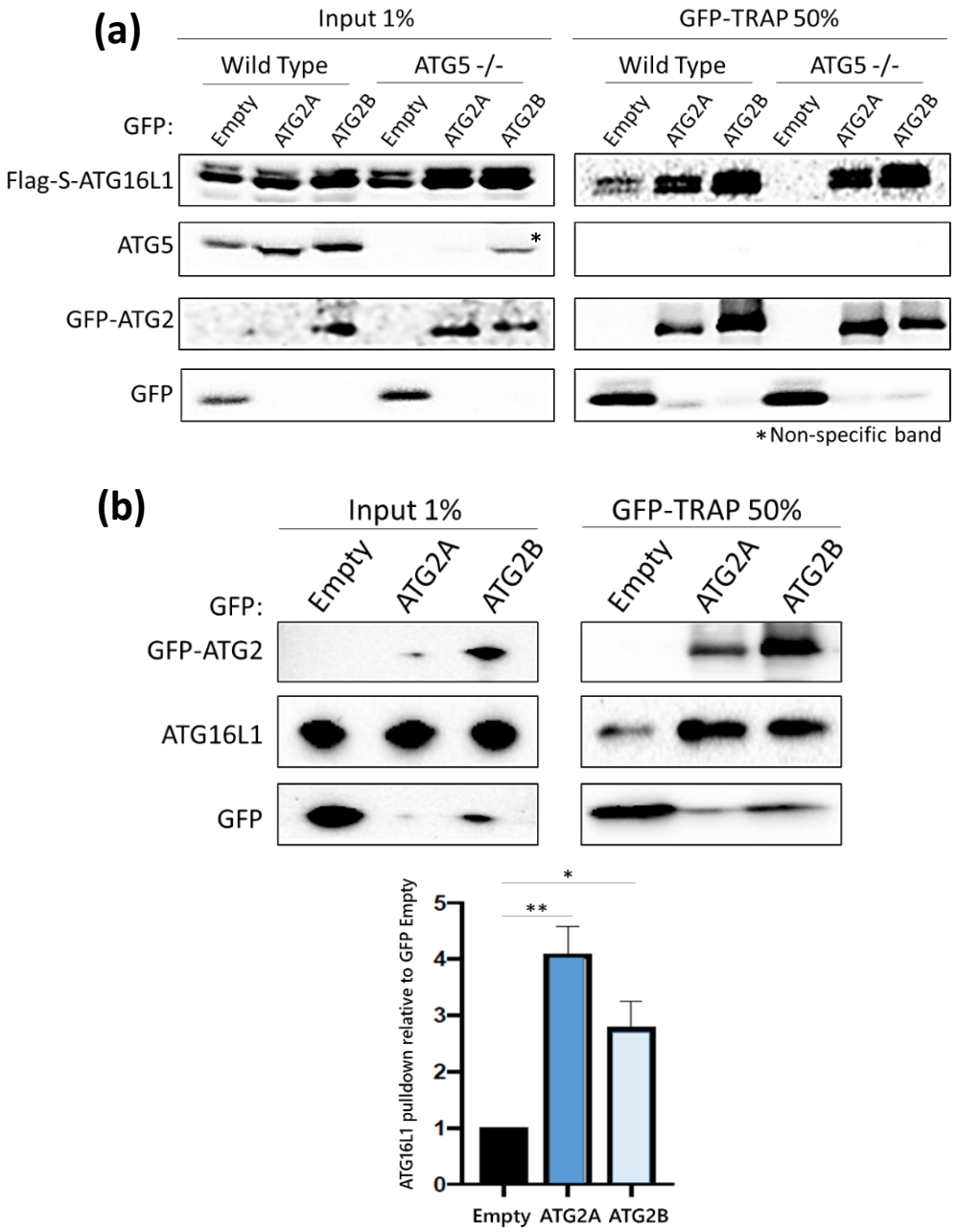

Figure 7.1 ATG16L1 interacts with ATG2.

(a) *Protein–protein interaction assay in cells transiently transfected with the indicated GFP constructs and Flag-S-ATG16L1 in wild type (WT) or ATG5 -/- HEK293T cell lines. GFP-TRAP pull-down was followed by immunoblotting using the indicated antibodies.* ***(b)*** *Protein–protein interaction assay of purified GFP-tagged proteins expressed in HEK293T cells and recombinant ATG16L1 protein. GFP-TRAP pulldown was followed by immunoblotting using the indicated antibodies. Quantification of pulldown with values normalised to GFP-Empty control is shown below. Mean + SD is shown from at three independent experiments. * p<0.05, ** p<0.01, assessed by unpaired Student's t-test.*

7.3.3 Mapping the ATG2-ATG16L1 interaction sites

Next, we aimed to determine the region within ATG16L1 essential for binding to ATG2a. Truncation mutants of ATG16L1 (Dudley et al., 2019; Gammoh et al., 2013) or HA-tagged ATG2a were expressed in ATG16L1 knockout HEK293T cells. Cell lysates were mixed and incubated in the presence of anti-HA beads. Pulldown of ATG2a showed that the N-terminal region of ATG16L1 does not bind ATG2a, whereas full length protein and C-terminal region co-precipitate with ATG2a (figure 7.2). C-terminal region of ATG16L1 consists of WD40 domains which are dispensable for autophagy (Fletcher et al., 2018). Therefore, these results indicate that the functional relevance of ATG2-ATG16L1 interaction is highly likely unrelated to autophagy.

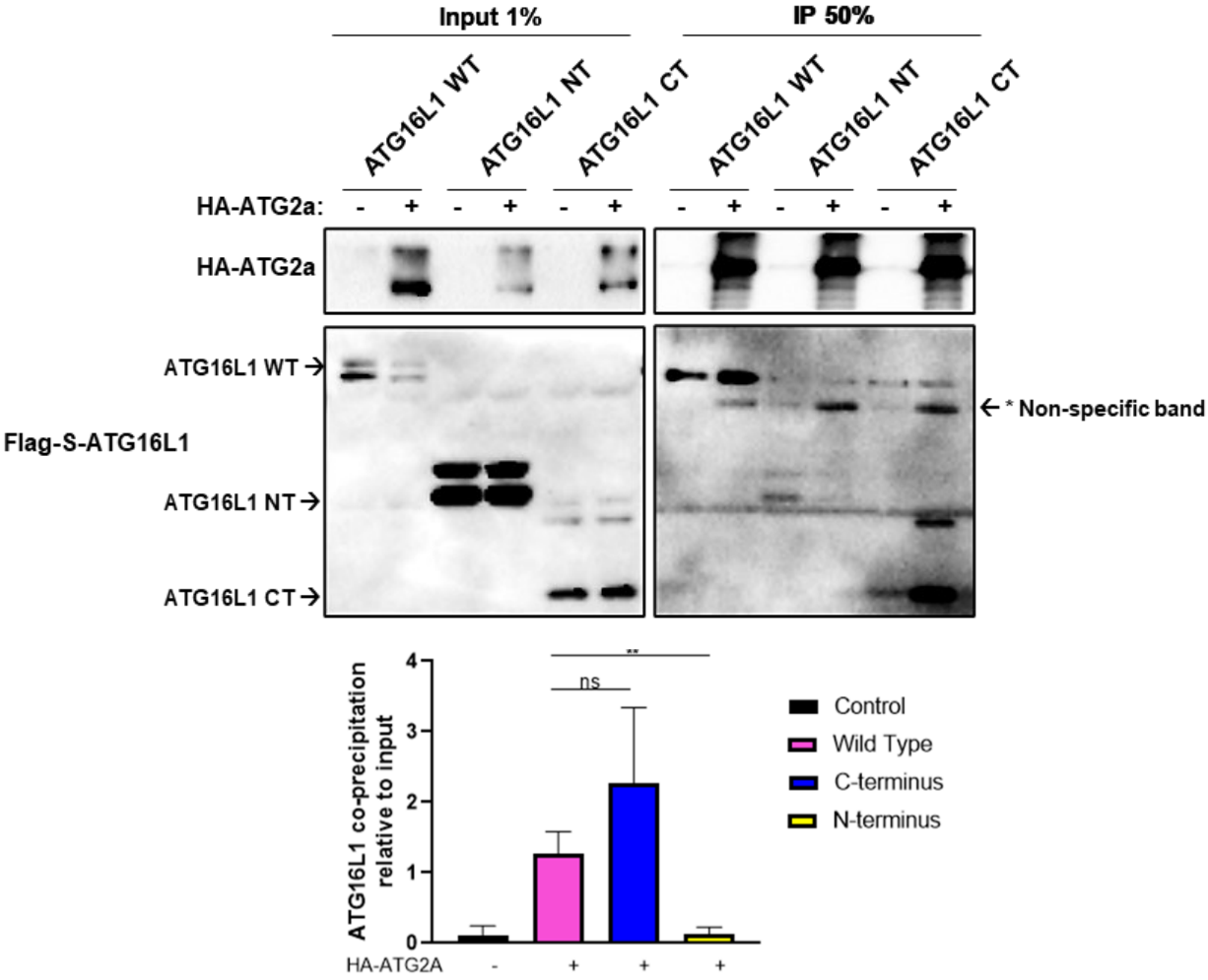

Figure 7.2 ATG16L1 interacts with ATG2 via C-terminus.

*Protein–protein interaction assay in ATG16L1 knockout HEK293T cells transiently transfected with HA-ATG2a or the indicated Flag-S-ATG16L1. Cell lysates were mixed and HA tag pull-down was performed followed by immunoblotting using the indicated antibodies. The following ATG16L1 proteins consist of the indicated amino acids: WT (wild type): 1-623, NT (N-terminus): 1-336, CT (C-terminus): 337–623. Quantification of relative ATG2a-ATG16L1 binding is shown below. Mean + SD is shown from at three independent experiments, non-significant (ns), ** p<0.01, assessed by unpaired Student's t-test.*

WIPI4 is another protein which consist of WD40 domains and was reported to interact with ATG2a (Bakula et al., 2017; Zheng et al., 2017). The residues on ATG2a essential for WIPI4 binding have been previously identified and were narrowed down to three residues (YFS) in the middle region of ATG2a protein (figure 7.3a) (Chowdhury et al., 2018; Zheng et al., 2017). Pulldown assay was performed to test whether WIPI4 binding mutant of ATG2a (YFS/AAA) is still able to interact with the WD40 domain of ATG16L1 located within its C-terminal half. The levels of ATG16L1 co-precipitating with ATG2a YFS/AAA mutant were significantly diminished but not completely abolished when compared to the wild type protein (figure 7.3b). This finding suggests that YFS residues on ATG2a could contribute to the interaction between ATG2a with ATG16L1.

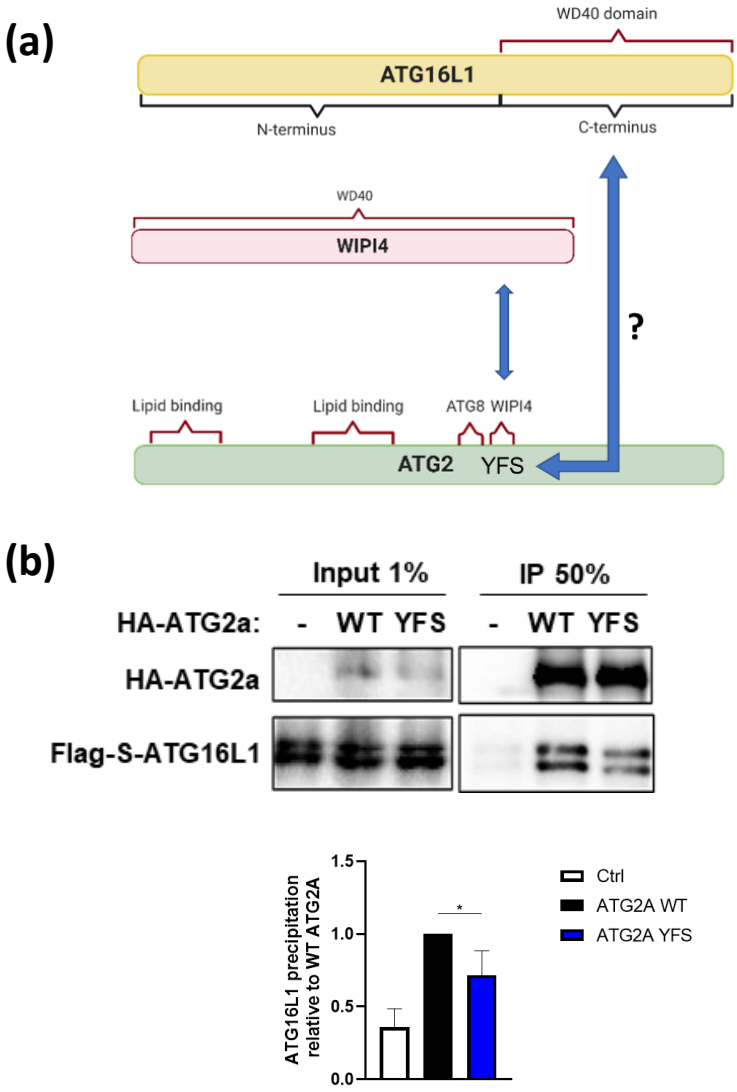

Figure 7.3 ATG2a YFS mutant shows reduced interaction with ATG16L1.

(a) *Schematic diagram of ATG2a and its potential binding to the WD40-containing proteins, WIPI4 and ATG16L1.* ***(b)*** *Protein–protein interaction assay in ATG16L1 knockout HEK293T cells transiently transfected with the indicated HA-ATG2a constructs or Flag-S-ATG16L1. Cell lysates expressing the indicated proteins were mixed and HA tag pull-down was performed, followed by immunoblotting using the indicated antibodies. Quantification of relative ATG2a-ATG16L1 binding is shown below. Mean + SD is shown from at three independent experiments, * p<0.05, assessed by unpaired Student's t-test.*

I proceeded with identifying the binding residues on ATG2a which are required to disrupt ATG16L1 binding. Although it is possible to obtain truncation mutants of ATG2a (Tamura et al., 2017), deletions within ATG2a can lead to failed expression or

protein degradation (Bozic et al., 2020). Alanine scanning mutagenesis (Lefèvre et al., 1997) of ATG2a was also unfeasible due to a relatively large size of ATG2a protein (~1,900-aa). Therefore, to investigate the binding site between ATG2a and ATG16L1, we utilised a peptide array approach. ATG2a protein was fragmented into overlapping peptide fragments and bound to a membrane (JPT Peptide Technologies). To exclude misleading data, unspecific binding of ATG2a fragments to the secondary antibody was assessed by incubating the membrane with secondary antibody only (figure 7.4a). Incubation of the ATG2a peptide array membrane with recombinant ATG16L1 revealed multiple fragments of ATG2a binding to ATG16L1 (figure 7.4b). I selected regions of ATG2a potentially involved in binding to ATG16L1 but not detected when membrane was incubated with secondary antibody alone (figure 7.4b). In agreement with previous reports, alanine substitution of ATG2a fragments resulted in failed expression or unstable protein levels of certain mutants (data not shown) (Bozic et al., 2020). However, we were able to express and test ATG2a mutant with residues 221 to 227 substituted to alanine (AA 221-227). This region is located after lipid binding domain identified at the N-terminus of the protein (Valverde et al., 2019). Pulldown assays showed a significantly reduced binding of ATG16L1 to AA 221-227 mutant when compared to wild type protein (figure 7.4c). This indicated that the mutated residues are essential for ATG16L1 binding and ATG2a AA 221-227 could potentially be used to study the functional relevance of the interaction of ATG2 with ATG16L1. Altogether, these data narrowed down regions on both ATG16L1 and ATG2a essential for the interaction between the two proteins.

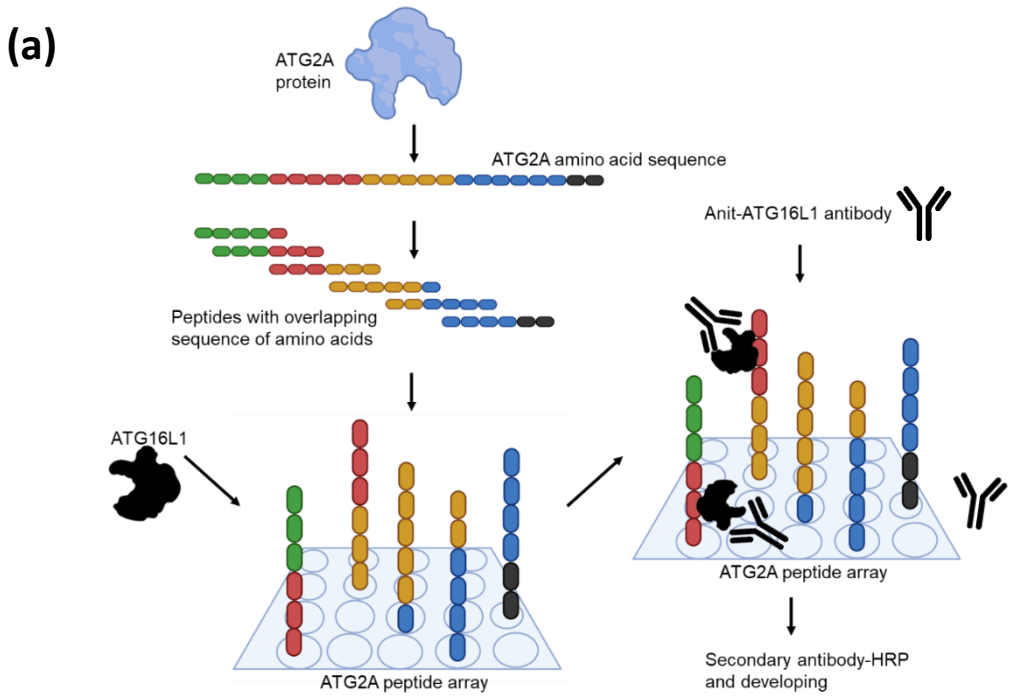
(a)
ATG2A protein
ATG2A amino acid sequence
Peptides with overlapping sequence of amino acids
ATG16L1
ATG2A peptide array
Anit-ATG16L1 antibody
ATG2A peptide array
Secondary antibody-HRP and developing

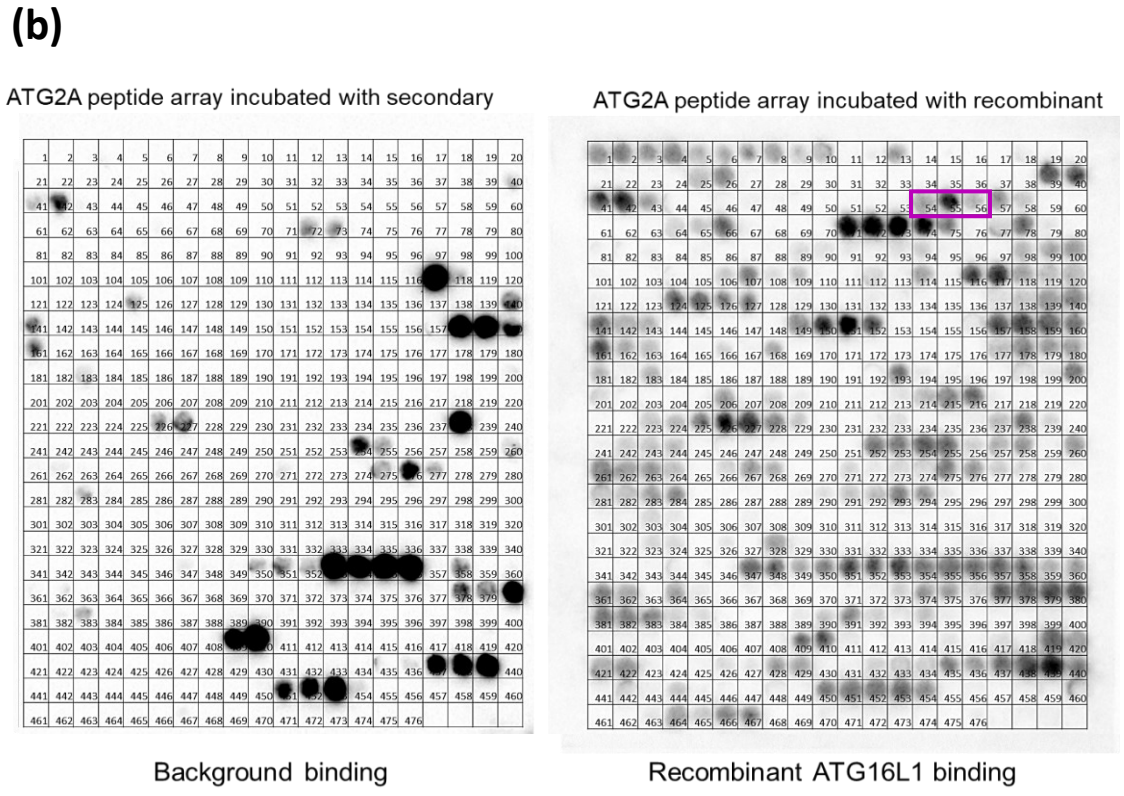
(b)
ATG2A peptide array incubated with secondary
ATG2A peptide array incubated with recombinant
Background binding
Recombinant ATG16L1 binding

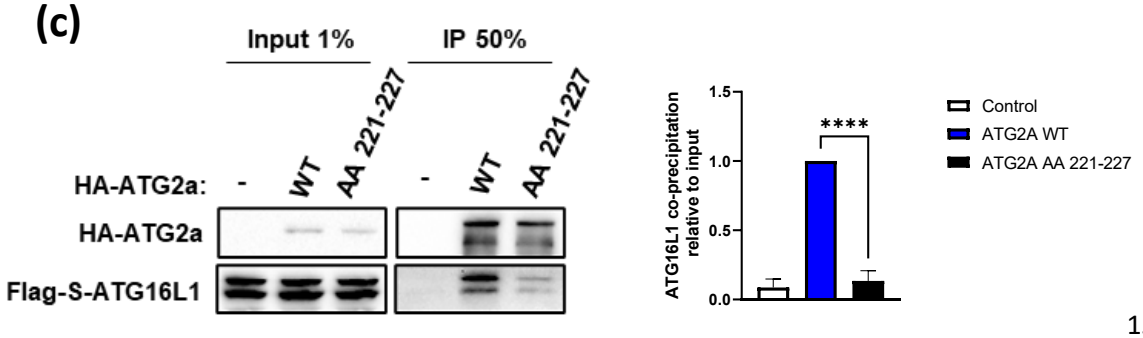
(c)
Input 1%
IP 50%
HA-ATG2a:
-
WT
AA 221-227
HA-ATG2a
Flag-S-ATG16L1
ATG16L1 co-precipitation relative to input
1.5
1.0
0.5
0.0
****
Control
ATG2A WT
ATG2A AA 221-227

Figure 7.4 Identification of residues on ATG2a essential for ATG16L1 binding.
(a) *Schematic diagram of ATG2a peptide array. Amino acid sequence of ATG2a was fragmented into overlapping peptide fragments bound to a nitrocellulose membrane. The peptide array was incubated with recombinant ATG16L1 and subsequently with the indicated antibodies. The membrane was then developed using chemiluminescence detection.* ***(b)*** *Left: To asses background binding, ATG2a peptide array was incubated with HRP conjugated secondary antibody. Right: ATG2a peptide array incubated with recombinant ATG16L1. Peptide fragments used for mutagenesis are indicated in magenta.* ***(c)*** *Protein–protein interaction assay in ATG16L1 knockout HEK293T cells transiently transfected with the indicated HA-ATG2a constructs or Flag-S-ATG16L1. Cell lysates expressing the indicated proteins were mixed and HA tag pull-down was performed followed by immunoblotting using the indicated antibodies. Quantification of relative ATG2a-ATG16L1 binding is shown on the right. Mean + SD is shown from at three independent experiments, **** p<0.0001, assessed by unpaired Student's t-test.*

7.3 Discussion

In this chapter, I have focused on determining whether two already established autophagy proteins, ATG2 and ATG16L1, are binding partners. ATG2b and ATG16L1 were detected in close proximity to one another in TurboID proximity labelling screen. The results from multiple binding assays confirmed the novel interaction between ATG2 and ATG16L1. This interaction is ATG5-independent and occurs between ATG2 proteins and ATG16L1. ATG2b exhibited higher levels of biotinylation than ATG2a in our MS analyses but did not exhibit higher association to ATG16L1 in *in vitro* settings. Therefore, it would be interesting to test whether ATG2b-ATG16L1 interaction is preferable between the endogenous proteins, or whether the higher biotinylation levels of ATG2b is a result of lower levels of endogenous ATG2a in MEF cells used in the proximity labelling assay. The preference of binding either ATG2a or ATG2b could be tested by pulling down endogenous ATG16L1 in a cell line with comparable levels of the two ATG2 proteins. The differences between the levels of ATG2a and ATG2b co-precipitating with ATG16L1 would help determine whether one of these interactions is more prevalent in an endogenous settings.

The binding residues on ATG16L1 required for ATG2 binding are yet to be further narrowed down. Pulldown of truncation mutants of ATG16L1 showed that the WD40

domains region of the protein is necessary to co-precipitate with ATG2a and ATG2b. The WD40 region is challenging to manipulate as mutations in these domains can disrupt the propeller structure and lead to protein instability (Xu and Min, 2011). For this reason, I have focused on finding the binding residues on ATG2a. Mutating a small region of ATG2a (AA 221-227) identified in the peptide array experiment showed a dramatic reduction in ATG16L1 binding. I also observed diminished ATG16L1 binding of ATG2a YFS/AAA mutant required to binding WIPI4. Whether a complete abolishment of ATG16L1 binding could be achieved by mutating both regions of ATG2a remains to be determined. It would also be interesting to check whether WIPI4 binding is affected in ATG2a AA 221-227 mutant and whether other interacting partners are able to bind to ATG2a through these amino acids. ATG2 proteins exhibit similarities in structure and function (Velikkakath et al., 2012) and it has been previously reported that the co-depletion of ATG2a and ATG2b is required to disrupt autophagy (Velikkakath et al., 2012). Therefore, experimental settings aiming to study a phenotype seen upon disrupting ATG2-ATG16L1 binding need to be carefully designed when mutating ATG2 residues and ATG2 mutants should be expressed in ATG2a/ATG2b double knockout cells.

The observation that WD40 region of ATG16L1 is sufficient to bind ATG2 indicates that the functional relevance of the ATG2-ATG16L1 binding could be related to the reported processes facilitated by this region rather than canonical autophagy. Binding of the WD40 domains of ATG16L1 to V-ATPase subunits and ubiquitin-decorated endosomes mediate the recognition of bacteria and initiate xenophagy (Fujita et al., 2013; Xu et al., 2019). The WD40 domains of ATG16L1 were also shown to be involved in plasma membrane damage repair upon bacteria infection (Tan et al., 2018). It would be interesting to test whether the absence of ATG16L1 and ATG2 interaction abrogates the ability of ATG16L1 to bind to the V-ATPase subunits or ubiquitin and has any effect on the xenophagy or plasma membrane integrity.

Moreover, WD40 domains of ATG16L1 are essential for CASM (Fletcher et al., 2018). Our preliminary data showed that LC3 lipidation on single membrane during LAP-like processes is inhibited in ATG2 double knockout cells (data not shown), which indicates that ATG2 could potentially play a role in CASM. The main quality of ATG2 involved in autophagy is its lipid transfer properties, which contribute to the expansion of the phagophore (Osawa and Noda, 2019; Valverde et al., 2019; van Vliet et al.,

2022). In CASM, the membrane on which ATG8 lipidation takes place is already present (Durgan and Florey, 2023; Florey et al., 2011a). If ATG2 is indeed essential for CASM, the role of ATG2 could be unrelated to lipid transfer qualities exhibited during autophagy. The residues we have identified as essential for ATG16L1 binding are not required for lipid transfer or interaction with known partners of ATG2 (Dudley et al., 2020). Altogether, this suggests that further investigation of ATG2-ATG16L1 could uncover unidentified properties of ATG2 in CASM or other processes.

To gain a better understanding of the consequences of disrupting ATG2-ATG16L1 interaction in an unbiased way, MS analyses of wild type cells and cells expressing ATG2-ATG16L1 binding mutant would be beneficial. Comparing whole cell proteome in the presence or absence of ATG2-ATG16L1 binding could help narrow down processes affected in the absence of this interaction. For example, certain proteins induce selective autophagy by engaging with the WD40 region of ATG16L1 (Boada-Romero et al., 2013; Hu et al., 2016), therefore accumulation of a subset of autophagy receptors in the absence of ATG2-ATG16L1 binding could help specify the affected cargo.

Altogether, data from this chapter confirm a novel binding between ATG2 and ATG16L1. The functional relevance of this binding is yet to be determined but analyses of the binding regions indicate that this interaction could be relevant to processes out with canonical autophagy.

Appendix 1

(a)

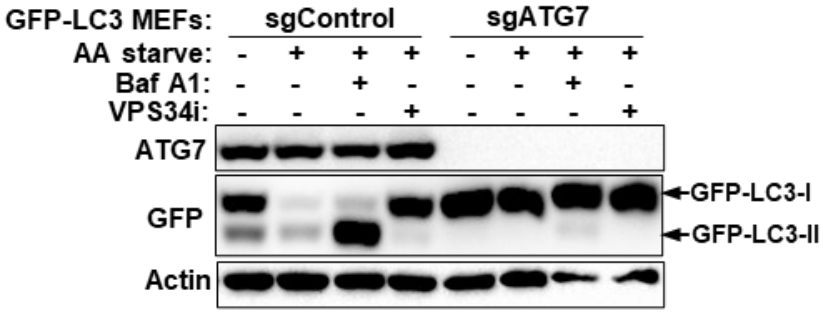

(b)

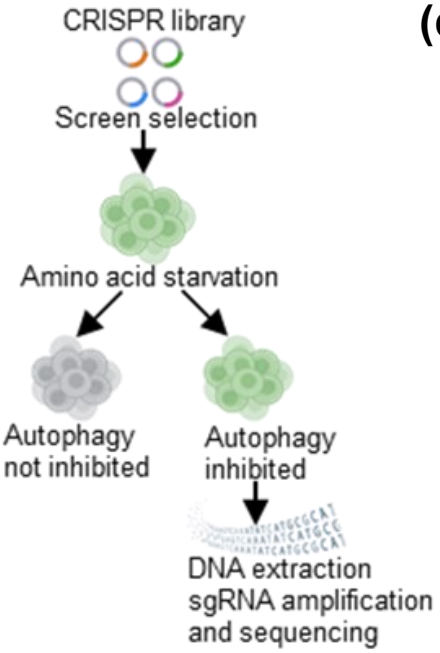

(c)

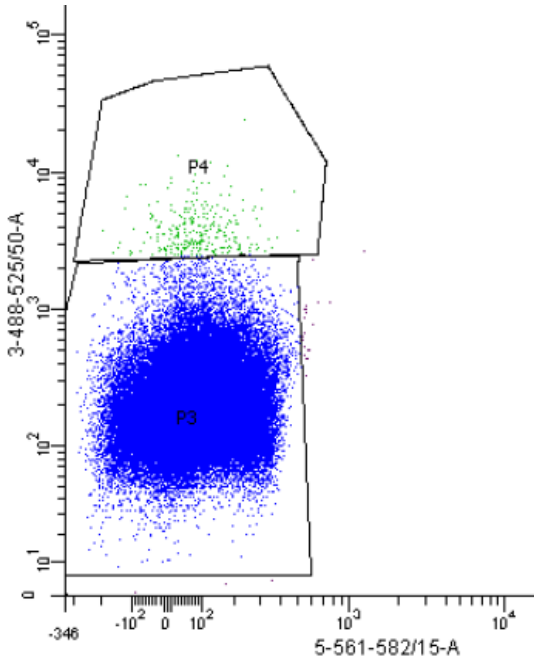

(d)

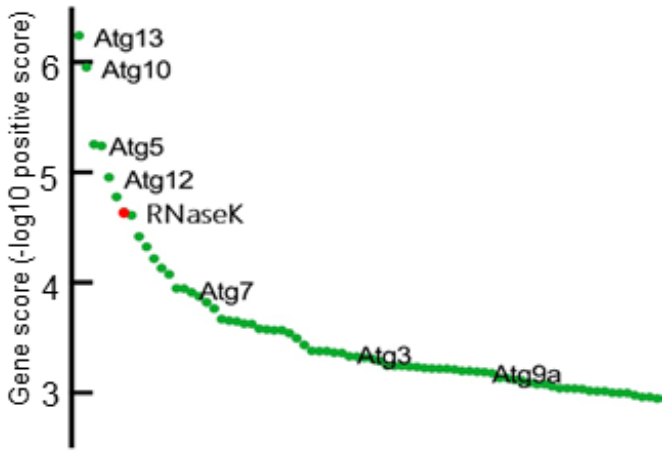

Appendix 1 Genome-wide CRISPR-Cas9 knockout screen identifies RNAseK as a novel autophagy regulator.

(a) *Validation of the reporter GFP-LC3 MEF cells. Cells were left untreated or amino acid (AA) starved for 2 h in the presence or absence of Baf A1 or VPS34 inhibitor (VPS34i). Cells were either expressing Cas9 alone (sgControl) or sgRNA targeting ATG7 (sgATG7). Cell lysates were subjected to western blot analyses using the indicated antibodies.* ***(b)*** *Work flow for the loss of function screen. MEFs stably expressing GFP-LC3 and Cas9 were transduced with sgRNA library and subjected to AA starvation (16 h) to induce autophagy and FACS sorting into GFP positive (autophagy deficient) and GFP negative (autophagy competent) populations. Genomic extraction and amplification was used to identify sgRNA sequences.* ***(c)*** *Representative scatterplot of FACS sorting of GFP positive (autophagy deficient) and GFP negative (autophagy competent) populations. GFP positive population is represented in green, GFP negative population is represented in blue.* ***(d)*** *Deep sequencing analysis of sorted GFP positive cells. Highlighted are top 100 identified hits, including the indicated Atg genes and Rnasek.*

Appendix 2

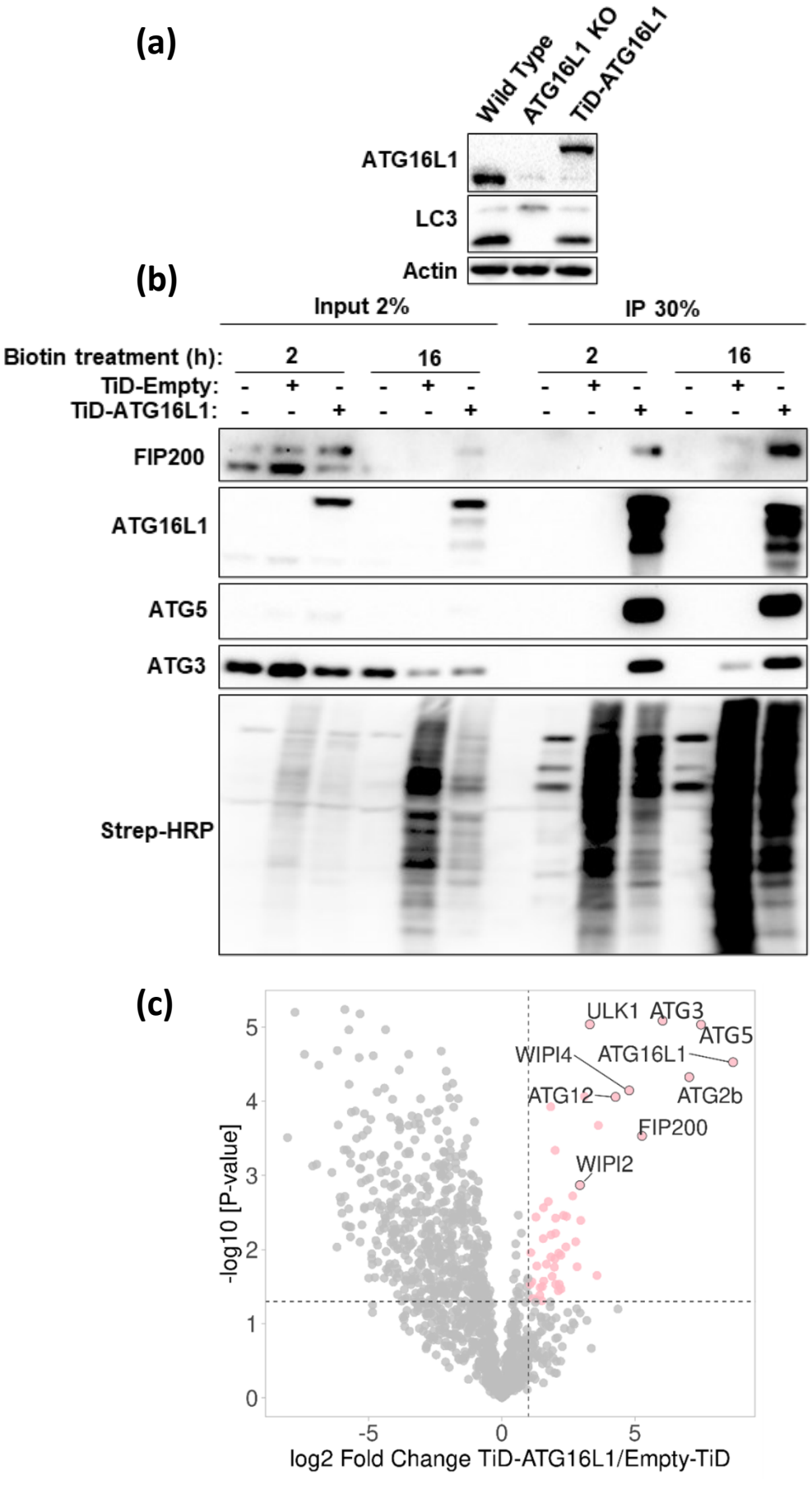
(a)
Wild Type
ATG16L1 KO
TiD-ATG16L1
ATG16L1
LC3
Actin
(b)
Input 2%
IP 30%
Biotin treatment (h):
2
16
2
16
TiD-Empty:
TiD-ATG16L1:
FIP200
ATG16L1
ATG5
ATG3
Strep-HRP
(c)
ULK1
ATG3
ATG5
WIPI4
ATG16L1
ATG12
ATG2b
FIP200
WIPI2
-log10 [P-value]
log2 Fold Change TiD-ATG16L1/Empty-TiD

Appendix 1 TurboID proximity screen identifies ATG2b in close proximity to ATG16L1. ***(a)*** *Validation of the TurboID-ATG16L1 MEF cell line. Cells were amino acid (AA) starved for 2 h in the presence of Baf A1.* ***(b)*** *MEFs stably expressing the indicated TurboID constructs were starved of amino acids with biotin treatment for the indicated times. The cell lysates were subjected to affinity purification using streptavidin-coupled beads. The pulldown samples were subjected to western blot analyses using the indicated antibodies.* ***(c)*** *Volcano plot analyses of TiD-ATG16L1 proximity labelling hits identified by MS presented as relative values to hits obtained from TurboID empty cells. Significant hits (P > 0.05; Fold Change > 2) are represented in pink.*

List of references

Abbas, Y.M., Wu, D., Bueler, S.A., Robinson, C. V., and Rubinstein, J.L. Structure of V-ATPase from the mammalian brain. Science (80-.). : 1240-1246.

Adell, M.A.Y., Vogel, G.F., Pakdel, M., Müller, M., Lindner, H., Hess, M.W., and Teis, D. (2014). Coordinated binding of Vps4 to ESCRT-III drives membrane neck constriction during MVB vesicle formation. J. Cell Biol. *205*, 33–49.

Alsaadi, R.M., Losier, T.T., Tian, W., Jackson, A., Guo, Z., Rubinsztein, D.C., and Russell, R.C. (2019). ULK1-mediated phosphorylation of ATG16L1 promotes xenophagy, but destabilizes the ATG16L1 Crohn's mutant. EMBO Rep. *20*, e46885.

Alvarez-Erviti, L., Seow, Y., Schapira, A.H., Gardiner, C., Sargent, I.L., Wood, M.J.A., and Cooper, J.M. (2011). Lysosomal dysfunction increases exosome-mediated alpha-synuclein release and transmission. Neurobiol. Dis. *42*, 360–367.

Aman, Y., Schmauck-Medina, T., Hansen, M., Morimoto, R.I., Simon, A.K., Bjedov, I., Palikaras, K., Simonsen, A., Johansen, T., Tavernarakis, N., et al. (2021). Autophagy in healthy aging and disease. Nat. Aging *1*, 634–650.

Ameis, D., Merkel, M., Eckerskorn, C., and Greten, H. (1994). Purification, characterization and molecular cloning of human hepatic lysosomal acid lipase. Eur. J. Biochem. *219*, 905–914.

Andrejewski, N., Punnonen, E.-L., Guhde, G., Tanaka, Y., Lüllmann-Rauch, R., Hartmann, D., von Figura, K., and Saftig, P. (1999). Normal Lysosomal Morphology and Function in LAMP-1-deficient Mice*. J. Biol. Chem. *274*, 12692–12701.

Axe, E.L., Walker, S.A., Manifava, M., Chandra, P., Roderick, H.L., Habermann, A., Griffiths, G., and Ktistakis, N.T. (2008). Autophagosome formation from membrane compartments enriched in phosphatidylinositol 3-phosphate and dynamically connected to the endoplasmic reticulum. J. Cell Biol. *182*, 685–701.

Bach, M., Larance, M., James, D.E., and Ramm, G. (2011). The serine/threonine kinase ULK1 is a target of multiple phosphorylation events. Biochem. J. *440*, 283–291.

Bagh, M.B., Peng, S., Chandra, G., Zhang, Z., Singh, S.P., Pattabiraman, N., Liu, A., and Mukherjee, A.B. (2017). Misrouting of v-ATPase subunit V0a1 dysregulates lysosomal acidification in a neurodegenerative lysosomal storage disease model. Nat. Commun. *8*, 14612.

Bakula, D., Müller, A.J., Zuleger, T., Takacs, Z., Franz-Wachtel, M., Thost, A.-K., Brigger, D., Tschan, M.P., Frickey, T., Robenek, H., et al. (2017). WIPI3 and WIPI4 β-propellers are scaffolds for LKB1-AMPK-TSC signalling circuits in the control of autophagy. Nat. Commun. *8*, 15637.

Bandyopadhyay, D., Cyphersmith, A., Zapata, J.A., Kim, Y.J., and Payne, C.K. (2014). Lysosome transport as a function of lysosome diameter. PLoS One *9*, e86847.

Belyaev, N.D., Kellett, K.A.B., Beckett, C., Makova, N.Z., Revett, T.J., Nalivaeva, N.N., Hooper, N.M., and Turner, A.J. (2010). The transcriptionally active amyloid precursor protein (APP) intracellular domain is preferentially produced from the 695 isoform of APP in a {beta}-secretase-dependent pathway. J. Biol. Chem. *285*, 41443–41454.

Bethani, I., Werner, A., Kadian, C., Geumann, U., Jahn, R., and Rizzoli, S.O. (2009). Endosomal Fusion upon SNARE Knockdown is Maintained by Residual SNARE Activity and Enhanced Docking. Traffic *10*, 1543–1559.

Bi, X., Haque, T.S., Zhou, J., Skillman, A.G., Lin, B., Lee, C.E., Kuntz, I.D., Ellman, J.A., and Lynch, G. (2000). Novel cathepsin D inhibitors block the formation of hyperphosphorylated tau fragments in hippocampus. J. Neurochem. *74*, 1469–1477.

Bishop, N., and Woodman, P. (2000). ATPase-defective mammalian VPS4 localizes to aberrant endosomes and impairs cholesterol trafficking. Mol. Biol. Cell *11*, 227–239.

Bjørkøy, G., Lamark, T., Brech, A., Outzen, H., Perander, M., Øvervatn, A., Stenmark, H., and Johansen, T. (2005). p62/SQSTM1 forms protein aggregates degraded by autophagy and has a protective effect on huntingtin-induced cell death . J. Cell Biol. *171*, 603–614.

Boada-Romero, E., Letek, M., Fleischer, A., Pallauf, K., Ramón-Barros, C., and Pimentel-Muiños, F.X. (2013). TMEM59 defines a novel ATG16L1-binding motif that promotes local activation of LC3. EMBO J. *32*, 566–582.

Bowman, B.J., and Bowman, E.J. (2002). Mutations in subunit C of the vacuolar ATPase confer resistance to bafilomycin and identify a conserved antibiotic binding site. J. Biol. Chem. *277*, 3965–3972.

Bozic, M., van den Bekerom, L., Milne, B.A., Goodman, N., Roberston, L., Prescott, A.R., Macartney, T.J., Dawe, N., and McEwan, D.G. (2020). A conserved ATG2-

GABARAP family interaction is critical for phagophore formation. EMBO Rep. *21*.
Brady, R.O., Kanfer, J.N., Mock, M.B., and Fredrickson, D.S. (1966). The metabolism of sphingomyelin. II. Evidence of an enzymatic deficiency in Niemann-Pick diseae. Proc. Natl. Acad. Sci. U. S. A. *55*, 366–369.
BRADY, R.O., KANFER, J.N., and SHAPIRO, D. (1965). METABOLISM OF GLUCOCEREBROSIDES. II. EVIDENCE OF AN ENZYMATIC DEFICIENCY IN GAUCHER'S DISEASE. Biochem. Biophys. Res. Commun. *18*, 221–225.
Branon, T.C., Bosch, J.A., Sanchez, A.D., Udeshi, N.D., Svinkina, T., Carr, S.A., Feldman, J.L., Perrimon, N., and Ting, A.Y. (2018). Efficient proximity labeling in living cells and organisms with TurboID. Nat. Biotechnol. *36*, 880–898.
Brown, H.A., Thomas, P.G., and Lindsley, C.W. (2017). Targeting phospholipase D in cancer, infection and neurodegenerative disorders. Nat. Rev. Drug Discov. *16*, 351–367.
Brown, W.J., Goodhouse, J., and Farquhar, M.G. (1986). Mannose-6-phosphate receptors for lysosomal enzymes cycle between the Golgi complex and endosomes. J. Cell Biol. *103*, 1235–1247.
Burke, J.E., and Dennis, E.A. (2009). Phospholipase A2 structure/function, mechanism, and signaling. J. Lipid Res. *50 Suppl*, S237-42.
Cai, M., Huang, Y., Ghirlando, R., Wilson, K.L., Craigie, R., and Clore, G.M. (2001). Solution structure of the constant region of nuclear envelope protein LAP2 reveals two LEM-domain structures: one binds BAF and the other binds DNA. EMBO J. *20*, 4399–4407.
Cann, G.M., Guignabert, C., Ying, L., Deshpande, N., Bekker, J.M., Wang, L., Zhou, B., and Rabinovitch, M. (2008). Developmental expression of LC3α and β: Absence of fibronectin or autophagy phenotype in LC3β knockout mice. Dev. Dyn. *237*, 187–195.
Cao, Y., and Klionsky, D.J. (2007). Physiological functions of Atg6/Beclin 1: a unique autophagy-related protein. Cell Res. *17*, 839–849.
Cao, M., Luo, X., Wu, K., and He, X. (2021). Targeting lysosomes in human disease: from basic research to clinical applications. Signal Transduct. Target. Ther. *6*, 379.
Cao, Q., Yang, Y., Zhong, X.Z., and Dong, X.-P. (2017). The lysosomal Ca(2+) release channel TRPML1 regulates lysosome size by activating calmodulin. J. Biol. Chem. *292*, 8424–8435.

Capella, M., Martín Caballero, L., Pfander, B., Braun, S., and Jentsch, S. (2020). ESCRT recruitment by the S. cerevisiae inner nuclear membrane protein Heh1 is regulated by Hub1-mediated alternative splicing. J. Cell Sci. *133*.

Carnio, S., LoVerso, F., Baraibar, M.A., Longa, E., Khan, M.M., Maffei, M., Reischl, M., Canepari, M., Loefler, S., Kern, H., et al. (2014). Autophagy impairment in muscle induces neuromuscular junction degeneration and precocious aging. Cell Rep. *8*, 1509–1521.

Carro, S.D., and Cherry, S. (2020). Beyond the Surface: Endocytosis of Mosquito-Borne Flaviviruses. Viruses *13*.

Chan, E.Y.W., Kir, S., and Tooze, S.A. (2007a). siRNA screening of the kinome identifies ULK1 as a multidomain modulator of autophagy. J. Biol. Chem. *282*, 25464–25474.

Chan, E.Y.W., Kir, S., and Tooze, S.A. (2007b). siRNA screening of the kinome identifies ULK1 as a multidomain modulator of autophagy. J. Biol. Chem.

Chen, S., Wang, C., Yeo, S., Liang, C.-C., Okamoto, T., Sun, S., Wen, J., and Guan, J.-L. (2016). Distinct roles of autophagy-dependent and -independent functions of FIP200 revealed by generation and analysis of a mutant knock-in mouse model. Genes Dev. *30*, 856–869.

Cheong, H., Wu, J., Gonzales, L.K., Guttentag, S.H., Thompson, C.B., and Lindsten, T. (2014). Analysis of a lung defect in autophagy-deficient mouse strains. Autophagy *10*, 45–56.

Cherf, G.M., and Cochran, J.R. (2015). Applications of Yeast Surface Display for Protein Engineering. Methods Mol. Biol. *1319*, 155–175.

Chiaruttini, N., Redondo-Morata, L., Colom, A., Humbert, F., Lenz, M., Scheuring, S., and Roux, A. (2015). Relaxation of Loaded ESCRT-III Spiral Springs Drives Membrane Deformation. Cell *163*, 866–879.

Choi-Rhee, E., Schulman, H., and Cronan, J.E. (2004). Promiscuous protein biotinylation by Escherichia coli biotin protein ligase. Protein Sci. *13*, 3043–3050.

Chowdhury, S., Otomo, C., Leitner, A., Ohashi, K., Aebersold, R., Lander, G.C., and Otomo, T. (2018). Insights into autophagosome biogenesis from structural and biochemical analyses of the ATG2A-WIPI4 complex. Proc. Natl. Acad. Sci. U. S. A. *115*, E9792–E9801.

Cook, N.R., Row, P.E., and Davidson, H.W. (2004). Lysosome Associated

Membrane Protein 1 (Lamp1) Traffics Directly from the TGN to Early Endosomes. Traffic *5*, 685–699.

CROCKER, A.C. (1961). The cerebral defect in Tay-Sachs disease and Niemann-Pick disease. J. Neurochem. *7*, 69–80.

Cruchaga, C., Karch, C.M., Jin, S.C., Benitez, B.A., Cai, Y., Guerreiro, R., Harari, O., Norton, J., Budde, J., Bertelsen, S., et al. (2014). Rare coding variants in the phospholipase D3 gene confer risk for Alzheimer's disease. Nature *505*, 550–554.

Cuervo, A.M., and Wong, E. (2014). Chaperone-mediated autophagy: Roles in disease and aging. Cell Res. *24*, 92–104.

Cui, Y., Yang, Z., and Teasdale, R.D. (2019). A role of GCC88 in the retrograde transport of CI-M6PR and the maintenance of lysosomal activity. Cell Biol. Int. *43*, 1234–1244.

Dahms, N.M., Lobel, P., Breitmeyer, J., Chirgwin, J.M., and Kornfeld, S. (1987). 46 kd mannose 6-phosphate receptor: cloning, expression, and homology to the 215 kd mannose 6-phosphate receptor. Cell *50*, 181–192.

Dairaku, T., Iwamoto, T., Nishimura, M., Endo, M., Ohashi, T., and Eto, Y. (2014). A practical fluorometric assay method to measure lysosomal acid lipase activity in dried blood spots for the screening of cholesteryl ester storage disease and Wolman disease. Mol. Genet. Metab. *111*, 193–196.

Danon, M.J., Oh, S.J., DiMauro, S., Manaligod, J.R., Eastwood, A., Naidu, S., and Schliselfeld, L.H. (1981). Lysosomal glycogen storage disease with normal acid maltase. Neurology *31*, 51–57.

Degenhardt, K., Mathew, R., Beaudoin, B., Bray, K., Anderson, D., Chen, G., Mukherjee, C., Shi, Y., Gélinas, C., Fan, Y., et al. (2006). Autophagy promotes tumor cell survival and restricts necrosis, inflammation, and tumorigenesis. Cancer Cell *10*, 51–64.

Dejesus, R., Moretti, F., McAllister, G., Wang, Z., Bergman, P., Liu, S., Frias, E., Alford, J., Reece-Hoyes, J.S., Lindeman, A., et al. (2016). Functional CRISPR screening identifies the ufmylation pathway as a regulator of SQSTM1/p62. Elife *5*.

Deltcheva, E., Chylinski, K., Sharma, C.M., Gonzales, K., Chao, Y., Pirzada, Z.A., Eckert, M.R., Vogel, J., and Charpentier, E. (2011). CRISPR RNA maturation by trans-encoded small RNA and host factor RNase III. Nature *471*, 602–607.

Demeter, A., Romero-Mulero, M.C., Csabai, L., Ölbei, M., Sudhakar, P., Haerty, W.,

and Korcsmáros, T. (2020). ULK1 and ULK2 are less redundant than previously thought: computational analysis uncovers distinct regulation and functions of these autophagy induction proteins. Sci. Rep. *10*, 10940.

Demirev, A.V., Song, H.-L., Cho, M.-H., Cho, K., Peak, J.-J., Yoo, H.J., Kim, D.-H., and Yoon, S.-Y. (2019). V232M substitution restricts a distinct O-glycosylation of PLD3 and its neuroprotective function. Neurobiol. Dis. *129*, 182–194.

Di, Y.-Q., Han, X.-L., Kang, X.-L., Wang, D., Chen, C.-H., Wang, J.-X., and Zhao, X.-F. (2021). Autophagy triggers CTSD (cathepsin D) maturation and localization inside cells to promote apoptosis. Autophagy *17*, 1170–1192.

Diaz, A., Zhang, J., Ollwerther, A., Wang, X., and Ahlquist, P. (2015). Host ESCRT proteins are required for bromovirus RNA replication compartment assembly and function. PLoS Pathog. *11*, e1004742.

Dikic, I. (2017). Proteasomal and Autophagic Degradation Systems. Annu. Rev. Biochem. *86*, 193–224.

Di Domenico, F., Coccia, R., Cocciolo, A., Murphy, M.P., Cenini, G., Head, E., Butterfield, D.A., Giorgi, A., Schinina, M.E., Mancuso, C., et al. (2013). Impairment of proteostasis network in Down syndrome prior to the development of Alzheimer's disease neuropathology: redox proteomics analysis of human brain. Biochim. Biophys. Acta *1832*, 1249–1259.

Dong, X.-P., Cheng, X., Mills, E., Delling, M., Wang, F., Kurz, T., and Xu, H. (2008). The type IV mucolipidosis-associated protein TRPML1 is an endolysosomal iron release channel. Nature *455*, 992–996.

Dooley, H.C., Razi, M., Polson, H.E.J., Girardin, S.E., Wilson, M.I., and Tooze, S.A. (2014). WIPI2 Links LC3 Conjugation with PI3P, Autophagosome Formation, and Pathogen Clearance by Recruiting Atg12-5-16L1. Mol. Cell *55*, 238–252.

Dossou, A.S., and Basu, A. (2019). The Emerging Roles of mTORC1 in Macromanaging Autophagy. Cancers (Basel). *11*.

Dudley, L.J., Cabodevilla, A.G., Makar, A.N., Sztacho, M., Michelberger, T., Marsh, J.A., Houston, D.R., Martens, S., Jiang, X., and Gammoh, N. (2019a). Intrinsic lipid binding activity of <scp>ATG</scp> 16L1 supports efficient membrane anchoring and autophagy. EMBO J. *38*.

Dudley, L.J., Cabodevilla, A.G., Makar, A.N., Sztacho, M., Michelberger, T., Marsh, J.A., Houston, D.R., Martens, S., Jiang, X., and Gammoh, N. (2019b). Intrinsic lipid

binding activity of ATG 16L1 supports efficient membrane anchoring and autophagy . EMBO J.

Dudley, L.J., Makar, A.N., and Gammoh, N. (2020). Membrane targeting of core autophagy players during autophagosome biogenesis. FEBS J. *287*, 4806–4821.

Durgan, J., and Florey, O. (2023). Many roads lead to CASM: Diverse stimuli of noncanonical autophagy share a unifying molecular mechanism. Sci. Adv. *8*, eabo1274.

Durgan, J., Lystad, A.H., Sloan, K., Carlsson, S.R., Wilson, M.I., Marcassa, E., Ulferts, R., Webster, J., Lopez-Clavijo, A.F., Wakelam, M.J., et al. (2021). Non-canonical autophagy drives alternative ATG8 conjugation to phosphatidylserine. Mol. Cell *81*, 2031-2040.e8.

DE DUVE, C., PRESSMAN, B.C., GIANETTO, R., WATTIAUX, R., and APPELMANS, F. (1955). Tissue fractionation studies. 6. Intracellular distribution patterns of enzymes in rat-liver tissue. Biochem. J. *60*, 604–617.

Ebner, P., Poetsch, I., Deszcz, L., Hoffmann, T., Zuber, J., and Ikeda, F. (2018). The IAP family member BRUCE regulates autophagosome–lysosome fusion. Nat. Commun. *9*, 599.

Economopoulou, M.-A.I., Fragoulis, E.G., and Sideris, D.C. (2007). Molecular cloning and characterization of the human RNase i, an ortholog of Cc RNase. Nucleic Acids Res. *35*, 6389–6398.

Egan, D.F., Chun, M.G.H., Vamos, M., Zou, H., Rong, J., Miller, C.J., Lou, H.J., Raveendra-Panickar, D., Yang, C.-C., Sheffler, D.J., et al. (2015). Small Molecule Inhibition of the Autophagy Kinase ULK1 and Identification of ULK1 Substrates. Mol. Cell *59*, 285–297.

Ehlert, K., Frosch, M., Fehse, N., Zander, A., Roth, J., and Vormoor, J. (2007). Farber disease: clinical presentation, pathogenesis and a new approach to treatment. Pediatr. Rheumatol. Online J. *5*, 15.

Epple, U.D., Suriapranata, I., Eskelinen, E.L., and Thumm, M. (2001). Aut5/Cvt17p, a putative lipase essential for disintegration of autophagic bodies inside the vacuole. J. Bacteriol. *183*, 5942–5955.

Eriksson, I., Wäster, P., and Öllinger, K. (2020). Restoration of lysosomal function after damage is accompanied by recycling of lysosomal membrane proteins. Cell Death Dis. *11*, 370.

Eskelinen, E.-L. (2006). Roles of LAMP-1 and LAMP-2 in lysosome biogenesis and autophagy. Mol. Aspects Med. *27*, 495–502.

Eskelinen, E.-L., Schmidt, C.K., Neu, S., Willenborg, M., Fuertes, G., Salvador, N., Tanaka, Y., Lüllmann-Rauch, R., Hartmann, D., Heeren, J., et al. (2004). Disturbed Cholesterol Traffic but Normal Proteolytic Function in LAMP-1/LAMP-2 Double-deficient Fibroblasts. Mol. Biol. Cell *15*, 3132–3145.

Fan, W., Nassiri, A., and Zhong, Q. (2011). Autophagosome targeting and membrane curvature sensing by Barkor/Atg14(L). Proc. Natl. Acad. Sci. *108*, 7769–7774.

Fang, E.F., Hou, Y., Palikaras, K., Adriaanse, B.A., Kerr, J.S., Yang, B., Lautrup, S., Hasan-Olive, M.M., Caponio, D., Dan, X., et al. (2019). Mitophagy inhibits amyloid-β and tau pathology and reverses cognitive deficits in models of Alzheimer's disease. Nat. Neurosci. *22*, 401–412.

Fazzari, P., Horre, K., Arranz, A.M., Frigerio, C.S., Saito, T., Saido, T.C., and De Strooper, B. (2017). PLD3 gene and processing of APP. Nature *541*, E1–E2.

Fedele, A.O., and Proud, C.G. (2020). Chloroquine and bafilomycin A mimic lysosomal storage disorders and impair mTORC1 signalling. Biosci. Rep. *40*, BSR20200905.

Fei, N., Wen, S., Ramanathan, R., Hogg, M.E., Zureikat, A.H., Lotze, M.T., Bahary, N., Singhi, A.D., Zeh, H.J., and Boone, B.A. (2021). SMAD4 loss is associated with response to neoadjuvant chemotherapy plus hydroxychloroquine in patients with pancreatic adenocarcinoma. Clin. Transl. Sci. *14*, 1822–1829.

Fernández, Á.F., Sebti, S., Wei, Y., Zou, Z., Shi, M., McMillan, K.L., He, C., Ting, T., Liu, Y., Chiang, W.-C., et al. (2018). Disruption of the beclin 1–BCL2 autophagy regulatory complex promotes longevity in mice. Nature *558*, 136–140.

Filippi-Chiela, E.C., Bueno e Silva, M.M., Thomé, M.P., and Lenz, G. (2015). Single-cell analysis challenges the connection between autophagy and senescence induced by DNA damage. Autophagy *11*, 1099–1113.

Fletcher, K., Ulferts, R., Jacquin, E., Veith, T., Gammoh, N., Arasteh, J.M., Mayer, U., Carding, S.R., Wileman, T., Beale, R., et al. (2018a). The WD 40 domain of ATG 16L1 is required for its non-canonical role in lipidation of LC 3 at single membranes . EMBO J.

Fletcher, K., Ulferts, R., Jacquin, E., Veith, T., Gammoh, N., Arasteh, J.M., Mayer,

U., Carding, S.R., Wileman, T., Beale, R., et al. (2018b). The <scp>WD</scp> 40 domain of <scp>ATG</scp> 16L1 is required for its non-canonical role in lipidation of <scp>LC</scp> 3 at single membranes. EMBO J. *37*.

Florey, O., Kim, S.E., Sandoval, C.P., Haynes, C.M., and Overholtzer, M. (2011a). Autophagy machinery mediates macroendocytic processing and entotic cell death by targeting single membranes. Nat. Cell Biol.

Florey, O., Kim, S.E., Sandoval, C.P., Haynes, C.M., and Overholtzer, M. (2011b). Autophagy machinery mediates macroendocytic processing and entotic cell death by targeting single membranes. Nat. Cell Biol. *13*, 1335–1343.

Florey, O., Gammoh, N., Kim, S.E., Jiang, X., and Overholtzer, M. (2015). V-ATPase and osmotic imbalances activate endolysosomal LC3 lipidation. Autophagy *11*, 88–99.

Fraile-Ramos, A., Pelchen-Matthews, A., Risco, C., Rejas, M.T., Emery, V.C., Hassan-Walker, A.F., Esteban, M., and Marsh, M. (2007). The ESCRT machinery is not required for human cytomegalovirus envelopment. Cell. Microbiol. *9*, 2955–2967.

Franken, L.E., Boekema, E.J., and Stuart, M.C.A. (2017). Transmission Electron Microscopy as a Tool for the Characterization of Soft Materials: Application and Interpretation. Adv. Sci. (Weinheim, Baden-Wurttemberg, Ger. *4*, 1600476.

Fujita, N., Itoh, T., Omori, H., Fukuda, M., Noda, T., and Yoshimori, T. (2008). The Atg16L complex specifies the site of LC3 lipidation for membrane biogenesis in autophagy. Mol. Biol. Cell *19*, 2092–2100.

Fujita, N., Morita, E., Itoh, T., Tanaka, A., Nakaoka, M., Osada, Y., Umemoto, T., Saitoh, T., Nakatogawa, H., Kobayashi, S., et al. (2013). Recruitment of the autophagic machinery to endosomes during infection is mediated by ubiquitin. J. Cell Biol. *203*, 115–128.

Furuya, N., Yu, J., Byfield, M., Pattingre, S., and Levine, B. (2005). The evolutionarily conserved domain of Beclin 1 is required for Vps34 binding, autophagy and tumor suppressor function. Autophagy *1*, 46–52.

Futai, M., Sun-Wada, G.-H., Wada, Y., Matsumoto, N., and Nakanishi-Matsui, M. (2019). Vacuolar-type ATPase: A proton pump to lysosomal trafficking. Proc. Jpn. Acad. Ser. B. Phys. Biol. Sci. *95*, 261–277.

Futter, C.E., Pearse, A., Hewlett, L.J., and Hopkins, C.R. (1996). Multivesicular endosomes containing internalized EGF-EGF receptor complexes mature and then

fuse directly with lysosomes. J. Cell Biol. *132*, 1011–1023.
Galluzzi, L., Pietrocola, F., Bravo-San Pedro, J.M., Amaravadi, R.K., Baehrecke, E.H., Cecconi, F., Codogno, P., Debnath, J., Gewirtz, D.A., Karantza, V., et al. (2015). Autophagy in malignant transformation and cancer progression. EMBO J. *34*, 856–880.
Gamblin, C., Rouault, C., Lacombe, A., Langa-Vives, F., Farabos, D., Lamaziere, A., Clément, K., Gautier, E.L., Yvan-Charvet, L., and Dugail, I. (2021). Lysosomal Acid Lipase Drives Adipocyte Cholesterol Homeostasis and Modulates Lipid Storage in Obesity, Independent of Autophagy. Diabetes *70*, 76–90.
Gammoh, N., Florey, O., Overholtzer, M., and Jiang, X. (2013). Interaction between FIP200 and ATG16L1 distinguishes ULK1 complex-dependent and-independent autophagy. Nat. Struct. Mol. Biol. *20*, 144–149.
Gan, B., Peng, X., Nagy, T., Alcaraz, A., Gu, H., and Guan, J.-L. (2006). Role of FIP200 in cardiac and liver development and its regulation of TNFalpha and TSC-mTOR signaling pathways. J. Cell Biol. *175*, 121–133.
Ganley, I.G., Lam, D.H., Wang, J., Ding, X., Chen, S., and Jiang, X. (2009). ULK1·ATG13·FIP200 complex mediates mTOR signaling and is essential for autophagy. J. Biol. Chem. *284*, 12297–12305.
Ganley, I.G., Wong, P.-M., and Jiang, X. (2011). Thapsigargin distinguishes membrane fusion in the late stages of endocytosis and autophagy. Autophagy *7*, 1397–1399.
Gavin, A.L., Huang, D., Huber, C., Mårtensson, A., Tardif, V., Skog, P.D., Blane, T.R., Thinnes, T.C., Osborn, K., Chong, H.S., et al. (2018). PLD3 and PLD4 are single-stranded acid exonucleases that regulate endosomal nucleic-acid sensing. Nat. Immunol. *19*, 942–953.
Ghosh, P., Dahms, N.M., and Kornfeld, S. (2003). Mannose 6-phosphate receptors: new twists in the tale. Nat. Rev. Mol. Cell Biol. *4*, 202–213.
Glick, D., Barth, S., and Macleod, K.F. (2010). Autophagy: cellular and molecular mechanisms. J. Pathol. *221*, 3–12.
Gomaraschi, M., Fracanzani, A.L., Dongiovanni, P., Pavanello, C., Giorgio, E., Da Dalt, L., Norata, G.D., Calabresi, L., Consonni, D., Lombardi, R., et al. (2019). Lipid accumulation impairs lysosomal acid lipase activity in hepatocytes: Evidence in NAFLD patients and cell cultures. Biochim. Biophys. Acta. Mol. Cell Biol. Lipids

1864, 158523.
Gonzalez, A.C., Schweizer, M., Jagdmann, S., Bernreuther, C., Reinheckel, T., Saftig, P., and Damme, M. (2018a). Unconventional Trafficking of Mammalian Phospholipase D3 to Lysosomes. Cell Rep. *22*, 1040–1053.
Gonzalez, A.C., Stroobants, S., Reisdorf, P., Gavin, A.L., Nemazee, D., Schwudke, D., D'Hooge, R., Saftig, P., and Damme, M. (2018b). PLD3 and spinocerebellar ataxia. Brain *141*, e78–e78.
Gubas, A., and Dikic, I. (2022). A guide to the regulation of selective autophagy receptors. FEBS J. *289*, 75–89.
Guerra, F., and Bucci, C. (2016). Multiple Roles of the Small GTPase Rab7. Cells *5*.
Guo, B., Liang, Q., Li, L., Hu, Z., Wu, F., Zhang, P., Ma, Y., Zhao, B., Kovács, A.L., Zhang, Z., et al. (2014). O-GlcNAc-modification of SNAP-29 regulates autophagosome maturation. Nat. Cell Biol. *16*, 1215–1226.
Guo, H., Chitiprolu, M., Roncevic, L., Javalet, C., Hemming, F.J., Trung, M.T., Meng, L., Latreille, E., Tanese de Souza, C., McCulloch, D., et al. (2017). Atg5 Disassociates the V(1)V(0)-ATPase to Promote Exosome Production and Tumor Metastasis Independent of Canonical Macroautophagy. Dev. Cell *43*, 716-730.e7.
Gutierrez, M.G., Munafó, D.B., Berón, W., and Colombo, M.I. (2004). Rab7 is required for the normal progression of the autophagic pathway in mammalian cells. J. Cell Sci. *117*, 2687–2697.
Gwinn, D.M., Shackelford, D.B., Egan, D.F., Mihaylova, M.M., Mery, A., Vasquez, D.S., Turk, B.E., and Shaw, R.J. (2008). AMPK phosphorylation of raptor mediates a metabolic checkpoint. Mol. Cell *30*, 214–226.
Hackett, B.A., and Cherry, S. (2018). Flavivirus internalization is regulated by a size-dependent endocytic pathway. Proc. Natl. Acad. Sci. U. S. A. *115*, 4246–4251.
Hackett, B.A., Yasunaga, A., Panda, D., Tartell, M.A., Hopkins, K.C., Hensley, S.E., and Cherry, S. (2015). RNASEK is required for internalization of diverse acid-dependent viruses. Proc. Natl. Acad. Sci. U. S. A. *112*, 7797–7802.
Haft, C.R., de la Luz Sierra, M., Barr, V.A., Haft, D.H., and Taylor, S.I. (1998). Identification of a family of sorting nexin molecules and characterization of their association with receptors. Mol. Cell. Biol. *18*, 7278–7287.
Haft, C.R., de la Luz Sierra, M., Bafford, R., Lesniak, M.A., Barr, V.A., and Taylor, S.I. (2000). Human orthologs of yeast vacuolar protein sorting proteins Vps26, 29,

and 35: assembly into multimeric complexes. Mol. Biol. Cell *11*, 4105–4116.
Hale, C.M., Cheng, Q., Ortuno, D., Huang, M., Nojima, D., Kassner, P.D., Wang, S., Ollmann, M.M., and Carlisle, H.J. (2016). Identification of modulators of autophagic flux in an image-based high content siRNA screen. Autophagy *12*, 713–726.
Han, J., Pluhackova, K., and Böckmann, R.A. (2017). The Multifaceted Role of SNARE Proteins in Membrane Fusion . Front. Physiol. *8*.
Hara, T., Takamura, A., Kishi, C., Iemura, S.I., Natsume, T., Guan, J.L., and Mizushima, N. (2008). FIP200, a ULK-interacting protein, is required for autophagosome formation in mammalian cells. J. Cell Biol. *181*, 497–510.
Hardie, D.G., Ross, F.A., and Hawley, S.A. (2012). AMPK: a nutrient and energy sensor that maintains energy homeostasis. Nat. Rev. Mol. Cell Biol. *13*, 251–262.
Harrison, D.E., Strong, R., Sharp, Z.D., Nelson, J.F., Astle, C.M., Flurkey, K., Nadon, N.L., Wilkinson, J.E., Frenkel, K., Carter, C.S., et al. (2009). Rapamycin fed late in life extends lifespan in genetically heterogeneous mice. Nature *460*, 392–395.
Hasegawa, T., Konno, M., Baba, T., Sugeno, N., Kikuchi, A., Kobayashi, M., Miura, E., Tanaka, N., Tamai, K., Furukawa, K., et al. (2011). The AAA-ATPase VPS4 regulates extracellular secretion and lysosomal targeting of α-synuclein. PLoS One *6*, e29460.
Heckmann, B.L., Teubner, B.J.W., Tummers, B., Boada-Romero, E., Harris, L., Yang, M., Guy, C.S., Zakharenko, S.S., and Green, D.R. (2019). LC3-Associated Endocytosis Facilitates β-Amyloid Clearance and Mitigates Neurodegeneration in Murine Alzheimer's Disease. Cell *178*, 536-551.e14.
HERS, H.G. (1963). alpha-Glucosidase deficiency in generalized glycogenstorage disease (Pompe's disease). Biochem. J. *86*, 11–16.
Hiesinger, P.R., Fayyazuddin, A., Mehta, S.Q., Rosenmund, T., Schulze, K.L., Zhai, R.G., Verstreken, P., Cao, Y., Zhou, Y., Kunz, J., et al. (2005). The v-ATPase V0 subunit a1 is required for a late step in synaptic vesicle exocytosis in Drosophila. Cell *121*, 607–620.
Hiraoka, M., Abe, A., and Shayman, J.A. (2005). Structure and function of lysosomal phospholipase A2: identification of the catalytic triad and the role of cysteine residues. J. Lipid Res. *46*, 2441–2447.
Hiraoka, M., Abe, A., Lu, Y., Yang, K., Han, X., Gross, R.W., and Shayman, J.A. (2006). Lysosomal phospholipase A2 and phospholipidosis. Mol. Cell. Biol. *26*,

6139–6148.
Hirata, E., Shirai, K., Kawaoka, T., Sato, K., Kodama, F., and Suzuki, K. (2021). Atg15 in Saccharomyces cerevisiae consists of two functionally distinct domains. Mol. Biol. Cell *32*, 645–663.
Hoflack, B., and Kornfeld, S. (1985). Purification and characterization of a cation-dependent mannose 6-phosphate receptor from murine P388D1 macrophages and bovine liver. J. Biol. Chem. *260*, 12008–12014.
Höning, S., Sosa, M., Hille-Rehfeld, A., and von Figura, K. (1997). The 46-kDa Mannose 6-Phosphate Receptor Contains Multiple Binding Sites for Clathrin Adaptors*. J. Biol. Chem. *272*, 19884–19890.
Hooper, K.M., Jacquin, E., Li, T., Goodwin, J.M., Brumell, J.H., Durgan, J., and Florey, O. (2022). V-ATPase is a universal regulator of LC3-associated phagocytosis and non-canonical autophagy. J. Cell Biol. *221*.
Hosokawa, N., Sasaki, T., Iemura, S.I., Natsume, T., Hara, T., and Mizushima, N. (2009). Atg101, a novel mammalian autophagy protein interacting with Atg13. Autophagy *5*, 973–979.
Hsu, J.B.-K., Lee, T.-Y., Cheng, S.-J., Lee, G.A., Chen, Y.-C., Le, N.Q.K., Huang, S.-W., Kuo, D.-P., Li, Y.-T., Chang, T.-H., et al. (2021). Identification of Differentially Expressed Genes in Different Glioblastoma Regions and Their Association with Cancer Stem Cell Development and Temozolomide Response. J. Pers. Med. *11*.
Hu, J., Li, G., Qu, L., Li, N., Liu, W., xia, D., Hongdu, B., Lin, X., Xu, C., Lou, Y., et al. (2016). TMEM166/EVA1A interacts with ATG16L1 and induces autophagosome formation and cell death. Cell Death Dis. *7*, e2323–e2323.
Huynh, K.K., Eskelinen, E.-L., Scott, C.C., Malevanets, A., Saftig, P., and Grinstein, S. (2007). LAMP proteins are required for fusion of lysosomes with phagosomes. EMBO J. *26*, 313–324.
Im, E., Jiang, Y., Stavrides, P., Darji, S., Erdjument-Bromage, H., Neubert, T.A., Bordi, M., Choi, J.Y., Lee, J.-H., and Nixon, R.A. (2022). Lysosomal dysfunction in Down Syndrome and Alzheimer mouse models is caused by selective v-ATPase inhibition by Tyr⁶⁸² phosphorylated APP βCTF. BioRxiv 2022.06.02.494546.
Imamura, H., Nakano, M., Noji, H., Muneyuki, E., Ohkuma, S., Yoshida, M., and Yokoyama, K. (2003). Evidence for rotation of V1-ATPase. Proc. Natl. Acad. Sci. U.

S. A. *100*, 2312–2315.
Infante, R.E., Wang, M.L., Radhakrishnan, A., Kwon, H.J., Brown, M.S., and Goldstein, J.L. (2008). NPC2 facilitates bidirectional transfer of cholesterol between NPC1 and lipid bilayers, a step in cholesterol egress from lysosomes. Proc. Natl. Acad. Sci. U. S. A. *105*, 15287–15292.
Inoki, K., Zhu, T., and Guan, K.-L. (2003). TSC2 mediates cellular energy response to control cell growth and survival. Cell *115*, 577–590.
Ishibashi, K., Uemura, T., Waguri, S., and Fukuda, M. (2012). Atg16L1, an essential factor for canonical autophagy, participates in hormone secretion from PC12 cells independently of autophagic activity. Mol. Biol. Cell *23*, 3193–3202.
Itakura, E., Kishi, C., Inoue, K., and Mizushima, N. (2008). Beclin 1 forms two distinct phosphatidylinositol 3-kinase complexes with mammalian Atg14 and UVRAG. Mol. Biol. Cell.
Itakura, E., Kishi-Itakura, C., and Mizushima, N. (2012). The hairpin-type tail-anchored SNARE syntaxin 17 targets to autophagosomes for fusion with endosomes/lysosomes. Cell *151*, 1256–1269.
Jacquin, E., Leclerc-Mercier, S., Judon, C., Blanchard, E., Fraitag, S., and Florey, O. (2017). Pharmacological modulators of autophagy activate a parallel noncanonical pathway driving unconventional LC3 lipidation. Autophagy *13*, 854–867.
Jadot, M., Canfield, W.M., Gregory, W., and Kornfeld, S. (1992). Characterization of the signal for rapid internalization of the bovine mannose 6-phosphate/insulin-like growth factor-II receptor. J. Biol. Chem. *267*, 11069–11077.
Jäger, S., Bucci, C., Tanida, I., Ueno, T., Kominami, E., Saftig, P., and Eskelinen, E.-L. (2004). Role for Rab7 in maturation of late autophagic vacuoles. J. Cell Sci. *117*, 4837–4848.
Jia, J., Claude-Taupin, A., Gu, Y., Choi, S.W., Peters, R., Bissa, B., Mudd, M.H., Allers, L., Pallikkuth, S., Lidke, K.A., et al. (2020). Galectin-3 Coordinates a Cellular System for Lysosomal Repair and Removal. Dev. Cell *52*, 69-87.e8.
Jia, S., Wang, Y., You, Z., Liu, B., Gao, J., and Liu, W. (2017). Mammalian Atg9 contributes to the post-Golgi transport of lysosomal hydrolases by interacting with adaptor protein-1. FEBS Lett. *591*, 4027–4038.
Jiang, P., Nishimura, T., Sakamaki, Y., Itakura, E., Hatta, T., Natsume, T., and Mizushima, N. (2014). The HOPS complex mediates autophagosome-lysosome

fusion through interaction with syntaxin 17. Mol. Biol. Cell *25*, 1327–1337.
Jiang, W., Chen, X., Ji, C., Zhang, W., Song, J., Li, J., and Wang, J. (2021). Key Regulators of Autophagosome Closure. Cells *10*.
Jinek, M., Chylinski, K., Fonfara, I., Hauer, M., Doudna, J.A., and Charpentier, E. (2012). A programmable dual-RNA-guided DNA endonuclease in adaptive bacterial immunity. Science *337*, 816–821.
Johnson, D.E., Ostrowski, P., Jaumouillé, V., and Grinstein, S. (2016). The position of lysosomes within the cell determines their luminal pH. J. Cell Biol. *212*, 677–692.
Jung, C.H., Ro, S.-H., Cao, J., Otto, N.M., and Kim, D.-H. (2010). mTOR regulation of autophagy. FEBS Lett. *584*, 1287–1295.
Kabeya, Y. (2000). LC3, a mammalian homologue of yeast Apg8p, is localized in autophagosome membranes after processing. EMBO J. *19: 5720-5*.
Kabeya, Y., Mizushima, N., Yamamoto, A., Oshitani-Okamoto, S., Ohsumi, Y., and Yoshimori, T. (2004). LC3, GABARAP and GATE16 localize to autophagosomal membrane depending on form-II formation. J. Cell Sci. *117*, 2805–2812.
Kageyama, S., Omori, H., Saitoh, T., Sone, T., Guan, J.-L., Akira, S., Imamoto, F., Noda, T., and Yoshimori, T. (2011). The LC3 recruitment mechanism is separate from Atg9L1-dependent membrane formation in the autophagic response against Salmonella. Mol. Biol. Cell *22*, 2290–2300.
Kanfer, G., Sarraf, S.A., Maman, Y., Baldwin, H., Dominguez-Martin, E., Johnson, K.R., Ward, M.E., Kampmann, M., Lippincott-Schwartz, J., and Youle, R.J. (2021). Image-based pooled whole-genome CRISPRi screening for subcellular phenotypes. J. Cell Biol. *220*.
Kaur, J., and Debnath, J. (2015). Autophagy at the crossroads of catabolism and anabolism. Nat. Rev. Mol. Cell Biol. *16*, 461–472.
Kaushik, S., Massey, A.C., and Cuervo, A.M. (2006). Lysosome membrane lipid microdomains: novel regulators of chaperone-mediated autophagy. EMBO J. *25*, 3921–3933.
Kim, D.I., Jensen, S.C., Noble, K.A., KC, B., Roux, K.H., Motamedchaboki, K., and Roux, K.J. (2016). An improved smaller biotin ligase for BioID proximity labeling. Mol. Biol. Cell *27*, 1188–1196.
Kim, J., Kundu, M., Viollet, B., and Guan, K.-L. (2011). AMPK and mTOR regulate autophagy through direct phosphorylation of Ulk1. Nat. Cell Biol. *13*, 132–141.

Kiritsi, M.N., Fragoulis, E.G., and Sideris, D.C. (2012). Essential cysteine residues for human RNase κ catalytic activity. FEBS J. *279*, 1318–1326.
Kishi-Itakura, C., Koyama-Honda, I., Itakura, E., and Mizushima, N. (2014). Ultrastructural analysis of autophagosome organization using mammalian autophagy-deficient cells. J. Cell Sci. *127*, 4089–4102.
Knopman, D.S., Amieva, H., Petersen, R.C., Chételat, G., Holtzman, D.M., Hyman, B.T., Nixon, R.A., and Jones, D.T. (2021). Alzheimer disease. Nat. Rev. Dis. Prim. *7*, 33.
Koch, B., Nijmeijer, B., Kueblbeck, M., Cai, Y., Walther, N., and Ellenberg, J. (2018). Generation and validation of homozygous fluorescent knock-in cells using CRISPR–Cas9 genome editing. Nat. Protoc. *13*, 1465–1487.
Koike, M., Nakanishi, H., Saftig, P., Ezaki, J., Isahara, K., Ohsawa, Y., Schulz-Schaeffer, W., Watanabe, T., Waguri, S., Kametaka, S., et al. (2000). Cathepsin D deficiency induces lysosomal storage with ceroid lipofuscin in mouse CNS neurons. J. Neurosci. Off. J. Soc. Neurosci. *20*, 6898–6906.
Komatsu, M., Waguri, S., Ueno, T., Iwata, J., Murata, S., Tanida, I., Ezaki, J., Mizushima, N., Ohsumi, Y., Uchiyama, Y., et al. (2005). Impairment of starvation-induced and constitutive autophagy in Atg7-deficient mice. J. Cell Biol. *169*, 425–434.
Kondo, Y., Kanzawa, T., Sawaya, R., and Kondo, S. (2005). The role of autophagy in cancer development and response to therapy. Nat. Rev. Cancer *5*, 726–734.
Korolchuk, V.I., Saiki, S., Lichtenberg, M., Siddiqi, F.H., Roberts, E.A., Imarisio, S., Jahreiss, L., Sarkar, S., Futter, M., Menzies, F.M., et al. (2011). Lysosomal positioning coordinates cellular nutrient responses. Nat. Cell Biol. *13*, 453–460.
Koyama-Honda, I., and Mizushima, N. (2022). Transient visit of STX17 (syntaxin 17) to autophagosomes. Autophagy *18*, 1213–1215.
Kozik, P., Hodson, N.A., Sahlender, D.A., Simecek, N., Soromani, C., Wu, J., Collinson, L.M., and Robinson, M.S. (2013). A human genome-wide screen for regulators of clathrin-coated vesicle formation reveals an unexpected role for the V-ATPase. Nat. Cell Biol. *15*, 50–60.
Kroemer, G., Mariño, G., and Levine, B. (2010). Autophagy and the integrated stress response. Mol. Cell *40*, 280–293.
Kuchitsu, Y., Homma, Y., Fujita, N., and Fukuda, M. (2018). Rab7 knockout unveils

regulated autolysosome maturation induced by glutamine starvation. J. Cell Sci. *131*, jcs215442.

Kuma, A., Hatano, M., Matsui, M., Yamamoto, A., Nakaya, H., Yoshimori, T., Ohsumi, Y., Tokuhisa, T., and Mizushima, N. (2004). The role of autophagy during the early neonatal starvation period. Nature *432*, 1032–1036.

Laurent-Matha, V., Derocq, D., Prébois, C., Katunuma, N., and Liaudet-Coopman, E. (2006). Processing of human cathepsin D is independent of its catalytic function and auto-activation: involvement of cathepsins L and B. J. Biochem. *139*, 363–371.

Lee, C.-W., Wilfling, F., Ronchi, P., Allegretti, M., Mosalaganti, S., Jentsch, S., Beck, M., and Pfander, B. (2020). Selective autophagy degrades nuclear pore complexes. Nat. Cell Biol. *22*, 159–166.

Lee, J.-H., Yang, D.-S., Goulbourne, C.N., Im, E., Stavrides, P., Pensalfini, A., Chan, H., Bouchet-Marquis, C., Bleiwas, C., Berg, M.J., et al. (2022). Faulty autolysosome acidification in Alzheimer's disease mouse models induces autophagic build-up of Aβ in neurons, yielding senile plaques. Nat. Neurosci. *25*, 688–701.

Lefèvre, F., Rémy, M.-H., and Masson, J.-M. (1997). Alanine-stretch scanning mutagenesis: a simple and efficient method to probe protein structure and function. Nucleic Acids Res. *25*, 447–448.

Leidal, A.M., Huang, H.H., Marsh, T., Solvik, T., Zhang, D., Ye, J., Kai, F., Goldsmith, J., Liu, J.Y., Huang, Y.-H., et al. (2020). The LC3-conjugation machinery specifies the loading of RNA-binding proteins into extracellular vesicles. Nat. Cell Biol. *22*, 187–199.

Lettieri Barbato, D., Tatulli, G., Aquilano, K., and Ciriolo, M.R. (2013). FoxO1 controls lysosomal acid lipase in adipocytes: implication of lipophagy during nutrient restriction and metformin treatment. Cell Death Dis. *4*, e861–e861.

Levine, B., and Klionsky, D.J. (2017). Autophagy wins the 2016 Nobel Prize in Physiology or Medicine: Breakthroughs in baker's yeast fuel advances in biomedical research. Proc. Natl. Acad. Sci. U. S. A. *114*, 201–205.

Li, F., and Zhang, H. (2019). Lysosomal Acid Lipase in Lipid Metabolism and Beyond. Arterioscler. Thromb. Vasc. Biol. *39*, 850–856.

Li, J., and Pfeffer, S.R. (2016). Lysosomal membrane glycoproteins bind cholesterol and contribute to lysosomal cholesterol export. Elife *5*, e21635.

Li, F., Zhao, X., Li, H., Liu, Y., Zhang, Y., Huang, X., Cao, J., Du, F., Wu, D., and Yu,

H. (2021). Hepatic lysosomal acid lipase drives the autophagy-lysosomal response and alleviates cholesterol metabolic disorder in ApoE deficient mice. Biochim. Biophys. Acta. Mol. Cell Biol. Lipids *1866*, 159027.

Li, S.-S., Zhang, M., Wang, J.-H., Yang, F., Kang, B., Xu, J.-J., and Chen, H.-Y. (2019). Monitoring the Changes of pH in Lysosomes during Autophagy and Apoptosis by Plasmon Enhanced Raman Imaging. Anal. Chem. *91*, 8398–8405.

Li, W.W., Li, J., and Bao, J.K. (2012). Microautophagy: Lesser-known self-eating. Cell. Mol. Life Sci. *69*, 1125–1136.

Li, X., Rydzewski, N., Hider, A., Zhang, X., Yang, J., Wang, W., Gao, Q., Cheng, X., and Xu, H. (2016). A molecular mechanism to regulate lysosome motility for lysosome positioning and tubulation. Nat. Cell Biol. *18*, 404–417.

Li, Y., Wang, X., Li, M., Yang, C., and Wang, X. (2022). M05B5.4 (lysosomal phospholipase A2) promotes disintegration of autophagic vesicles to maintain C. elegans development. Autophagy *18*, 595–607.

Liang, J.R., and Corn, J.E. (2022). A CRISPR view on autophagy. Trends Cell Biol. *32*, 1008–1022.

Liang, C., Lee, J., Inn, K., Gack, M.U., Li, Q., Roberts, E.A., Vergne, I., Deretic, V., Feng, P., Akazawa, C., et al. (2008). Beclin1-binding UVRAG targets the class C Vps complex to coordinate autophagosome maturation and endocytic trafficking. Nat. Cell Biol. *10*, 776–787.

Liang, J.R., Lingeman, E., Luong, T., Ahmed, S., Muhar, M., Nguyen, T., Olzmann, J.A., and Corn, J.E. (2020). A Genome-wide ER-phagy Screen Highlights Key Roles of Mitochondrial Metabolism and ER-Resident UFMylation. Cell *180*, 1160-1177.e20.

Lin, X., Li, S., Zhao, Y., Ma, X., Zhang, K., He, X., and Wang, Z. (2013). Interaction domains of p62: a bridge between p62 and selective autophagy. DNA Cell Biol. *32*, 220–227.

Lipinski, M.M., Zheng, B., Lu, T., Yan, Z., Py, B.F., Ng, A., Xavier, R.J., Li, C., Yankner, B.A., Scherzer, C.R., et al. (2010). Genome-wide analysis reveals mechanisms modulating autophagy in normal brain aging and in Alzheimer's disease. Proc. Natl. Acad. Sci. U. S. A. *107*, 14164–14169.

Liu, W.J., Ye, L., Huang, W.F., Guo, L.J., Xu, Z.G., Wu, H.L., Yang, C., and Liu, H.F. (2016). p62 links the autophagy pathway and the ubiqutin–proteasome system upon

ubiquitinated protein degradation. Cell. Mol. Biol. Lett. *21*, 29.
López-Otín, C., Blasco, M.A., Partridge, L., Serrano, M., and Kroemer, G. (2013). The hallmarks of aging. Cell *153*, 1194–1217.
Lőrincz, P., and Juhász, G. (2020). Autophagosome-Lysosome Fusion. J. Mol. Biol. *432*, 2462–2482.
Lürick, A., Gao, J., Kuhlee, A., Yavavli, E., Langemeyer, L., Perz, A., Raunser, S., and Ungermann, C. (2017). Multivalent Rab interactions determine tether-mediated membrane fusion. Mol. Biol. Cell *28*, 322–332.
Lystad, A.H., Carlsson, S.R., de la Ballina, L.R., Kauffman, K.J., Nag, S., Yoshimori, T., Melia, T.J., and Simonsen, A. (2019). Distinct functions of ATG16L1 isoforms in membrane binding and LC3B lipidation in autophagy-related processes. Nat. Cell Biol.
Maeda, S., Otomo, C., and Otomo, T. (2019). The autophagic membrane tether ATG2A transfers lipids between membranes. Elife *8*.
Maeda, S., Yamamoto, H., Kinch, L.N., Garza, C.M., Takahashi, S., Otomo, C., Grishin, N. V, Forli, S., Mizushima, N., and Otomo, T. (2020). Structure, lipid scrambling activity and role in autophagosome formation of ATG9A. Nat. Struct. Mol. Biol. *27*, 1194–1201.
Maeda, Y., Oku, M., and Sakai, Y. (2015). A defect of the vacuolar putative lipase Atg15 accelerates degradation of lipid droplets through lipolysis. Autophagy *11*, 1247–1258.
Maehira, F., Nakada, F., and Hokama, T. (1984). Characteristics of acid esterase in Wolman's disease. Biochem. Med. *32*, 322–330.
Maharjan, Y., Dutta, R.K., Son, J., Wei, X., Park, C., Kwon, H.M., and Park, R. (2022). Intracellular cholesterol transport inhibition Impairs autophagy flux by decreasing autophagosome–lysosome fusion. Cell Commun. Signal. *20*, 189.
Mahuran, D.J. (1999). Biochemical consequences of mutations causing the GM2 gangliosidoses. Biochim. Biophys. Acta *1455*, 105–138.
Maria Fimia, G., Stoykova, A., Romagnoli, A., Giunta, L., Di Bartolomeo, S., Nardacci, R., Corazzari, M., Fuoco, C., Ucar, A., Schwartz, P., et al. (2007). Ambra1 regulates autophagy and development of the nervous system. Nature *447*, 1121–1125.
Martinez, J., Malireddi, R.K.S., Lu, Q., Cunha, L.D., Pelletier, S., Gingras, S.,

Orchard, R., Guan, J.-L., Tan, H., Peng, J., et al. (2015). Molecular characterization of LC3-associated phagocytosis reveals distinct roles for Rubicon, NOX2 and autophagy proteins. Nat. Cell Biol. *17*, 893–906.

Maruyama, T., and Noda, N.N. (2018). Autophagy-regulating protease Atg4: structure, function, regulation and inhibition. J. Antibiot. (Tokyo). *71*, 72–78.

Matsui, T., Jiang, P., Nakano, S., Sakamaki, Y., Yamamoto, H., and Mizushima, N. (2018). Autophagosomal YKT6 is required for fusion with lysosomes independently of syntaxin 17. J. Cell Biol. *217*, 2633–2645.

Matsushita, M., Suzuki, N.N., Obara, K., Fujioka, Y., Ohsumi, Y., and Inagaki, F. (2007). Structure of Atg5·Atg16, a Complex Essential for Autophagy*. J. Biol. Chem. *282*, 6763–6772.

Mauthe, M., Orhon, I., Rocchi, C., Zhou, X., Luhr, M., Hijlkema, K.-J., Coppes, R.P., Engedal, N., Mari, M., and Reggiori, F. (2018). Chloroquine inhibits autophagic flux by decreasing autophagosome-lysosome fusion. Autophagy *14*, 1435–1455.

Mauvezin, C., Nagy, P., Juhász, G., and Neufeld, T.P. (2015). Autophagosome–lysosome fusion is independent of V-ATPase-mediated acidification. Nat. Commun. *6*, 7007.

May, D.G., Scott, K.L., Campos, A.R., and Roux, K.J. (2020). Comparative Application of BioID and TurboID for Protein-Proximity Biotinylation. Cells *9*.

Mazhab-Jafari, M.T., Rohou, A., Schmidt, C., Bueler, S.A., Benlekbir, S., Robinson, C. V, and Rubinstein, J.L. (2016). Atomic model for the membrane-embedded VO motor of a eukaryotic V-ATPase. Nature *539*, 118–122.

McDonald, E.R. 3rd, de Weck, A., Schlabach, M.R., Billy, E., Mavrakis, K.J., Hoffman, G.R., Belur, D., Castelletti, D., Frias, E., Gampa, K., et al. (2017). Project DRIVE: A Compendium of Cancer Dependencies and Synthetic Lethal Relationships Uncovered by Large-Scale, Deep RNAi Screening. Cell *170*, 577-592.e10.

McEwan, D.G., Popovic, D., Gubas, A., Terawaki, S., Suzuki, H., Stadel, D., Coxon, F.P., Miranda de Stegmann, D., Bhogaraju, S., Maddi, K., et al. (2015). PLEKHM1 regulates autophagosome-lysosome fusion through HOPS complex and LC3/GABARAP proteins. Mol. Cell *57*, 39–54.

Medina, D.L., Di Paola, S., Peluso, I., Armani, A., De Stefani, D., Venditti, R., Montefusco, S., Scotto-Rosato, A., Prezioso, C., Forrester, A., et al. (2015).

Lysosomal calcium signalling regulates autophagy through calcineurin and TFEB. Nat. Cell Biol. *17*, 288–299.

Mercer, C.A., Kaliappan, A., and Dennis, P.B. (2009). A novel, human Atg13 binding protein, Atg101, interacts with ULK1 and is essential for macroautophagy. Autophagy *5*, 649–662.

Mijaljica, D., Prescott, M., and Devenish, R.J. (2011). V-ATPase engagement in autophagic processes. Autophagy *7*, 666–668.

Mimura, K., Sakamaki, J.-I., Morishita, H., Kawazu, M., Mano, H., and Mizushima, N. (2021). Genome-wide CRISPR screening reveals nucleotide synthesis negatively regulates autophagy. J. Biol. Chem. *296*, 100780.

Mizushima, N., and Levine, B. (2010). Autophagy in mammalian development and differentiation. Nat. Cell Biol. *12*, 823–830.

Mizushima, N., Yoshimori, T., and Levine, B. (2010). Methods in Mammalian Autophagy Research. Cell *140*, 313–326.

Mo, D., Chen, Y., Jiang, N., Shen, J., and Zhang, J. (2020). Investigation of Isoform Specific Functions of the V-ATPase a Subunit During Drosophila Wing Development . Front. Genet. *11*.

Mohsen, S., Sobash, P.T., Algwaiz, G.F., Nasef, N., Al-Zeidaneen, S.A., and Karim, N.A. (2022). Autophagy Agents in Clinical Trials for Cancer Therapy: A Brief Review. Curr. Oncol. *29*, 1695–1708.

Morita, K., Hama, Y., Izume, T., Tamura, N., Ueno, T., Yamashita, Y., Sakamaki, Y., Mimura, K., Morishita, H., Shihoya, W., et al. (2018). Genome-wide CRISPR screen identifies TMEM41B as a gene required for autophagosome formation. J. Cell Biol. *217*, 3817–3828.

Moriya, H. (2015). Quantitative nature of overexpression experiments. Mol. Biol. Cell *26*, 3932–3939.

Mortimore, G.E., and Schworer, C.M. (1977). Induction of autophagy by amino-acid deprivation in perfused rat liver. Nature *270*, 174–176.

Muhammad, A., Flores, I., Zhang, H., Yu, R., Staniszewski, A., Planel, E., Herman, M., Ho, L., Kreber, R., Honig, L.S., et al. (2008). Retromer deficiency observed in Alzheimer's disease causes hippocampal dysfunction, neurodegeneration, and Abeta accumulation. Proc. Natl. Acad. Sci. U. S. A. *105*, 7327–7332.

Mukadam, A.S., Breusegem, S.Y., and Seaman, M.N.J. (2018). Analysis of novel

endosome-to-Golgi retrieval genes reveals a role for PLD3 in regulating endosomal protein sorting and amyloid precursor protein processing. Cell. Mol. Life Sci. *75*, 2613–2625.

Nackenoff, A.G., Hohman, T.J., Neuner, S.M., Akers, C.S., Weitzel, N.C., Shostak, A., Ferguson, S.M., Mobley, B., Bennett, D.A., Schneider, J.A., et al. (2021). PLD3 is a neuronal lysosomal phospholipase D associated with β-amyloid plaques and cognitive function in Alzheimer's disease. PLoS Genet. *17*, e1009406.

Neggers, J.E., Paolella, B.R., Asfaw, A., Rothberg, M. V, Skipper, T.A., Yang, A., Kalekar, R.L., Krill-Burger, J.M., Dharia, N. V, Kugener, G., et al. (2020). Synthetic Lethal Interaction between the ESCRT Paralog Enzymes VPS4A and VPS4B in Cancers Harboring Loss of Chromosome 18q or 16q. Cell Rep. *33*, 108493.

Nibbeling, E.A.R., Duarri, A., Verschuuren-Bemelmans, C.C., Fokkens, M.R., Karjalainen, J.M., Smeets, C.J.L.M., de Boer-Bergsma, J.J., van der Vries, G., Dooijes, D., Bampi, G.B., et al. (2017). Exome sequencing and network analysis identifies shared mechanisms underlying spinocerebellar ataxia. Brain *140*, 2860–2878.

Nickerson, D.P., West, M., Henry, R., and Odorizzi, G. (2010). Regulators of Vps4 ATPase Activity at Endosomes Differentially Influence the Size and Rate of Formation of Intralumenal Vesicles. Mol. Biol. Cell *21*, 1023–1032.

Nishimura, T., Kaizuka, T., Cadwell, K., Sahani, M.H., Saitoh, T., Akira, S., Virgin, H.W., and Mizushima, N. (2013). FIP200 regulates targeting of Atg16L1 to the isolation membrane. EMBO Rep. *14*, 284–291.

Nixon, R.A. (2020). The aging lysosome: An essential catalyst for late-onset neurodegenerative diseases. Biochim. Biophys. Acta. Proteins Proteomics *1868*, 140443.

Nixon, R.A., and Yang, D.-S. (2011). Autophagy failure in Alzheimer's disease--locating the primary defect. Neurobiol. Dis. *43*, 38–45.

Novikoff, A.B., Beaufay, H., and de Duve, C. (1956). ELECTRON MICROSCOPY OF LYSOSOME-RICH FRACTIONS FROM RAT LIVER . J. Biophys. Biochem. Cytol. *2*, 179–184.

O'Sullivan, G.A., Kneussel, M., Elazar, Z., and Betz, H. (2005). GABARAP is not essential for GABA receptor targeting to the synapse. Eur. J. Neurosci. *22*, 2644–2648.

Ohashi, T. (2012). Enzyme replacement therapy for lysosomal storage diseases. Pediatr. Endocrinol. Rev. *10 Suppl 1*, 26–34.

Ohkuma, S., and Poole, B. (1978). Fluorescence probe measurement of the intralysosomal pH in living cells and the perturbation of pH by various agents. Proc. Natl. Acad. Sci. U. S. A. *75*, 3327–3331.

Ohnstad, A.E., Delgado, J.M., North, B.J., Nasa, I., Kettenbach, A.N., Schultz, S.W., and Shoemaker, C.J. (2020). Receptor-mediated clustering of FIP200 bypasses the role of LC3 lipidation in autophagy. EMBO J. *39*, e104948.

Olson, L.J., Hindsgaul, O., Dahms, N.M., and Kim, J.-J.P. (2008). Structural insights into the mechanism of pH-dependent ligand binding and release by the cation-dependent mannose 6-phosphate receptor. J. Biol. Chem. *283*, 10124–10134.

Oot, R.A., Couoh-Cardel, S., Sharma, S., Stam, N.J., and Wilkens, S. (2017). Breaking up and making up: The secret life of the vacuolar H(+) -ATPase. Protein Sci. *26*, 896–909.

Orsi, A., Razi, M., Dooley, H.C., Robinson, D., Weston, A.E., Collinson, L.M., and Tooze, S.A. (2012). Dynamic and transient interactions of Atg9 with autophagosomes, but not membrane integration, are required for autophagy. Mol. Biol. Cell.

Orvedahl, A., Sumpter, R.J., Xiao, G., Ng, A., Zou, Z., Tang, Y., Narimatsu, M., Gilpin, C., Sun, Q., Roth, M., et al. (2011). Image-based genome-wide siRNA screen identifies selective autophagy factors. Nature *480*, 113–117.

Osawa, T., and Noda, N.N. (2019). Atg2: A novel phospholipid transfer protein that mediates de novo autophagosome biogenesis. Protein Sci. *28*, 1005–1012.

Ott, C., König, J., Höhn, A., Jung, T., and Grune, T. (2016). Macroautophagy is impaired in old murine brain tissue as well as in senescent human fibroblasts. Redox Biol. *10*, 266–273.

Packer, M.S., and Liu, D.R. (2015). Methods for the directed evolution of proteins. Nat. Rev. Genet. *16*, 379–394.

Pamarthy, S., Kulshrestha, A., Katara, G.K., and Beaman, K.D. (2018). The curious case of vacuolar ATPase: regulation of signaling pathways. Mol. Cancer *17*, 41.

Parenti, G., Medina, D.L., and Ballabio, A. (2021). The rapidly evolving view of lysosomal storage diseases. EMBO Mol. Med. *13*, e12836.

Parzych, K.R., and Klionsky, D.J. (2014). An overview of autophagy: morphology,

mechanism, and regulation. Antioxid. Redox Signal. *20*, 460–473.
Pedersen, K.M., Finsen, B., Celis, J.E., and Jensen, N.A. (1998). Expression of a Novel Murine Phospholipase D Homolog Coincides with Late Neuronal Development in the Forebrain*. J. Biol. Chem. *273*, 31494–31504.
Perez, S.E., He, B., Nadeem, M., Wuu, J., Ginsberg, S.D., Ikonomovic, M.D., and Mufson, E.J. (2015). Hippocampal endosomal, lysosomal, and autophagic dysregulation in mild cognitive impairment: correlation with aβ and tau pathology. J. Neuropathol. Exp. Neurol. *74*, 345–358.
Perreira, J.M., Aker, A.M., Savidis, G., Chin, C.R., McDougall, W.M., Portmann, J.M., Meraner, P., Smith, M.C., Rahman, M., Baker, R.E., et al. (2015a). RNASEK Is a V-ATPase-Associated Factor Required for Endocytosis and the Replication of Rhinovirus, Influenza A Virus, and Dengue Virus. Cell Rep. *12*, 850–863.
Perreira, J.M., Aker, A.M., Savidis, G., Chin, C.R., McDougall, W.M., Portmann, J.M., Meraner, P., Smith, M.C., Rahman, M., Baker, R.E., et al. (2015b). RNASEK Is a V-ATPase-Associated Factor Required for Endocytosis and the Replication of Rhinovirus, Influenza A Virus, and Dengue Virus. Cell Rep. *12*, 850–863.
Peters, C., Bayer, M.J., Bühler, S., Andersen, J.S., Mann, M., and Mayer, A. (2001). Trans-complex formation by proteolipid channels in the terminal phase of membrane fusion. Nature *409*, 581–588.
Piao, S., and Amaravadi, R.K. (2016). Targeting the lysosome in cancer. Ann. N. Y. Acad. Sci. *1371*, 45–54.
Pickford, F., Masliah, E., Britschgi, M., Lucin, K., Narasimhan, R., Jaeger, P.A., Small, S., Spencer, B., Rockenstein, E., Levine, B., et al. (2008). The autophagy-related protein beclin 1 shows reduced expression in early Alzheimer disease and regulates amyloid beta accumulation in mice. J. Clin. Invest. *118*, 2190–2199.
Platt, F.M., d'Azzo, A., Davidson, B.L., Neufeld, E.F., and Tifft, C.J. (2018). Lysosomal storage diseases. Nat. Rev. Dis. Prim. *4*, 27.
Polson, H.E.J., De Lartigue, J., Rigden, D.J., Reedijk, M., Urbé, S., Clague, M.J., and Tooze, S.A. (2010). Mammalian Atg18 (WIPI2) localizes to omegasome-anchored phagophores and positively regulates LC3 lipidation. Autophagy *6*, 506–522.
Poole, B., and Ohkuma, S. (1981). Effect of weak bases on the intralysosomal pH in mouse peritoneal macrophages. J. Cell Biol. *90*, 665–669.

Popovic, D., and Dikic, I. (2014). TBC1D5 and the AP2 complex regulate ATG9 trafficking and initiation of autophagy. EMBO Rep. *15*, 392–401.

Poreba, M., Groborz, K., Vizovisek, M., Maruggi, M., Turk, D., Turk, B., Powis, G., Drag, M., and Salvesen, G.S. (2019). Fluorescent probes towards selective cathepsin B detection and visualization in cancer cells and patient samples. Chem. Sci. *10*, 8461–8477.

Proikas-Cezanne, T., Takacs, Z., Dönnes, P., and Kohlbacher, O. (2015). WIPI proteins: essential PtdIns3P effectors at the nascent autophagosome. J. Cell Sci. *128*, 207–217.

Puertollano, R., Ferguson, S.M., Brugarolas, J., and Ballabio, A. (2018). The complex relationship between TFEB transcription factor phosphorylation and subcellular localization. EMBO J. *37*.

Pungercar, J.R., Caglic, D., Sajid, M., Dolinar, M., Vasiljeva, O., Pozgan, U., Turk, D., Bogyo, M., Turk, V., and Turk, B. (2009). Autocatalytic processing of procathepsin B is triggered by proenzyme activity. FEBS J. *276*, 660–668.

Pyo, J.-O., Yoo, S.-M., Ahn, H.-H., Nah, J., Hong, S.-H., Kam, T.-I., Jung, S., and Jung, Y.-K. (2013). Overexpression of Atg5 in mice activates autophagy and extends lifespan. Nat. Commun. *4*, 2300.

Qian, M., Sleat, D.E., Zheng, H., Moore, D., and Lobel, P. (2008). Proteomics analysis of serum from mutant mice reveals lysosomal proteins selectively transported by each of the two mannose 6-phosphate receptors. Mol. Cell. Proteomics *7*, 58–70.

Qin, W., Cho, K.F., Cavanagh, P.E., and Ting, A.Y. (2021). Deciphering molecular interactions by proximity labeling. Nat. Methods *18*, 133–143.

Qureshi, Y.H., Berman, D.E., Marsh, S.E., Klein, R.L., Patel, V.M., Simoes, S., Kannan, S., Petsko, G.A., Stevens, B., and Small, S.A. (2022). The neuronal retromer can regulate both neuronal and microglial phenotypes of Alzheimer's disease. Cell Rep. *38*, 110262.

Radulovic, M., Schink, K.O., Wenzel, E.M., Nähse, V., Bongiovanni, A., Lafont, F., and Stenmark, H. (2018). ESCRT-mediated lysosome repair precedes lysophagy and promotes cell survival. EMBO J. *37*.

Rai, S., Arasteh, M., Jefferson, M., Pearson, T., Wang, Y., Zhang, W., Bicsak, B., Divekar, D., Powell, P.P., Naumann, R., et al. (2019). The ATG5-binding and coiled

coil domains of ATG16L1 maintain autophagy and tissue homeostasis in mice independently of the WD domain required for LC3-associated phagocytosis. Autophagy *15*, 599–612.
Raiborg, C., and Stenmark, H. (2009). The ESCRT machinery in endosomal sorting of ubiquitylated membrane proteins. Nature *458*, 445–452.
Ramanathan, M., Majzoub, K., Rao, D.S., Neela, P.H., Zarnegar, B.J., Mondal, S., Roth, J.G., Gai, H., Kovalski, J.R., Siprashvili, Z., et al. (2018). RNA–protein interaction detection in living cells. Nat. Methods *15*, 207–212.
Ratto, E., Chowdhury, S.R., Siefert, N.S., Schneider, M., Wittmann, M., Helm, D., and Palm, W. (2022). Direct control of lysosomal catabolic activity by mTORC1 through regulation of V-ATPase assembly. Nat. Commun. *13*, 4848.
Rawat, S., Chatterjee, D., Marwaha, R., Charak, G., Kumar, G., Shaw, S., Khatter, D., Sharma, S., de Heus, C., Liv, N., et al. (2022). RUFY1 binds Arl8b and mediates endosome-to-TGN CI-M6PR retrieval for cargo sorting to lysosomes. J. Cell Biol. *222*, e202108001.
Ries, S., Büchler, C., Langmann, T., Fehringer, P., Aslanidis, C., and Schmitz, G. (1998). Transcriptional regulation of lysosomal acid lipase in differentiating monocytes is mediated by transcription factors Sp1 and AP-2. J. Lipid Res. *39*, 2125–2134.
Rieter, E., Vinke, F., Bakula, D., Cebollero, E., Ungermann, C., Proikas-Cezanne, T., and Reggiori, F. (2013). Atg18 function in autophagy is regulated by specific sites within its β-propeller. J. Cell Sci. *126*, 593–604.
Rocchi, A., Yamamoto, S., Ting, T., Fan, Y., Sadleir, K., Wang, Y., Zhang, W., Huang, S., Levine, B., Vassar, R., et al. (2017). A Becn1 mutation mediates hyperactive autophagic sequestration of amyloid oligomers and improved cognition in Alzheimer's disease. PLoS Genet. *13*, e1006962.
Rodger, C., Flex, E., Allison, R.J., Sanchis-Juan, A., Hasenahuer, M.A., Cecchetti, S., French, C.E., Edgar, J.R., Carpentieri, G., Ciolfi, A., et al. (2020). De Novo VPS4A Mutations Cause Multisystem Disease with Abnormal Neurodevelopment. Am. J. Hum. Genet. *107*, 1129–1148.
Rojas, R., van Vlijmen, T., Mardones, G.A., Prabhu, Y., Rojas, A.L., Mohammed, S., Heck, A.J.R., Raposo, G., van der Sluijs, P., and Bonifacino, J.S. (2008). Regulation of retromer recruitment to endosomes by sequential action of Rab5 and Rab7. J.

Cell Biol. *183*, 513–526.
Romanyuk, D., Polak, A., Maleszewska, A., Sieńko, M., Grynberg, M., and Zoładek, T. (2011). Human hAtg2A protein expressed in yeast is recruited to preautophagosomal structure but does not complement autophagy defects of atg2Δ strain. Acta Biochim. Pol.
Ronan, B., Flamand, O., Vescovi, L., Dureuil, C., Durand, L., Fassy, F., Bachelot, M.-F., Lamberton, A., Mathieu, M., Bertrand, T., et al. (2014). A highly potent and selective Vps34 inhibitor alters vesicle trafficking and autophagy. Nat. Chem. Biol. *10*, 1013–1019.
Roux, K.J., Kim, D.I., Raida, M., and Burke, B. (2012). A promiscuous biotin ligase fusion protein identifies proximal and interacting proteins in mammalian cells. J. Cell Biol. *196*, 801–810.
Rudnik, S., and Damme, M. (2021). The lysosomal membrane—export of metabolites and beyond. FEBS J. *288*, 4168–4182.
Rumin, J., Bonnefond, H., Saint-Jean, B., Rouxel, C., Sciandra, A., Bernard, O., Cadoret, J.-P., and Bougaran, G. (2015). The use of fluorescent Nile red and BODIPY for lipid measurement in microalgae. Biotechnol. Biofuels *8*, 42.
Runwal, G., Stamatakou, E., Siddiqi, F.H., Puri, C., Zhu, Y., and Rubinsztein, D.C. (2019). LC3-positive structures are prominent in autophagy-deficient cells. Sci. Rep. *9*, 10147.
Russell, R.C., Tian, Y., Yuan, H., Park, H.W., Chang, Y.Y., Kim, J., Kim, H., Neufeld, T.P., Dillin, A., and Guan, K.L. (2013). ULK1 induces autophagy by phosphorylating Beclin-1 and activating VPS34 lipid kinase. Nat. Cell Biol.
Sabatini, D.D., and Adesnik, M. (2013). Christian de Duve: Explorer of the cell who discovered new organelles by using a centrifuge. Proc. Natl. Acad. Sci. *110*, 13234–13235.
Saitoh, T., Fujita, N., Hayashi, T., Takahara, K., Satoh, T., Lee, H., Matsunaga, K., Kageyama, S., Omori, H., Noda, T., et al. (2009). Atg9a controls dsDNA-driven dynamic translocation of STING and the innate immune response. Proc. Natl. Acad. Sci. U. S. A. *106*, 20842–20846.
Sakoh-Nakatogawa, M., Matoba, K., Asai, E., Kirisako, H., Ishii, J., Noda, N.N., Inagaki, F., Nakatogawa, H., and Ohsumi, Y. (2013). Atg12-Atg5 conjugate enhances E2 activity of Atg3 by rearranging its catalytic site. Nat. Struct. Mol. Biol.

20, 433–439.
Samie, M., Wang, X., Zhang, X., Goschka, A., Li, X., Cheng, X., Gregg, E., Azar, M., Zhuo, Y., Garrity, A.G., et al. (2013). A TRP channel in the lysosome regulates large particle phagocytosis via focal exocytosis. Dev. Cell *26*, 511–524.
Sancak, Y., Bar-Peled, L., Zoncu, R., Markhard, A.L., Nada, S., and Sabatini, D.M. (2010). Ragulator-Rag complex targets mTORC1 to the lysosomal surface and is necessary for its activation by amino acids. Cell *141*, 290–303.
Sanjana, N.E., Shalem, O., and Zhang, F. (2014). Improved vectors and genome-wide libraries for CRISPR screening. Nat. Methods *11*, 783–784.
Sanjuan, M.A., Dillon, C.P., Tait, S.W.G., Moshiach, S., Dorsey, F., Connell, S., Komatsu, M., Tanaka, K., Cleveland, J.L., Withoff, S., et al. (2007). Toll-like receptor signalling in macrophages links the autophagy pathway to phagocytosis. Nature *450*, 1253–1257.
Sarkar, S., Carroll, B., Buganim, Y., Maetzel, D., Ng, A.H.M., Cassady, J.P., Cohen, M.A., Chakraborty, S., Wang, H., Spooner, E., et al. (2013). Impaired autophagy in the lipid-storage disorder Niemann-Pick type C1 disease. Cell Rep. *5*, 1302–1315.
Satoh, J.-I., Kino, Y., Yamamoto, Y., Kawana, N., Ishida, T., Saito, Y., and Arima, K. (2014). PLD3 is accumulated on neuritic plaques in Alzheimer's disease brains. Alzheimers. Res. Ther. *6*, 70.
Scheuring, S., Röhricht, R.A., Schöning-Burkhardt, B., Beyer, A., Müller, S., Abts, H.F., and Köhrer, K. (2001). Mammalian Cells Express Two VPS4 Proteins Both of Which are Involved in Intracellular Protein Trafficking. J. Mol. Biol. *312*, 469–480.
Schott, M.B., Weller, S.G., Schulze, R.J., Krueger, E.W., Drizyte-Miller, K., Casey, C.A., and McNiven, M.A. (2019). Lipid droplet size directs lipolysis and lipophagy catabolism in hepatocytes. J. Cell Biol. *218*, 3320–3335.
Schwagerl, A.L., Mohan, P.S., Cataldo, A.M., Vonsattel, J.P., Kowall, N.W., and Nixon, R.A. (1995). Elevated levels of the endosomal-lysosomal proteinase cathepsin D in cerebrospinal fluid in Alzheimer disease. J. Neurochem. *64*, 443–446.
Scotto Rosato, A., Montefusco, S., Soldati, C., Di Paola, S., Capuozzo, A., Monfregola, J., Polishchuk, E., Amabile, A., Grimm, C., Lombardo, A., et al. (2019). TRPML1 links lysosomal calcium to autophagosome biogenesis through the activation of the CaMKKβ/VPS34 pathway. Nat. Commun. *10*, 5630.

Selvy, P.E., Lavieri, R.R., Lindsley, C.W., and Brown, H.A. (2011). Phospholipase D: enzymology, functionality, and chemical modulation. Chem. Rev. *111*, 6064–6119.
Shalem, O., Sanjana, N.E., Hartenian, E., Shi, X., Scott, D.A., Mikkelsen, T.S., Heckl, D., Ebert, B.L., Root, D.E., Doench, J.G., et al. (2014). Genome-scale CRISPR-Cas9 knockout screening in human cells. Science (80-.). *343*, 84–87.
Shayman, J.A., and Tesmer, J.J.G. (2019). Lysosomal phospholipase A2. Biochim. Biophys. Acta. Mol. Cell Biol. Lipids *1864*, 932–940.
Shintani, T., and Klionsky, D.J. (2004). Autophagy in health and disease: a double-edged sword. Science *306*, 990–995.
Shrivastav, M., De Haro, L.P., and Nickoloff, J.A. (2008). Regulation of DNA double-strand break repair pathway choice. Cell Res. *18*, 134–147.
Sigismund, S., Argenzio, E., Tosoni, D., Cavallaro, E., Polo, S., and Di Fiore, P.P. (2008). Clathrin-Mediated Internalization Is Essential for Sustained EGFR Signaling but Dispensable for Degradation. Dev. Cell *15*, 209–219.
Singh, J., Kaade, E., Muntel, J., Bruderer, R., Reiter, L., Thelen, M., and Winter, D. (2020). Systematic Comparison of Strategies for the Enrichment of Lysosomes by Data Independent Acquisition. J. Proteome Res. *19*, 371–381.
Skowyra, M.L., Schlesinger, P.H., Naismith, T. V, and Hanson, P.I. (2018). Triggered recruitment of ESCRT machinery promotes endolysosomal repair. Science *360*.
Sorbara, M.T., Foerster, E.G., Tsalikis, J., Abdel-Nour, M., Mangiapane, J., Sirluck-Schroeder, I., Tattoli, I., van Dalen, R., Isenman, D.E., Rohde, J.R., et al. (2018). Complement C3 Drives Autophagy-Dependent Restriction of Cyto-invasive Bacteria. Cell Host Microbe *23*, 644-652.e5.
Sou, Y.S., Waguri, S., Iwata, J.I., Ueno, T., Fujimura, T., Hara, T., Sawada, N., Yamada, A., Mizushima, N., Uchiyama, Y., et al. (2008). The Atg8 conjugation system is indispensable for proper development of autophagic isolation membranes in mice. Mol. Biol. Cell *19*, 4762–4775.
Spang, A. (2016). Membrane Tethering Complexes in the Endosomal System. Front. Cell Dev. Biol. *4*, 35.
Staudt, C., Puissant, E., and Boonen, M. (2016). Subcellular Trafficking of Mammalian Lysosomal Proteins: An Extended View. Int. J. Mol. Sci. *18*.
Strauss, K., Goebel, C., Runz, H., Möbius, W., Weiss, S., Feussner, I., Simons, M., and Schneider, A. (2010). Exosome secretion ameliorates lysosomal storage of

cholesterol in Niemann-Pick type C disease. J. Biol. Chem. *285*, 26279–26288.
Sun-Wada, G.-H., Toyomura, T., Murata, Y., Yamamoto, A., Futai, M., and Wada, Y. (2006). The a3 isoform of V-ATPase regulates insulin secretion from pancreatic beta-cells. J. Cell Sci. *119*, 4531–4540.
Sun, M., Goldin, E., Stahl, S., Falardeau, J.L., Kennedy, J.C., Acierno Jr, J.S., Bove, C., Kaneski, C.R., Nagle, J., Bromley, M.C., et al. (2000). Mucolipidosis type IV is caused by mutations in a gene encoding a novel transient receptor potential channel. Hum. Mol. Genet. *9*, 2471–2478.
Sun, Z.-C., Jiang, Z., Xu, X., Li, M., Zeng, Q., Zhu, Y., Wang, S., Li, Y., Tian, X.-L., and Hu, C. (2021). Fish Paralog Proteins RNASEK-a and -b Enhance Type I Interferon Secretion and Promote Apoptosis . Front. Immunol. *12*.
Suzuki, K., Kubota, Y., Sekito, T., and Ohsumi, Y. (2007). Hierarchy of Atg proteins in pre-autophagosomal structure organization. Genes to Cells *12*, 209–218.
SWEELEY, C.C., and KLIONSKY, B. (1963). FABRY'S DISEASE: CLASSIFICATION AS A SPHINGOLIPIDOSIS AND PARTIAL CHARACTERIZATION OF A NOVEL GLYCOLIPID. J. Biol. Chem. *238*, 3148–3150.
Szymańska, E., Nowak, P., Kolmus, K., Cybulska, M., Goryca, K., Derezińska-Wołek, E., Szumera-Ciećkiewicz, A., Brewińska-Olchowik, M., Grochowska, A., Piwocka, K., et al. (2020). Synthetic lethality between VPS4A and VPS4B triggers an inflammatory response in colorectal cancer. EMBO Mol. Med. *12*, e10812.
Takahara, T., Amemiya, Y., Sugiyama, R., Maki, M., and Shibata, H. (2020). Amino acid-dependent control of mTORC1 signaling: a variety of regulatory modes. J. Biomed. Sci. *27*, 87.
Takahashi, Y., He, H., Tang, Z., Hattori, T., Liu, Y., Young, M.M., Serfass, J.M., Chen, L., Gebru, M., Chen, C., et al. (2018a). An autophagy assay reveals the ESCRT-III component CHMP2A as a regulator of phagophore closure. Nat. Commun. *9*, 1–13.
Takahashi, Y., He, H., Tang, Z., Hattori, T., Liu, Y., Young, M.M., Serfass, J.M., Chen, L., Gebru, M., Chen, C., et al. (2018b). An autophagy assay reveals the ESCRT-III component CHMP2A as a regulator of phagophore closure. Nat. Commun. *9*, 2855.
Takahashi, Y., Liang, X., Hattori, T., Tang, Z., He, H., Chen, H., Liu, X., Abraham, T., Imamura-Kawasawa, Y., Buchkovich, N.J., et al. (2019). VPS37A directs ESCRT

recruitment for phagophore closure. J. Cell Biol. *218*, 3336–3354.
Takeshige, K., Baba, M., Tsuboi, S., Noda, T., and Ohsumi, Y. (1992). Autophagy in yeast demonstrated with proteinase-deficient mutants and conditions for its induction. J. Cell Biol. *119*, 301–311.
Tamura, N., Nishimura, T., Sakamaki, Y., Koyama-Honda, I., Yamamoto, H., and Mizushima, N. (2017). Differential requirement for ATG2A domains for localization to autophagic membranes and lipid droplets. FEBS Lett. *591*, 3819–3830.
Tan, J.M.J., Mellouk, N., Osborne, S.E., Ammendolia, D.A., Dyer, D.N., Li, R., Brunen, D., van Rijn, J.M., Huang, J., Czuczman, M.A., et al. (2018). An ATG16L1-dependent pathway promotes plasma membrane repair and limits Listeria monocytogenes cell-to-cell spread. Nat. Microbiol. *3*, 1472–1485.
Tan, M., Li, J., Ma, F., Zhang, X., Zhao, Q., and Cao, X. (2019). PLD3 Rare Variants Identified in Late-Onset Alzheimer's Disease Affect Amyloid-β Levels in Cellular Model. Front. Neurosci. *13*, 116.
Tanaka, Y., Guhde, G., Suter, A., Eskelinen, E.-L., Hartmann, D., Lüllmann-Rauch, R., Janssen, P.M.L., Blanz, J., von Figura, K., and Saftig, P. (2000). Accumulation of autophagic vacuoles and cardiomyopathy in LAMP-2-deficient mice. Nature *406*, 902–906.
Tang, C.-H., Lee, J.-W., Galvez, M.G., Robillard, L., Mole, S.E., and Chapman, H.A. (2006). Murine cathepsin F deficiency causes neuronal lipofuscinosis and late-onset neurological disease. Mol. Cell. Biol. *26*, 2309–2316.
Tang, Z., Takahashi, Y., He, H., Hattori, T., Chen, C., Liang, X., Chen, H., Young, M.M., and Wang, H.G. (2019). TOM40 Targets Atg2 to Mitochondria-Associated ER Membranes for Phagophore Expansion. Cell Rep. *28*, 1744-1757.e5.
Tanida, I., Ueno, T., and Kominami, E. (2004). LC3 conjugation system in mammalian autophagy. Int. J. Biochem. Cell Biol. *36*, 2503–2518.
Teter, S.A., Eggerton, K.P., Scott, S. V., Kim, J., Fischer, A.M., and Klionsky, D.J. (2001). Degradation of lipid vesicles in the yeast vacuole requires function of Cvt17, a putative lipase. J. Biol. Chem. *276*, 2083–2087.
Thelen, M., Winter, D., Braulke, T., and Gieselmann, V. (2017). SILAC-Based Comparative Proteomic Analysis of Lysosomes from Mammalian Cells Using LC-MS/MS BT - Lysosomes: Methods and Protocols. K. Öllinger, and H. Appelqvist, eds. (New York, NY: Springer New York), pp. 1–18.

Tiede, S., Storch, S., Lübke, T., Henrissat, B., Bargal, R., Raas-Rothschild, A., and Braulke, T. (2005). Mucolipidosis II is caused by mutations in GNPTA encoding the alpha/beta GlcNAc-1-phosphotransferase. Nat. Med. *11*, 1109–1112.
Toei, M., Saum, R., and Forgac, M. (2010). Regulation and isoform function of the V-ATPases. Biochemistry *49*, 4715–4723.
Trivedi, P.C., Bartlett, J.J., and Pulinilkunnil, T. (2020). Lysosomal Biology and Function: Modern View of Cellular Debris Bin. Cells *9*, 1131.
Tsuboyama, K., Koyama-Honda, I., Sakamaki, Y., Koike, M., Morishita, H., and Mizushima, N. (2016). The ATG conjugation systems are important for degradation of the inner autophagosomal membrane. Science (80-.). *354*, 1036–1041.
Tsukada, M., and Ohsumi, Y. (1993). Isolation and characterization of autophagy-defective mutants of Saccharomyces cerevisiae. FEBS Lett. *333*, 169–174.
Turk, V., Stoka, V., Vasiljeva, O., Renko, M., Sun, T., Turk, B., and Turk, D. (2012). Cysteine cathepsins: From structure, function and regulation to new frontiers. Biochim. Biophys. Acta - Proteins Proteomics *1824*, 68–88.
Ueno, T., and Komatsu, M. (2020). Monitoring Autophagy Flux and Activity: Principles and Applications. BioEssays *42*, 2000122.
Vajjhala, P.R., Nguyen, C.H., Landsberg, M.J., Kistler, C., Gan, A.-L., King, G.F., Hankamer, B., and Munn, A.L. (2008). The Vps4 C-terminal helix is a critical determinant for assembly and ATPase activity and has elements conserved in other members of the meiotic clade of AAA ATPases. FEBS J. *275*, 1427–1449.
Valverde, D.P., Yu, S., Boggavarapu, V., Kumar, N., Lees, J.A., Walz, T., Reinisch, K.M., and Melia, T.J. (2019). ATG2 transports lipids to promote autophagosome biogenesis. J. Cell Biol. *218*, 1787–1798.
Velho, R.V., Harms, F.L., Danyukova, T., Ludwig, N.F., Friez, M.J., Cathey, S.S., Filocamo, M., Tappino, B., Güneş, N., Tüysüz, B., et al. (2019). The lysosomal storage disorders mucolipidosis type II, type III alpha/beta, and type III gamma: Update on GNPTAB and GNPTG mutations. Hum. Mutat. *40*, 842–864.
Velikkakath, A.K.G., Nishimura, T., Oita, E., Ishihara, N., and Mizushima, N. (2012). Mammalian Atg2 proteins are essential for autophagosome formation and important for regulation of size and distribution of lipid droplets. Mol. Biol. Cell *23*, 896–909.
Verbaanderd, C., Maes, H., Schaaf, M.B., Sukhatme, V.P., Pantziarka, P., Sukhatme, V., Agostinis, P., and Bouche, G. (2017). Repurposing Drugs in Oncology

(ReDO)-chloroquine and hydroxychloroquine as anti-cancer agents. Ecancermedicalscience *11*, 781.

Vietri, M., Radulovic, M., and Stenmark, H. (2020). The many functions of ESCRTs. Nat. Rev. Mol. Cell Biol. *21*, 25–42.

van Vliet, A.R., Chiduza, G.N., Maslen, S.L., Pye, V.E., Joshi, D., De Tito, S., Jefferies, H.B.J., Christodoulou, E., Roustan, C., Punch, E., et al. (2022). ATG9A and ATG2A form a heteromeric complex essential for autophagosome formation. Mol. Cell *82*, 4324-4339.e8.

Wang, D., Wan, X., Du, X., Zhong, Z., Peng, J., Xiong, Q., Chai, J., and Jiang, S. (2021a). Insights into the Interaction of Lysosomal Amino Acid Transporters SLC38A9 and SLC36A1 Involved in mTORC1 Signaling in C2C12 Cells. Biomolecules *11*.

Wang, F., Gómez-Sintes, R., and Boya, P. (2018). Lysosomal membrane permeabilization and cell death. Traffic *19*, 918–931.

Wang, H., Wang, X., Zhang, K., Wang, Q., Cao, X., Wang, Z., Zhang, S., Li, A., Liu, K., and Fang, Y. (2019). Rapid depletion of ESCRT protein Vps4 underlies injury-induced autophagic impediment and Wallerian degeneration. Sci. Adv. *5*, eaav4971.

Wang, L., Wu, D., Robinson, C. V, Wu, H., and Fu, T.-M. (2020). Structures of a Complete Human V-ATPase Reveal Mechanisms of Its Assembly. Mol. Cell *80*, 501-511.e3.

Wang, T., Wang, L., Zhang, Y., Sun, J., Xie, Y., Yuan, Y., Gu, J., Bian, J., Liu, Z., and Zou, H. (2021b). Puerarin Restores Autophagosome-Lysosome Fusion to Alleviate Cadmium-Induced Autophagy Blockade via Restoring the Expression of Rab7 in Hepatocytes . Front. Pharmacol. *12*.

Wang, Z., Miao, G., Xue, X., Guo, X., Yuan, C., Wang, Z., Zhang, G., Chen, Y., Feng, D., Hu, J., et al. (2016). The Vici Syndrome Protein EPG5 Is a Rab7 Effector that Determines the Fusion Specificity of Autophagosomes with Late Endosomes/Lysosomes. Mol. Cell *63*, 781–795.

Weidberg, H., Shvets, E., Shpilka, T., Shimron, F., Shinder, V., and Elazar, Z. (2010). LC3 and GATE-16/GABARAP subfamilies are both essential yet act differently in autophagosome biogenesis. EMBO J. *29*, 1792–1802.

Weindruch, R., and Walford, R.L. (1982). Dietary restriction in mice beginning at 1 year of age: effect on life-span and spontaneous cancer incidence. Science *215*,

1415–1418.
Wesselborg, S., and Stork, B. (2015). Autophagy signal transduction by ATG proteins: from hierarchies to networks. Cell. Mol. Life Sci. *72*, 4721–4757.
Westermann, L., Neubauer, B., and Köttgen, M. (2021). Nobel Prize 2020 in Chemistry honors CRISPR: a tool for rewriting the code of life. Pflügers Arch. - Eur. J. Physiol. *473*, 1–2.
Wilfling, F., Lee, C.-W., Erdmann, P.S., Zheng, Y., Sherpa, D., Jentsch, S., Pfander, B., Schulman, B.A., and Baumeister, W. (2020). A Selective Autophagy Pathway for Phase-Separated Endocytic Protein Deposits. Mol. Cell *80*, 764-778.e7.
Willén, K., Edgar, J.R., Hasegawa, T., Tanaka, N., Futter, C.E., and Gouras, G.K. (2017). Aβ accumulation causes MVB enlargement and is modelled by dominant negative VPS4A. Mol. Neurodegener. *12*, 61.
Wirth, M., Zhang, W., Razi, M., Nyoni, L., Joshi, D., O'Reilly, N., Johansen, T., Tooze, S.A., and Mouilleron, S. (2019). Molecular determinants regulating selective binding of autophagy adapters and receptors to ATG8 proteins. Nat. Commun. *10*, 2055.
Wold, M.S., Lim, J., Lachance, V., Deng, Z., and Yue, Z. (2016). ULK1-mediated phosphorylation of ATG14 promotes autophagy and is impaired in Huntington's disease models. Mol. Neurodegener. *11*, 76.
Wu, Z., Bagarolo, G.I., Thoröe-Boveleth, S., and Jankowski, J. (2020). "Lipidomics": Mass spectrometric and chemometric analyses of lipids. Adv. Drug Deliv. Rev. *159*, 294–307.
Xia, Y., Liu, N., Xie, X., Bi, G., Ba, H., Li, L., Zhang, J., Deng, X., Yao, Y., Tang, Z., et al. (2019). The macrophage-specific V-ATPase subunit ATP6V0D2 restricts inflammasome activation and bacterial infection by facilitating autophagosome-lysosome fusion. Autophagy *15*, 960–975.
Xu, C., and Min, J. (2011). Structure and function of WD40 domain proteins. Protein Cell *2*, 202–214.
Xu, H., and Ren, D. (2015). Lysosomal Physiology. Annu. Rev. Physiol. *77*, 57–80.
Xu, Y., Zhou, P., Cheng, S., Lu, Q., Nowak, K., Hopp, A.-K., Li, L., Shi, X., Zhou, Z., Gao, W., et al. (2019). A Bacterial Effector Reveals the V-ATPase-ATG16L1 Axis that Initiates Xenophagy. Cell *178*, 552-566.e20.
Yadati, T., Houben, T., Bitorina, A., and Shiri-Sverdlov, R. (2020). The Ins and Outs

of Cathepsins: Physiological Function and Role in Disease Management. Cells *9*.
Yan, J., Kuroyanagi, H., Kuroiwa, A., Matsuda, Y., Tokumitsu, H., Tomoda, T., Shirasawa, T., and Muramatsu, M. (1998). Identification of mouse ULK1, a novel protein kinase structurally related to C. elegans UNC-51. Biochem. Biophys. Res. Commun. *246*, 222–227.
Yan, Y., Flinn, R.J., Wu, H., Schnur, R.S., and Backer, J.M. (2009). HVps15, but not Ca2+/CaM, is required for the activity and regulation of hVps34 in mammalian cells. Biochem. J. *417*, 747–755.
Yan, Y., Xu, Z., Dai, S., Qian, L., Sun, L., and Gong, Z. (2016). Targeting autophagy to sensitive glioma to temozolomide treatment. J. Exp. Clin. Cancer Res. *35*, 23.
Yang, Y., Zheng, L., Zheng, X., and Ge, L. (2021). Autophagosomal Membrane Origin and Formation. Adv. Exp. Med. Biol. *1208*, 17–42.
Yang, Z., Funke, B.H., Cripe, L.H., Vick, G.W., Mancini-Dinardo, D., Peña, L.S., Kanter, R.J., Wong, B., Westerfield, B.H., Varela, J.J., et al. (2010). LAMP2 Microdeletions in Patients With Danon Disease. Circ. Cardiovasc. Genet. *3*, 129–137.
Yim, W.W.-Y., and Mizushima, N. (2020a). Lysosome biology in autophagy. Cell Discov. *6*, 6.
Yim, W.W.Y., and Mizushima, N. (2020b). Lysosome biology in autophagy. Cell Discov. *6*, 1–12.
Yoon, T.-Y., and Munson, M. (2018). SNARE complex assembly and disassembly. Curr. Biol. *28*, R397–R401.
Yoshii, S.R., and Mizushima, N. (2017). Monitoring and Measuring Autophagy. Int. J. Mol. Sci. *18*, 1865.
Yoshii, S.R., Kuma, A., Akashi, T., Hara, T., Yamamoto, A., Kurikawa, Y., Itakura, E., Tsukamoto, S., Shitara, H., Eishi, Y., et al. (2016). Systemic Analysis of Atg5-Null Mice Rescued from Neonatal Lethality by Transgenic ATG5 Expression in Neurons. Dev. Cell *39*, 116–130.
Yoshimori, T., Yamamoto, A., Moriyama, Y., Futai, M., and Tashiro, Y. (1991). Bafilomycin A1, a specific inhibitor of vacuolar-type H(+)-ATPase, inhibits acidification and protein degradation in lysosomes of cultured cells. J. Biol. Chem. *266*, 17707–17712.
Young, A.R.J., Chan, E.Y.W., Hu, X.W., Köchl, R., Crawshaw, S.G., High, S., Hailey,

D.W., Lippincott-Schwartz, J., and Tooze, S.A. (2006). Starvation and ULK1-dependent cycling of mammalian Atg9 between the TGN and endosomes. J. Cell Sci. *119*, 3888–3900.

Yuan, P., Zhang, M., Tong, L., Morse, T.M., McDougal, R.A., Ding, H., Chan, D., Cai, Y., and Grutzendler, J. (2022). PLD3 affects axonal spheroids and network defects in Alzheimer's disease. Nature *612*, 328–337.

Yue, Z., Jin, S., Yang, C., Levine, A.J., and Heintz, N. (2003). Beclin 1, an autophagy gene essential for early embryonic development, is a haploinsufficient tumor suppressor. Proc. Natl. Acad. Sci. U. S. A. *100*, 15077–15082.

Yue, Z., Niu, X., Yuan, Z., Qin, Q., Jiang, W., He, L., Gao, J., Ding, Y., Liu, Y., Xu, Z., et al. (2022). RSPO2 and RANKL signal through LGR4 to regulate osteoclastic premetastatic niche formation and bone metastasis. J. Clin. Invest. *132*.

Zhang, S., Peng, X., Yang, S., Li, X., Huang, M., Wei, S., Liu, J., He, G., Zheng, H., Yang, L., et al. (2022). The regulation, function, and role of lipophagy, a form of selective autophagy, in metabolic disorders. Cell Death Dis. *13*, 132.

Zhen, Y., Spangenberg, H., Munson, M.J., Brech, A., Schink, K.O., Tan, K.-W., Sørensen, V., Wenzel, E.M., Radulovic, M., Engedal, N., et al. (2020). ESCRT-mediated phagophore sealing during mitophagy. Autophagy *16*, 826–841.

Zheng, J.X., Li, Y., Ding, Y.H., Liu, J.J., Zhang, M.J., Dong, M.Q., Wang, H.W., and Yu, L. (2017). Architecture of the ATG2B-WDR45 complex and an aromatic Y/HF motif crucial for complex formation. Autophagy *13*, 1870–1883.

Zhou, J., Tan, S.H., Nicolas, V., Bauvy, C., Yang, N. Di, Zhang, J., Xue, Y., Codogno, P., and Shen, H.M. (2013). Activation of lysosomal function in the course of autophagy via mTORC1 suppression and autophagosome-lysosome fusion. Cell Res. *23*, 508–523.

Zoncu, R., Bar-Peled, L., Efeyan, A., Wang, S., Sancak, Y., and Sabatini, D.M. (2011). mTORC1 senses lysosomal amino acids through an inside-out mechanism that requires the vacuolar H(+)-ATPase. Science *334*, 678–683.

van Zutphen, T., Todde, V., de Boer, R., Kreim, M., Hofbauer, H.F., Wolinski, H., Veenhuis, M., van der Klei, I.J., and Kohlwein, S.D. (2014). Lipid droplet autophagy in the yeast Saccharomyces cerevisiae. Mol. Biol. Cell *25*, 290–301.